KAPL-P-000198
(K97132)

HEAT TRANSFER CHARACTERISTICS OF POROUS SLUDGE DEPOSITS AND THEIR IMPACT ON THE PERFORMANCE OF COMMERCIAL STEAM GENERATORS

D. Duncan, et. al.

December 1998

NOTICE

KAPL ATOMIC POWER LABORATORY SCHENECTADY, NEW YORK 10701

Operated for the U. S. Department of Energy
by KAPL, Inc. a Lockheed Martin company

DOMINION ENGINEERING, INC.

Heat Transfer Characteristics of Porous Sludge Deposits and Their Impact on the Performance of Commercial Steam Generators

DEI-518
Revision 0

September 1997

Principal Investigators

M. A. Kreider
G. A. White
R. D. Varrin
P. J. Ouzts

6862 ELM STREET McLEAN, VIRGINIA 22101 PHONE: 703/790-5544 FAX: 703/790-0027

ACKNOWLEDGMENTS

Dominion Engineering acknowledges the contributions of the Electric Power Research Institute (EPRI), which supplied the ATHOS code and associated sludge deposition module for use in the project. Equally important, the participating utilities provided essential plant data and information for use in the project. The authors would like to thank the following people for their time and effort spent in providing support on this project: Govinda Srikantiah, Al Matheny, Michael Schwaebe, Oscar Flores, Steve Ewens, Tim Pettus, Warren Witt, Gary Boles, David Goetcheus, Bob Dolan, and Ron Baker.

Table of Contents

List of Tables

List of Figures

List of Attachments

NOMENCLATURE

This section lists and defines the symbols and abbreviations used in this report. Physical quantities are also listed with the units used. Most subscripts suggest their own meanings; full definitions are located where they are first introduced.

Symbols

A = heat-transfer area (ft^2); a "0" subscript indicates the original, new area (i.e., no plugged tubes).

Δ = operator used to indicate a change in the quantity that follows. Also used to denote statistical uncertainty.

F = factor used in defining log-mean temperature difference (dimensionless).

h = heat-transfer coefficient

k = thermal conductivity (BTU/hr-ft-°F).

N = number of tubes (dimensionless).

p or P = pressure (psia or psig).

q'' = local heat flux (BTU/hr-ft^2).

Q = heat-transfer rate, i.e., thermal power (BTU/hr or MWt). Q may also be used to denote volumetric flow rate (ft^3/hr).

R = global heat-transfer resistance (hr-°F/BTU). Defined to be $1/(UA)$.

R'' = area-based global heat-transfer resistance (hr-ft^2-°F/BTU). Defined to be $1/U$.

R_f'' = global area-based fouling factor (hr-ft^2-°F/BTU), which is defined as the change in area-based heat-transfer resistance ($\Delta R''$).

t = thickness (inches or mils).

T = temperature (°F); often used with subscripts "hot", "cold", "sat", etc., to indicate specific values. Temperature differences are indicated with a leading Δ.

ΔT_{lm} = log-mean temperature difference (°F); given by $F(\Delta T_2 - \Delta T_1)/\ln(\Delta T_2/\Delta T_1)$ for two arbitrary temperature differences "1" and "2". Used as a single-parameter characterization of the temperature difference along the length of heat exchanger tubes. (This is also used as an approximation to ΔT_m, the actual average temperature difference (integrated over the heat-transfer area).)

U = global heat-transfer coefficient (BTU/hr-ft^2-°F); a "0" subscript indicates new or clean conditions. Other subscripts are defined as they are used.

v = Used to denote volume fraction, a dimensionless quantity.

x = steam quality, i.e., percentage of water mass flow rate in the gaseous phase (dimensionless)
Also used to denote a generic variable.

Subscripts

The following are some of the commonly used subscripts applied to the above symbols:

ave	Denotes an average of reactor hot-leg and cold-leg properties
boil	Denotes boiling conditions
cold	Denotes reactor cold-leg property values
FW	Denotes final feedwater property values
global	Denotes property values defined for the SG tube bundle
hot	Denotes reactor hot-leg property values
local	Denotes property values at a specific location in the SG
sat	Denotes property values at secondary-side saturation conditions
0	Generally indicates property values under new or clean conditions in the SG

Abbreviations

AVT	All Volatile Treatment
BET	Brunnauer, Emmet, and Teller Surface Area Analysis
CANDU	Canadian Deuterium-Uranium nuclear plant or reactor
EFPY	Effective Full Power Years
EOC	End of [Operating] Cycle
ETA	Ethanolamine
HeP	Helium Pychnometry
ICP	Inductively Coupled Plasma Spectrometry
LMTD	Log-mean temperature difference
NSSS	Nuclear Steam Supply System
PHWR	Pressurized Heavy Water Reactor
PWR	Pressurized Water Reactor
SG/RSG	Steam Generator, Recirculating SG
SNUPPS	Standardized Nuclear Unit Power Plant System
TGA	Thermogravimetric Analysis
TSP	Tube Support Plate
TTS	Top of Tube Sheet

RTD	Resistance Temperature Detector
VWO	Valves Wide Open—refers to the fully open position of the turbine governor valves used to throttle the steam turbine
XRD	X-Ray Diffraction
XRF	X-Ray Fluorescence

I. INTRODUCTION

Steam generator (SG) fouling, in the form of corrosion deposits on the secondary sides of SG tubes, has been known to occur in almost all commercial US nuclear PWR (pressurized water reactor) plants. The level of fouling, as measured by the quantity of corrosion products that form, varies widely from plant to plant. In addition, the effect of SG fouling, as measured by a decrease in effective heat-transfer coefficient, has also varied substantially among commercial US plants. While some have observed large decreases in heat transfer, others have noted little change in performance despite the presence of significant quantities of secondary corrosion layers on their SG tubes. This observation has led to considerable confusion about what role secondary deposits play in causing heat-transfer degradation in SGs. As will become clear later in this report, secondary deposits can have a wide range of effects on heat transfer, from highly resistive to slightly enhancing (reflected by "negative fouling"). These different behaviors are the result of differences in deposit thickness, composition, and morphology. The main focus of this report is an investigation of the effects of secondary deposits on SG thermal performance. This investigation includes compilation of detailed information on the properties of tube scale at five commercial US nuclear plants and corresponding information characterizing SG thermal performance at these plants.

As indicated above, commercial US plants have exhibited a wide range of SG fouling behavior and SG tube scale properties. As a result, this project comprised an effort to collect, document, and analyze plant data in order to evaluate the effects of secondary tube scale on SG thermal performance. ATHOS, a thermal-hydraulics code developed by the Electric Power Research Institute (EPRI) specifically for steam generators, was an important tool used in these evaluations. As such, the project involved a number of separate tasks, which can be briefly summarized as follows:

1. Collect data relating to SG tube scale properties for five commercial US plants, including available information on composition, morphology, thickness, and spatial distribution.
2. Perform global fouling analyses for the SGs at the same five units to ascertain the effects of tube deposits on heat transfer. As part of this effort, other causes of SG thermal performance degradation were identified and evaluated in order not to incorrectly attribute their effects to secondary deposits. The main results of these analyses are estimates of the global fouling factor and SG steam pressure loss attributable to secondary tube scale.
3. Perform thermal-hydraulic analyses of the SGs at the five commercial plants chosen for the study. These analyses were performed using ATHOS, an industry-standard tool for evaluating SG thermal hydraulics. (Reference (29) discusses the use of ATHOS in

greater detail.) The analyses incorporated the scale thickness and spatial distribution data collected for the five plants in order to predict the effects of the deposits on SG heat transfer. To facilitate this effort, the ATHOS source code was modified to accept a spatially varying fouling factor.

The data and analyses presented in this report are believed to represent the most comprehensive collection of such information compiled to date.

Report Outline

A more detailed discussion of the work presented in this report is given below. Each topic listed in boldface corresponds to a separate section of the report as indicated.

TUBE SCALE CHARACTERIZATION (SECTION III). For a chosen group of US plants, available information regarding the characteristics of tube scale, including data on composition, morphology, thickness, and spatial distribution, was collected and evaluated. In some cases, data from other US plants were used to supplement those gathered for the five plants of interest.

One focus of this task is the chemical and physical characteristics of tube scale. Properties such as chemical composition, bulk density, porosity, pore size distribution, specific surface area, and internal structure (e.g., sub-layers) were catalogued for the participating plants. To the extent possible, data for multiple times during the plant history were gathered. This information is subsequently used in conjunction with industry data to evaluate the potential impact of a given plant scale on heat transfer.

A second focus of this task is the evaluation of scale thickness at the participating plants. In particular, variation in scale thickness with operating time and also the spatial thickness distribution throughout the SG are investigated. The data forming the basis for this evaluation include

- Mass removals during chemical cleanings and routine top-of-tube-sheet sludge lancing operations.
- Feedwater impurity concentration histories.
- Measurements of tube scale flakes retrieved from the participating plants (including data from pulled tubes).
- Low-frequency eddy current sludge profiles, both for the plants of interest and for other similar US plants.
- Visual inspections of the SGs at the participating plants.

Based on composition, morphology, and thickness data, estimates of thermal resistance and associated steam pressure loss are documented for each plant. These estimates are independent of those based on global thermal-hydraulic data discussed in Sections IV and V.

GLOBAL FOULING FACTOR ANALYSES (SECTION IV). For each participating plant, thermal-hydraulic measurements have been collected over the history of plant operation and analyzed using the overall heat-transfer equation. The resulting calculations indicate how both SG steam pressure and global fouling factor have varied over plant life. Because the fouling factor inherently adjusts for changes in plant operating temperatures, heat-transfer area, and thermal power, it provides greater insight into the effects of secondary deposits than SG steam pressure alone.

CAUSES OF SG PRESSURE LOSS (SECTION V). Although the global fouling factor accounts for variations in primary temperatures, heat-transfer area, and thermal power, it does not account for a number of other non-deposit-related causes of SG pressure loss (e.g., moisture separator fouling and hot-leg streaming among others). Consequently, a detailed accounting of SG steam pressure loss by cause is documented for each plant in the study, resulting in a best-estimate prediction of pressure loss due to deposits. Note that these estimates are based solely on the global fouling factor analyses and evaluations of other causes of pressure loss; no consideration is given to specific deposit properties for these estimates. Such estimates are made in Section III.

ATHOS THERMAL-HYDRAULIC ANALYSES (SECTION VI). The ATHOS3 computer program is an industry-standard tool for analyzing the thermal hydraulics of SGs. As part of this project, ATHOS was used to perform the following analyses:

- For "clean" conditions (i.e., unfouled), the spatial variation of temperature, pressure, heat flux, void fraction, and quality have been calculated for the four SG geometries represented by the five plants participating in this study. In each case, thermal-hydraulic inputs typical of actual plant operation were used. The results provide insight into which regions in a particular SG are likely to be most susceptible to tube deposits, and also help reveal correlations between local SG conditions and plant observations of deposit thickness distribution.
- With the analytical sludge deposition model included in ATHOS, predictions of scale thickness distribution throughout the SG were prepared for the five participating plants for typical operating conditions.
- The sensitivity of SG steam pressure to the axial thermal resistance distribution was investigated with the aid of an ATHOS code modification to allow input of a spatially varying thermal resistance. This analysis was designed to reveal how sensitive SG thermal performance is to the relative distribution of scale loading as opposed to the magnitude of total scale loading.

Participating Plants Used as Case Studies

In order to facilitate the tasks outlined above, five commercial US plants volunteered to participate in this project. After obtaining specific permission from the operating utilities, we proceeded to gather available tube scale characterization and thickness data and also the required plant instrument thermal-hydraulic data. The five plants A through E listed in the table on the next page participated in this project.* A sixth plant, Ginna,† which was known to have significant secondary fouling, was added to the study in view of the thin deposits and minimal fouling that were found at Plant C. Not all of the information collected for Plants A through E was available for Ginna, known in this study as Plant F. As a result, only the following information and analyses are included for Plant F.

- In Section III, deposit characterization information. Most of this information is taken from tests performed on a pulled tube taken from Plant F in 1991 (1, 28).
- In Section IV, a global fouling factor analysis based on measured SG steam pressures in Reference (20) and design values of other thermal-hydraulic parameters.
- In Section IV, analysis of heat-transfer tests performed by B&W Nuclear Technologies (now Framatome Technologies, Inc.) on a pulled tube taken from Plant F in 1991 (1, 27).

Plants Participating in Study

Unit	Plant A	Plant B	Plant C	Plant D	Plant E	Added: Plant F
SG Model	W Model F	W Model 51	W Model E2	W Model 51	CE Model 3410	W Model 44
Comm. Operation	1984	1981	1988	1981	1983	1970
No. SGs	4	4	4	4	2	2
Chemical Cleaning	Yes (3/95)	Yes (9/95)	No	No	Yes (12/96)	No*
Current Age (EFPY†)	9.5	7.8	5.0	8.0	10.1	15.6**
FW Chemistry	AVT‡ (ETA since 1993)	AVT	AVT	AVT	AVT (ETA since 1996)	PO_4 1970-74 AVT 1974-
Illustration	Fig. I-1 (22)	Fig. I-2 (23)	Fig. I-3 (22)	Fig. I-2 (23)	Fig. I-4	Similar to 51

* No chemical cleaning was performed; however, the SGs were replaced in 1996 due to tube corrosion problems.

** As of the most recent available thermal-hydraulic data in 1990.

† EFPY stands for "effective full power years," a standard measure of a plant's age.

‡ AVT stands for "all volatile treatment" and is usually characterized by the presence of ammonia (NH_3) and hydrazine (N_2H_4). Some plants using AVT chemistry have also incorporated other additives like ethanolamine (ETA) and morpholine.

---

* Based on the request of the participating utilities, plant names are not used in this report.

† Ginna is identified because all information used in the project is available in published sources.

Plants Participating in Study

Unit	Plant A	Plant B	Plant C	Plant D	Plant E	Added: Plant F
SG Model	W Model F	W Model 51	W Model E2	W Model 51	CE Model 3410	W Model 44
Comm. Operation	1984	1981	1988	1981	1983	1970
No. SGs	4	4	4	4	2	2
Chemical Cleaning	Yes (3/95)	Yes (9/95)	No	No	Yes (12/96)	No*
Current Age (EFPY†)	9.5	7.8	5.0	8.0	10.1	15.6**
FW Chemistry	AVT‡ (ETA since 1993)	AVT	AVT	AVT	AVT (ETA since 1996)	PO_4 1970-74 AVT 1974-
Illustration	Fig. I-1 (22)	Fig. I-2 (23)	Fig. I-3 (22)	Fig. I-2 (23)	Fig. I-4	Similar to 51

* No chemical cleaning was performed; however, the SGs were replaced in 1996 due to tube corrosion problems.

** As of the most recent available thermal-hydraulic data in 1990.

† EFPY stands for "effective full power years," a standard measure of a plant's age.

‡ AVT stands for "all volatile treatment" and is usually characterized by the presence of ammonia (NH_3) and hydrazine (N_2H_4). Some plants using AVT chemistry have also incorporated other additives like ethanolamine (ETA) and morpholine.

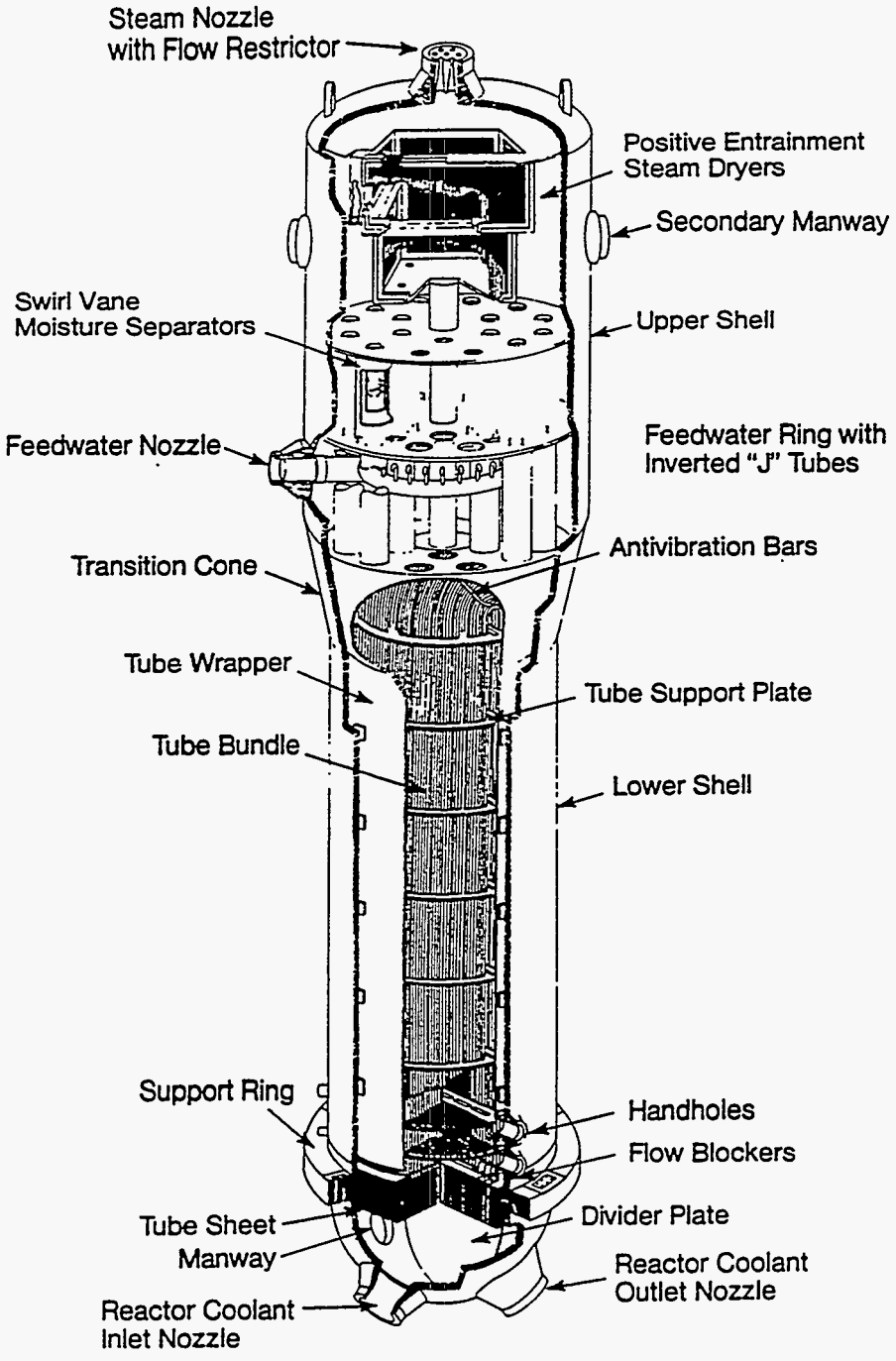

Figure I-1. Schematic of a Westinghouse Model F Steam Generator (22)

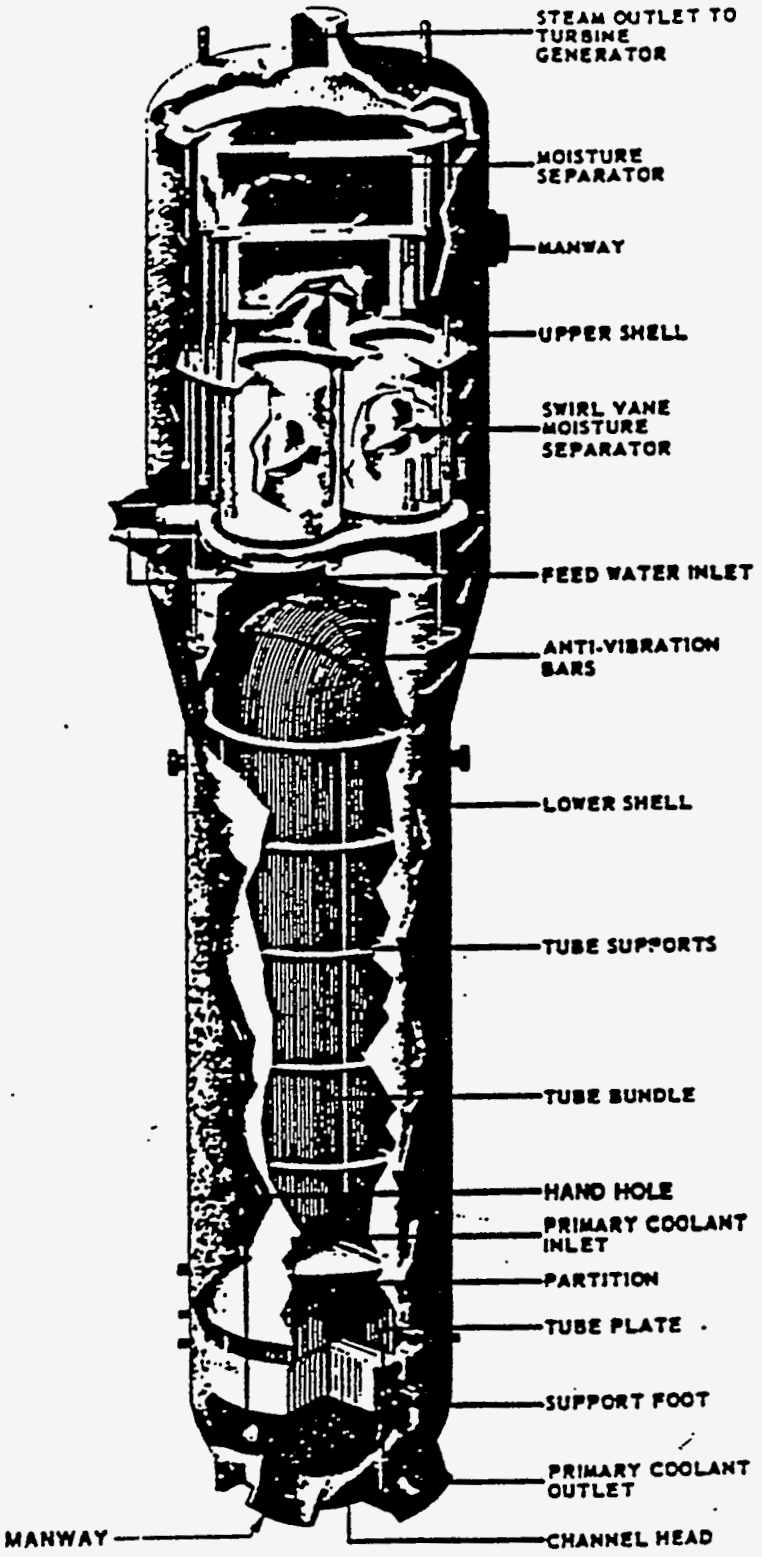

Figure I-2. Schematic of a Westinghouse Model 51 Steam Generator (23)

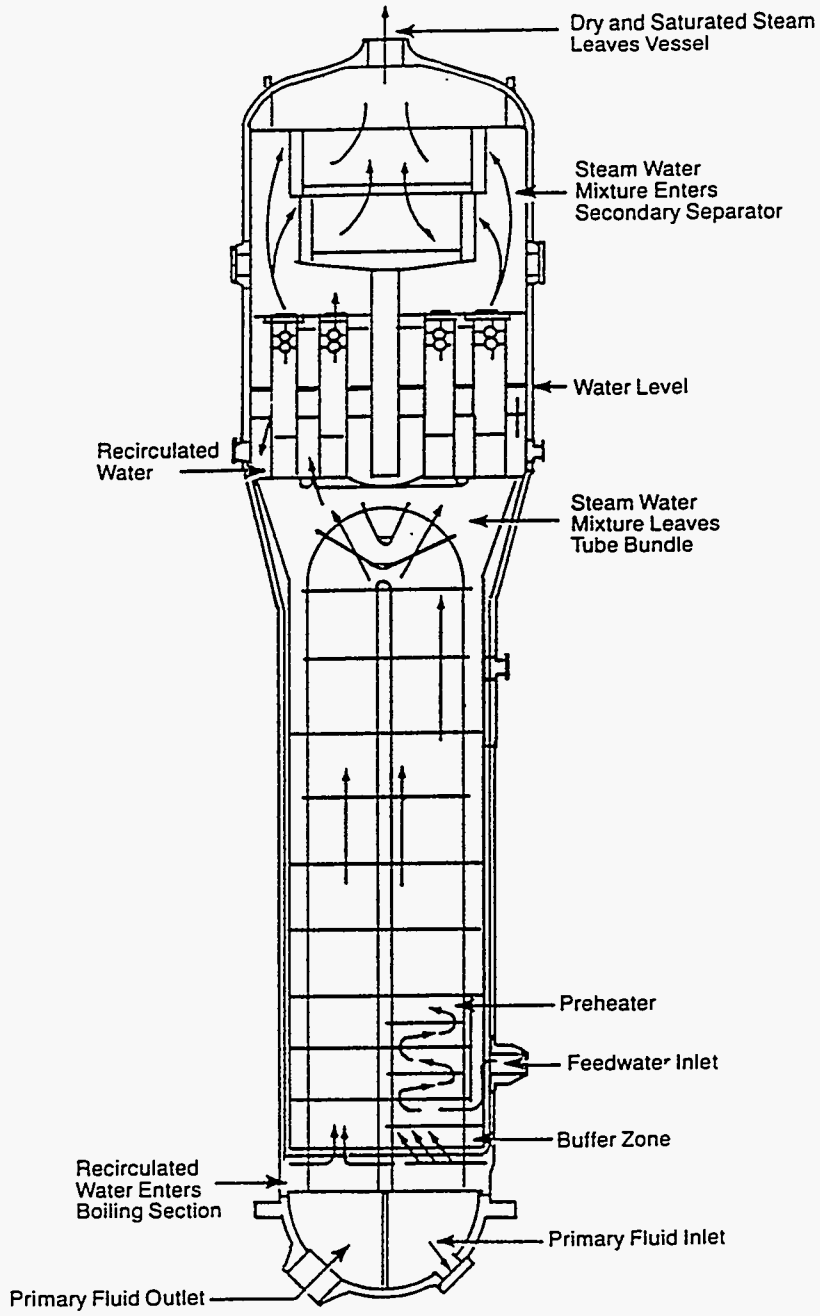

Figure I-3. Schematic of a Westinghouse Model E2 Steam Generator (22)

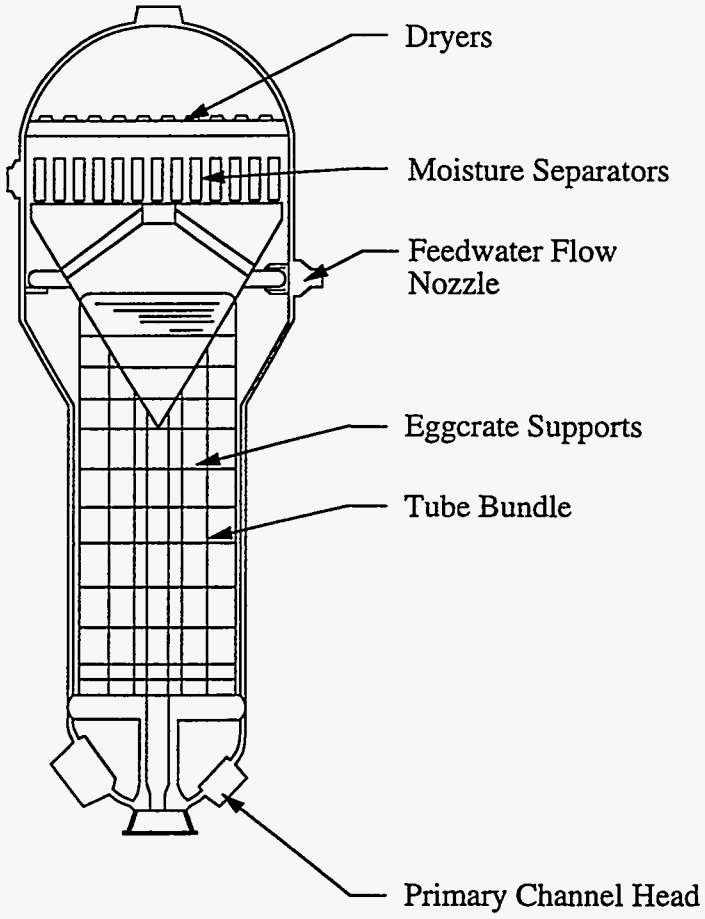

Figure I-4. Schematic of Combustion Engineering Model 3410 Steam Generator

II. SUMMARY OF RESULTS AND CONCLUSIONS

Included in this section is a summary of the key results and conclusions generated by the project. Brief summaries of commercial scale characterization data, commercial scale thickness and distribution data, and fouling factor analyses and pressure loss breakdowns for five commercial units are provided. The key conclusions reached during this project include the following:

- Thin secondary tube deposits (thinner than about 4 mils) tend to have little effect on SG thermal performance and may even be performance-enhancing. Thick deposits (thicker than about 9 mils) tend to be nearly nonporous at the tube wall and consequently very thermally resistive, causing significant performance degradation.
- Sources of SG performance degradation vary substantially from plant to plant. Although tube scale can be a major cause of such performance degradation, it is not the only one or always the most significant one.
- As demonstrated by an ATHOS sensitivity study, the spatial distribution of tube scale mass within an SG, while significant, has a smaller effect on SG thermal performance compared to the magnitude of the scale loading (i.e., average thickness).
- Based on the ATHOS code and associated sludge deposition postprocessor, the variables which most strongly affect sludge deposition are fluid velocity, void fraction, and heat flux.

Scale Characterization Data

COMPOSITION. Chemical analyses indicated that scale from all five plants is primarily composed of magnetite or other forms of iron oxide (50% up to 90-95%, depending on the plant). Tube scale and sludge samples from Plants B and E contained significant amounts of copper (10-25%), while samples from Plants A and C exhibited very little copper (typically less than 1%). Primary and significant minor scale constituents are listed at the top of Table II-1.

MORPHOLOGY. Examinations of flake cross sections revealed the following morphological information:

- Plant-A scale from 1993 varied in thickness from 0.9 to 6 mils and sometimes exhibited a double-layer structure, including a very thin copper-rich layer adjacent to the tube interface and a thicker, more porous outer layer.
- Plant-B scale flakes from 1990 exhibited a two-layered morphology with significant copper inclusions. The outer layer of Plant-B scale was sometimes extremely porous (as high as 80-90%).
- Inspections of Plant-E flakes indicated a three-layer structure, including a low-porosity inner layer representing about 40% of the total thickness, a highly porous middle layer containing what appear to be large enclosed voids (typically about 10-15% of the total

scale thickness), and an outer layer exhibiting a connected network of capillaries. This layer represented about 50% of the total thickness.

- Plant-F scale exhibited a two-layer structure with increased porosity in the outside part of the outer layer and a calcium-phosphorus compound in the dense inner layer, a result of early operation with phosphate water chemistry (1). Overall, Plant-F scale was observed to be more dense than the scale from the other plants.

Key morphological properties for the scale at each plant are summarized in Table II-1.

THICKNESS. Best estimates of average tube scale thickness based on chemical cleaning mass removals, feedwater impurity concentration histories, and direct flake measurements were prepared for each plant in the study. For the first two methods, adjustments were made to account for the accumulation of sludge on the tube support surfaces and the tube sheet. The resulting overall best estimates, considering all estimation methods, are summarized in Table II-2. Note that Plant E (prior to chemical cleaning) and Plant F (prior to replacement) have the highest estimated thicknesses.

DISTRIBUTION. In addition to the average thickness at each plant, best estimates of representative scale mass distributions were generated using low-frequency eddy-current test (ECT) sludge profiles, which report the relative mass per unit length for selected tubes. Data for plants in the study and, when available, from other plants in the industry were used to generate composite distributions applicable to the SG designs examined in the project. These distributions can be used as inputs to thermal-hydraulic analyses for evaluating the effects of scale distribution on SG thermal performance.

ESTIMATES OF THERMAL RESISTANCE. Best estimates of thermal resistance associated with each plant scale were prepared. Note that these estimates are independent of the global fouling analyses (see below), but are based instead on the specific information collected for scale at each plant (thickness, composition, porosity, etc.), heat-transfer experiments, and engineering judgment. The results are reported at the bottom of Table II-1 and suggest significant thermal performance loss at Plants E and F.

Fouling Factor Analyses and Pressure Loss Summary

The results of global fouling factor analyses performed for each plant, including computed uncertainties, are summarized in Table II-3. These fouling factors were translated into secondary-deposit SG pressure losses after accounting for other possible causes of pressure loss. The results, summarized in Table II-4, indicate that Plants E and F experienced large pressure

losses due to secondary deposits. Based on the calculations, Plant A scale enhanced heat transfer slightly, scale at Plants B and D caused moderate SG steam pressure losses, and Plant C experienced either no effect at all or a slight heat-transfer enhancement. Note that these estimates are based solely on measured thermal-hydraulic data and are thus independent of the estimates at the bottom of Table II-1. The agreement between the calculated global fouling factors in Table II-3 and the estimates based on deposit characterization in Table II-1 provides added confidence in the fouling factor calculations.

Effects of Thermal Resistance Distribution on SG Thermal Performance

A sensitivity study was performed to evaluate the sensitivity of SG steam pressure to the axial distribution of thermal resistance. The results for 60 10^{-6} h-ft^2-°/BTU and 200 10^{-6} h-ft^2-°/BTU area-averaged thermal resistances distributed linearly from the top of the tube sheet indicate that the average thermal resistance has a significantly greater impact on pressure loss than the distribution, even in cases where the thermal resistance is very uneven.

Table II-1. Summary of Tube Scale Characterization Data

Plant	A	B	C	D*	E	F
Primary Constituents	Fe_3O_4, Fe_2O_3	Fe_3O_4, Cu	Fe_3O_4	Fe_3O_4	Fe_3O_4	Fe_3O_4, $Ca_{10}(PO_4)_6(OH)_2$
Significant Minor Constituents	Ca, Al, SiO_2	SiO_2	NA	Cu	Cu, ZnO	Cu
Morphology	Double Layer: Consolidated Inner, Porous Outer	Double Layer: Consolidated Inner Very Porous Outside	NA	NA	Three Layer: Consolidated Inner, Void-Filled Middle, Porous Outer	Double Layer: Consolidated Inner, Slightly Porous Outer
Skeletal Density (g/cm^3)	NA	5.41	NA	5.38	5.14	4.61
Total Porosity	NA	55%	NA	34%	22%	9%
Flake Thickness Range (mils)	0.9-6	2.5-5.5	0.3-1.1	NA	7.4-18.8	8.1-9.3
Estimated Fouling Factor (10^{-6} h-ft^2-°F/BTU)	-15	44	0	65	185	192

NA = Not Available

*Data for Plant-D sister station

Table II-2. Best Estimates of Average Tube Scale Thickness

Plant	Est. Avg. Thickness (mils)	Corresponding Plant Age (EFPY)
A	4.1±0.5	8.6
B	5.7±1.0	7.5
C	0.7±0.5	5.0
D	5.9±2.0	8.0
E	10.4±1.0	10.0
F	8.7±2.5	15.6

Table II-3. Computed Fouling Factors and Uncertainties (10^{-6} h-ft^2-°F/BTU)

Value	Plant A		Plant B		Plant C	Plant D	Plant E	Plant F
	Before CC	Recent Oper.	Before CC	Recent Oper.	Recent Oper.	Recent Oper.	Recent Oper.	As of 1990
Best Estimate	-28	-5	+21	+42	+30	+51	+172	+190
Est. Uncertainty	±25	±25	±24	±24	±46	±89	±48	–
Est. Lower-Bound	-47	-24	-3	+18	-16	-37	+124	–
Est. Upper-Bound	-9	+14	+45	+66	+76	+140	+220	–

Table II-4. Estimated Pressure Loss Due to Secondary Deposits Based on Other Causes

Pressure Loss (psi)	PLANT A		PLANT B		PLANT C	PLANT D	PLANT E	PLANT F
	Before CC	Recent Oper.	Before CC	Recent Oper.	Recent Oper.	Recent Oper.	Before CC	1980-1990
Best Estimate	-5	5	8	14	-8	17	66	32*
Estimated Tolerance	±5	±5	±7	±7	±10	±7	±5	±20
Est. Upper Bound	0	10	15	21	2	24	71	52
Est. Lower Bound	-10	0	1	7	-18	10	61	12

*Estimated to be approximately 62 psi compared to early operation.

III. EVALUATION OF TUBE SCALE CHARACTERIZATION DATA FOR FIVE US PLANTS

In a PWR SG, the resistance to heat transfer between the primary coolant and the secondary-side fluid is the sum of several individual thermal resistances. Under clean design conditions, this total resistance includes boundary-layer resistances in both the primary and secondary fluids at the heat exchanger surfaces (i.e., the ID and OD surfaces of the SG tubes) plus the resistance of the tube wall, which depends on the thermal conductivity of the tube material and the tube geometry. After sufficient operating time, both the ID and the OD surfaces of the tubes can become covered with layers of corrosion products (i.e., become fouled). This process effectively introduces two additional thermal resistances which can be quantified in terms of the effective thermal conductivities of the corrosion layers. If these resistances are large enough, they can have a significant effect on the overall heat-transfer performance of SGs. For commercial PWR SGs, primary deposits are believed to have relatively little impact on SG thermal performance (see Appendix E for details). However, secondary deposits can have a wide range of possible effects on heat transfer depending on the composition and physical properties of the deposit layers.

This section focuses on the properties of the secondary tube deposits that have developed over the operating histories of the five plants examined in this study.* Specifically, information in the following areas will be presented.

- SCALE COMPOSITION. Both elemental and compound summaries are provided for the scale at each plant as available. In addition, the feedwater chemistry, including notable impurity concentrations, is summarized for each unit.
- SCALE MORPHOLOGY. Physical characteristics relevant to heat transfer are documented for the plants in this study, including internal layered structure, bulk density, total porosity, pore size distribution, and specific surface area.
- MEASUREMENT TECHNIQUES FOR SCALE CHARACTERIZATION
- PLANT FEEDWATER IMPURITIES
- SCALE THICKNESS AND DISTRIBUTION. Several approaches are used to estimate deposit thicknesses and distributions for each plant, including
  - Chemical cleaning and sludge lance mass removals
  - Time integration of corrosion product concentration histories
  - Direct scale measurement (including measurement of flakes and data from tube pulls)

---

* Some additional information is included for a sixth plant (Plant F) in view of the very thin deposits believed to be present at Plant C.

- Low-frequency eddy-current sludge profiling
- Visual inspections

Some of these techniques can only provide information regarding the average deposit thickness (e.g., chemical cleaning results, integrated corrosion product concentrations, and usually flake measurements). Such average thicknesses are combined with the available data concerning distribution throughout the bundle to generate thickness distributions.

Scale Composition

Some chemical tests indicate which elements are present in secondary deposit samples (and in what proportion) while others indicate the compounds in which those elements appear. Results of both types of test are summarized for each plant as applicable.

PLANT A. Five sludge samples taken from the Plant-A SGs prior to the chemical cleaning in 1995 (presumably from the previous outage in 1993) were chemically analyzed. Three of the samples comprised powder taken from three different SGs following sludge lancing, the fourth sample was powder removed after a pressure pulse cleaning application, and the fifth sample consisted of tube flakes.* Both inductively coupled plasma spectrometry (ICP) and X-ray diffraction (XRD) tests were performed; the results are summarized in the leftmost columns of Table III-1. Note that the powder samples were tested to be nearly 100% iron oxide according to both ICP and XRD. According to both tests, the flake sample comprised only a little over 50% iron oxide, with potentially large fractions of hardness species (5% calcium, 3% silicon, 3% aluminum, and 2% phosphorus†).

PLANT B. Deposits taken from the Plant-B SGs at several different times were analyzed. The dates of the analyses and corresponding plant operating times are listed below along with brief summaries of the chemical composition results. A tabular summary of the 1990-1993 data is provided as part of Table III-1.

April 1987 (2.85 EFPY): Energy dispersive spectroscopy (EDS) yielded semi-quantitative results for both powder and flake samples. Approximately 95% (by volume) of the powder particles analyzed were predominantly iron (presumably in the form of iron oxides). About 1% by volume were chiefly silicon, and the remaining 4% by volume were a mixture of iron and copper. The flake samples

* Note that the report accompanying the chemical analysis suggests that the postulated outer layer of the tube scale flake may have broken off the sample prior to the analysis, potentially affecting the results.

† Note that these values do not match those listed in Table III-1. The values in the text are weight percents of the stated elements while the values in the table are weight percents of the assumed compound.

were characterized as having high iron concentrations and lower copper and nickel concentrations. EDS dot maps revealed locally concentrated areas of copper.

August 1990 (4.02 EFPY) — X-ray fluorescence (XRF) tests indicated mainly iron (presumably in the form of magnetite or other iron oxides), although a large fraction of copper was present in all samples tested (about 20%). An independent ICP test indicated about 70% iron oxides and 28% copper.

February 1992 (5.25 EFPY) — The combined results of XRF and ICP indicated that both powder and tube scale samples from all four SGs contained approximately 60% iron by weight (which is equivalent to about 80% magnetite) and 10% copper. All other constituents were measured at concentrations of 1% or less.

June 1993 (6.25 EFPY) — The combined results of XRF and ICP analyses are indicated in Table III-1 for both bulk sludge samples and tube scale samples. The values shown are averages for samples taken from each of the four SGs. Note that the copper content in the tube scale is significantly higher than in the bulk sludge collected from the top of the tube sheet.

PLANT C. Chemical analyses were performed on tube deposits on pulled tubes taken from the Plant-C SGs in 1993 and 1995. These analyses indicated more than 25% magnetite (no specific value provided), with only small amounts of other elements, including copper (less than about 1%).*

PLANT D. Unfortunately, no deposit composition data were available specifically for Plant D. However, results of an analysis for Plant D's sister unit (same station) are available. According to ICP analyses, a sample consisting of about 75% powder (with the remainder flakes) comprised about 90% iron oxide, 8% copper, and only small amounts of other elements (<1%). The results are summarized in Table III-1.

PLANT E. Deposit chemical composition data were available for two outages: 1991 (5.72 EFPY) and 1995 (8.63 EFPY). The results are summarized in Table III-1. Note that tube scale from both times was composed of approximately 90% magnetite and 5-10% copper, with lesser amounts of zinc. All other constituents, including silicon, were present in concentrations of less than 1%.

---

* Some samples taken from the region of the tube support plates were higher in copper—about 7%. Also, manganese was found in significant concentrations (about 10%) in the vicinity of some tube support plates.

PLANT F. Because analysis of the deposits at Plant C indicated very thin deposits (see the latter part of this section), a sixth plant, which exhibited a high level of thermal performance degradation, has also been included in this study. The U-bend portion of a single tube was removed from one of the Plant-F SGs in 1991, and the secondary deposits were examined (1). The composition of the deposits on this tube segment was evaluated using XRF (elemental analysis) and XRD (compound identification). Both powder and flake samples were examined; the results are summarized in Table III-1. The presence of magnetite (Fe_3O_4), elemental copper (Cu), calcium hydroxyapatite ($Ca_{10}(PO_4)_6(OH)_2$), zinc oxide (ZnO), and hematite (Fe_2O_3) were all confirmed with XRD. It is important to note that the presence of the phosphorus compound in Plant-F scale is the result of early operation on phosphate water chemistry (1970 through 1974). All other plants in this study have used all-volatile treatment (AVT) water chemistry, which does not transport phosphorus to the SGs in significant quantities.

Scale Morphology

The physical characteristics of secondary scale can have a greater effect on heat transfer than the chemical constituents do. The parameters which are expected to determine the heat-transfer properties are the total porosity, the pore size distribution, and the flow permeability.* Some of these parameters (and related quantities like the range of particle sizes) were recorded for scale samples at two of the five original plants included in the study (B and E), the sister station of a third plant (D),† and also for Plant F. The results are summarized in Table III-2. Note that Plant-B scale had much higher porosity than scale from Plants D, E, and F; it also exhibited a correspondingly lower bulk density. Also note that the average pore size at Plant E is significantly lower than that at Plants B and D.

Further insight into the heat-transfer effects of plant scale can be gained through microscopic inspection of flake cross sections. Such cross sections can reveal internal structures that impact heat transfer. Cross sectional photos were available for Plants A, B, E, and F and are briefly discussed below.

---

* The total porosity can be calculated by measuring the bulk density and skeletal density. Flow permeability is not normally measured directly. Also note that the range of particle sizes is related to the pore size distribution but is often independently measured.

† In the following discussion on scale morphology, all references to Plant-D scale apply to the measured values for Plant D's sister unit unless otherwise noted.

PLANT A. Cross sections of several flakes removed from the Plant-A SGs in 1993 were prepared. The flakes measured between 0.9 mils and 6 mils in thickness, and exhibited the following additional characteristics:

- An apparent double-layer structure.
- Highly variable thickness locally in some cases, suggesting a high degree of roughness.
- A high level of porosity in the outermost layer of each flake.
- In some cases, a very thin (small fraction of 1 mil) copper-rich inner layer adjacent to the tube interface.

Figures III-1a and III-1b show several photomicrographs of Plant-A scale from 1993; in all cases the tube interface surface is located at the lower part of the photo. The top photo in Figure III-1a depicts a scale layer 0.9 mils thick. Note the high level of porosity, particularly near the outer surface. The lower photo in Figure III-1a shows a portion of 6-mil thick scale with significant porosity (especially at the outer surface). The samples shown in Figure III-1b are both relatively thin (approximately 1 to 2 mils or less). In each, a very thin layer of copper near the tube interface surface is visible. The lower photo also reveals a local area of concentrated copper inclusions. In the top photo, a double-layer structure is suggested: an outer porous layer and a more consolidated inner layer.

PLANT B. Flake samples collected in 1990 were mounted for this project. A sample set of five flakes was examined, leading to the following observations:

- With no magnification, samples were dull black on the outer surface with a somewhat rough appearance. The inner surface was shiny black and smoother than the outer surface.
- The thickness was variable between approximately 2.5 mils and 5.5 mils.
- For the thin flakes (2-3 mils), the structure was characterized by two layers: an inner layer about 2 mils thick exhibiting low porosity and many metallic inclusions (probably copper, based on the chemical analyses of Plant-B scale) and an outer layer 0.5-1 mil thick marked by much higher porosity and few metallic inclusions. Figure III-2a depicts two views of the same flake magnified at 400X.* Note that the thickness is about 2.5 to 3 mils in each case.
- For thicker flakes (4-5.5 mils), the two-layer structure is even more pronounced. As with the thin flakes, the inner layer is 2-3 mils thick and is marked by relatively low porosity and numerous metal inclusions (up to 30 or 40% locally). The outer layer of the thicker flakes was 1.5-2.5 mils thick with porosity varying from moderately high (estimated at about 50%) to very high (estimated at 80 to 90%). Photos of two separate flakes in this

* The tube interface surface in each photo in Figures III-2a and III-2b is located at the lower portion of the picture.

category are shown in Figure III-2b. The upper flake is about 4.5 mils thick while the lower flake is nearly 5.5 mils thick. Note the extremely high porosity in the outer layer shown in the top part of the upper photo.

PLANT E. Twelve tube scale flakes ranging from 7.4 mils to 18.8 mils in total thickness were taken from Plant E's SGs in 1995 and examined visually under magnification. The cross sections revealed the following morphological details:

- An innermost layer (adjacent to tube interface) with low porosity and dispersed inclusions of zinc oxide and copper. Adjacent to the tube interface surface, significant quantities of other metal oxides appear to be present (e.g., zinc oxide, manganese oxide, and nickel ferrite). This layer typically represented about 40% of the total deposit thickness.
- A middle, highly porous layer with large, apparently enclosed voids. The voids appear to be lined with optically active materials (perhaps silicates or sulfates). This layer usually comprised about 10-15% of the total deposit thickness.
- An outermost layer comprising a porous, crystalline magnetite band. The pores in this layer appear to represent a well-connected network of capillaries rather than the large enclosed voids of the middle layer. The outer layer represented about 50% of the total flake thickness in most cases.

Figure III-3 shows two photomicrographs of Plant-E tube scale removed from one of the SGs in 1995. The top photo (a dark field image) clearly shows the three distinct layers described above; the total thickness of this sample is 14 mils. The lower photo (phase contrast) highlights the inclusions (probably composed of silica and/or sulfate) lining the voids in the middle layer. This flake sample was 8 mils thick.

PLANT F. Several cross sections of the secondary deposits on the U-bend portion of a single tube removed from Plant F in 1991 were prepared (1). The salient features of this scale are illustrated in Figure III-4 and include

- A thick, porous outer layer (7-8 mils) characterized by magnetite (light gray in the photo) and copper inclusions (white in the photo). Note the high degree of porosity (black) near the outer surface of the deposit.
- A thinner, more consolidated inner layer (0.5-2 mils) characterized primarily by calcium hydroxyapatite and some form of magnesium oxide (dark gray in the photo). There are also some copper inclusions in the inner layer, although generally fewer than in the outer layer.

Measurement Techniques for Scale Characterization

Much of the information presented above concerning scale composition and morphology was gathered using the techniques described below. In particular, ICP, XRF, and XRD were used to

measure the compositions reported in Table III-1, helium pychnometry was used to measure the skeletal densities reported in Table III-2, mercury porosimetry was used to evaluate the range of pore sizes and the average pore sizes in Table III-2, and BET was used to measure the specific surface areas in Table III-2.

INDUCTIVELY COUPLED PLASMA SPECTROMETRY (ICP). This technique is typically performed on a liquid sample of 1 to 5 grams and involves initial dissolution in an acid medium followed by heating of the specimen and observation of the resulting emitted light. Only elemental composition can be determined with this method. The accuracy of ICP is generally ±0.2%.

X-RAY FLUORESCENCE (XRF). Also used to measure elemental composition, XRF consists of bombarding the specimen with intense x-rays and examining the emission spectra for wavelengths characteristic of particular elements. The concentration of constituent elements can be determined from the intensity of the emission spectra. The accuracy of XRF is highly dependent on the equipment sophistication and the manner in which the system is calibrated with standards. When properly calibrated, XRF systems can exhibit accuracies comparable to ICP for many elements (e.g., less than 0.5%). Use of improperly calibrated XRF systems may result in uncertainties as high as ±10%.

X-RAY DIFFRACTION (XRD). Most compound analyses employ this technique, which is implemented by passing x-rays through the compound and observing the resulting diffraction pattern. Compounds are identified by comparing the images with previously catalogued images for known crystal structures. Usually the laboratory performing the analysis is provided with a list of potential compounds that may be represented in the sample(s); only those compounds that are included in the search list can be identified. The accuracy of XRD analysis is generally taken to be approximately ±0.5%.

HELIUM PYCHNOMETRY. This technique is used to determine the skeletal density of a deposit sample. It requires placement of the sample, usually 0.5 to 5 grams, in a chamber of known volume. After the chamber is sealed, it is evacuated and then pressurized with dry helium gas to approximately 20 psig. The ideal gas law and knowledge of the empty sample chamber volume can then be used to calculate the total volume occupied by the deposit sample (less the sum of the pore volumes). Skeletal density is then calculated by dividing the sample weight by the net volume of the sample. Note that helium pychnometry cannot account for voids in the deposit samples if they are completely isolated from the penetrating helium gas. This can lead to a low

bias in the calculations (i.e., a lower density).* The inherent accuracy of helium pychnometers is dependent on: (1) the accuracies of the pressure measurements, (2) temperature changes of the gas during the measurement, and most importantly, (3) the degree to which the helium can penetrate the voids within the samples. Overall, the first two sources of error are generally believed to contribute errors on the order of 1%. The error associated with the third issue is highly sample dependent, but could be as much as 5 to 10%.

System calibration of helium pychnometers can be achieved in several ways, but the most common method involves measuring the density of non-porous materials with known densities. DEI calibrates its Micromeritics Model 1305 helium pychnometer with copper powder.

WATER PYCHNOMETRY. This simple technique involves: (1) measuring the weight of a water-filled sample container (typically 5 to 20 ml in volume with a capillary overflow tube which permits filling to the same level repeatably), (2) recording the temperature of the water (to allow for accurate assessment of the water density), (3) removing all or part of the water, (4) submerging a pre-weighed and dried deposit sample in the partially filled container, (5) back-filling the sample chamber with water to exactly the same level as was used in the initial weighing, (6) re-weighing the water/deposit filled system, and finally (7) calculating the density of the sample via knowledge of the deposit weight and the weight of the water displaced by the sample. Water displacement pychnometry is used to measure bulk density since the water will tend to fill open pores (until the surface tension of the water cannot be overcome by capillary forces). The accuracy of water displacement pychnometry depends on the accuracy of the balances used to weigh the samples, as well as the accuracy of the water temperature measurements. DEI uses a water displacement pychnometer with an integral precision mercury thermometer to minimize errors in the temperature measurements. In general, the repeatability of the device is expected to be on the order of 1%, but the absolute accuracy is highly dependent on the sample morphology.

BET SURFACE AREA MEASUREMENT. This technique is used to measure the total surface area of a deposit sample, including that area provided by the inner surfaces of pores. The technique involves cooling the sample to the temperature of liquid nitrogen, flowing a mixture of nitrogen and a lower boiling point gas (e.g., helium) over the sample while it is cold, and then warming the sample while simultaneously measuring the amount of nitrogen that condensed on the surface. The quantity of nitrogen is measured by a thermal conductivity detector. Several

* This may be particularly relevant for the deposits at Plant E, which exhibited numerous, apparently enclosed voids.

equations which describe "adsorption isotherms" can be used to estimate the surface area from the amount of adsorbed nitrogen and the sample weight, the most common being that developed by Brunnauer, Emmet, and Teller (hence BET technique).

MERCURY POROSIMETRY. This technique is used to determine the porosity and pore size distribution of a solid sample. A sample is placed in a sample chamber known as a penetrometer. Usually, a minimum of 1 gram of sample material is used. After evacuating the sample chamber, liquid mercury is admitted to the chamber and the volume required to initially fill the chamber (no sample penetration) is recorded. This allows for a measurement of the bulk density of the sample. Upon completion of the initial fill, additional mercury is forced into the penetrometer and as such into the deposit sample pores. The pressure of the "intrusion" is increased gradually, and pressure-intrusion volumes are recorded. Complete penetration may require pressures as high as 60,000 to 80,000 psi. Analysis of the pressure-intrusion volume data allows for a determination of total porosity, pore size distribution (since the surface tension of mercury is well characterized, the size of the pores intruded at a particular pressure can be calculated), and specific surface area.

The accuracy of the mercury porosimetry technique is subject to debate since much depends on the data manipulation, but it is reasonable to assume it is accurate to with a few percent.

Plant Feedwater Impurities

Key impurities in the SG feedwater contribute to the composition and hence the properties of resultant tube scale. Consequently, for each plant examined in this study, available feedwater impurity data have been compiled. Note that each plant uses all-volatile treatment (AVT) with hydrazine concentrations ranging from about 30 to 130 ppb to control the secondary-side pH. Table III-3 summarizes the available average or typical values of several important impurities for each plant in the study. Values in the top portion of the table reflect concentrations in the final feedwater. Due to the lack of complete data on feedwater concentrations, these values are supplemented in the lower half of the table with additional measurements of blowdown concentrations.

It should be noted that for a given impurity, the relationship between the blowdown concentration and the final feedwater concentration is complex, depending primarily on the specific tendencies of individual species. For a nonvolatile impurity that does not tend to form secondary deposits (e.g., sulfates), most of the incoming mass exits via the blowdown. In this

case, a simple mass balance indicates that the blowdown concentration of this impurity is larger than the final feedwater concentration by approximately the ratio of the flow rates (e.g., a factor of about 50-200, depending on the plant).* However, for volatile impurities, which are likely to exit with the steam (e.g., chlorides), or other species that form secondary deposits (e.g., iron and copper), the blowdown concentration will be closer to the feedwater concentration.

Plant-specific details associated with Table III-3 are provided below.

PLANT A. The iron and copper concentrations in Table III-3 reflect integrated collection sampler measurements made on average about once every 8 to 10 days in the final feedwater. Silicon values represent the average of readings taken for blowdown grab samples from each of the four SGs about once every 1.5 days.† The averaged values are then adjusted by multiplying by the ratio of blowdown flow rate to total feedwater flow rate, which is equivalent to assuming that most of the incoming silicon leaves via blowdown (and therefore does not deposit on tubes). If, on the other hand, 50% of the incoming silicon deposited on tubes (for example), then the listed concentrations would need to be increased by a factor of two. The sodium values listed in Table III-3 reflect a limited set of feedwater measurements—about 200 values recorded during 1986 and one value each during 1993 and 1995.

PLANT B. The iron values listed in Table III-3 are approximate averages based on a utility review of corrosion product sampler measurements. The silicon values reflect only reactive silicon (i.e., ionic Si) detected via spectrophotometer; non-dissociated forms (SiO_2, for example) are not included in the measurements.‡

PLANT C. Feedwater iron and copper concentrations are best estimates made by the utility. The silicon values are blowdown measurements adjusted in the manner discussed above for Plant A. The sodium values are unadjusted blowdown measurements.

---

* Note that there is evidence that in some cases, the blowdown concentration is lower than this method would indicate due to "contamination" with feedwater (i.e., incomplete mixing). This effect may reduce the blowdown concentration by as much as a factor of two.

† Note that some of the values were recorded as "<10 ppb" or "<20 ppb"; these readings were counted as 10 ppb or 20 ppb, respectively, when computing the averages.

‡ Note that silica measurements of concentrations below 5-10 ppb are difficult to make accurately.

PLANT D. Feedwater iron and copper values are averages of measurements taken approximately once every two weeks between 1988 and 1990 (3.5 to 5.4 EFPY). The silicon value is an estimated average of blowdown measurements adjusted as described earlier for Plant A.

PLANT E. The iron and copper concentrations are taken from a deposit-loading study performed for the utility prior to chemical cleaning of the SGs. The silicon values are calculated based on projected silicon mass values present in the SGs and the assumption that most of the incoming silicon is removed through the blowdown (about 99% as with Plant A). If this fraction were significantly different, the listed concentration estimates would consequently need to be adjusted. The sodium, chloride, and sulfate values are average blowdown concentrations for each operating cycle.

GENERIC OPERATING GUIDELINES. In addition to the impurity data discussed above, further insight is provided by the industry guidelines established for secondary water chemistry by EPRI.* References (30) and (31) indicate the main parameters recommended to be controlled in PWR SG feedwater as of 1982 and 1996, respectively. They include the suggested upper limits for power operation shown in the table below. Note that cation conductivity is a measure of the total concentration of soluble anions.

	Suggested Feedwater Concentration Limit		Suggested Blowdown Concentration Limit	
Parameter	1982	1996	1982	1996
Total Iron (ppb)	20	5	–	–
Total Copper (ppb)	2	1	–	–
Sodium (ppb)	3	–	20	5
Chloride (ppb)	–	–	20	10
Silica (ppb)	–	–	300	300*
Cation Conductivity (μmho/cm)	0.2	0.2*	0.8	1

*These quantities are designated as "diagnostic parameters". Values are characterized as typical.

* Citation of these guidelines does not imply that the subject plants always met them. Except as indicated by Table III-3, it is not known how successful each plant has been in meeting the guidelines.

It is noteworthy that no direct control is suggested for other species potentially detrimental to heat transfer (e.g., calcium or phosphorus). Also note that suggested iron and copper concentration limits have decreased significantly.

Average Scale Thickness

Because heat must be conducted (and/or convected) through any secondary deposit, the thickness of the deposit has a direct bearing on its thermal properties. Potentially relevant to the thermal hydraulics of a steam generator are both the average deposit thickness and also the spatial thickness distribution throughout the SG. Estimates of the average scale thickness derived from the following different methods are discussed below:

- Total mass removed through chemical cleaning and sludge lancing
- Projected mass accumulation from feedwater impurity concentration data
- Direct flake measurements, including measurements of deposits on pulled tubes

CHEMICAL CLEANING MASS REMOVALS. Three of the five plants examined in this study implemented full-height chemical cleanings of the SGs within the last three years. Because chemical cleaning removes nearly all of the secondary-side corrosion products (typically over 95%), the total mass removed facilitates a good estimate of the total mass on the tube OD surfaces and hence a good estimate of the average scale thickness. Note, however, that in addition to the total mass removed during the cleaning, the following inputs must also be evaluated in order to compute the average scale thickness:

- The mass remaining in the SGs after the cleaning.
- The mass of corrosion products on the top of the tube sheet known as the "sludge pile." This mass does not contribute to the secondary deposit layers on the tubes.
- The mass of corrosion products accumulated on the tube supports, other structural elements, and the wrapper prior to the cleaning. This total includes the mass of flakes which have spalled from the tube surfaces.
- The reduction in scale-covered heat-transfer area which accompanies spalling. Making this adjustment increases the calculated thickness on the remaining area compared to the assumption that all tube surfaces are uniformly covered.
- The average bulk density of the tube scale.

A summary of the inputs and resulting calculated thicknesses is provided in Table III-4; bases for the inputs and relevant assumptions are discussed below for each plant.

Plant A. According to utility information, a total of 16,837 pounds of magnetite and copper were removed from the four SGs (an average of 4,209 pounds per SG). Following the cleaning, a video inspection of one SG near the top of the tube bundle indicated that essentially all visible deposits were removed from the tube surfaces, the top of a tube support plate, and the broach hole areas. As a result, it is estimated that only 2% of the total corrosion products remained in each SG after the cleaning (less than 100 pounds per SG).

The mass of corrosion products present on the tube sheet prior to the cleaning can be estimated by examining the mass removed during recent prior sludge lancing operations. For Plant A, the sludge lancing in 1993 prior to the chemical cleaning removed an average of 141 pounds per SG (see Table III-5 for details). This value is considered a reasonable estimate of the mass in the sludge pile at the time of the chemical cleaning.

The mass accumulated on each of the tube support plates within the SGs is estimated to be, on average, 10% of the total mass on the tube sheet plus a fraction of the mass of spalled flakes from the tube surfaces.* It is estimated based on the tube support geometry at Plant A (broached-hole plates) and inspection videos at Plant B that two-thirds of the mass of spalled flakes eventually comes to rest on the tube supports.† The 10% value is based on industry experience and inspection videos that indicate much greater accumulation on the tube sheet than on the supports. Possible reasons for this include:

- Secondary velocities through the holes in the support plates are high enough to prevent large, stable accumulations via gravitational settling.
- For feedring units (all of the plants in this study except Plant C), the feedwater enters the SG through the downcomer, allowing the largest impurity particles to settle on the tube sheet before reaching the tube supports.

As indicated in Table III-4, the estimated mass on the supports is about 125 pounds per SG.

Due to the relatively thin deposits at Plant A, the lack of consistent steam pressure transients following plant startups, and a video inspection of one SG prior to chemical cleaning, it is believed that tube scale spalling was very minor (1% or less). Hence, 99% of the tube surface area is assumed to have been scale-covered at the time of the cleaning.

---

* Note that some support plates likely have more mass than others. For example, it is likely that lower support plates are more heavily loaded than upper ones.

† The other one-third of the spalled flakes are believed to have fallen to the tube-sheet surface.

No plant-specific scale density measurements were available for Plant A. For the purpose of estimating scale thickness, a limited industry average value of 3.35 g/cm^3 is used as the best estimate. The resulting best-estimate average scale thickness is computed to be 4.2 mils. Upper- and lower-bound scale thickness calculations are also made based on upper-bound and lower-bound estimates of two key parameters, scale bulk density and percentage of heat-transfer area exposed by spalling. For Plant A, the bounding densities are estimated to be 25% lower and higher, respectively, than the best estimate, and the bounding spalled heat-transfer surface areas are estimated to be 0% and 5%. As shown in Table III-4, the resulting bounding scale thicknesses are calculated to be 3.4 mils and 5.4 mils.

Plant B. The 1995 chemical cleaning at Plant B removed a total of 20,405 pounds of corrosion products, an average of 5,101 pounds per SG. Although no specific information was available regarding the effectiveness of the cleaning, it is estimated that at least 95% of the corrosion products were removed. Thus, a maximum of 255 pounds per SG (on average) is estimated to have remained after the cleaning. Using the sludge lancing history at Plant B prior to the cleaning, an estimated 258 pounds per SG of additional corrosion products were present in the sludge pile immediately prior to the cleaning.

As with Plant A, the amount of deposit material on the tube support surfaces is estimated to be 10% of the tube sheet sludge mass (per support) plus a fraction of the mass of spalled flakes. Based on visual inspections of all four Plant-B SGs in 1993, which revealed widespread spalling of flakes from the tube surfaces, it is estimated that 15% of the tube surface area initially covered by deposits became exposed as a result of spalling prior to the cleaning. Based on the 1993 inspection video and also on the tube support geometry (drilled-hole plates), it is estimated that two-thirds of the spalled flakes remained on the tube support surfaces. Thus, the total calculated mass on the tube support surfaces is about 625 pounds per SG.

In 1990, the Plant-B scale bulk density was measured to be 2.44 g/cm^3. Due to scale ripening, in which porous areas become clogged with additional contaminants, the density in 1995 is likely to have been significantly higher. Consequently, the industry average value (3.35 g/cm^3) is used as a best estimate of the 1995 density. As shown in Table III-4, the resulting best-estimate average scale thickness is 5.9 mils. Upper and lower bounds of ±25% on scale density and bounds of 5% and 25% on the spalled heat-transfer area were used to calculate upper- and lower-bound scale thickness estimates of 7.8 mils and 4.5 mils.

Plant E. Chemical cleaning in late 1996 removed a total of 32,508 pounds of tube deposits and sludge (16,254 pounds per SG). Inspection photographs taken following the cleaning show very clean tubes, suggesting only a minimal amount of residual sludge in the SGs. As with Plant A, this amount is estimated to be 2% of the total removal, or 325 pounds per SG in this case. The sludge lance history at Plant E reveals that about 550 pounds of dry sludge were removed from each SG during the outage prior to the chemical cleaning. Because recent sludge lancing applications are believed to be nearly 100% effective at removing sludge at the top of the tube sheet, this same quantity is estimated to have been present on the tube sheet at the time of the cleaning.

The quantity of deposits present on the tube supports (in this case eggcrates rather than solid plates) is estimated to be 2% of the mass of the tube sheet plus a portion of the mass of spalled flakes rather than the 10% assumed for plants with solid support plates.* Like Plant B, Plant E exhibited large numbers of spalled flakes as documented in pre-cleaning visual inspection reports. Using the same 15% estimate of spalled heat-transfer area as for Plant B, and assuming that only 20% of these flakes remain on the supports,† we compute a total of about 560 pounds per SG on the tube supports.

The Plant-E tube scale bulk density was measured in 1995 to be 3.98 g/cm^3. However, this measurement is judged to be slightly higher than the actual average bulk density for three reasons:

- Only a single sample was used to make the measurement. It is possible that this sample came from the top portion of the bundle where a mechanical cleaning took place. It is believed that enhanced chemical concentration in the U-bend portion of the bundle will generate more consolidated, lower-porosity scale compared to that at lower elevations.
- Numerous flakes taken from the Plant-E SGs at the same time exhibit a layer of very high porosity (enclosed voids). This suggests that the single sample used for the density measurement may have been atypically dense.
- Data from other units in the industry (3.35 g/cm^3 on average) suggest that a lower density is likely.

Consequently, the measured value is lowered by about 10% for a best-estimate density of 3.6 g/cm^3. Table III-4 indicates a resultant best-estimate average scale thickness of 9.3 mils.

---

* The lower value reflects the much lower horizontal surface area associated with lattice supports compared to that associated with solid supports.

† Because Plant E has eggcrate lattice supports rather than solid support plates, it is estimated that fewer of the spalled flakes can accumulate on the supports; most fall to the tube sheet surface.

Upper- and lower-bound density estimates of ±25% and bounding spalled heat-transfer areas of 5% and 25% yield bounding scale thickness estimates of 6.8 mils and 12.9 mils.

FEEDWATER IMPURITY CONCENTRATION HISTORIES. A second method for estimating average deposit thickness consists of integrating impurity concentration histories in order to compute the total quantity of impurities deposited in the SGs. Because secondary deposits are composed predominantly of magnetite, the historical iron concentration is of primary interest. Depending on the plant, the historical copper concentration can also be important, although to a lesser extent. As was done with the chemical cleaning estimates, adjustments must be made for the mass of corrosion products accumulated on the top of the tube sheet and on the tube supports. The basic methodology for calculating the average thickness comprises the following steps:

- Multiply the average feedwater iron concentration for a given period of operation by the average feedwater mass flow rate (per SG) and the effective operating time to yield the mass of iron deposited in each SG. It is assumed for all plants that the quantity of iron removed via blowdown is negligible. While this is not strictly accurate, the iron removed through blowdown is believed to be significantly smaller than the quantity of iron transported during plant transients (i.e., trips and outages) and is thus considered to be part of the uncertainty in the transient factors used for each plant (see next paragraph).

  Note that the Plant-E data are taken from a deposit loading analysis performed for the utility in preparation for chemical cleaning. In this analysis, an explicit factor was used to account for increases in impurity transport to the SGs due to plant transients (startups, trips, power reductions, etc.). This factor is listed in the third row of Table III-6. In the absence of any specific information about transients at the other plants, it is set equal to 1. Exceptions are Plants B and D, which are discussed below.

- Assuming all of the iron is present in the form of magnetite, convert the mass of iron to an equivalent mass of magnetite. This is accomplished by multiplying by the ratio of the atomic mass of magnetite (231.4) to the atomic mass of the constituent iron (167.4). The resulting factor is 1.382.

- Multiply the average copper concentration for the period of operation by the average feedwater mass flow rate (per SG) and the effective operating time, resulting in the mass of copper metal deposited in each SG.

- Based on deposit characterization analyses, estimate the total mass of other corrosion products (aside from iron and copper) using the percentage of the deposit samples which were not composed of iron compounds or copper.

- Estimate the total mass that had historically accumulated on the tube sheet surface by summing historical sludge lancing mass removals during the period of interest (Table III-5). Included in this total is the mass of spalled deposits assumed to have fallen to the tube sheet surface (see bullet below).

- Estimate the total mass of deposits on tube support surfaces using the same method that was used earlier. That is, this mass is estimated to be 10% of the mass in the sludge pile

(per tube support) plus a fraction of the mass of spalled flakes. This method was adjusted in two cases:

  - For Plant B, this method resulted in decreasing scale thicknesses, which is believed to be unrealistic. As a consequence, a fraction of the mass accumulating on the tube supports during one period of operation is assumed to be displaced to the tube sheet by subsequent plant transients. This is consistent with large numbers of spalled flakes falling to the tube sheet during the transients.
  - For Plant E, the tube supports are egg-crate lattices rather than solid plates. As a result, only 2% of the mass in the sludge pile is assumed to collect on each support.

- Estimate the percentage of heat-transfer surface area uncovered by spalling of deposits. For recent periods, this estimate is based on visual inspection data. Earlier values are extrapolations of the later values based on engineering judgment.
- Using estimates or measurements of the average scale density, compute the average scale thickness at the end of the stated operating period.

The results of the calculations are summarized in Table III-6; descriptions of plant-specific inputs and assumptions are discussed below.

Plant A. Utility sources provided feedwater iron concentration measurements taken over the history of operation. As indicated in Table III-6, the data were broken into three major intervals; the first was characterized by an average iron concentration of 11.5 ppb, the second by an average concentration of 8.0 ppb, and the third by an average concentration of 3.2 ppb. The computed mass of copper shown in Table III-6 is based on average concentrations of 1.0 ppb, 0.5 ppb, and 0.02 ppb for the same respective periods.* The mass of other impurities, based on deposit composition analyses and engineering judgment, is estimated to be 15% of the total corrosion-product mass.

The total mass accumulated on the tube sheet over the history of Plant A (per sludge lance records) is shown in Table III-6; as of the chemical cleaning in 1995, this mass was about 370 pounds per SG.† The total mass on tube support surfaces, calculated in the manner discussed earlier, is estimated to be about 280 pounds per SG in 1995.

Using a spalled heat-transfer area of 1% and a scale bulk density of 3.35 g/cm^3 (both per earlier discussion), the best-estimate average scale thickness as of 1995 is 3.9 mils. Using ±25% as

---

* The copper mass calculated using this method is significantly higher than deposit analyses and chemical cleaning mass removals would indicate, perhaps meaning that the early concentration measurements were higher than the actual values.

† Sludge lance masses were adjusted to account for water content since most reported weights reflect wet sludge. The adjustment is based on wet and dry densities measured for Plant E.

bounding estimates of the scale density and 0% and 5% as bounds for spalled heat-transfer area leads to bounding average scale thicknesses of 3.1 mils and 5.0 mils.

Plant B. Utility sources indicated average feedwater iron concentrations of 10 ppb (until 1990), 0.8 ppb (between 1990 and 1993), and 3 ppb (from 1993 until the chemical cleaning in 1995). In addition, the explicit transient factor discussed earlier is varied parametrically in order to achieve two results:

1. Make the ratio of deposits on the tube sheet to the total mass of corrosion products a reasonable value. Setting the transient factor to 1 results in a ratio of tube sheet mass to total deposit mass of over 75%. This is believed to be unrealistically high. Based on the early value used at Plant E, 2.0 is chosen for operation up to 1990. The resulting fraction of deposit mass on the tube sheet is calculated to be 34%.

2. Make the calculated mass of deposits on the tubes increase with operating time. Use of low transient factors for operation after 1990 results in calculated scale thicknesses that decrease. This is also believed to be unrealistic. As a best estimate, the transient factors for operation after 1990 (18 and 4.2) were selected in order to maintain the same ratio of tube sheet deposit mass to total mass (34%). These large factors are consistent with the relatively high number of trips experienced by Plant B (more than 10 per EFPY of operation).

It should be noted that the above assumptions significantly increase the uncertainty of this calculation for Plant B.

Feedwater concentrations of copper at Plant B were unavailable. Instead, the mass of copper transported to each Plant-B SG is assumed to equal that removed via the chemical cleaning. (The mass of copper at earlier dates is estimated by multiplying the total copper removed during the cleaning by the ratio of magnetite calculated for the earlier times to the magnetite calculated to be in each SG at the time of the chemical cleaning.) Based on the data for flakes in Table III-1, about 5% of the total deposit mass is assumed to comprise impurities other than iron and copper (zinc, silicon, etc.).

The total mass historically accumulated on the tube sheet is computed from sludge lance mass removal records (a total of over 2300 pounds per SG).* The total mass on tube support surfaces is calculated using the method outlined earlier; the result is about 920 pounds per SG prior to the chemical cleaning.

---

* Sludge lance masses were adjusted to account for water content. The adjustment is based on wet and dry densities measured for Plant E.

The final Plant-B inputs (a scale bulk density of 3.35 g/cm^3 and a spalled heat-transfer area of 15%) were discussed earlier. The resulting best-estimate average scale thickness is 5.0 mils as indicated in Table III-6. Using bounding values for scale density and spalled heat-transfer area (±25% and 5%/25%, respectively) leads to bounding scale thicknesses of 3.6 mils and 6.3 mils.

Plant C. Utility sources indicated a best-estimate feedwater iron concentration of 12-15 ppb for operation up to 1994. Subsequent operation was characterized by an average concentration of 4-5 ppb per measurements. For all operation, the average feedwater copper concentration was 0.05 ppb. Other impurities are assumed to make up 5% of the total deposit weight based in part on Plant C deposit analyses and in part on industry data.

For Plant C, only one sludge lance value was available (see Table III-5). The total mass on the tube sheet is thus estimated using the rate of accumulation suggested by this value (16 pounds per SG during 0.4 EFPY of operation). The mass on the tube supports is estimated using the previous methodology; in this case, the resulting estimate is slightly less than 200 pounds per SG.

Lastly, the tube scale bulk density is assigned the industry average value of 3.35 g/cm^3, and the spalled heat-transfer area is estimated to be 5%. The resulting calculated average scale thickness as of early 1996 is 2.1 mils. Computing bounds with densities of ±25% and spalled areas of 1% and 15% yields 1.6 mils and 2.7 mils.

Plant D. Feedwater iron and copper concentration measurements made between 1988 and 1990 were reported by the utility for Plant D. Excepting a few very large transients, the iron values averaged 9.2 ppb. A factor of 1.5 is used to account for the observed transients in the data. Values for operation prior to 1988 were not available; a best estimate 25% higher is used since plants have generally lowered iron transport as water chemistry strategies have improved. For operation since 1990, a single value (also 9.2 ppb) reflecting operation in 1994 is used. Note that the calculations associated with these concentrations are considerably uncertain due to the scarcity of data for Plant D.

Feedwater copper concentration measurements were also available for operation between 1988 and 1990. Omitting several large apparent transients results in an average concentration of about 1 ppb. To account for the transients, the average concentration is doubled to 2 ppb. As with

iron, no values prior to 1988 were available; a best estimate of 2.5 ppb is used for that period. A single 1994 value of 0.3 ppb is used for operation since 1990. Based on industry data, other impurities are assumed to comprise 5% of the total corrosion-product mass.

Historical sludge lance results for Plant D, adjusted for water content, indicate that about 265 pounds per SG were present on the tube sheet surface as of June 1995 prior to the most recent sludge lancing. The total mass on tube support surfaces is computed in the same fashion as for Plant B, which also has Model 51 SGs. The result (254 pounds per SG) is shown in Table III-6.

The final inputs for Plant D are the scale bulk density and the spalled heat-transfer area. The best-estimate values used are 3.35 g/cm^3 (industry average) and 2% (based on visual inspection videos which show no appreciable spalling). The resulting best-estimate scale thickness is computed to be 5.9 mils. Using ±25% bounds for scale density and bounds of 1% and 15% for spalled heat-transfer area yields thickness bounds of 4.7 mils and 7.8 mils.

Plant E. The Plant-E calculations are based on a deposit-loading study performed for the utility in preparation for chemical cleaning. The cycle-by-cycle average values for iron feedwater concentration, transient factor, and copper transport mass used in this study are listed in Table III-6.

Historical tube sheet mass loading was available from sludge lance records; the total mass removed over the operating history was over 1700 pounds per SG. Deposit loading on the tube supports (in this case eggcrate lattices) is estimated as described earlier. The calculated mass is about 800 pounds per SG at the time of the chemical cleaning in 1996.

As discussed earlier, the best-estimate scale bulk density (3.6 g/cm^3 based on measurements and deposit characterization information) and spalled heat-transfer area (15%) are the final inputs to the scale thickness calculation for Plant E. The best-estimate result is an average thickness of 9.9 mils. Bounding scale densities of ±25% and spalled heat-transfer areas of 5% and 25% yield bounding average scale thicknesses of 7.3 mils and 13.8 mils.

TUBE FLAKE MEASUREMENTS. A third means of estimating average scale thickness is through direct measurement of scale flakes retrieved from the SGs. Potential problems with using this method to estimate average thickness include the following:

- The sample of flakes used may be too small to be statistically significant and/or may reflect scale from a limited portion of the tube bundle (e.g., the highest elevations) rather than the bundle as a whole. In cases where the tube scale layer is nonuniform throughout the SG, the measured thicknesses could be either higher or lower than the actual average thickness throughout the bundle.
- The flakes may have been altered during the collection process (e.g., sub-layers may have delaminated, causing the measured thickness to be smaller than the actual thickness).

In spite of these cautions, thickness measurements of individual flakes are very accurate, and measurement of many samples can help assure that the resulting average thickness is representative of the tube bundle. Measurements taken for scale samples at Plants A, B, C, E, and F are discussed below.

Plant A. Flakes removed during a 1993 outage varied from 0.9 mils to 6 mils in thickness. Insufficient measurements were available to determine a statistically relevant average thickness based on flake measurements. These two extreme values are consistent with Plant-A low-frequency eddy-current test data that show a predominance of deposit mass on the hot-leg side of the tube bundle and very thin deposits on the cold leg (see later part of this section).

Plant B. Two sets of flakes removed in 1987 (reflecting 2.85 EFPY) averaged 2.0 mils in thickness, with a maximum of 3.0 mils and a minimum of 0.96 mils. One set of flakes removed in 1990 (reflecting 4.02 EFPY) ranged in thickness from 1.6 mils to 3.9 mils, with the greatest number of measurements between 2.0 mils and 2.4 mils (no averages were provided). A second set of flakes removed in 1990 was mounted and measured for this project. The results are indicated below.

SCALE THICKNESS MEASUREMENTS FOR PLANT B (1990)

Flake No.	Observed Thickness Range (mils)	Est. Average Thickness (mils)
1	2.3-2.7	2.6
2	3.5-4.5	4.0
3	4.0-5.5	4.5
4	4.5-5.3	5.0
5	2.3-2.8	2.5

Plant C. Limited information on tube OD deposits at Plant C was provided for tubes pulled from the lower hot-leg side of two out of the four SGs in 1993 (2.96 EFPY). Measurements made by

examining 630X micrographs of metallographic mounts indicate that the average deposit thickness for the four tubes was about 0.3 mils, with a maximum of 1.1 mils.

Plant E. The thicknesses of tube scale flakes from 1995 were evaluated by measuring photographs (12 samples) and also using a ball-end micrometer (35 samples). The results are indicated below.

PLANT E THICKNESS MEASUREMENTS

Quantity (mils)	Photographs	Micrometer
Avg. Thickness	10.9	11.5
Standard Deviation	4.2	2.1
Minimum Thickness	7.4	7.0
Maximum Thickness	18.8	14.5

Plant F. According to Reference (1), five tube scale samples from the U-bend region of a single tube were measured in five locations each by examining photomicrographs at magnifications up to 1500X. The overall average of the measurements was 8.7 mils in total thickness. This average thickness reflected operation until the time the tube was pulled from the SG in 1991 after 15.6 EFPY of operation.

OVERALL BEST-ESTIMATE AVERAGE THICKNESSES. The three methods described above are used to make overall best estimates of the average scale thickness throughout the tube bundle of each unit in the study. The results are summarized in Table III-7. For each plant, the best estimates were made as described below:

- Plant A: The chemical cleaning and feedwater estimates were used to make the overall best estimate.
- Plant B: At the time of the chemical cleaning, both the cleaning and feedwater transport estimates were considered. Due to the uncertainty associated with the latter, more weight was given to the cleaning estimate. Estimates of the average thickness at earlier points in Plant B's life are based both on the feedwater transport estimates and on flake measurements.
- Plant C: Flake measurements from pulled tubes are believed to provide the most reliable estimate of scale thickness.* The feedwater transport estimate was given a lesser weight.†

* Note, however, that deposits can be damaged during tube pull operations, potentially affecting any scale thickness measurements.

† The sludge lancing history at Plant C was incomplete. If a significant quantity of sludge was removed from the Plant-C SGs via lancing, then the scale-thickness estimate based on feedwater transport is too high.

- Plant D: The best estimate is based only on the feedwater transport data; this estimate is consequently more uncertain than that for most of the other plants as indicated in Table III-7.
- Plant E: All three types of estimate were considered.
- Plant F: Only the flake thickness measurements in Reference (1) were available for this unit, making the best estimate somewhat uncertain.

These average thickness estimates are used in conjunction with deposit distribution data to generate input for some of the ATHOS thermal-hydraulic analyses discussed in Section VI.

Scale Thickness Distribution

In addition to the average thickness of a secondary deposit layer, the manner in which the deposits are distributed throughout the SG tube bundle has an impact on overall heat transfer (e.g., thicker deposits at higher elevations). Methods that can be used for evaluating scale thickness distribution include

- LOW-FREQUENCY EDDY-CURRENT TEST (ECT) PROFILES. Non-destructive evaluations using low-frequency eddy-current probes can provide a quantitative evaluation of magnetite mass distribution per unit length of the tube(s) examined. Based on discussions with one of the developers of the technique, the accuracy of this form of sludge profiling is about ±15%. Each profile must be combined with an estimate of scale density in order to generate a scale thickness profile. It is important to note that few or no data exist regarding the variation of scale density throughout the tube bundle. As a consequence, the simplest assumption—constant scale density—is assumed when evaluating ECT profiles in this study.
- VISUAL INSPECTIONS. To a limited extent, these inspections can reveal areas of greater deposit loading in the tube bundle, particularly if spalling has taken place and flakes are abundant. It should be noted that estimates of deposit distribution based on visual inspections are qualitative or semi-quantitative.
- DIRECT FLAKE MEASUREMENT. If tube scale flakes from different known locations within the bundle are available for measurement, then an estimate of the scale distribution can be made. Unfortunately, flakes are usually collected during sludge lancing operations; as a result, the original location of the flakes is unknown. No significant data of this type are available for any of the plants in this study.

Available scale distribution data of the first two types are discussed below.

LOW-FREQUENCY ECT PROFILES. During the last decade a number of plants had low-frequency ECT profiles generated for some of their SG tubes in order to aid in evaluating deposit loading. For this project, the following such profiles were available:

SG Model	Plant	No. Tubes
Model F	A	10
	A1	16
	A2	7
Model 51/51F	B	1
	B1*	10
	B2	1
	B3	1
CE Model 80	G	3

The above-listed profiles were digitized electronically by scanning hard copies and tracing the prominent features using a CAD program. The results are shown in Figures III-5 through III-10. To the right of each profile, the tube location within the SG is listed as designated by row and column. Note that although each tube forms a U shape, the profiles are stretched into straight lines. Each of the vertical lines drawn on the profiles represents a tube support elevation (e.g., 1H is the first hot-leg tube support, 7C is the seventh cold-leg tube support, etc.). The portion in the middle of each profile (e.g., between 7C and 7H on Figure III-5) represents the U-bend region.

The circumferential/radial locations of the tubes profiled are depicted graphically in Figures III-11 and III-12. In the former, all Model F tubes are shown. Note that the figure represents half of an SG (either the hot-leg or the cold leg); the full length of each tube was profiled, including the symmetric half not shown. It is clear from Figure III-11 that a reasonable overall sampling of the tubes in Model F SGs is available; only tubes in very low and very high column locations are not represented. The sampling of Model 51 tubes indicated in Figure III-12 is less complete: no tubes with high column numbers were profiled, and only a single tube near the center of the bundle was chosen.

Noteworthy features of the profiles in Figures III-5 through III-10 include

1. Without exception, the hot-leg sides of all tubes showed greater scale mass accumulation than the corresponding cold-leg sides.

2. The Model F profiles exhibited approximately two to three times as much deposit loading on the hot leg as on the corresponding cold leg. (In most cases, a sharp change

* Sister unit of Plant B (same station).

in deposit loading occurs in the U-bend region.) This trend is specifically applicable to the 10 Plant-A profiles.

3. The Model 51 profiles exhibit an almost linear tube scale profile with the largest accumulations on the hot-leg side. There is generally not a sharp transition in loading in the U-bend region. The profiles applicable to Plant B and its sister station exhibit both of these characteristics.

4. The only CE plant for which profiles were available (a preheater unit) exhibited heavy deposits at low elevations on both the hot leg and cold leg sides and to a lesser extent in the U-bend region. Less deposit loading was observed at high elevations on both sides.

VISUAL INSPECTIONS. Video inspections of the tube bundles at Plants B, D, and E were made available for this project. In addition, written reports discussing visual inspections were provided for Plant E.

Plant B. A series of visual inspections made during 1993 (6.25 EFPY) revealed that Plant-B scale has a tendency to spall frequently, creating numerous flakes on the tube support plate surfaces and the tube sheet. Although it is impractical to determine the magnitude of scale thickness from the videotape, some idea of deposit distribution is indicated by the location and quantity of the spalled flakes. From several videotapes taken inside each of the four SGs at Plant B, it was apparent that spalled flakes were more numerous on the hot-leg side and at lower elevations. Spalling is caused by the difference in thermal expansion coefficient for the tube and for the deposit material combined with temperature transients. It is thus more likely that thicker flakes (which develop greater temperature differences across the thickness and which are less compliant than thin flakes) will spall more readily than thinner flakes. It can thus be concluded that the hot-leg side was loaded with generally thicker deposits than the cold-leg side.* This conclusion is consistent with the low-frequency ECT profiles obtained for Model 51 SGs (including Plant B and its sister station).

Plant D. A visual inspection of the Plant-D SGs was conducted in early 1996 during the most recent outage. This inspection covered all support-plate elevations (the first through the seventh) and portions of the tube free spans from the viewpoint of the flow slots, which are located between the hot leg and the cold leg. Consequently, most of the tubes viewed are Row-1 tubes, which have the smallest radius U-bends. The video indicated an apparently uniform layer of orange-brown scale covering both the tubes and the support plates. No significant variation in

* It is not necessarily true that greater numbers of spalled flakes at lower elevations indicate thicker deposits there—spalled deposits from higher elevations could easily fall to lower tube support elevations or even to the tube sheet surface.

scale appearance could be discerned over the height of the SG, including the U-bend region. No evidence of spalling—bare patches on the tubes or loose flakes on tube support surfaces—could be seen.

Plant E. A visual inspection of the Plant-E SGs was performed prior to the chemical cleaning in 1996. The inspection covered mainly peripheral tubes in the U-bend region and the upper tube support elevations (seventh to tenth). Deposits in the U-bend region appeared to be a dark orange or brown in color and uniform in thickness.* No difference could be seen between the hot-leg and cold-leg sides of the U-bends. Spalling of tube deposits was minor in the vicinity of the ninth and tenth tube supports; however, much larger numbers of spalled flakes were observed near the seventh and eighth supports, possibly suggesting thicker deposits at lower elevations.

COMPOSITE SCALE DISTRIBUTIONS. The scale mass distributions described by the data presented above are used to generate several composite mass distributions relevant to the plants examined in this study. The procedure employed to compute the mass distribution on particular tubes is as follows:

- Discretize the graphical ECT profiles shown in Figures III-5 through III-10 by breaking each into piecewise-constant segments between each pair of tube supports. For example, for tube R26C64 (see Figure III-5), the tube span between the tube sheet and the first tube support plate on the cold-leg side was measured to have an average scale mass per unit length of 0.01 units, and the tube span immediately above it was measured to have an average mass per unit length of 0.03 units.†
- Using the relative mass per unit length, calculate the total mass for each portion of tube length. Since tube supports are approximately the same distance apart, the only adjustment required is for the U-bends, which vary in length depending on the tube location within the bundle. The adjustment is made by scaling the mass per unit length by the ratio of the U-bend length to the typical distance between tube supports.
- Convert the total mass to a fraction of total deposit loading present within a specific region (e.g., 5% of the total deposit mass on tube R10C20 is located between the third and fourth tube support elevations on the cold-leg side). These fractions are combined with the average thickness discussed earlier in this section to calculate thickness distributions used in Section VI to evaluate the effect of spatial variations in thermal resistance on SG thermal performance.

The composite distributions used for Plants A through F are discussed below.

---

* An additional inspection of the U-bend portions of tubes in the interior of the bundle sometimes revealed deposits having a nonuniform thickness.

† Note that the actual units are unimportant; ECT profiles provide only relative mass per unit length. The magnitude of the thickness must be determined by also considering the average scale thickness for the SG (see the earlier part of Section III).

Model F. A total of 33 ECT profiles from Model-F tubes were examined. Based on the similarity of the profiles from plant to plant and also from tube to tube within a single SG, it was judged appropriate to compute a single relative mass distribution based on all of these profiles. This composite profile was computed in the following manner:

- The discretization scheme used to apply scale thicknesses to ATHOS models involves a total of 30 regions (five axial regions (including the U-bend area), three radial regions, and a split between the hot leg and the cold leg).* As a result, the Model F tubes are split into three groups based on radial location. Specifically, regions of equal area were drawn on the tube cross section map in Figure III-11 using concentric circles; tubes within the innermost circle are grouped together, tubes in the middle circle are grouped together, and tubes in the peripheral circle are grouped together.
- The average relative total mass for each tube free span between supports (and in the U-bend region) is calculated for each grouping of tubes.
- For each tube, the total mass for each axial region is converted to a fraction of total mass by dividing by the total mass in all axial regions.
- Based on the number of tube support locations (e.g., eight for the Plant A1 tubes in Figure III-6), the mass is distributed axially into four regions on both the hot-leg and cold-leg sides. For example, the mass fraction located on the hot leg between the tube sheet and the first support and the mass fraction located between the first and second supports are added together, resulting in the mass fraction for the first hot-leg axial region.

The results are shown in the left portion of Table III-8 and graphically in Figure III-13. Note that the fraction of deposit mass in the U-bend region increases toward the periphery of the bundle (e.g., Radial Region 3 versus Radial Region 1) because the U-bends are longer for the peripheral tubes profiled (see Figure III-11).

Model 51. A total of 11 profiles from Model 51 SGs were used to calculate a composite scale mass distribution for the outermost radial region in the same manner described for the Model F distribution. However, since only two profiles were available for tubes in the innermost radial regions (see Figure III-12), estimated mass distributions for these regions were computed by assuming that the average scale masses on the inner tubes are the same as the average masses on the outer tubes.† The resulting mass distribution is shown numerically in Table III-8 and pictorially in Figure III-14. Note that there is less mass concentrated in the U-bend region compared to the Model-F distribution. This distribution is applicable to Plants B and D.

---

* These regions are illustrated in a sketch below Table III-8. See Section VI for greater detail.

† The masses applied to the U-bend segments of the inner tubes were adjusted to account for the differences in average U-bend length.

Preheater. No ECT profiles for Plant C (with preheater SGs) were available. However, profiles for three tubes in the preheater SGs at another plant were supplied for this project. Because the preheater significantly alters the thermal-hydraulics within the SG, it was judged most appropriate to use the profiles for these tubes as the basis for postulating a tube scale mass distribution at Plant C.* The mass distribution was determined in the same fashion as the Model-51 distributions, including the adjustment for U-bend length. (All three tubes were located in the outermost radial region and had relatively long U-bends.) The resulting distribution, shown in Figure III-15, shows large concentrations of tube scale at low elevations in the bundle. Note that no ATHOS analyses using this distribution were performed due to the thin deposits and low level of SG thermal performance degradation exhibited by Plant C.

Hybrid Composite. Other than inconclusive visual inspections, no information directly applicable to the Plant-E scale mass distribution was available. As a consequence, the average of the Model-F and Model-51 distributions is judged applicable to Plant E. This average distribution, shown in Figure III-16, does not differ markedly from the two distributions used to compute it.

Independent Estimates of Deposit Thermal Resistance

Based on the composition, structure, and thickness data presented in this section, estimates of deposit thermal resistance are calculated and presented in Table III-9 for Plants A through F. In this table, each plant scale is divided into up to three layers of different morphology: an inner consolidated layer transferring heat by conduction alone, a middle layer transferring heat also by conduction, and an outer layer transferring heat by a combination of conduction and convection. The thermal resistances of conduction layers are calculated using composition information and Bruggeman's Equation (see Appendix E), and the thermal resistances of outer porous layers are estimated based on morphological data, cross-section photos, industry and laboratory data, and engineering judgment.

Note that the Table III-9 estimates are independent of the global fouling analyses presented in Section IV. From Table III-9 it is clear that scale layers from Plants A through D are predicted to be mildly enhancing (Plant A before chemical cleaning) to moderately resistive (Plants B and D) to heat transfer. Plants E and F are both calculated to be highly resistive, with best-estimate

* In addition, due to the low overall deposit loading at Plant C, the scale mass distribution is not critical for determining the impact on SG heat transfer.

fouling factors near 200 10^{-6} h-ft^2-°F/BTU. It is noteworthy that all of the estimates are marked by considerable uncertainty as reflected by the upper- and lower-bound calculations also shown in Table III-9.

Table III-10 shows the approximate steam pressure losses that correspond to the secondary deposit fouling factors estimated in Table III-9. The steam pressure sensitivity values needed for this calculation are those computed and reported in Appendix D (Tables D-1 through D-5).

Table III-1. Chemical Composition of Powder and Scale Samples[1]
(Page 1 of 2)

Unit		Plant A					Plant B				
Date/Plant Age (EFPY)		1993/7.33					1990/4.02		1992/5.25	1993/6.25	
Test Type		ICPS		XRD			XRF		ICPS & XRF	ICPS & XRF[6]	
Element	Compound[2]	Powder[4]	Flakes	Powder	Flakes (OD)	Flakes (ID)	Bulk Sludge	Flakes	Powder & Flakes[5]	Bulk Sludge	Flakes
Fe	Fe_3O_4 (magnetite)	96.7	56.0	49.0	30.0	53.0	72.5	76.8	82.9	95.5	79.3
Fe	Fe_2O_3 (maghemite)	–	–	33.3	18.0	15.0	–	–	–	–	–
Fe	Fe_2O_3 (hematite)	–	–	–	–	–	–	–	–	–	–
Fe	Unidentified Oxide	–	–	17.5	–	–	–	–	–	–	–
Ni	NiO	0.7	1.1	–	–	–	2.0	1.8	–	1.6	2.6
Cu	Cu	0.2	1.9	–	–	–	21.0	20.3	10.0	8.6	17.7
Mn	MnO	0.2	2.5	–	–	–	1.0	1.8	–	0.4	2.0
Cr	Cr_2O_3	0.2	0.6	–	–	–	–	–	–	–	–
Si	SiO_2	–	6.3	–	–	–	3.5	0.0	–	0.5	0.7
Ca	CaO	–	6.7	–	–	–	–	–	–	–	–
Al	Al_2O_3	–	6.1	–	–	–	–	–	–	–	–
P	P_2O_5	–	5.1	–	–	–	–	–	–	–	–
Nb	Nb_2O_5	–	9.0	–	–	–	–	–	–	–	–
Zn	ZnO	–	–	–	–	–	–	–	–	–	–
Cd	CdO	–	–	–	–	–	–	–	–	–	–
Ti	TiO_2	–	–	–	–	–	–	–	–	–	–
Zr	ZrO_2	–	–	–	–	–	–	–	–	–	–
Mg	MgO	–	–	–	–	–	–	–	–	–	–
Sn	SnO_2	–	–	–	–	–	–	–	–	–	–
Co	Co_2O_3	–	–	–	–	–	–	–	–	–	–
Mo	MoO_3	–	–	–	–	–	–	–	–	–	–
S	SO_2	–	–	–	–	–	–	–	–	–	–
C	C	–	–	–	–	–	–	–	–	–	–
Ca, P	Calcium Hydroxyapatite $Ca_{10}(PO_4)_6(OH)_2$	–	–	–	–	–	–	–	–	–	–
Al	Boehmite AlO(OH)	–	–	–	24.0	21.0	–	–	–	–	–
Ca, Al, Si	Bicchulite $Ca_2Al_2SiO_6(OH)_2$	–	–	–	12.0	–	–	–	–	–	–
Ca, P	Calcium Phosphate CaP_2O_6	–	–	–	8.0	–	–	–	–	–	–
,	Unidentified Compound	–	–	–	8.0	11.0	–	–	–	–	–

KEY:

ICPS Inductively Coupled Plasma Spectrophotometry
ND Not Detected
NM Not Measured
XRD X-Ray Diffraction
XRF X-Ray Fluorescence
– Not measured, not detected, or not available

NOTES:

1. Values are weight percents of the listed compound.
2. For ICPS and XRF tests, this is assumed to be the primary form in which the element is found. XRD identifies the compound.
3. Weight percents from XRF analysis have been converted to weight percent of oxide. Compounds identified with XRD.
4. Reflects the average of four samples taken from three of the four SGs.
5. Several constituents were present in quantities of 1% or less.
6. The values shown are averages for samples taken from each of the four SGs.

Table III-1. Chemical Composition of Powder and Scale Samples[1]
(Page 2 of 2)

Unit		Plant D Sister Unit	Plant E				Plant F
Date/Plant Age (EFPY)		1989/6.88	1991/5.72		1995/8.63		1991/15.63
Test Type		ICPS	ICPS				XRF & XRD[3]
Element	Compound[2]	75% Powder 25% Flakes	Powder	Scale	Powder	Scale	Powder & Flakes
Fe	Fe_3O_4 (magnetite)	88.6	88.6	82.6	87.1	90.3	53.9
Fe	Fe_2O_3 (maghemite)	–	–	–	–	–	–
Fe	Fe_2O_3 (hematite)	–	–	–	–	–	trace
Fe	Unidentified Oxide	–	–	–	–	–	–
Ni	NiO	0.1	0.8	0.9	0.8	0.5	2.7
Cu	Cu	8.4	10.5	13.2	9.1	5.6	11.1
Mn	MnO	0.9	0.5	0.7	0.4	0.4	0.9
Cr	Cr_2O_3	0.3	0.2	0.0	0.1	0.1	trace
Si	SiO_2	0.4	0.3	0.0	NM	0.3	–
Ca	CaO	0.3	0.0	0.0	0.0	0.4	–
Al	Al_2O_3	0.2	0.1	0.1	NM	0.1	–
P	P_2O_5	–	0.1	0.2	0.1	0.1	–
Nb	Nb_2O_5	–	–	–	–	–	–
Zn	ZnO	0.3	4.6	7.3	2.2	2.4	2.9
Cd	CdO	0.0	0.0	NM	NM	ND	–
Ti	TiO_2	0.3	0.1	0.0	0.1	0.0	–
Zr	ZrO_2	–	0.0	0.0	0.0	ND	–
Mg	MgO	0.1	0.0	0.0	0.0	0.0	–
Sn	SnO_2	–	0.1	0.2	0.1	ND	–
Co	Co_2O_3	0.1	0.0	0.0	0.0	0.0	–
Mo	MoO_3	0.1	0.0	0.0	0.0	0.1	trace
S	SO_2	–	0.0	0.0	0.0	0.0	–
C	C	–	0.3	0.2	0.3	NM	–
Ca, P	Calcium Hydroxyapatite $Ca_{10}(PO_4)_6(OH)_2$	–	–	–	–	–	16.4
Al	Boehmite AlO(OH)	–	–	–	–	–	–
Ca, Al, Si	Bicchulite $Ca_2Al_2SiO_6(OH)_2$	–	–	–	–	–	–
Ca, P	Calcium Phosphate CaP_2O_6	–	–	–	–	–	–
	Unidentified Compound	–	–	–	–	–	–

KEY:

ICPS Inductively Coupled Plasma Spectrophotometry
ND Not Detected
NM Not Measured
XRD X-Ray Diffraction
XRF X-Ray Fluorescence
– Not measured, not detected, or not available

NOTES:

1. Values are weight percents of the listed compound.
2. For ICPS and XRF tests, this is assumed to be the primary form in which the element is found. XRD identifies the compound.
3. Weight percents from XRF analysis have been converted to weight percent of oxide. Compounds identified with XRD.
4. Reflects the average of four samples taken from three of the four SGs.
5. Several constituents were present in quantities of 1% or less.
6. The values shown are averages for samples taken from each of the four SGs.

Table III-2. Selected Tube Scale Morphology Parameters

Parameter	Plant			
	B	D*	E	F
Date	1990	1989	1995	1991
Plant Age (EFPY)	4.02	6.88	8.63	15.63
Skeletal density (g/cm^3)	5.41	5.38	5.14	5.03
Bulk density (g/cm^3)	2.44	3.57	3.98	4.61**
Total porosity	55%	34%	22%	9%
Range of pore sizes (microns)	0.04-4.0	0.02-100	0.003-122	NA
Avg. Pore Size (microns)	0.45	0.36	0.10	NA
Predominant Particle Size (microns)	20-40	4-15	NA	NA
Weight % of Particles >150 microns	90	94	NA	NA
Specific surface area (m^2/g)	1.24	0.99	0.34	NA

NA = Not Currently Available

*Data provided for Plant D's sister unit.

**Calculated from skeletal density and total porosity.

Table III-3. Plant Feedwater Impurity Ingress Data (ppb)[1,6,7]

Unit	Plant A			Plant B			Plant C				Plant D	Plant E						
Age (EFPY)	<4.5	<6.8	<8.6	<4.5	<6.2	<7.9	<3.0	<3.4	<4.3	<4.7	3.5-5.4	<1.0	<1.7	<2.8	<4.3	<5.7	<7.2	<8.6	<10.1
Impurity	Feedwater Concentrations																		
Iron (Fe)	11.5	8.0	3.2	10	0.8	3	13.5		4.5		9.2	28	30	10	10	12	7	6	6
Copper (Cu)	0.8	0.4	0.03	–	–	–	<0.05				2.0	9.9	1.0	2.2	0.5	0.2	0.3	2.4	2.4
Silicon (Si)[2]	*0.5*	*0.4*	*0.8*	<5	<5	<5	*1.7*		*0.7*		*0.15*	*15.2*	*16.3*	*10.4*	*5.4*	*7.1*	*4.1*	*4.6*	*4.7*
Impurity	Blowdown Concentrations																		
Sodium (Na)[3,4,5]	*0.5*	*0.1*	*0.1*	2.5	2	1.2	2.0		<0.8		<0.3	–	30.0	6.1	2.2	1.2	0.3	0.3	0.2	0.0
Chloride (Cl)[5]	–	–	–	–	–	–	–	–	–	–	–	59.6	11.1	3.0	1.7	0.5	0.4	0.2	0.3
Sulfate (SO_4^{2-})[5]	–	–	–	–	–	–	–	–	–	–	–	29.4	14.7	2.2	0.5	0.1	0.4	0.1	0.1

NOTES

1. Each value in the table represents an average for operation between the previous plant age and the listed plant age. For example, Plant E's iron concentration averaged 30 ppb from 1.0 EFPY up to 1.7 EPFY.
2. Values for Plants A, C, and D are based on concentrations in the SG blowdown that have been adjusted to reflect approximate FW values. The values for Plant B reflect only ionic silicon in the feedwater, and the values for Plant E reflect estimated feedwater concentrations based on utility sludge mass projections prior to chemical cleaning.
3. The "0.5" value for Plant A reflects operation during 1986 only, and the "0.1" values are based on single readings.
4. Plant-C values reflect SG blowdown, which has averaged about 0.9% of the total FW flow over plant life. The concentration in the FW is likely to have been significantly lower.
5. Plant-E values are believed to reflect the SG blowdown, which has averaged 0.5% of total FW flow over the life of Plant E. The concentration in the FW is likely to have been significantly lower.
6. "–" indicates this value not available.
7. Values in italics are estimates.

Table III-4. Average Tube Scale Thickness Estimates Based on Chemical Cleaning Mass Removal

Unit	Plant A					Plant B					Plant E		
Date	March 1995					September 1995					December 1996		
Operating Age	8.63 EFPY					7.49 EFPY					10.1 EFPY		
Quantity (lb)	SG 1	SG 2	SG 3	SG 4	Avg.	SG 1	SG 2	SG 3	SG 4	Avg.	SG 1	SG 2	Avg.
Total Magnetite[1]	4228	4019	4859	3621	4182	4520	4634	4059	4652	4466	13746	13536	13641
Total Copper[1]	26	31	31	21	27	635	622	618	664	635	1578	1634	1606
Other Constituents[2]	0	0	0	0	0	0	0	0	0	0	1027	987	1007
Total Mass Removed by CC	4254	4050	4890	3642	4209	5156	5256	4678	5316	5101	16351	16157	16254
Est. Mass Remaining After CC	85	81	98	73	84	258	263	234	266	255	327	323	325
Total Deposit Mass in SGs Before CC	4340	4131	4988	3714	4293	5414	5519	4911	5581	5356	16678	16480	16579
Est. Mass on TS Before CC	141	141	141	141	141	258	258	258	258	258	550	550	550
Est. Mass on Support Plate Surfaces	126	124	130	122	126	633	642	587	648	628	566	560	563
Deposit Mass on Tube Surfaces	4073	3866	4717	3452	4027	4523	4618	4066	4675	4471	15562	15370	15466
Est. Percentage of Spalled HT Area[3]	1%	1%	1%	1%	1%	15%	15%	15%	15%	15%	15%	15%	15%
Calculated Scale Thickness (mils)													
Lower Bound[4]	3.4	3.2	4.0	2.9	3.4	4.5	4.6	4.1	4.7	4.5	6.8	6.7	6.8
Best Estimate	4.3	4.1	5.0	3.6	4.2	5.9	6.1	5.3	6.1	5.9	9.3	9.2	9.3
Upper Bound[4]	5.4	5.2	6.3	4.6	5.4	7.9	8.1	7.1	8.2	7.8	13.0	12.8	12.9

NOTES

1. Includes mass from sludge lancing. Note that sludge lance masses are assumed to represent wet sludge; an adjustment was made to reflect dry sludge.
2. Other constituents are assumed to be included in the magnetite total for Plants A and B. The quantities are believed to be small (i.e., less than 10%).
3. Reflects spalling of deposits from tube surfaces. Visual inspections at both Plants B and E revealed widespread spalling.
4. Lower and upper bounds are calculated using bounding estimates of scale bulk density and spalled heat-transfer area.

Table III-5. Sludge Lance Mass Removals[1]

Plant A			Plant B			Plant C			Plant D			Plant E		
Outage Date	Approx. EFPY	Avg. Removal per SG (lb)	Outage Date	Approx. EFPY	Avg. Removal per SG (lb)	Outage Date	Approx. EFPY	Avg. Removal per SG	Outage Date	Approx. EFPY	Avg. Removal per SG (lb)	Outage Date	Approx. EFPY	Avg. Removal per SG (lb)
2/86	1.1	8	9/81	0.3	193	9/89	0.8	NA[2]	1/83	1.2	77	10/84	0.8	0
4/87	1.9	8	9/82	1.1	259	3/90	1.2	NA[2]	10/84	1.6	15	4/86	1.0	0
9/87	2.2	0	9/83	1.7	270	11/90	1.6	16	10/86	2.7	18	9/87	2.8	72
3/89	3.5	12	2/84	1.9	177	9/92	2.9	NA[2]	9/88	4.0	38	8/89	4.3	140
9/90	4.7	11	8/85	2.9	304	2/93	3.0	NA[2]	3/90	5.0	32	8/91	5.7	200
3/92	6.0	46	3/90	4.0	324	3/95	3.9	NA[2]	11/91	6.1	34	6/93	7.2	241
10/93	7.3	141	10/91	5.3	285	5/96	5.0	NA[2]	3/93	6.8	32	2/95	8.6	550
3/95	8.6	447	4/93	6.3	258				10/94	7.8	NA[2]	12/96	10.1	3619
10/96	10.0	12	9/95	7.5	618				6/95	8.0	19			

NOTES

1. Values are adjusted to reflect dry sludge rather than wet sludge using typical values from Plant E (1.50 g/cm^3 for dry sludge and 2.16 g/cm^3 for wet sludge).
2. This value not available.

Table III-6. Average Tube Scale Thickness Estimates Based on Historical Feedwater Transport Data

Unit	Plant A			Plant B			Plant C		Plant D			Plant E							
Date	7/90	3/93	3/95	9/90	2/93	9/95	8/94	1/96	1/88	12/90	6/95	10/84	4/86	9/87	8/89	8/91	6/93	2/95	12/96
Operating Age (EFPY)	4.5	6.8	8.6	4.5	6.2	7.5	3.4	4.7	3.4	5.4	8.0	1.0	1.7	2.8	4.3	5.7	7.2	8.6	10.1
Average FW Iron Concentration (ppb)	11.5	8.0	3.2	10	0.8	3	13.5	4.5	*12*	9.2	9.2	28	30	10	10	12	7	6	6
Average Feedwater Flow Rate (10^6 lb/h)	3.827	3.937	3.941	3.712	3.754	3.762	4.263	4.270	3.692	3.704	3.768	7.452	7.530	7.558	7.503	7.489	7.476	7.370	7.360
Factor Accounting for Transients[1]	1.0	1.0	1.0	2.0	*18.0*	*4.2*	1.0	1.0	1.5	1.5	1.0	2.0	1.5	1.3	1.3	1.2	1.2	1.1	1.1
Cum. Mass of Fe Transported to each SG (lb)	1735	2356	2560	2927	3732	4267	1689	1908	1919	2774	3588	3667	5831	6790	8042	9370	10163	10790	11411
Cum. Mass of Magnetite in each SG (lb)	2398	3256	3539	4045	5158	5899	2335	2637	2653	3835	4960	5068	8060	9386	11117	12953	14048	14915	15774
Est. Cum. Mass of Copper in each SG (lb)	151	190	191	435	555	635	6	9	278	402	429	1296	1369	1580	1642	1664	1698	1949	2198
Est. Cum. Mass of Other Impurities per SG (lb)	450	608	658	236	301	344	123	139	154	223	284	414	613	713	829	950	1024	1096	1168
Est. Cum. Total Deposit Mass in each SG (lb)	2999	4054	4388	4717	6014	6878	2464	2785	3085	4460	5672	6779	10041	11679	13588	15567	16770	17960	19139
Total Mass Accumulated on TS per SG (lb)	39	173	367	1584	2034	2328	134	186	130	192	265	0	0	72	212	412	653	1203	1753
Total Mass on Support Plates per SG (lb)	47	146	282	475	648	730	150	246	110	162	254	14	20	128	170	370	431	698	813
Deposit Mass on Tube Surfaces per SG (lb)	2913	3734	3739	2658	3332	3819	2180	2353	2845	4107	5154	6765	10021	11479	13206	14785	15686	16059	16574
Est. Percentage of Spalled HT Area[2]	1%	1%	1%	7%	10%	15%	2%	5%	1%	1%	2%	1%	1%	5%	5%	10%	10%	15%	15%
Calculated Scale Thickness (mils)																			
Lower Bound[3]	2.4	3.1	3.1	3.2	3.5	3.6	1.5	1.6	2.6	3.7	4.7	2.8	4.1	4.7	5.4	6.3	6.7	7.0	7.3
Best Estimate	3.1	3.9	3.9	4.4	4.7	5.0	1.9	2.1	3.2	4.6	5.9	3.5	5.2	6.2	7.1	8.4	8.9	9.6	9.9
Upper Bound[3]	3.9	5.0	5.0	5.4	5.9	6.3	2.5	2.7	4.2	6.0	7.8	4.5	6.7	8.1	9.3	11.6	12.3	13.4	13.8

NOTES

1. For the last two columns under "Plant B," this factor is used as a parameter to keep the ratio of tube sheet deposit mass to total deposit mass constant. See text for details.
2. Reflects spalling of deposits from tube surfaces. Average scale thicknesses are calculated for the remaining surface area.
3. Lower and upper bounds are calculated using bounding estimates of scale bulk density and spalled heat-transfer area.

Table III-7. Summary of Overall Best-Estimate Average Scale Thicknesses (in mils)

Unit	Plant A	Plant B			Plant C	Plant D	Plant E								Plant F
Year	1995	1987	1990	1995	1993	1995	1984	1986	1987	1989	1991	1993	1995	1996	1991
Operating Time (EFPY)	8.6	2.9	4.0	7.5	3.0	8.0	1.0	1.7	2.8	4.3	5.7	7.2	8.6	10.1	15.6
Chemical Cleaning Removal	4.2	–	–	5.9	–	–	–	–	–	–	–	–	–	9.3	–
Feedwater Transport History	3.9	2.8	3.9	5.0	1.7	5.9	3.5	5.2	6.2	7.1	8.4	8.9	9.6	9.9	–
Direct Flake Measurement	–	2.0	3.7	–	0.3	–	–	–	–	–	–	–	11.3	–	8.7
Overall Best Estimate	**4.1**	**2.4**	**3.8**	**5.7**	**0.7**	**5.9**	**3.5**	**5.2**	**6.2**	**7.1**	**8.4**	**8.9**	**10.1**	**10.4**	**8.7**
Best-Estimate Tolerance	±0.5	±0.5	±1.0	±1.0	±0.5	±2.0	±1.5	±1.5	±1.5	±1.5	±1.5	±1.5	±1.0	±1.0	±2.5
Est. Upper Bound	4.6	2.9	4.8	6.7	1.2	7.9	5.0	6.7	7.7	8.6	9.9	10.4	11.1	11.4	11.2
Est. Lower Bound	3.6	1.9	2.8	4.7	0.2	3.9	2.0	3.7	4.7	5.6	6.9	7.4	9.1	9.4	6.2

Table III-8. Composite Tube Scale Distributions Based on Low-Frequency ECT Profiles*

Region	Model F (Plant A)			Model 51 (Plants B and D)			Preheater Profile (Plant C)			Overall (Plant E)		
	Radial 1	Radial 2	Radial 3	Radial 1	Radial 2	Radial 3	Radial 1	Radial 2	Radial 3	Radial 1	Radial 2	Radial 3
Cold Axial 1	0.029	0.018	0.016	0.047	0.042	0.041	0.060	0.053	0.052	0.038	0.030	0.028
Cold Axial 2	0.046	0.038	0.032	0.075	0.066	0.064	0.161	0.143	0.139	0.060	0.052	0.048
Cold Axial 3	0.053	0.049	0.043	0.079	0.070	0.068	0.073	0.065	0.063	0.066	0.059	0.055
Cold Axial 4	0.084	0.047	0.044	0.082	0.072	0.070	0.044	0.039	0.038	0.083	0.060	0.057
UB Cold	0.109	0.184	0.188	0.092	0.138	0.137	0.095	0.142	0.142	0.100	0.161	0.163
UB Hot	0.134	0.232	0.276	0.092	0.141	0.162	0.080	0.123	0.142	0.113	0.186	0.219
Hot Axial 4	0.170	0.130	0.111	0.124	0.110	0.107	0.078	0.070	0.068	0.147	0.120	0.109
Hot Axial 3	0.165	0.130	0.117	0.134	0.118	0.115	0.101	0.090	0.088	0.150	0.124	0.116
Hot Axial 2	0.107	0.078	0.099	0.143	0.126	0.123	0.157	0.139	0.136	0.125	0.102	0.111
Hot Axial 1	0.103	0.093	0.074	0.132	0.117	0.113	0.153	0.136	0.132	0.118	0.105	0.094

*Values are fractions of total deposit mass located within the indicated radial regions.

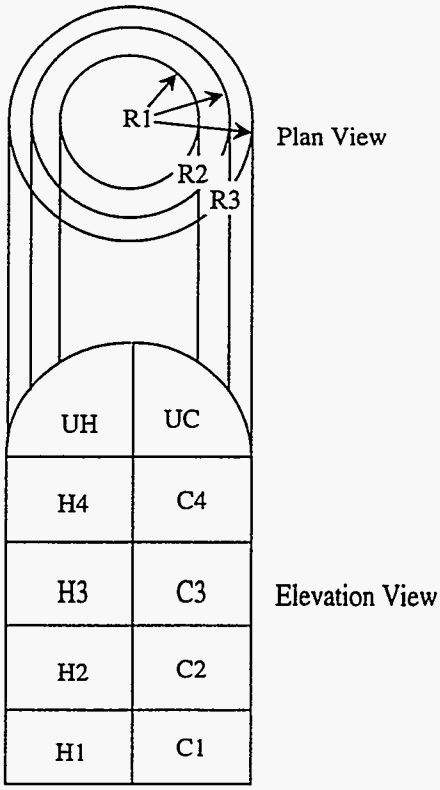

Sketch of SG Regions
Cn = Cold-Leg Axial Region n
Hn = Hot-Leg Axial Region n
UC = Cold-Leg U-Bend Region
UH = Hot-Leg U-Bend Region

Table III-9. Secondary and Primary Deposit Local Fouling Factor Predictions Based on Deposit Characterization (p. 1 of 2)

		Plant A Before Chem Clean			Plant A Now (1/96-4/96)			Plant B Before Chem Clean			Plant B Now (3/96-5/96)		
Nominal tube outside diameter (in)		0.688			0.688			0.875			0.875		
Nominal tube thickness (in)		0.040			0.040			0.050			0.050		
Tube inside diameter (in)		0.608			0.608			0.775			0.775		
Ratio of outside to inside surface areas		1.132			1.132			1.129			1.129		
Total outside surface area (ft^2)		55,000			55,000			51,500			51,500		
Secondary Fouling Factor Calculation (10^{-6} h-ft^2-°F/Btu)		Lower Bound	Best Estimate	Upper Bound	Lower Bound	Best Estimate	Upper Bound	Lower Bound	Best Estimate	Upper Bound	Lower Bound	Best Estimate	Upper Bound
Inner Nonporous Layer	Thickness (mils)	0.1	0.1	0.1				1.0	2.0	3.0			
	Continuous/dispersed phases	Cu (no dispersed)						Fe_3O_4/Cu					
	Dispersed phase volume fraction	0.00	0.00	0.00				0.30	0.20	0.10			
	Cont. thermal cond (BTU/h-ft-°F) (5)	219	219	219				2.0	2.0	2.0			
	Disp. thermal cond (BTU/h-ft-°F)							219	219	219			
	Effective thermal cond (BTU/h-ft-°F) (1)	219	219	219				5.53	3.80	2.71			
	Fouling factor	0.04	0.04	0.04				15.0	43.8	92.0			
Middle Layer	Thickness (mils)												
	Continuous/dispersed phases												
	Dispersed phase volume fraction												
	Cont. thermal cond (BTU/h-ft-°F)												
	Disp. thermal cond (BTU/h-ft-°F)												
	Effective thermal cond (BTU/h-ft-°F) (1)												
	Fouling factor												
Outer Porous Layer	Thickness (mils)	2.2	3.6	5.0				2.7	3.7	4.7			
	Porous matrix phase	Fe_3O_4						Fe_3O_4 + 20% Cu					
	Fe_3O_4 thermal cond (BTU/h-ft-°F)	2.0	2.0	2.0				5.6	3.8	2.7			
	Total porosity fraction all layers	0.350	0.350	0.350				0.550	0.550	0.550			
	Total porosity fraction outer layer	0.366	0.360	0.357				0.550	0.550	0.550			
	Chimney diameter (µm)	10.0	10.0	10.0				NA	NA	NA			
	Fraction of porosity in chimneys	0.54	0.38	0.22				NA	NA	NA			
	Chimney density (mm^{-2})	2500	1750	1000				NA	NA	NA			
	Porous shell porosity fraction	0.211	0.258	0.302				NA	NA	NA			
	Bulk Na concentration (ppb) (2)	0.01	0.02	0.04				NA	NA	NA			
	Bulk NaOH concentration (ppb)	0.017	0.035	0.070				NA	NA	NA			
	Nominal system pressure (psia)	1000	1000	1000				857	857	857			
	Nominal heat flux (BTU/h-ft^2)	55.509	55.509	55.509				56.698	56.698	56.698			
	Concentration factor Pan model	35	89	149				NA	NA	NA			
	ΔT predicted by Pan model (°F)	0.85	1.12	1.67				NA	NA	NA			
	Fouling factor engineering judgment (3)	-30.0	-15.0	0.0				-30.0	-15.0	15.0			
	Effective thermal cond (BTU/h-ft-°F)	-6.1	-19.9	∞				-7.5	-20.5	26.0			
Mass of silicates deposited after cleaning (lb)					25	75	150				25	75	150
Assumed density of silicates (g/cm^3)					3.0	3.0	3.0				3.0	3.0	3.0
Calculated silicate volume (ft^3)					0.133	0.400	0.801				0.133	0.400	0.801
Calculated silicate thickness (mils)					0.029	0.087	0.175				0.029	0.087	0.175
Silicate thermal conductivity (BTU/h-ft-°F)					1.00	0.75	0.50				1.00	0.75	0.50
Secondary deposit fouling factor		-30.0	-15.0	0.0	2.4	9.7	29.1	-15.0	28.8	107	2.4	9.7	29.1
Primary Fouling Factor Calculation (10^{-6} h-ft^2-°F/BTU)		Lower Bound	Best Estimate	Upper Bound	Lower Bound	Best Estimate	Upper Bound	Lower Bound	Best Estimate	Upper Bound	Lower Bound	Best Estimate	Upper Bound
Primary deposit layer thickness (µm)		0.5	1.0	5.0	0.5	1.0	5.0	0.5	1.0	5.0	0.5	1.0	5.0
Primary deposit layer thickness (mils)		0.020	0.039	0.197	0.020	0.039	0.197	0.020	0.039	0.197	0.020	0.039	0.197
Primary layer thermal cond. (BTU/h-ft-°F)		4.6	1.8	0.6	4.6	1.8	0.6	4.6	1.8	0.6	4.6	1.8	0.6
Primary fouling factor (based on inside area)		0.4	1.8	27.3	0.4	1.8	27.3	0.4	1.8	27.3	0.4	1.8	27.3
Primary fouling factor (based on outside area)		0.4	2.1	30.9	0.4	2.1	30.9	0.4	2.1	30.9	0.4	2.1	30.9

(1) Effective thermal conductivity per Bruggeman's equation.

(2) Nominal Plant-E values given by "Chemistry Status Report" dated October 3, 1994.

(3) Fouling factor based on fouling factor heat transfer experiments, literature values, and engineering judgment.

(4) "NA" indicates this information is not available.

(5) Plant-F value from Appendix E of Reference (1).

Table III-9. Secondary and Primary Deposit Local Fouling Factor Predictions Based on Deposit Characterization (p. 2 of 2)

		Plant C Now (2/96-6/96)			Plant D Now (4/95-6/95)			Plant E Before Chem Clean			Plant F as of 1990		
Nominal tube outside diameter (in)		0.750			0.875			0.750			0.875		
Nominal tube thickness (in)		0.043			0.050			0.048			0.050		
Tube inside diameter (in)		0.664			0.775			0.654			0.775		
Ratio of outside to inside surface areas		1.130			1.129			1.147			1.129		
Total outside surface area (ft^2)		68,000			51,500			104,130			44,430		
Secondary Fouling Factor Calculation (10^{-6} h-ft^2-°F/Btu)		Lower Bound	Best Estimate	Upper Bound	Lower Bound	Best Estimate	Upper Bound	Lower Bound	Best Estimate	Upper Bound	Lower Bound	Best Estimate	Upper Bound
Inner Nonporous Layer	Thickness (mils)				1.0	2.0	3.0	2.5	3.9	5.3	1.0	1.7	2.5
	Continuous/dispersed phases				Fe_3O_4			Fe_3O_4/Cu			$Ca_{10}(PO_4)_6(OH)_2$/MgO		
	Dispersed phase volume fraction				0.15	0.10	0.03	0.30	0.25	0.20	0.35	0.30	0.25
	Cont. thermal cond (BTU/h-ft-°F) (5)				2.0	2.0	2.0	2.0	2.0	2.0	2.5	0.7	0.5
	Disp. thermal cond (BTU/h-ft-°F)				100	25	10	219	219	219	20	10	7
	Effective thermal cond (BTU/h-ft-°F) (1)				3.14	2.54	2.10	5.53	4.56	3.80	5.35	1.54	0.95
	Fouling factor				26.5	65.4	118.6	37.5	70.9	115.6	15.6	92.0	217.8
Middle Layer	Thickness (mils)							1.0	1.5	2.0			
	Continuous/dispersed phases							Fe_3O_4/H_20(l) voids					
	Dispersed phase volume fraction							0.20	0.38	0.56			
	Cont. thermal cond (BTU/h-ft-°F)							2.0	2.0	2.0			
	Disp. thermal cond (BTU/h-ft-°F)							0.32	0.32	0.32			
	Effective thermal cond (BTU/h-ft-°F) (1)							1.55	1.20	0.88			
	Fouling factor							53.6	104.3	188.3			
Outer Porous Layer	Thickness (mils)	0.1	0.5	2.1	2.9	3.9	4.9	3.5	4.9	6.3	5.2	7.0	8.7
	Porous matrix phase	Fe_3O_4			Fe_3O_4			Fe_3O_4			Fe_3O_4 + 12% Cu		
	Fe_3O_4 thermal cond (BTU/h-ft-°F)	2.0	2.0	2.0	2.9	2.6	2.3	2.0	2.0	2.0	3.2	2.9	2.7
	Total porosity fraction all layers	NA	NA	NA	0.340	0.340	0.340	0.224	0.224	0.224	0.09	0.09	0.09
	Total porosity fraction outer layer	NA	NA	NA	0.340	0.340	0.340	0.391	0.355	0.306	0.17	0.17	0.17
	Chimney diameter (µm)	NA	NA	NA	NA	NA	NA	2.5	2.5	2.5	NA	NA	NA
	Fraction of porosity in chimneys	NA	NA	NA	NA	NA	NA	0.12	0.12	0.12	NA	NA	NA
	Chimney density (mm^{-2})	NA	NA	NA	NA	NA	NA	9555	8667	7475	NA	NA	NA
	Porous shell porosity fraction	NA	NA	NA	NA	NA	NA	0.361	0.326	0.279	NA	NA	NA
	Bulk Na concentration (ppb) (2)	NA	NA	NA	NA	NA	NA	0.05	0.09	0.18	NA	NA	NA
	Bulk NaOH concentration (ppb)	NA	NA	NA	NA	NA	NA	0.078	0.157	0.313	NA	NA	NA
	Nominal system pressure (psia)	1100	1100	1100	815	815	815	900	900	900	821	821	821
	Nominal heat flux (BTU/h-ft^2)	47,883	47,883	47,883	56,698	56,698	56,698	55,863	55,863	55,863	58,366	58,366	58,366
	Concentration factor Pan model	NA	NA	NA	NA	NA	NA	15	72	623	NA	NA	NA
	ΔT predicted by Pan model (°F)	NA	NA	NA	NA	NA	NA	1.30	1.30	1.33	NA	NA	NA
	Fouling factor engineering judgment (3)	-15.0	0.0	5.0	-30.0	0.0	30.0	-40.0	10.0	60.0	50.0	100.0	200.0
	Effective thermal cond (BTU/h-ft-°F)	-0.6	∞	34.9	-8.0	∞	13.5	-7.3	40.6	8.7	8.6	5.8	3.6
Mass of silicates deposited after cleaning (lb)													
Assumed density of silicates (g/cm^3)													
Calculated silicate volume (ft^3)													
Calculated silicate thickness (mils)													
Silicate thermal conductivity (BTU/h-ft-°F)													
Secondary deposit fouling factor		-15.0	0.0	5.0	-3.5	65.4	149	51.1	185	364	65.6	192	418
Primary Fouling Factor Calculation (10^{-6} h-ft^2-°F/BTU)		Lower Bound	Best Estimate	Upper Bound	Lower Bound	Best Estimate	Upper Bound	Lower Bound	Best Estimate	Upper Bound	Lower Bound	Best Estimate	Upper Bound
Primary deposit layer thickness (µm)		0.5	1.0	5.0	0.5	1.0	5.0	0.5	1.0	5.0	0.5	1.0	5.0
Primary deposit layer thickness (mils)		0.020	0.039	0.197	0.020	0.039	0.197	0.020	0.039	0.197	0.020	0.039	0.197
Primary layer thermal cond. (BTU/h-ft-°F)		4.6	1.8	0.6	4.6	1.8	0.6	4.6	1.8	0.6	4.6	1.8	0.6
Primary fouling factor (based on inside area)		0.4	1.8	27.3	0.4	1.8	27.3	0.4	1.8	27.3	0.4	1.8	27.3
Primary fouling factor (based on outside area)		0.4	2.1	30.9	0.4	2.1	30.9	0.4	2.1	30.9	0.4	2.1	30.9

(1) Effective thermal conductivity per Bruggeman's equation.

(2) Nominal Plant-E values given by "Chemistry Status Report" dated October 3, 1994.

(3) Fouling factor based on fouling factor heat transfer experiments, literature values, and engineering judgment.

(4) "NA" indicates this information is not available.

(5) Plant-F value from Appendix E of Reference (1).

Table III-10. Predicted Pressure Loss Due to Secondary Deposits Based on Deposit Characterization

Unit	Plant A		Plant B		Plant C	Plant D	Plant E	Plant F
Time	3/95	4/96	9/95	5/96	6/96	6/95	11/96	3/91
Age	8.6	9.5	7.5	7.8	5.0	8.0	10.1	15.6
Secondary Deposit Fouling Factor (10^{-6} h-ft^2-°F/BTU)	-15.0	9.7	43.8	9.7	0.0	65.4	185	192
Steam Pressure Sensitivity (psi/10^{-6} h-ft^2-°F/BTU)	-0.36	-0.36	-0.36	-0.36	-0.24	-0.34	-0.39	-0.38
Loss in Steam Pressure Due to Deposits (psi)	**-5**	**4**	**16**	**3**	**0**	**22**	**72**	**73**

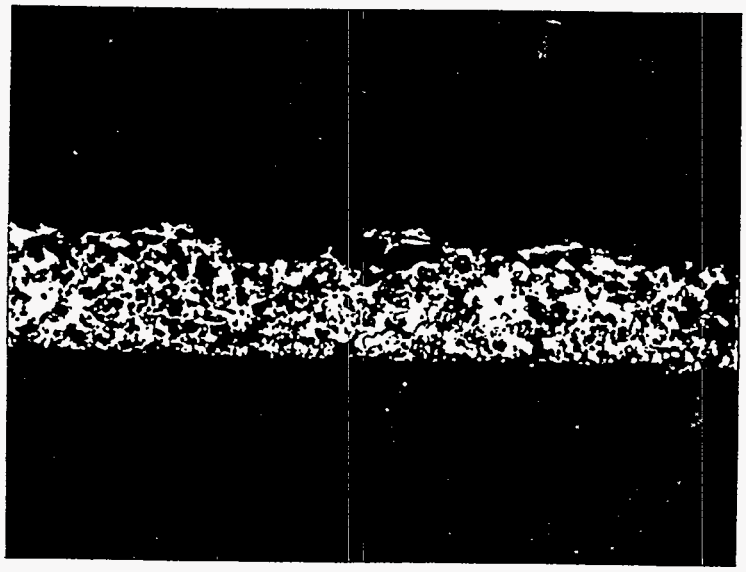

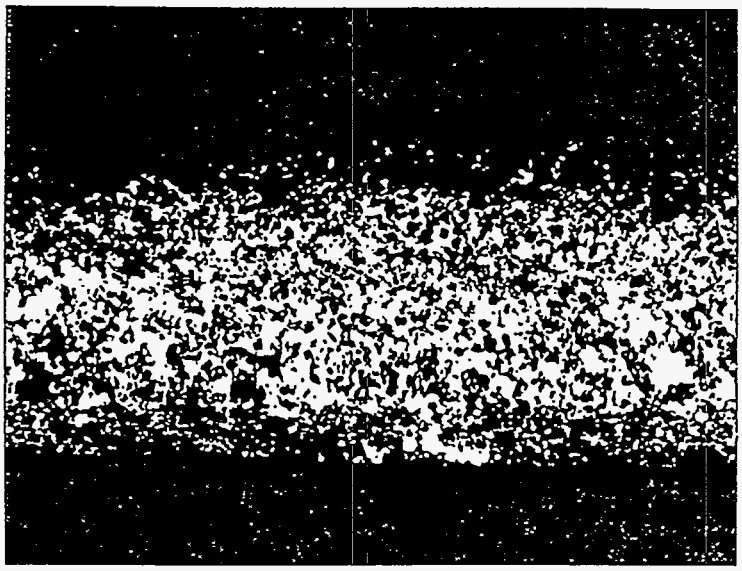

Figure III-1a. Photomicrographs of Thin and Thick Secondary Tube Deposits at Plant A

Figure III-1b. Photomicrographs of Thin Tube Deposits at Plant A (Double Layer Structure and Copper Inclusions)

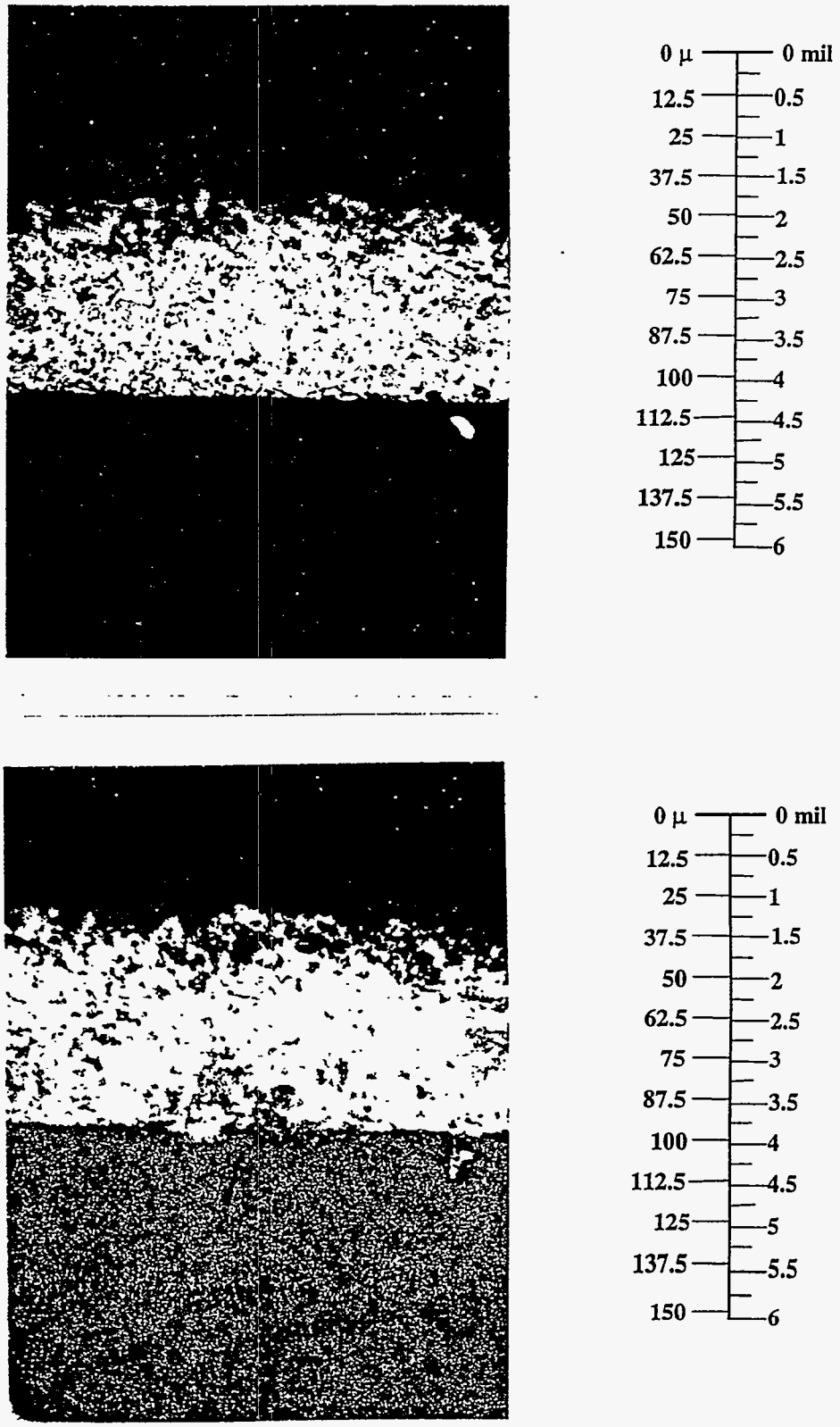

Figure III-2a. Photomicrographs of Secondary Tube Deposits at Plant B (Thin Flake)

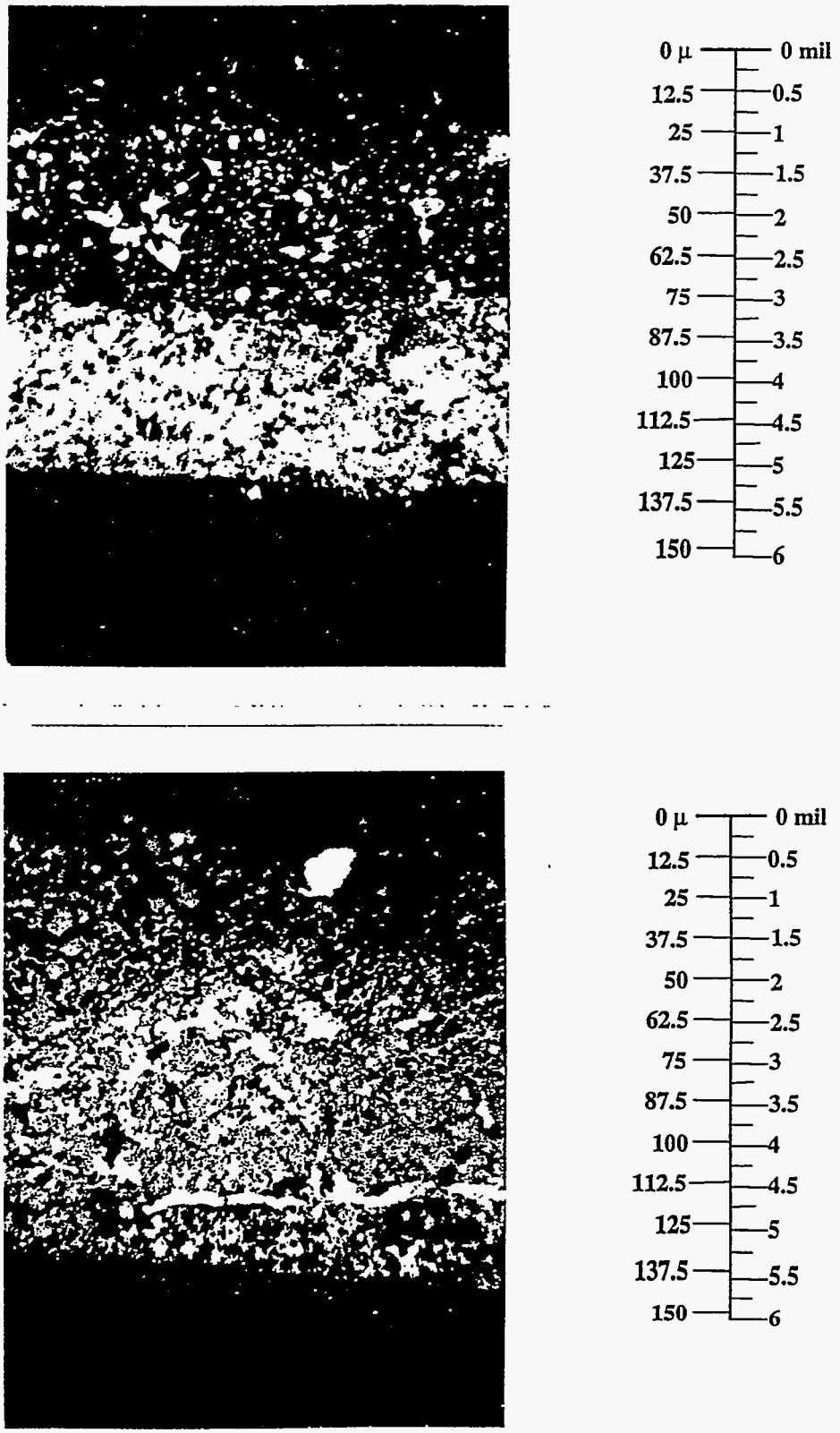

Figure III-2b. Photomicrographs of Secondary Tube Deposits at Plant B (Thick Flakes)

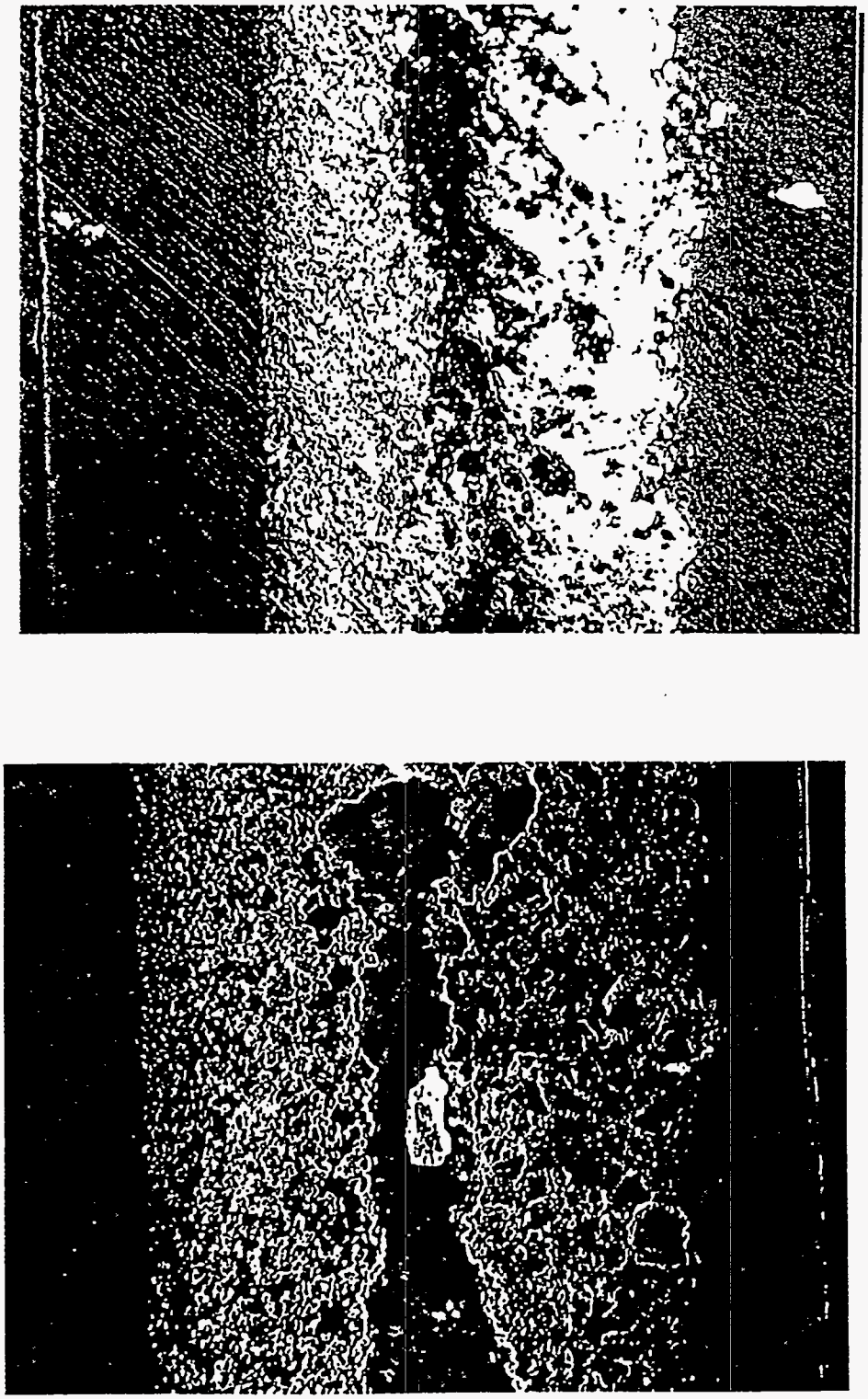

Figure III-3. Photomicrographs of Secondary Tube Deposits at Plant E

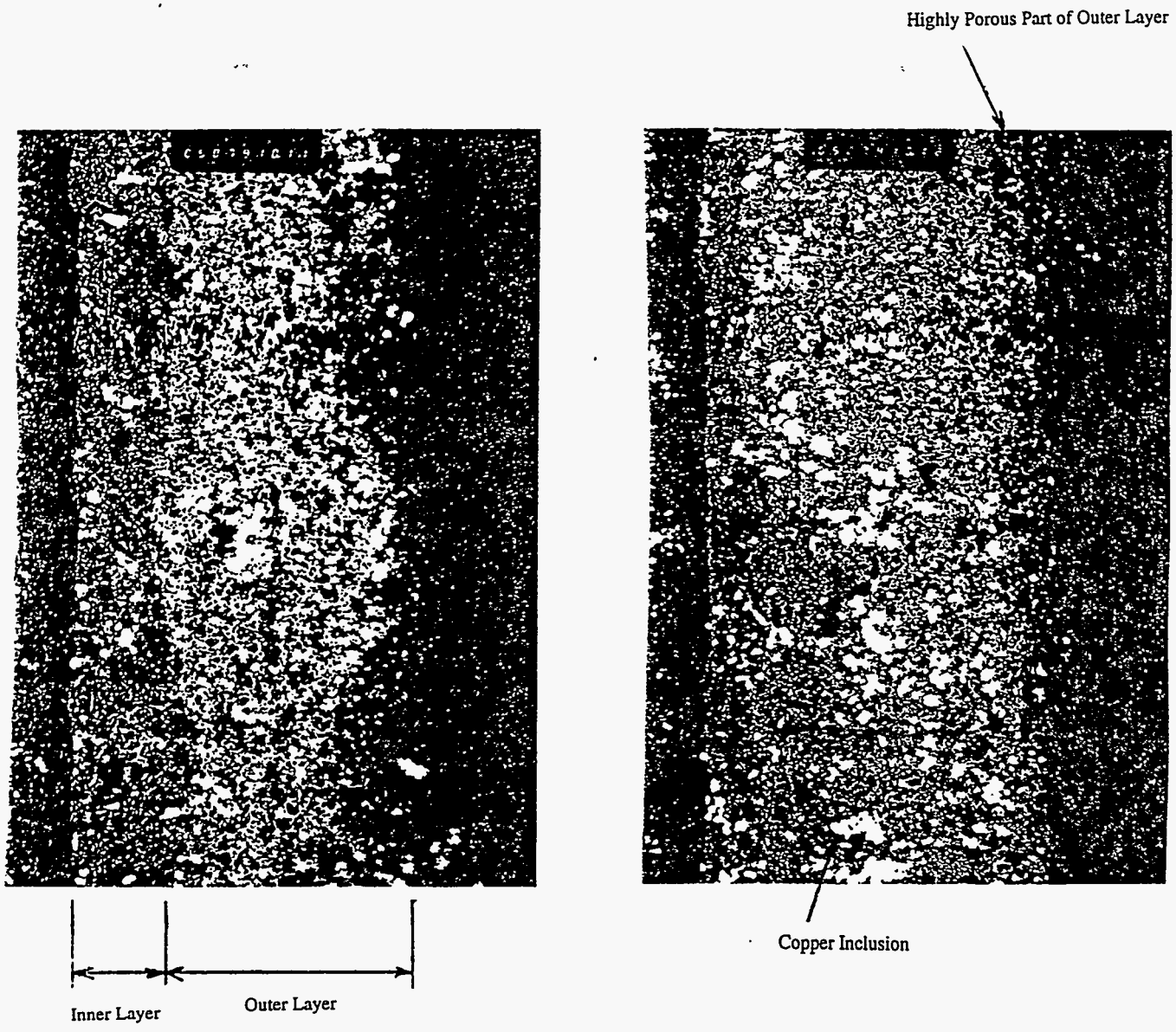

Figure III-4. Photomicrographs of Secondary Tube Deposits at Plant F

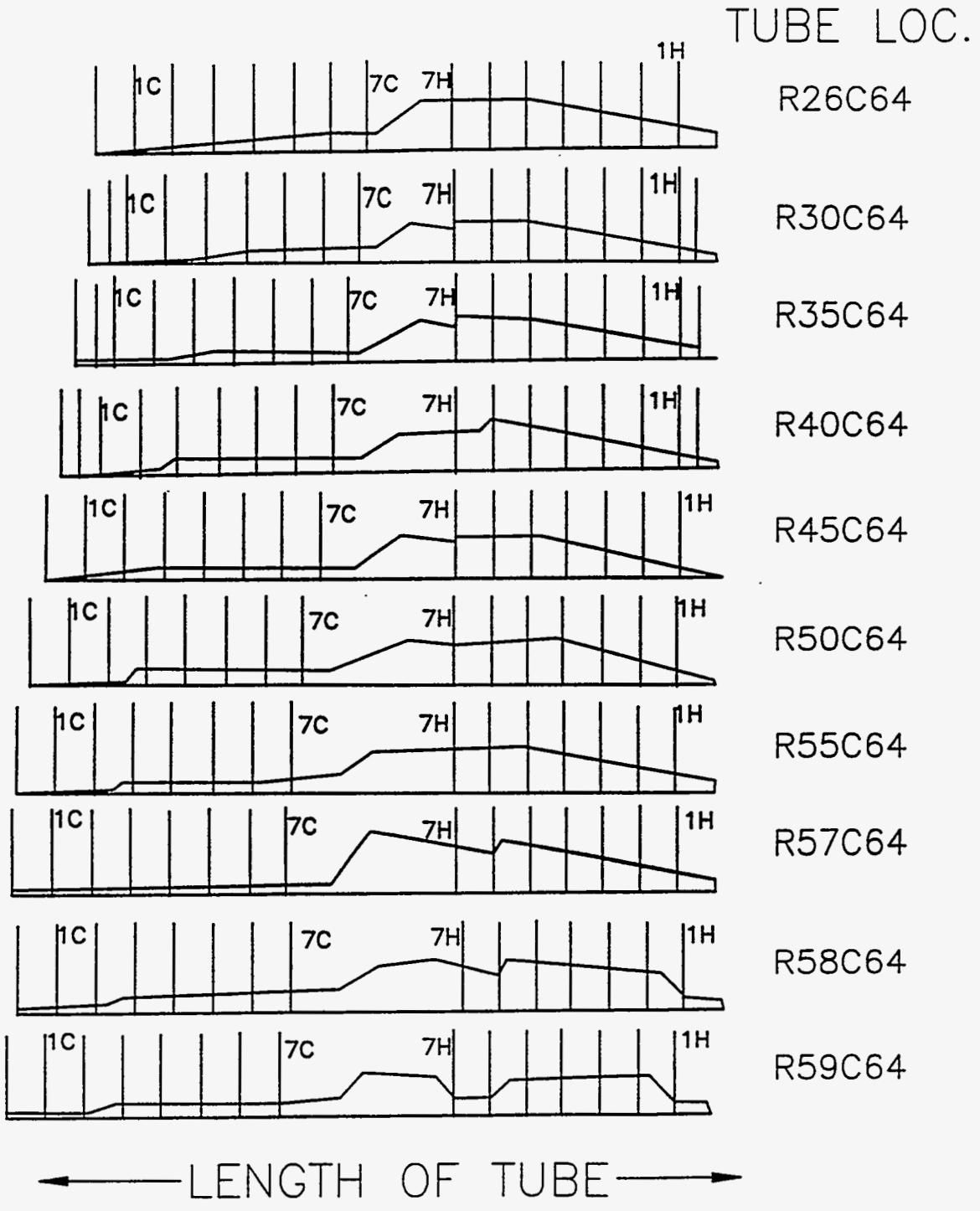

Figure III-5. Low-Frequency ECT Sludge Profiles for Plant A

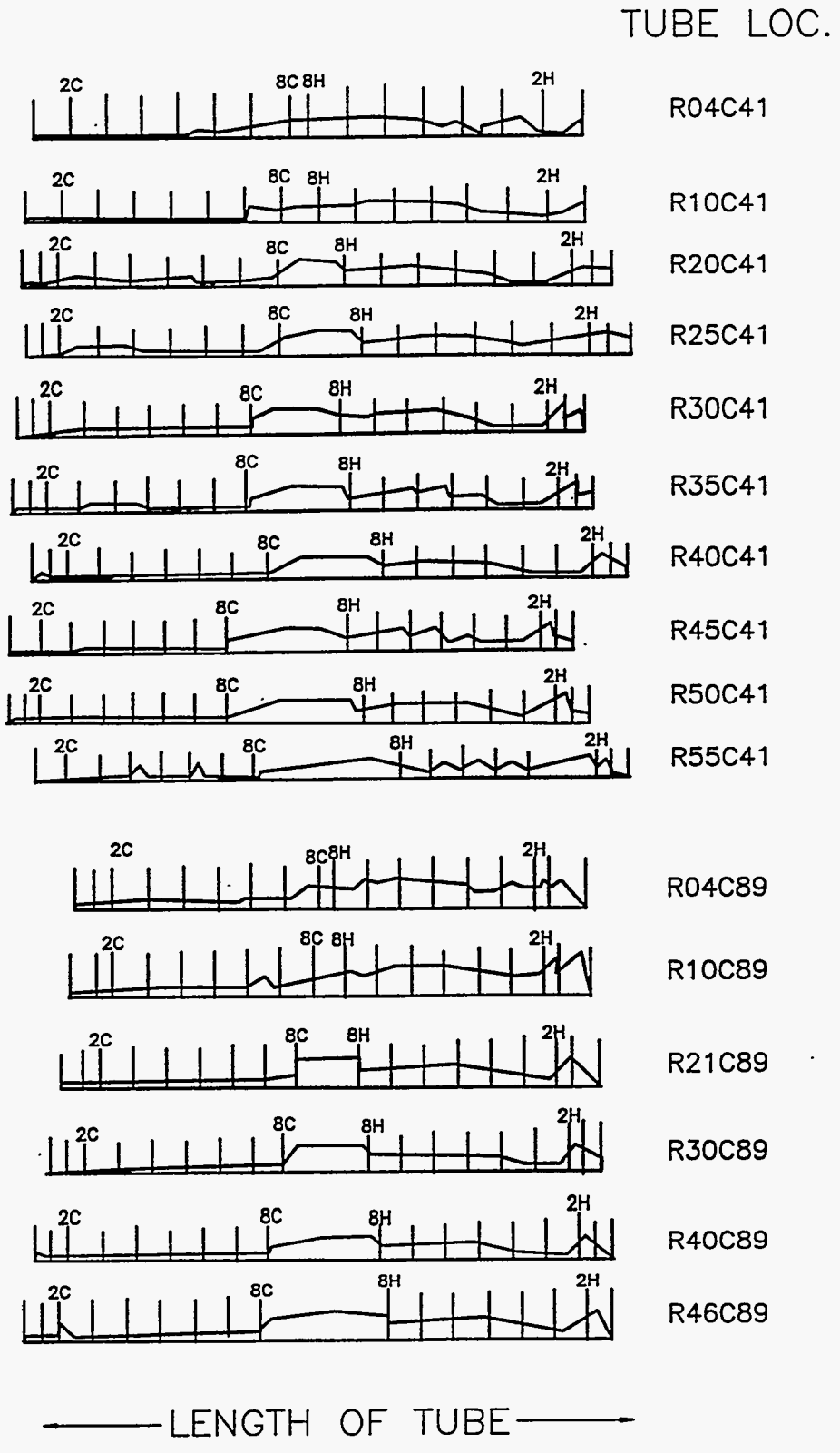

Figure III-6. Low-Frequency ECT Sludge Profiles for Plant A1

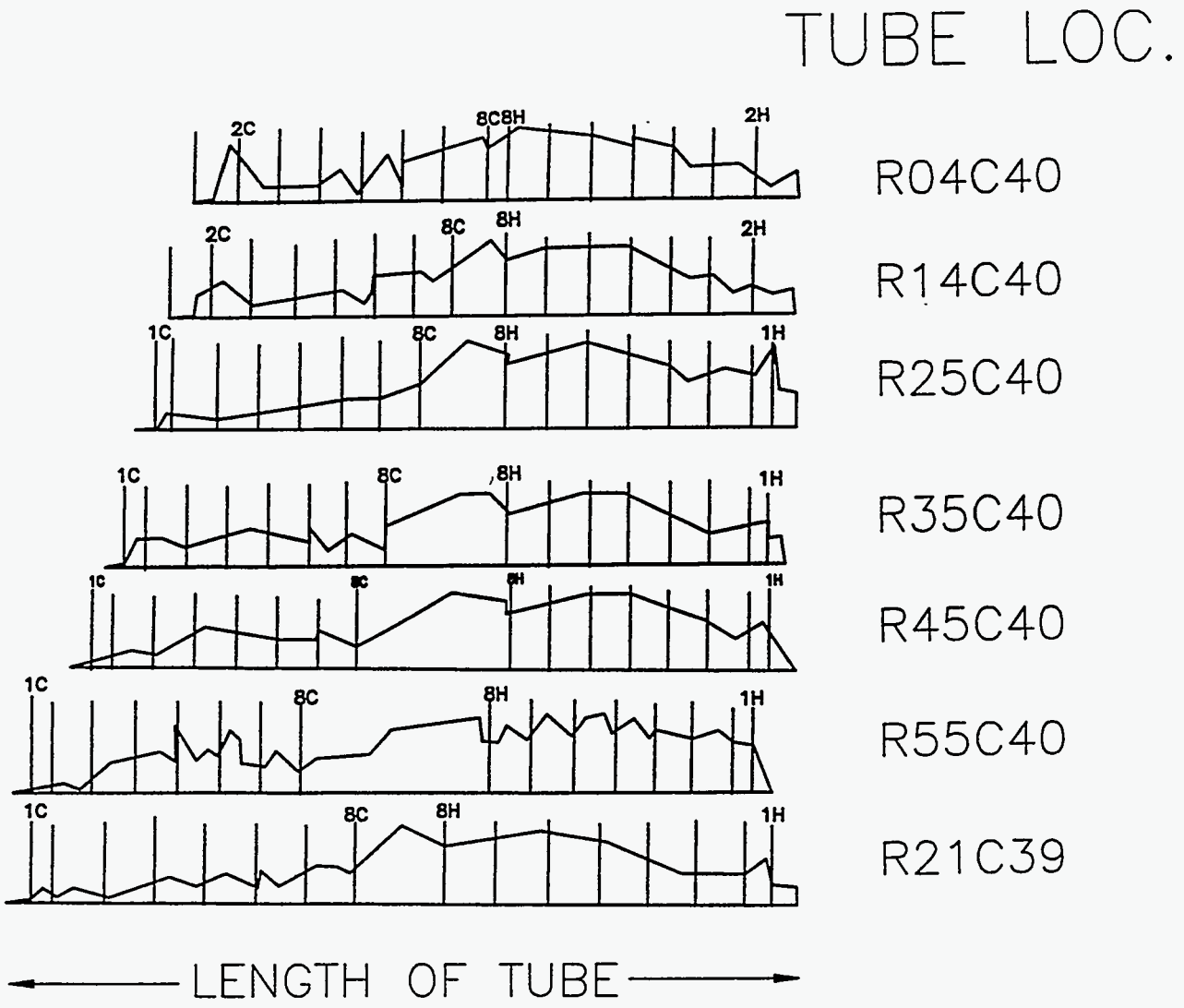

Figure III-7. Low-Frequency ECT Sludge Profiles for Plant A2

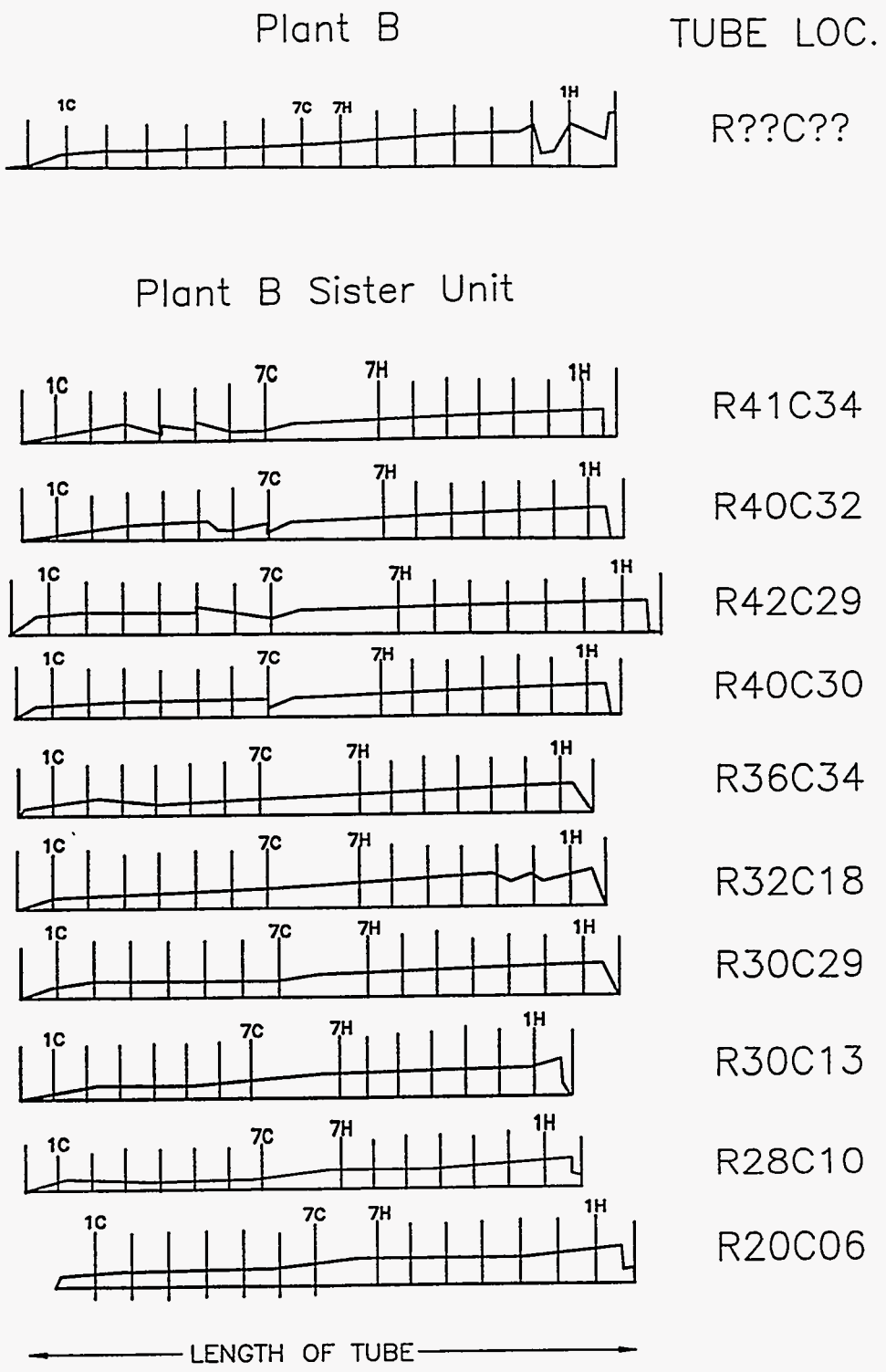

Figure III-8. Low-Frequency ECT Sludge Profiles for Plants B and B1

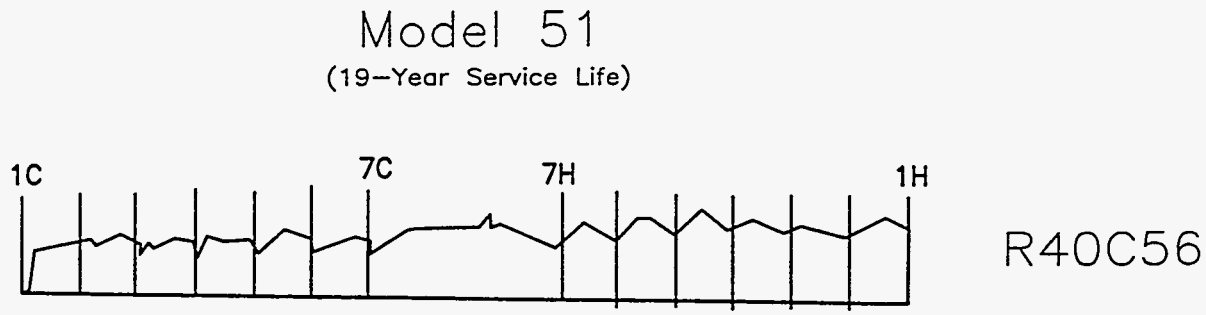

Plant B2

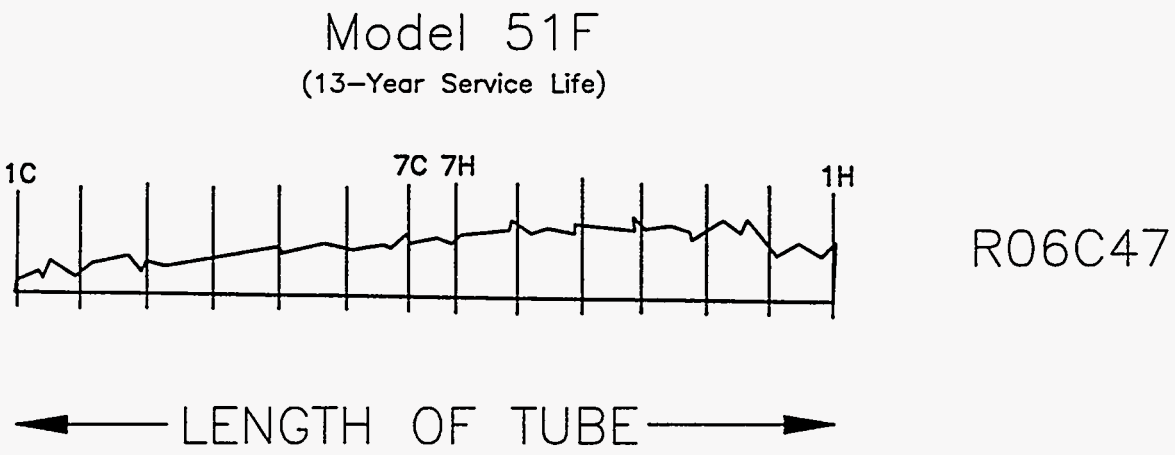

Plant B3

Figure III-9. Low-Frequency ECT Sludge Profiles for Plants B2 and B3

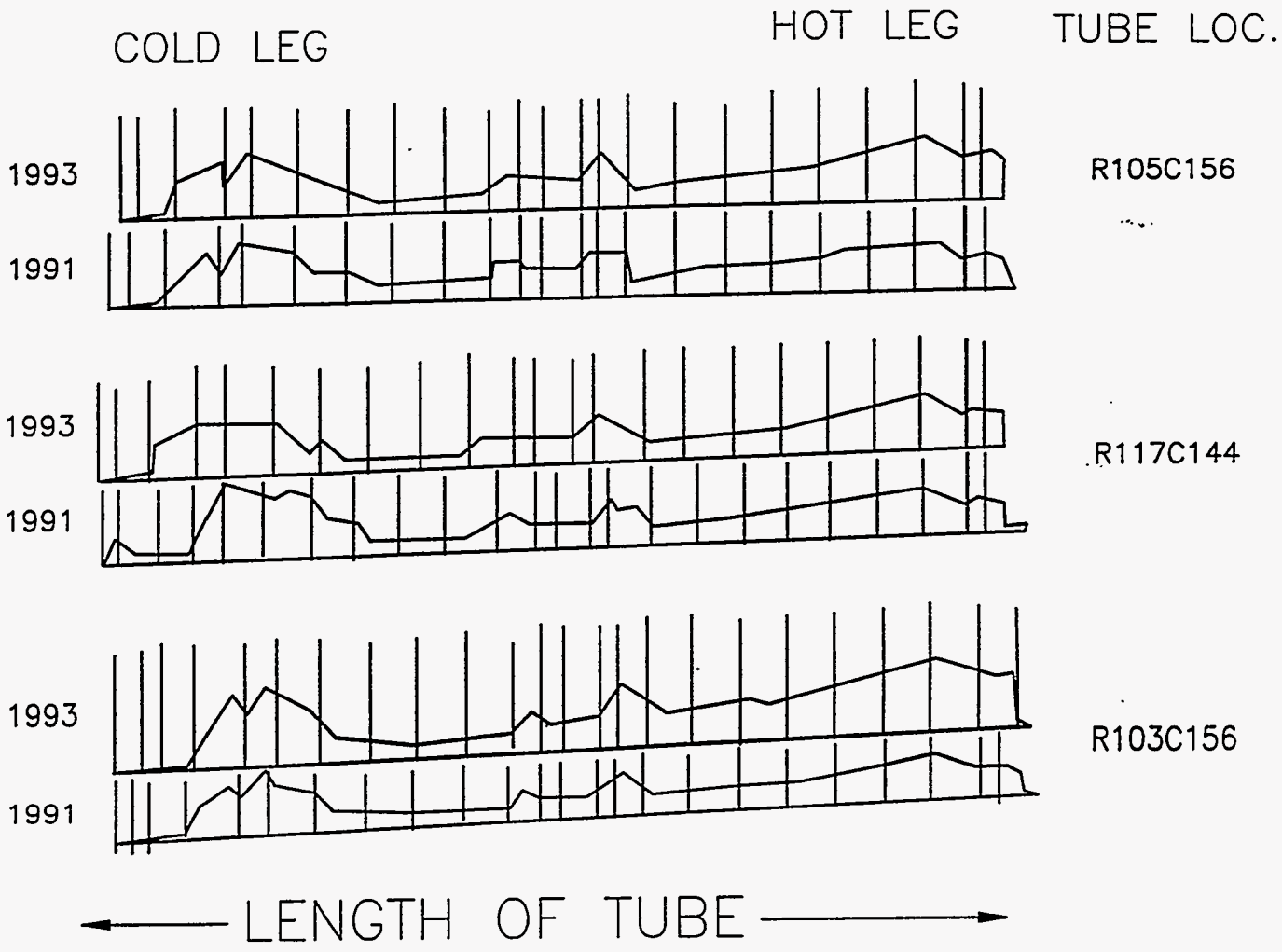

Figure III-10. Low-Frequency ECT Sludge Profiles for Plant G

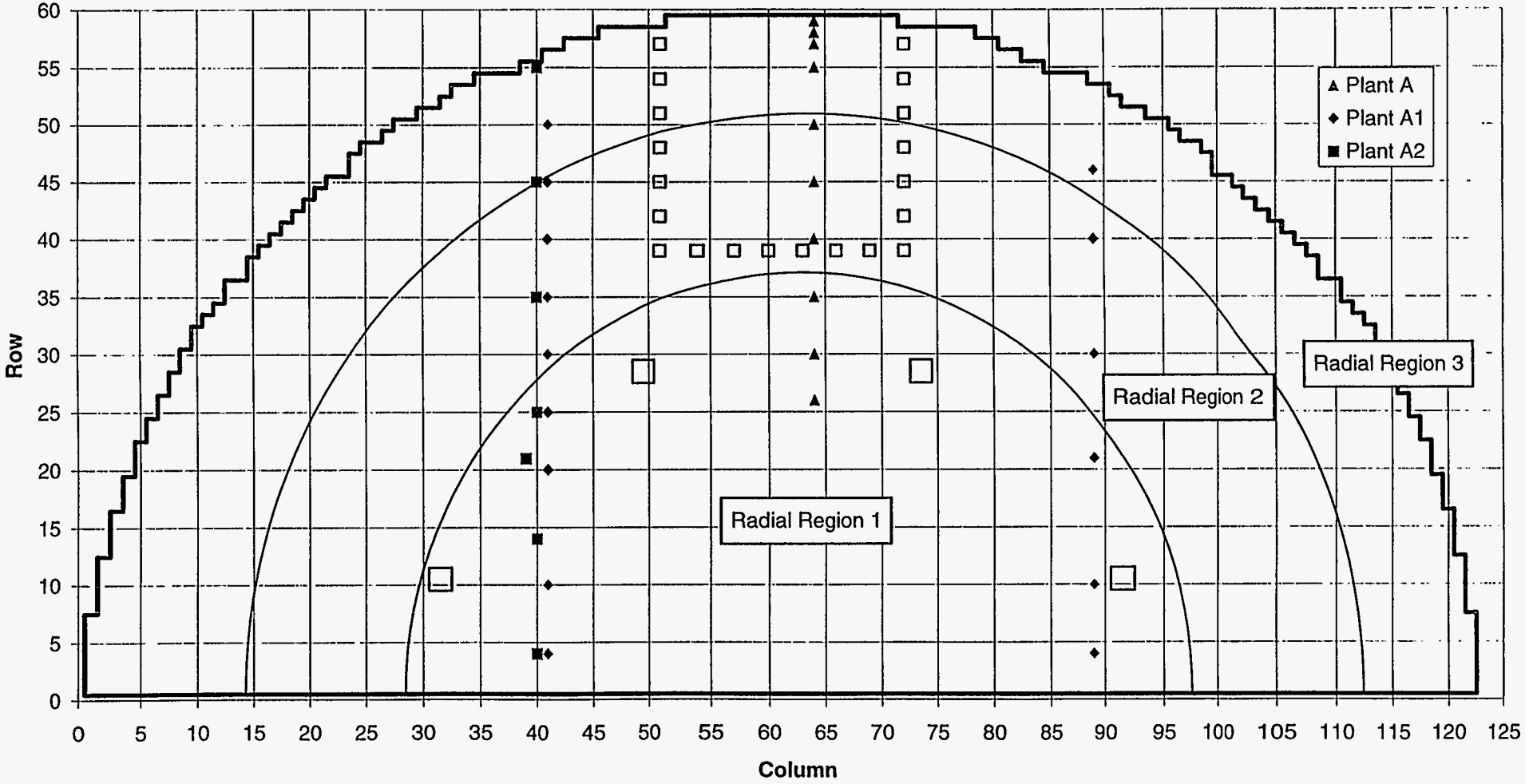

Figure III-11. Location of Tubes with ECT Sludge Profiles – Model F Units

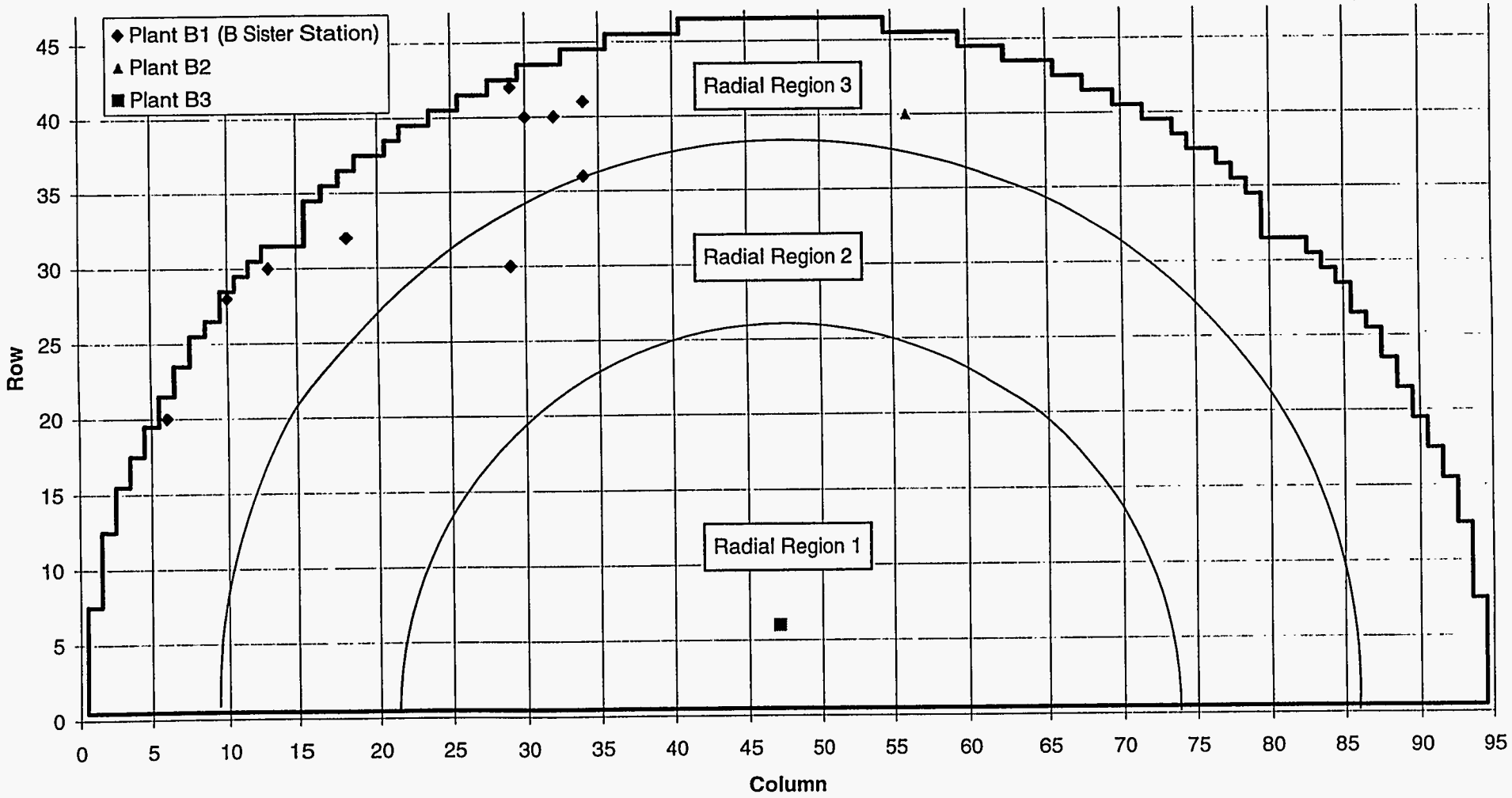

Figure III-12. Location of Tubes with ECT Sludge Profiles – Model 51 Units

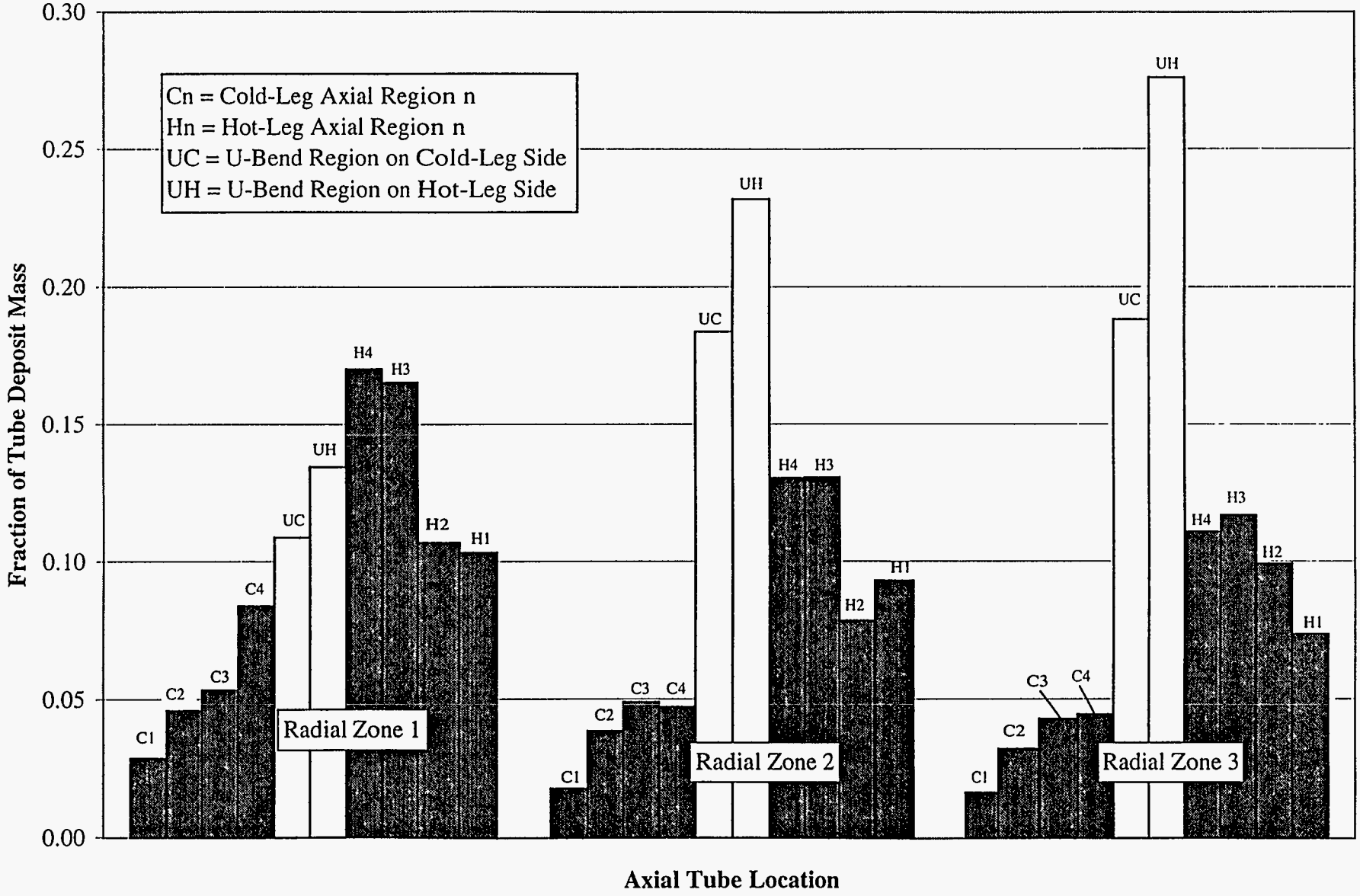

Figure III-13. Model F Composite Tube Scale Distribution

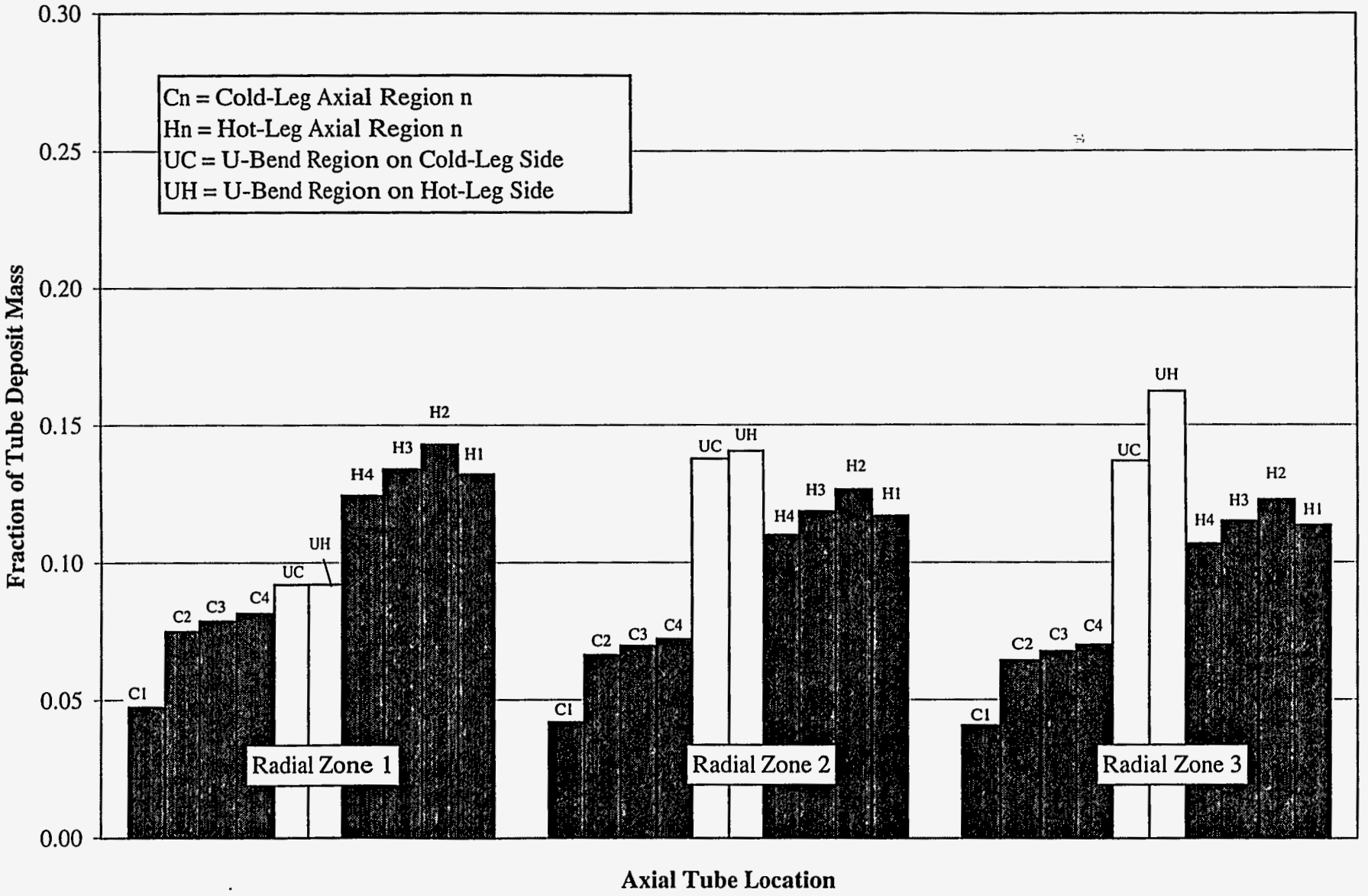

Figure III-14. Model 51 Composite Tube Scale Distribution

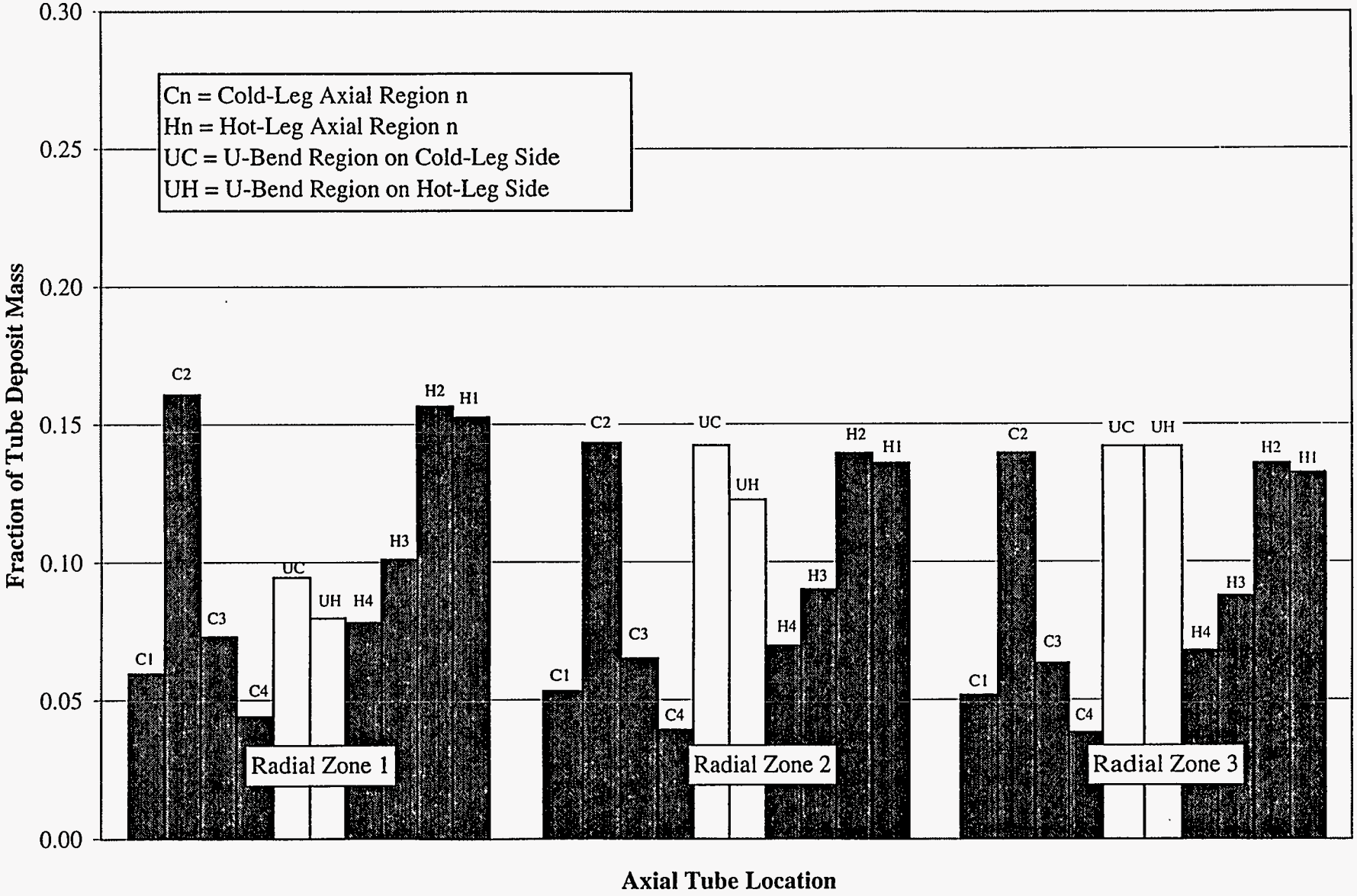

Figure III-15. Preheater Composite Tube Scale Distribution

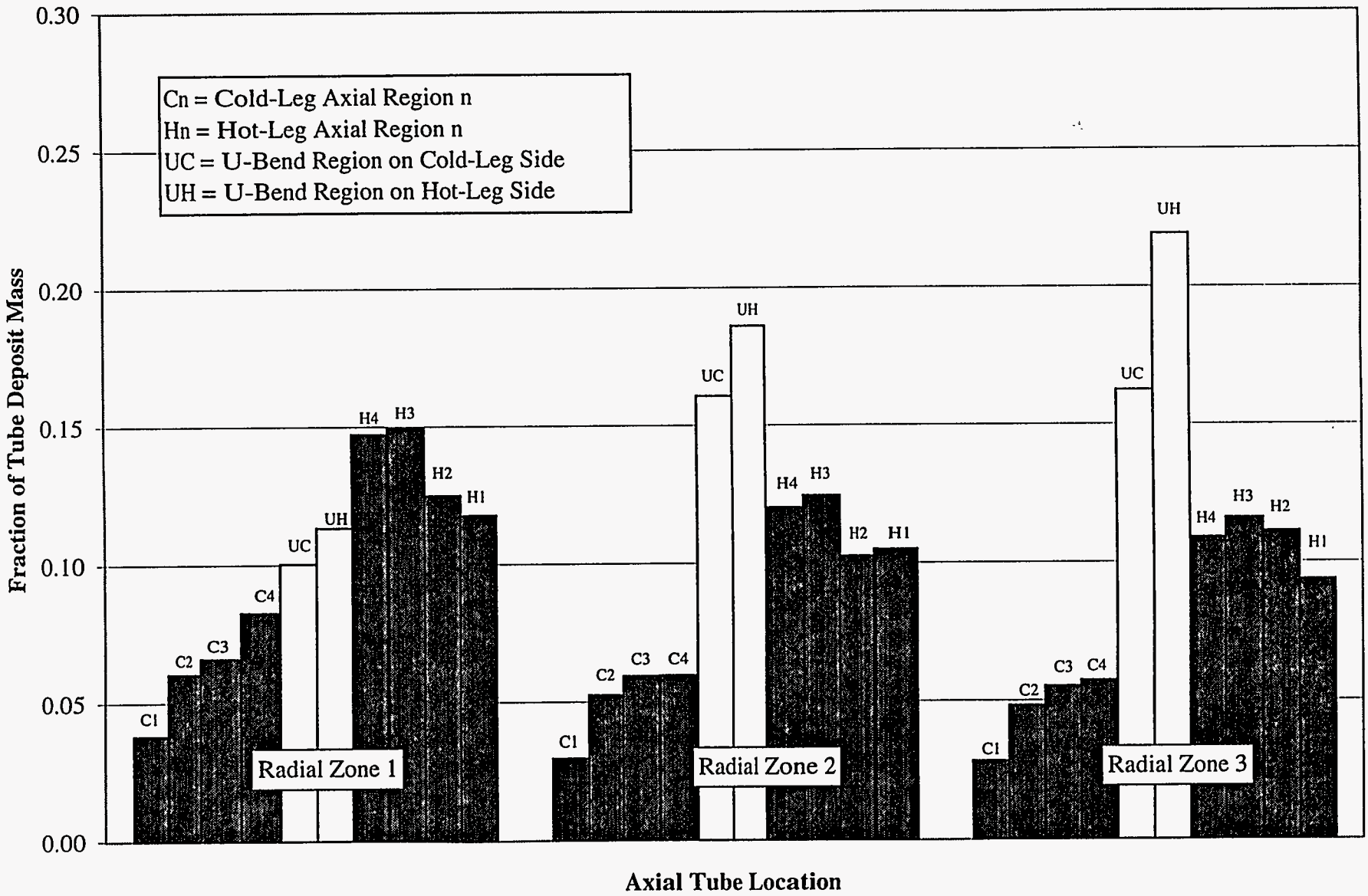

Figure III-16. Overall Composite Tube Scale Distribution

IV. GLOBAL FOULING FACTOR ANALYSES FOR FIVE US PLANTS

The primary focus of this project is on the heat-transfer effects of secondary tube scale. When this scale is thermally resistive, it tends to lower SG steam pressure. However, other factors unrelated to secondary deposits can also lower steam pressure. As discussed in more detail in Section V, the global fouling factor methodology aids in attributing SG pressure losses to the proper causes by accounting for changes in key thermal-hydraulic parameters. This section provides a brief background on the topic of SG thermal performance degradation and then discusses application of the global fouling factor methodology to the plants selected for this study, which is the first step in determining the observed heat-transfer effects of secondary deposits at these plants.

SG Thermal Performance Degradation—Definition

In order to accurately assess the heat-transfer effects of secondary deposits, it is necessary first to develop a working definition of SG thermal performance degradation. In a narrow sense, it can be defined as a decrease in the overall SG tube bundle heat-transfer coefficient. Stated another way, it is a loss of capacity to transfer heat given constant primary and secondary inlet temperatures, pressures, and mass flow rates. This type of performance degradation is most often the result of SG tube fouling, usually on the secondary-side surfaces of the tubes.* A broader definition of thermal performance degradation is given below:

> ***Thermal performance degradation refers to a decrease in SG outlet pressure and/or thermal power,† which can be caused by three different sources:***
>
> - ***Decrease in overall tube bundle heat transfer coefficient***
> - ***Other sources within the SG shell (e.g., extra moisture separator pressure drop)***
> - ***External sources (e.g., hot-leg streaming)***

As indicated above, the first type is usually caused by secondary deposits. The other two categories, on the other hand, are caused by factors unrelated to deposits. However, all three types can lead to a decrease in steam pressure. Consequently, for a particular plant of interest, all of these causes must be evaluated in order to attribute the proper portion of the observed change in steam pressure to secondary deposits (see Section V).

---

* Most data for US plants suggest that primary-side corrosion layers are very thin and probably cause little reduction in heat transfer. Note also that for SGs with preheaters, fouling of the preheater baffle plates can also cause a reduction in the apparent heat-transfer coefficient of the tube bundle as a whole.

† Note that excessive moisture carryover, steam carryunder, and water-level oscillations may also be considered forms of SG performance degradation. These forms are not directly relevant to the goals of this project.

Historical Background on Secondary Deposits in US Commercial SGs

Until recently, many throughout the nuclear industry had assumed that decreased SG thermal performance was due exclusively to the presence of secondary tube scale. This conclusion was generally consistent with the fact that nearly all of the plants and SG designs experiencing performance degradation have reported the presence of these deposits, which typically consist of iron oxides, copper metal, hardness species, and a host of minor constituents including alumino-silicates, salts, debris, and organics (see *Characterization of PWR Steam Generator Deposits,* EPRI Report TR-106048 (2), for more information). In addition, the role of secondary deposits in causing heat-transfer degradation was confirmed for the Ginna plant in the early 1990s (see EPRI Report TR-100866 (1)). Experiments documented in Reference (1) showed that fouling caused by corrosion products and impurities on the secondary side of SG tube surfaces was primarily responsible for the performance degradation at Ginna. The experience at Ginna (Plant F) is further discussed later in this section.

The belief that secondary deposits cause pressure loss in part led another unit, Plant A, to chemically clean the secondary side of their SGs. The objective was to remove an estimated 4 mils of tube scale that was believed to be the root cause of SG thermal performance problems. At the completion of the cleaning, during which approximately 5,000 pounds of deposits were removed from each of the four SGs, secondary-side visual inspections confirmed that essentially all deposits had been removed and tube surfaces were cleaned to what appeared to be bare metal. Much to the industry's surprise, the plant restarted after the cleaning only to have an even greater reduction in steam pressure compared to the pressure loss observed prior to the cleaning.

Another unit, Plant E, also chemically cleaned its SGs, removing over 16,000 pounds of corrosion products from each one. In contrast to Plant A, Plant E restarted with a substantially higher steam pressure than that recorded just prior to the chemical cleaning. As suggested by these two cases, secondary deposits can have a markedly different effect depending upon the plant. Such differences are the result of variation in the composition, morphology, and thickness of secondary deposits (see Section III).

Fouling Factor Methodology

An exact quantitative measure of the heat-transfer effects of secondary deposits is difficult to obtain due to the complex nature of SG thermal hydraulics. Accurate modeling of the details requires sophisticated thermal-hydraulics software specially designed for the SG geometry (e.g.,

ATHOS); even then, significant assumptions must be made. However, important insight into the performance of SGs can be achieved with the use of the standard global heat-transfer equation. The purpose of a fouling factor calculation is to quantify the degradation of the ability of a heat exchanger to transfer heat. At a local level, the ability to transfer heat from the primary coolant to the secondary fluid is given by the local heat transfer coefficient U_{local}:

$$q'' = U_{local}\left(T_{prim} - T_{sec}\right) \qquad \text{[IV-1]}$$

where q" is the local heat flux. This equation can also be written in terms of the local resistance to heat transfer R''_{local}:

$$q'' = \frac{T_{prim} - T_{sec}}{R''_{local}} \qquad \text{[IV-2]}$$

The local resistance is made up of the conductive resistance of the tube wall, the boundary layer resistances of the primary and secondary fluids, and the resistances resulting from the accumulation of any deposit layers on the inside and outside tube surfaces. The local fouling factor is the sum of these last two resistances and, in practice, is defined as the change in local resistance from the local resistance at initial operation:

$$R''_{f,local} = \Delta R''_{local} = R''_{local} - R''_{local,0} \qquad \text{[IV-3]}$$

As the local fouling factor increases due to the accumulation of deposits, the driving temperature difference must increase at the same rate in order for the same heat flux to be transferred.

The local fouling analysis can be extended to a global fouling analysis of an entire heat exchanger by defining a global heat transfer coefficient U and a global heat transfer resistance R (or a global area-based resistance R"):

$$Q = UA\Delta T_m = \frac{\Delta T_m}{R} = \frac{A\Delta T_m}{R''} \qquad \text{[IV-4]}$$

where Q is the total thermal power transferred, A is the active heat transfer area (defined using the outside tube surface area), and ΔT_m is the mean temperature difference between the two fluids. This equation is called the overall heat transfer equation.

Under certain assumptions, the mean temperature difference is equal to the log-mean temperature difference (LMTD), which is defined as

$$\Delta T_{lm} = F \frac{\Delta T_2 - \Delta T_1}{\ln\left(\Delta T_2 / \Delta T_1\right)} \qquad \text{[IV-5]}$$

where ΔT_1 and ΔT_2 are the terminal temperature differences corresponding to a pure counterflow heat exchanger and F is a factor less than or equal to one that accounts for the deviation from pure counterflow. This equation is strictly valid only if the local heat transfer coefficient is constant throughout the heat exchanger and the specific heat of each fluid can be considered constant. A commercial PWR steam generator does not strictly meet these two conditions because the secondary boundary layer resistance changes with the mode of heat transfer (boiling versus single-phase convection) and heat flux, flow rate, and quality (for boiling); and also because the specific heat of the secondary fluid jumps from a finite value to infinity at the inception of boiling. The first violation may cause only a slight uncertainty because the secondary boundary layer resistance is only about 15% of the total resistance. The effect of the second violation is illustrated in Figure IV-1, which shows the fluid temperature distribution of the primary and secondary fluids assuming pure counterflow. By using a log-mean temperature analysis, the secondary fluid temperature must be modeled as a logarithmic curve or as a constant. Figure IV-1 shows that the secondary fluid temperature distribution is best approximated by neglecting the subcooling of the fluid entering the bottom of the tube bundle from the downcomer. For a heat exchanger with the temperature of one fluid held constant by phase change, the factor F is one regardless of heat exchanger geometry.

Then the overall heat transfer equation for a PWR steam generator becomes

$$Q = UA \frac{\left(T_{hot} - T_{sat}\right) - \left(T_{cold} - T_{sat}\right)}{\ln\left(\frac{T_{hot} - T_{sat}}{T_{cold} - T_{sat}}\right)} \qquad \text{[IV-6]}$$

or

$$Q = UA \frac{T_{hot} - T_{cold}}{\ln\left(\frac{T_{hot} - T_{sat}(p_{sat})}{T_{cold} - T_{sat}(p_{sat})}\right)} \qquad \text{[IV-7]}$$

As was the local fouling factor, the global fouling factor is defined using the reduction in the overall heat transfer coefficient:

$$R_f'' = \Delta R'' = R'' - R_0'' = \frac{1}{U} - \frac{1}{U_0} \qquad \text{[IV-8]}$$

The utility of this approach is that all the quantities which appear in the overall heat transfer equation and in the definition of global fouling factor are normally tracked for PWR steam generators. If the local fouling factor is relatively uniform throughout the steam generator, then the global fouling factor is equal to the local fouling factor with some relatively small error, most likely principally due to the neglect of the downcomer subcooling. If the local fouling factor is not relatively uniform, then the global fouling factor is still a legitimate average value of the distribution of local fouling factors, but with a somewhat higher level of uncertainty.

Figures IV-2 and IV-3 illustrate the changes in resistance to heat transfer that occur during fouling. Figure IV-2 shows that the total resistance may increase over steam generator life to the point that the turbine throttle valves must be completely opened in order to lower the steam generator pressure and saturation temperature so that a large enough LMTD exists to transfer 100% thermal power. Further increases in resistance necessitate significant loss of electrical output unless remedial secondary cycle modifications are instituted. Figure IV-3 shows how the temperature difference from the primary coolant to secondary fluid must increase with fouling.

The extra resistance to heat transfer due to the presence of tube deposits can be quantified using a fouling factor analysis. However, the following issues must be considered when using the fouling factor methodology on a PWR steam generator:

- FOULING FACTOR UNCERTAINTY. The fouling factor calculation may be subject to significant measurement error due mainly to the uncertainties in the primary temperatures, feedwater flow rate, and steam generator pressure. Therefore, a calculated fouling factor should be reported with an uncertainty tolerance.

- SOURCES OF PERFORMANCE DEGRADATION OTHER THAN FOULING. Sources of pressure loss other than fouling must be identified so that they are not attributed to the calculated fouling factor. The sources that are explicitly accounted for by the fouling factor calculation—tube plugging, power increases, and primary temperature decreases—are straightforward to evaluate. Sources that are not usually factored out, such as extra separator/dryer pressure drop, are more difficult to evaluate. Section V and Appendix D provide further details.

- POTENTIAL CHANGES IN BOUNDARY LAYER RESISTANCES. The global fouling factor does not distinguish between resistance due to fouling layers and that due to changes in thermal hydraulics. Therefore, changes in primary tube velocity due to plugging and changes in boiling heat transfer coefficient due to changes in recirculation ratio (change in velocity and quality) could have an effect.

- UNCERTAINTY IN FOULING FACTOR DUE TO NEGLECT OF SUBCOOLING. As discussed above, the fouling factor calculation does not capture the effect of variations in the degree of downcomer subcooling. Changes in subcooling affect the true mean temperature difference as well as the distribution of secondary side heat transfer coefficients.
- PRESENCE OF AN INTEGRAL PREHEATER. Certain issues specific to preheaters (e.g., fouling of the preheater baffle plates, difference in meaning of LMTD, etc.) must be considered before applying the global fouling factor methodology to SGs with preheaters. See Appendix A for further details. Plant C is the only plant in this study with preheaters integral to its SGs.

Design and Actual Measured Thermal-Hydraulic Data

In order to perform the fouling factor calculations, data describing the intended design operating parameters are required to determine a design "baseline" for expected performance. In addition, operating parameters recorded during full-power operation are required to calculate the actual performance, which can then be compared to the predicted design baseline performance, or to the beginning-of-life actual performance, to generate a fouling factor.*

Design Data

The relevant thermal-hydraulic design data used for each of the five plants are used to develop a baseline for the fouling factor and are summarized in Table IV-1. Note the following comparisons:

- Design primary temperatures are all similar. T_{hot} values span a narrow range between 610°F to 626°F.
- Design steam temperatures range from 520°F up to 557°F.
- Design average heat fluxes are within 15%; four of the five designs are within 2%. (The Model E2 SGs in Plant C have a smaller average heat flux.)
- Heat-transfer area is similar for three of the five plants (about 50,000 ft^2), while Plants C and E are significantly larger (68,000 and 104,000 ft^2, respectively).

Measured Operating Data

Data for full-power operation were provided by each of the participating utilities. A brief summary of these data is given here; greater detail is provided in Appendix B.

* It should be noted that the initial startup performance may not match the design baseline. Any such difference that contributes to the fouling factor cannot be attributed to secondary deposits, which do not exist at initial startup.

TIME SPAN OF DATA. For each plant, data were provided for the entire operating history. In some cases, particularly long gaps in the data exist. Notable examples include

- A 1.3-EFPY gap for Plant B between 1983 and 1989
- No data during Cycles 1, 2, and 5 for Plant D (except for several isolated records)

Average data frequencies for the five plants ranged from once per operating week down to about once per operating month. This frequency varied both from plant to plant and also from cycle to cycle for a given plant. Generally, more measurements were available for recent operation.

TYPES OF MEASURED DATA. The various measured quantities obtained from the plants in this study in order to calculate the global fouling factor history are summarized below. Further detail is provided in Appendix B.

- Outage Dates and Effective Full-Power Years (EFPY). These are used to calculate effective operating time, which is used as an independent variable in place of calendar time.
- Number of Plugged Tubes. This information was collected for each outage so that heat-transfer area could be calculated as a function of operating time.
- Primary Temperatures (T_{hot}, T_{cold}, and/or T_{ave}). Where possible, narrow-range measurements, which are more accurate than wide-range measurements, are used in the calculations.
- Feedwater Temperature and Pressure. In some cases, the design feedwater pressure is used in place of unavailable measured values because the calculated fouling factor is weakly dependent on this variable.
- Feedwater Mass Flow Rate. When possible, corrections are applied for known errors such as venturi fouling or venturi bypass flow.
- Steam Mass Flow Rate. This variable is redundant if feedwater mass flow rate and blowdown flow rate are known. However, it may be useful for detecting inconsistencies in the measurements caused, for example, by venturi fouling. This item was provided for several of the plants in the study.
- Blowdown Flow Rate. Since blowdown is typically ≤1% of the feedwater flow rate, errors in the blowdown rate do not have a significant impact on the calculated fouling factor. As a result, for a couple of the plants, assumptions are made as necessary (e.g., unavailable early blowdown flow rates were assumed equal to the average rate recorded during recent cycles).
- SG Steam Pressure. If more than one measurement per loop was reported, the average is used in the fouling factor calculations. As required, corrections to the reported values include 1) conversion from gage to absolute (ΔP = 14.7 psi), 2) an addition for pressure drop between the average bundle pressure and the SG dome (or outlet), and 3) an addition for the pressure drop between the SG dome and the measurement location (often downstream on the main steam piping). Note that #2 includes any additional pressure drop attributable to fouled moisture separators and dryers if known.

- Calorimetric Thermal Power. This quantity can be used as an alternate basis for computing the fouling factor and may therefore be useful for discerning the effects of measurements errors (e.g., venturi fouling).

Graphical representations for histories of the key measured parameters discussed above are provided as part of Appendix B.

Fouling Factor Calculations

With the data summarized above (and discussed in greater detail in Appendix B), the global fouling factor is calculated for the operating history of Plants A, B, C, D, and E. In addition, due to the low fouling factor and thin deposits at Plant C, the global fouling factor is also computed for a sixth plant (Plant F) with information from Reference (20). (Note that the thermal-hydraulic data described above were not available for Plant F for use in this project. Consequently, design values are employed in the calculations. See the end of Appendix B and Appendix C for greater detail.*) Unless otherwise noted, the fouling factor for each plant is computed relative to the design value for the "clean" resistance R_0^*. The details of these calculations for Plants A through E are provided in Appendix C; the most important results (and the results for Plant F) are summarized here.

Measured SG steam pressure and the corresponding calculated global fouling factor are pictured in Figures IV-4 through IV-9 for Plants A through F, respectively. Key features of these plots include the following:

PLANT A – FIGURE IV-4

- Accompanied by a substantial increase in SG pressure (about 30 psi), the fouling factor decreased sharply during the first cycle of operation. This may reflect the development of heat-transfer-enhancing deposits on the secondary side of the SG tubes.
- Plant A increased its thermal power rating while the fouling factor was negative, temporarily allowing continued operation at 100% power. A subsequent decrease in performance caused Plant A to operate in the valves-wide-open (VWO) condition, resulting in lost electrical capacity. As expected, the uprate and the beginning of VWO operation do not cause any step changes in the fouling factor. However, the uprate did cause a step decrease of 15 psi in SG pressure, thereby lowering available fouling and plugging margins.

* Note that efforts were made to obtain from the operating utility the SG steam pressure history for early operation not included in Reference (1) (i.e., for operation before 1980). However, this information was not available in the plant archives.

- During the end-of-cycle (EOC) 7 outage, a chemical cleaning of the SG secondary side was performed in each of the four SGs. Upon restart in Cycle 8, the fouling factor exhibits a step increase. This suggests that the deposits removed by the chemical cleaning were in fact beneficial to heat transfer (i.e., responsible for a decrease in the fouling factor). Relatively thin deposits with particular composition and morphology often cause this behavior (see Section III).

- The net change in SG steam pressure and calculated global fouling factor for Plant A since early operation are indicated in Table IV-2, along with the rate of fouling factor increase characterizing 1) the last 3 cycles of operation prior to the chemical cleaning, and 2) operation since the chemical cleaning (part of one cycle).

PLANT B – FIGURE IV-5

- The SG pressure and fouling factor show similar trends as for Plant A.*
  - An initial pressure increase accompanied by a fouling factor decrease over the first cycle of operation.
  - A period of near-zero fouling for several cycles.
  - Increased fouling at a modest rate over the most recent cycles.

  Note, however, that these trends are not as pronounced as at Plant A. For example, the early increase in pressure is approximately 15 psi (compared to 30 psi at Plant A).

- The fouling factor shows perhaps a slight step increase after chemical cleaning. However, this step change is less convincing than the one at Plant A, perhaps because of the frequency of data near the outage of interest.

- The trends listed in the first bullet above, along with the possible step increase in fouling factor after chemical cleaning, are consistent with the presence of heat-transfer-enhancing scale prior to chemical cleaning. However, it should be noted that the data are not definitive. Slightly resistive tube deposits would not necessarily contradict the fouling factor history, particularly in light of the calculated fouling factor, which is slightly positive (see Table IV-2). It should also be noted that the increase in fouling factor following chemical cleaning is consistent with the presence of a thin, resistive deposit layer which was left on the tubes after the cleaning, or re-deposited on the tubes shortly thereafter.

- The net change in SG steam pressure and calculated global fouling factor for Plant B since early operation are indicated in Table IV-2, together with the fouling factor slope characteristic of 1) the last 3 cycles of operation prior to the chemical cleaning, and 2) operation since the chemical cleaning (part of one cycle).

---

* Note that the fouling factor shown in Figure IV-5 reflects a correction for 2°F of primary-temperature error due to hot-leg streaming—see Appendix D for further details.

PLANT C – FIGURE IV-6

- Unlike Plants A and B, Plant C does not show a noticeable decrease in fouling during the first cycle. This suggests that any tube scale that developed early in life had little effect on heat transfer. This conclusion is consistent with 1993 tube scale thickness measurements which averaged less than 0.5 mils. Scale this thin is typically expected to have little effect on heat transfer based on experimental data such as the measurements made at Chalk River Laboratories for DEI and industry data reported by Mitsubishi Heavy Industries (MHI) (17).

- The initial calculated fouling factor is in excess of 100 10^{-6} h-ft^2-°F/BTU, suggesting that the clean thermal resistance of the SGs is larger than the design values would indicate.

- The net change in SG steam pressure and calculated global fouling factor for Plant C since early operation are indicated in Table IV-2, along with the fouling factor slope for the last few EFPY.

- Most of the net increase in fouling has taken place over the last one or two operating cycles, potentially consistent with increasingly resistive secondary deposits.

- From Figure IV-6, there are at least two distinct transients in the fouling factor and SG pressure (at about 2 EFPY and again at 3.9 EFPY). In each case, the fouling factor increases by about 50 10^{-6} h-ft^2-°F/BTU and then decreases by the same amount, while SG pressure decreases by about 15-20 psi before recovering.* According to the utility, similar transients (at least in SG pressure, which is monitored) occur after each outage or trip, although such transients are not readily apparent from the figure due to the low frequency of available data.

  One possible explanation for these transients is partial tube scale exfoliation, which can create a steam-blanketed gap between the tube wall and the deposit, reducing heat transfer. Differences in thermal expansion could cause partial exfoliation to occur during plant transients. Subsequent total exfoliation a short time after restart would be responsible for the pressure recovery. Approximate calculations indicate that partial exfoliation covering less than 5% of the tube surface area could be responsible for the magnitude of the observed transients.

  A second possible explanation is fouling of the preheater baffle plates which could cause non-optimal flow distribution exiting through the top and bottom of the preheater, reducing its efficiency. No data are available for Plant C to confirm this possibility. Note that Plant C is the only plant in this study with integral preheaters in its SGs.

---

* Note that the pressure "recovery" associated with the second transient is difficult to see from Figure IV-6 due to the effects of a primary temperature decrease at the beginning of Cycle 7.

PLANT D – FIGURE IV-7

- The lack of early operating data (Cycles 1 and 2) makes it difficult to determine whether the early fouling behavior included a decrease like Plants A and B. As a result, the initial thermal resistance is more uncertain for Plant D than for the other plants.
- Recent fouling (Cycles 6-9) appears to be negligible. Note, however, that the data recorded during Cycles 6-8 are subject to additional uncertainty due to 1) estimated primary temperatures and 2) significant venturi bypass flow (4.5%).*
- The net change in SG steam pressure and calculated global fouling factor for Plant D since early operation are indicated in Table IV-2. Also shown is the approximate fouling rate over the last several EFPY. The uncertainty associated with all of these values is appreciably greater than for the other plants for the reasons discussed earlier.
- The increase in fouling factor is potentially consistent with slightly to moderately resistive secondary deposits. (If, however, lack of early data is concealing an early decrease in fouling factor such as occurred at Plant A, then the current effect of secondary deposits might be closer to zero.)

PLANT E – FIGURE IV-8

- Like Plant A, Plant E exhibited a significant decrease in fouling factor (and a concomitant increase in SG pressure) during early operation, consistent with heat-transfer-enhancing tube scale.
- Unlike at any of the previous plants, the Plant E fouling factor rapidly increased starting near the end of Cycle 2. The increase continued until a recent chemical cleaning.
- The net change in SG steam pressure and calculated global fouling factor for Plant E since early operation are indicated in Table IV-2, together with the average fouling rate since approximately Cycle 2. Note that this rate is significantly greater than for the other plants.
- This level of fouling far exceeds that calculated for any of Plants A through D and is consistent with highly resistive secondary deposits.
- A recent chemical cleaning of Plant E's SGs resulted in a net steam pressure increase of 61 psi due to deposit removal.† This substantial increase is consistent with the large calculated fouling factor prior to the cleaning.

PLANT F – FIGURE IV-9

- The computed fouling factor, +190 10^{-6} h-ft^2-°F/BTU, is comparable to that computed for Plant E (+172 10^{-6}).

---

* The venturi bypass error has been accounted for in the fouling factor calculations, but the error nevertheless increases the uncertainty of the results.

† This total is adjusted for a 6-psi decrease due to newly plugged tubes. The observed increase was 55 psi.

- For the operating period examined, the fouling factor increased significantly (over 100 10^{-6} h-ft^2-°F/BTU). As the bottom graph in Figure IV-9 indicates, the increase in fouling factor was marked by four or five large transient increases that occurred following refueling outages. Recovery of the transient during subsequent operation was typically incomplete (i.e., the transient resulted in a net increase).
- For the same period of operation, 6.5 EFPY to 10 EFPY, Plants E and F experienced similar increases in fouling factor (93 10^{-6} versus 87 10^{-6} h-ft^2-°F/BTU).
- Data for early operation at Plant F were unavailable; hence it is not possible to determine if incipient scale enhanced heat transfer.
- Table IV-2 indicates the net change in SG steam pressure and calculated global fouling factor as well as the average fouling rate for Plant F over the time span covered by the available data.

EXPERIMENTAL FOULING FACTORS MEASURED FOR PLANT F. In addition to the calculated global fouling factor discussed above, a good estimate of the Plant-F fouling factor as of 1990 can be obtained from the heat-transfer experiments documented in References (1), (27), and (28). These references document the results of heat transfer tests of the U-bend portion of a tube removed from a Plant-F SG both before and after cleaning by an EPRI/SGOG process. The results cited in (1) are summarized in the second column from the right in Table IV-3; the average fouling factor calculated there is 247 10^{-6} h-ft^2-°F/BTU.* Note, however, that these values reflect clean and fouled tube segments experiencing different heat fluxes. For an actual SG at full power, the heat flux across the tubes remains nearly constant regardless of the deposit layer. As a result, the values in (1) are adjusted to reflect the difference in heat flux using the Thom correlation (see, for example, p. 12-44 of Reference (24)), which is given by

$$\Delta T = \frac{0.072}{e^{p/1260}}\sqrt{q''} \qquad \text{[IV-9]}$$

where ΔT is the temperature difference between the saturation temperature and the tube surface (in °F), p is fluid pressure (in psia), and q'' is heat flux (in BTU/h-ft^2). Noting that $\Delta T = q''/h_{boil}$, the heat-transfer coefficient for boiling can be expressed as

$$h_{boil} = \frac{1}{0.072}e^{p/1260}\sqrt{q''} \qquad \text{[IV-10]}$$

The left side of Table IV-3 lists the heat-transfer rates and pressures for the heat-transfer tests on both clean and fouled tubes described in (1). These inputs are used to calculate the ratio of

* The values listed in Table IV-3 do not match those in Table 4-6 of Reference (1) exactly because of the area ratio correction used in (1). However, this factor is nearly 1 in all cases and is therefore neglected here.

boiling heat-transfer coefficient for each fouled tube to the corresponding coefficient for the cleaned tube. This ratio is then multiplied by the overall heat-transfer coefficient measured for the clean tubes to adjust for the higher heat fluxes in those tests. The resulting adjusted boiling heat-transfer coefficient is used with the measured fouled values to compute an adjusted fouling factor, shown in the last column of Table IV-3. The adjusted values average approximately 225 10^{-6} h-ft^2-°F/BTU (i.e., 25 10^{-6} lower than the values cited in (1)). The following qualifications should be noted with regard to this result:

- The heat-transfer tests reflect deposits in the U-bend region. These deposits are probably somewhat thicker and higher in density and thermal resistance than the deposits present in the remainder of the tube bundle. As a result, the fouling factor in Table IV-3 is likely to be slightly higher than the average bundle fouling factor.
- The secondary mass flow rate used in the tests was not necessarily typical of the actual Plant-F SGs.

Even in spite of the qualifications, the fouling factor suggested by the heat-transfer tests (225 10^{-6}) is reasonably consistent with the calculated fouling factor based on the steam pressure history (190 10^{-6} versus design thermal resistance) and with the best-estimate calculation based on deposit properties (192 10^{-6} h-ft^2-°F/BTU per Table III-9).

Fouling Factor Uncertainty Analyses

Because the calculated fouling factors discussed above rely on measured values that have an inherent degree of uncertainty, it is necessary to compute the resultant fouling factor uncertainty. The required inputs and the details of the calculations are presented in Appendix C. The results are summarized in the Table IV-4. For all of the plants in this study, the most important variables contributing to the calculated uncertainties are SG steam pressure, feedwater mass flow rate, and primary temperatures (especially T_{cold}). See Appendix C for further details.

Comparison of Global Fouling Factors and Independent Thermal-Resistance Estimates Based on Deposit Characterization

In Section III, estimates of thermal resistance based on observed deposit properties were presented. Those estimates are independent of the calculated fouling factors discussed in this section. Table IV-5 compares the estimates based on deposit characteristics with the calculated fouling factors discussed earlier in this section. All of the estimates agree within the calculated and estimated tolerances. Note in particular that both methods suggest heat-transfer enhancing scale at Plant A and very resistive scale at Plants E and F. The agreement provides added confidence in the global fouling factor calculations.

Table IV-1. Design SG Heat-Transfer Parameters (per SG)

Parameter	Units	Plant A	Plant B	Plant C	Plant D	Plant E
T_{hot}	°F	620	609.7	626.1	610.8	611
T_{cold}	°F	557	546.7	559.7	544.7	553
Steam Generator Dome Pressure	psia	1000.0	857.0	1100.0	815.0	900.0
Steam Generator Average Bundle Pressure	psia	1011.5	865.0	1107.1	823.0	910.0
Saturation Temp. for Avg. Bundle Pressure	°F	546.1	527.3	557.1	520.4	533.3
Thermal Power (per SG)	MWt	895	856	954	856	1705
Thermal Power (per SG)	BTU/h	3.053E+09	2.920E+09	3.256E+09	2.920E+09	5.818E+09
Heat Transfer Area (OD)	ft^2	55,000	51,500	68,000	51,500	104,130
Average Heat Flux (Based on OD Area)	BTU/h-ft^2	55,509	56,698	47,882	56,698	55,869
Design Plugging Margin	–	15%	0%	0%	10%	10%
Number of Tubes (per SG)	–	5626	3388	4864	3388	9350
Feedwater Temperature	°F	446.0	434.5	440.0	432.8	445.0
Feedwater Pressure	psia	1025	876	1129	836	936
Secondary Mass Flow Rate	lb_m/h	3.963E+06	3.749E+06	4.240E+06	3.709E+06	7.619E+06
Blowdown Flow Rate	lb_m/h	31,250	20,000	39,000	0	0

Table IV-2. Pressure and Fouling Trends Compared to Early Operation

Plant	Time	Δ EFPY	Net Change in SG Pressure (psi differential)	Net Change in Fouling Factor (10^{-6} h-ft^2-°F/BTU)	Fouling Factor Slope (10^{-6} h-ft^2-°F/BTU/EFPY)
A	Pre-Chemical Cleaning (1995)	8.6	-17	-28	+9
	Recently (mid-1996)	9.5	-28	-5	-15
B	Pre-Chemical Cleaning (1995)	7.5	-25	+21	+14
	Recently (mid-1996)	7.9	-36	+42	0
C	Recently (mid-1996)	5.0	-63	+30	+9
D	Recently (mid-1996)	8.0	-30	+51	+6
E	Pre-Chemical Cleaning (1996)	10.1	-77	+172	+23
F	Operation in 1990 vs. 1980	9.1	-67	+117	+16

Table IV-3. Summary of Ginna Heat-Transfer Thermal Resistance Experiments (1)

	Test Heat Flux		Test Steam Pressure		Ratio of Boiling Coeff.[1]	Overall Heat-Transfer Coefficient[1]			Fouling Factor	
EPRI Test Nos.	Q_{clean} (BTU/h)	Q_{foul} (BTU/h)	P_{clean} (psia)	P_{foul} (psia)	$h_{boil,f}/h_{boil,c}$ –	$h_{o,clean}$ (EPRI)[2] (BTU/h-ft^2-°F)	$h_{o,clean}$ (adj.)[3] (BTU/h-ft^2-°F)	$h_{o,foul}$ (BTU/h-ft^2-°F)	R_f" (EPRI) (h-ft^2-°F/BTU)	R_f" (adj.)[3] (h-ft^2-°F/BTU)
GNHT 18 and 35	28088	21878	788	778	0.876	6841.8	5990.6	2469.4	258.8	238.0
GNHT 21 and 36	43533	33196	773	772	0.873	8673.2	7567.8	2929.0	226.1	209.3
GNHT 22 and 37	54016	39750	776	778	0.859	9218.0	7920.2	2822.5	245.8	228.0
GNHT 23 and 38	61337	46562	788	781	0.866	10015.0	8677.5	3100.0	222.7	207.3
GNHT 25 and 42	27338	21148	778	783	0.883	4555.9	4023.0	2329.4	209.8	180.7
GNHT 26 and 44	38789	29960	785	778	0.874	5457.3	4769.6	2280.6	255.2	228.8
GNHT 28 and 45	51337	37336	779	782	0.855	6684.3	5714.0	2359.0	274.3	248.9
GNHT 29 and 47	58824	42723	784	785	0.853	7526.5	6419.4	2415.9	281.1	258.1
								Average	**246.7**	**224.9**

NOTES

1. Calculated using the Thom correlation.
2. The EPRI value does not include the area correction factor discussed in Reference (1).
3. These values reflect an adjustment for unequal heat fluxes in the clean and fouled tubes using the Thom correlation.

Table IV-4. Computed Fouling Factors and Uncertainties (10^{-6} h-ft^2-°F/BTU)

Value	Plant A		Plant B		Plant C	Plant D	Plant E	Plant F
	Before CC	Recent Oper.	Before CC	Recent Oper.	Recent Oper.	Recent Oper.	Recent Oper.	1991
Best Estimate	-28	-5	+21	+42	+30	+51	+172	+190
Computed Uncertainty	±25	±25	±24	±24	±96	±89	±48	–
Lower-Bound Estimate	-53	-30	-3	+18	-66	-38	+124	–
Upper-Bound Estimate	-3	+20	+45	+66	+126	+140	+220	–

Table IV-5. Comparison of Predicted Fouling Factors Based on Deposit Properties and Calculated Fouling Factors Based on T/H Data

Unit	Plant A		Plant B		Plant C	Plant D	Plant E	Plant F
Time	3/95	4/96	9/95	5/96	6/96	6/95	2/95	3/91
Operating Time (EFPY)	8.6	9.5	7.5	7.8	5.0	8.0	8.6	15.6
FF Based on Deposit Characterization (10^{-6} h-ft^2-°F/BTU)	-15	10†	44	10†	0	65	185	192
FF Based on T/H Data (10^{-6} h-ft^2-°F/BTU)	-28	-5	21	42	30	51	172	117*

*Does not reflect fouling due to deposits between 1970 and 1980 (i.e., the first 6.5 EFPY of operation).

†Based on postulated re-deposition of a thin layer of resistive scale—no specific scale data available.

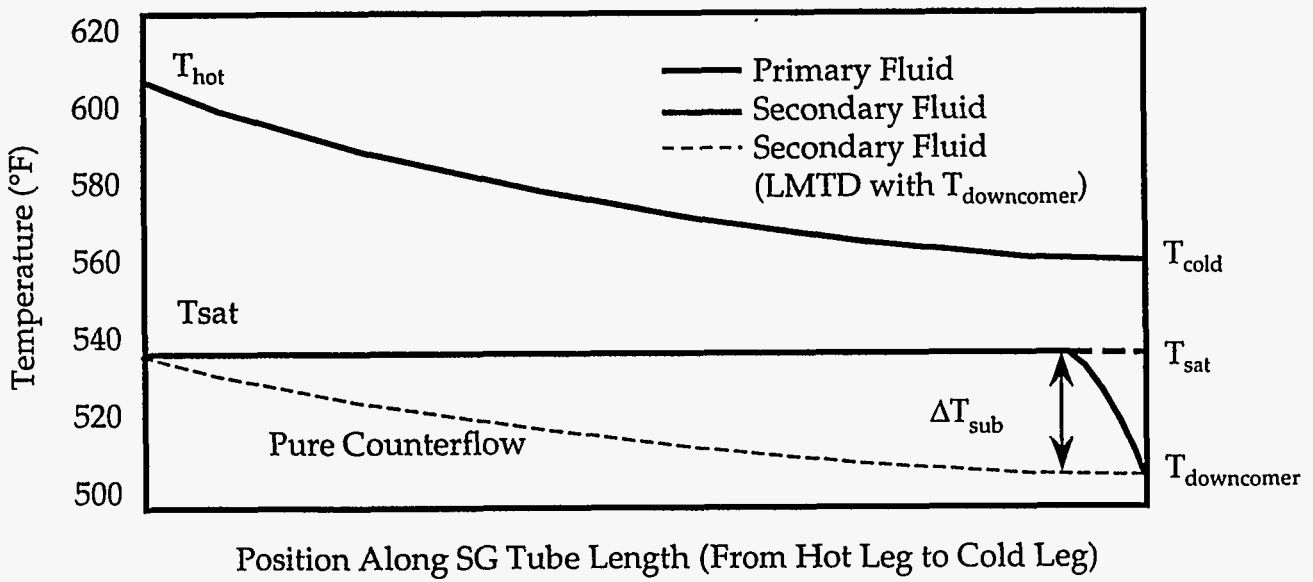

Figure IV-1. Steam Generator Temperature Distribution Assumed in Fouling Factor Calculations

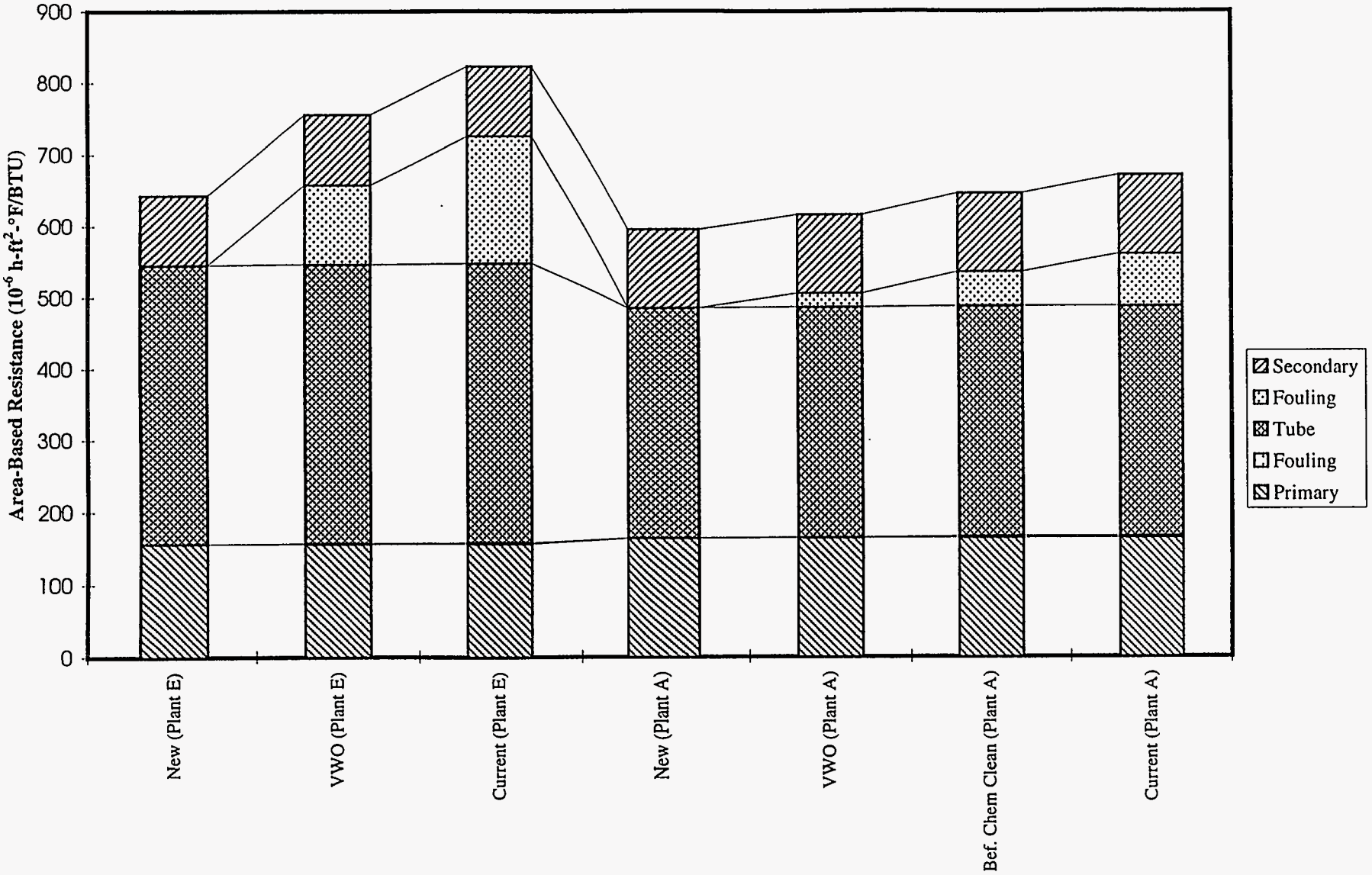

Figure IV-2. Theoretical Components of Heat Transfer Resistance

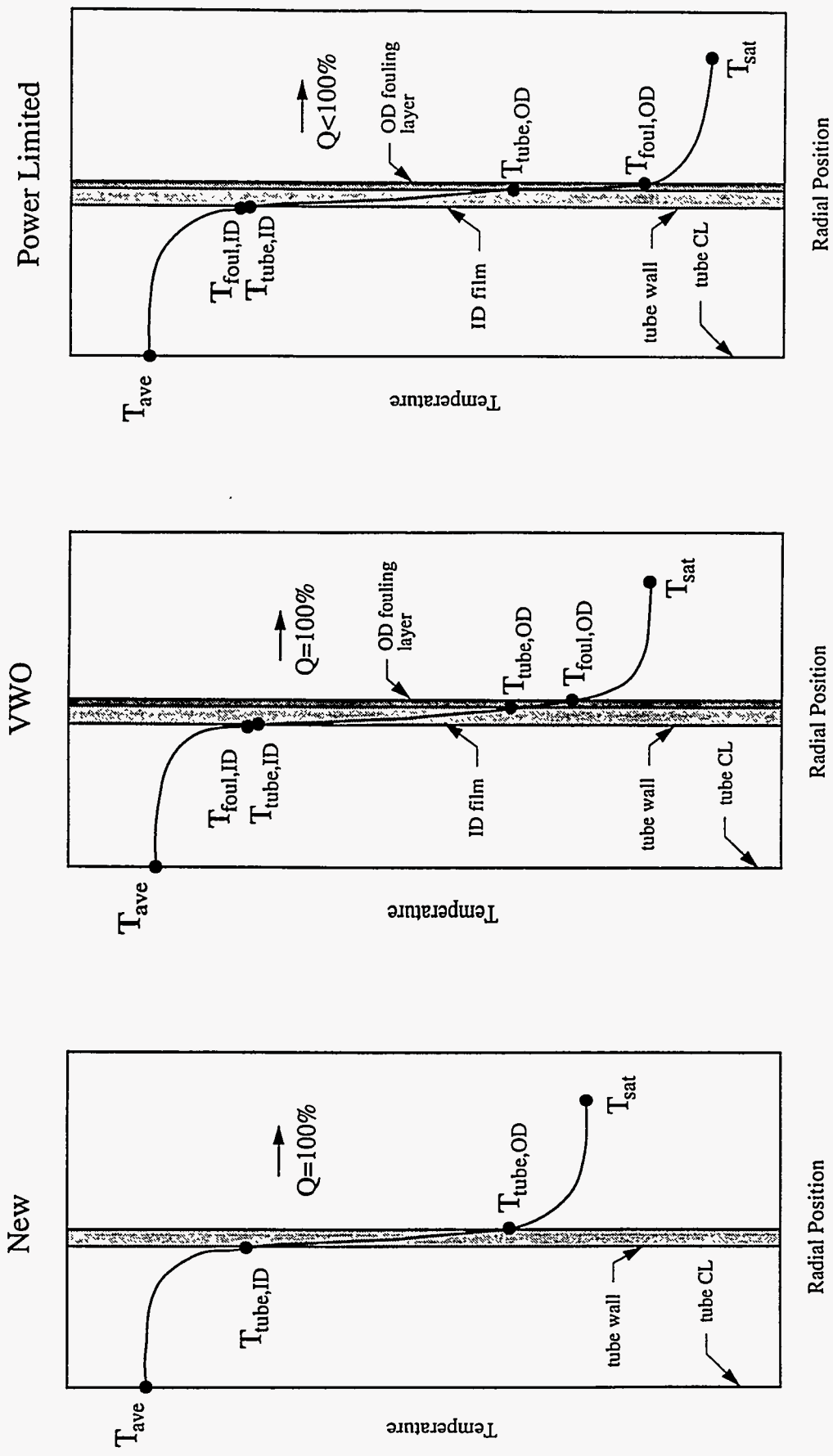

Figure IV-3. Change in Temperature Profile from Primary to Secondary Fluids Due to Fouling

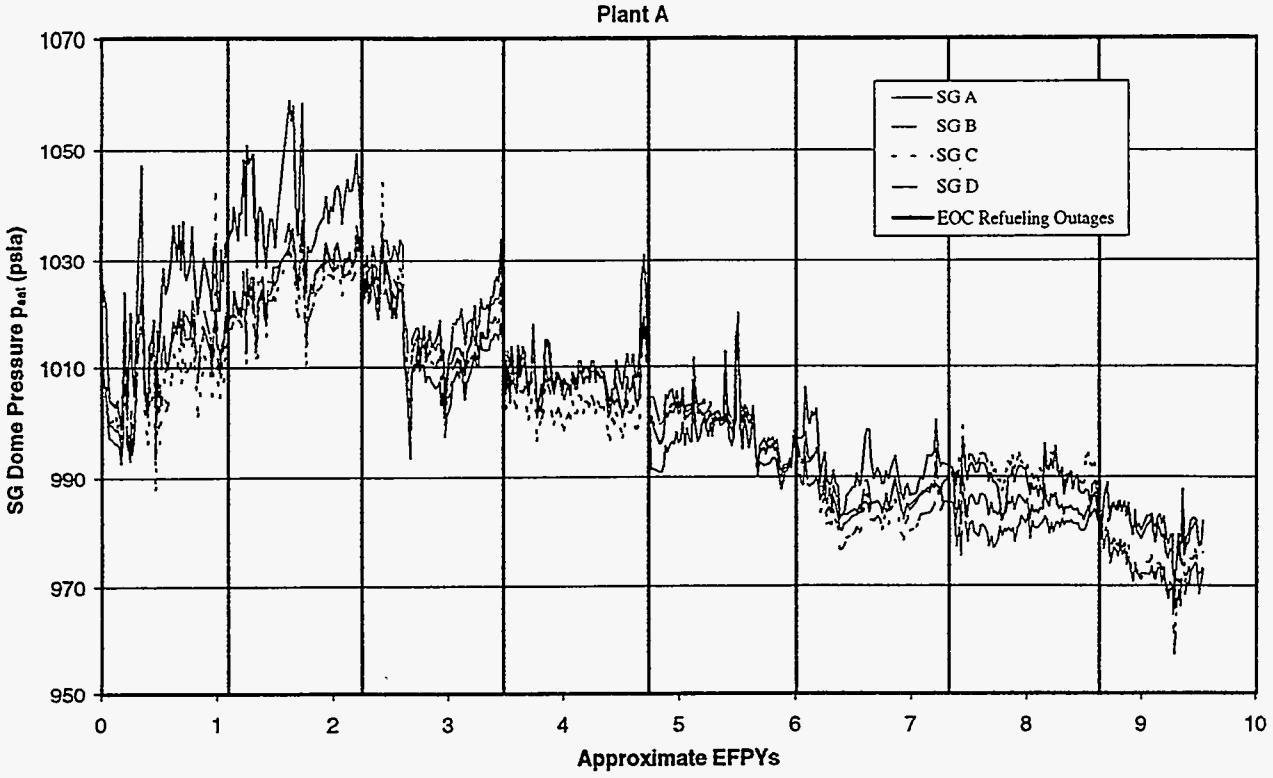

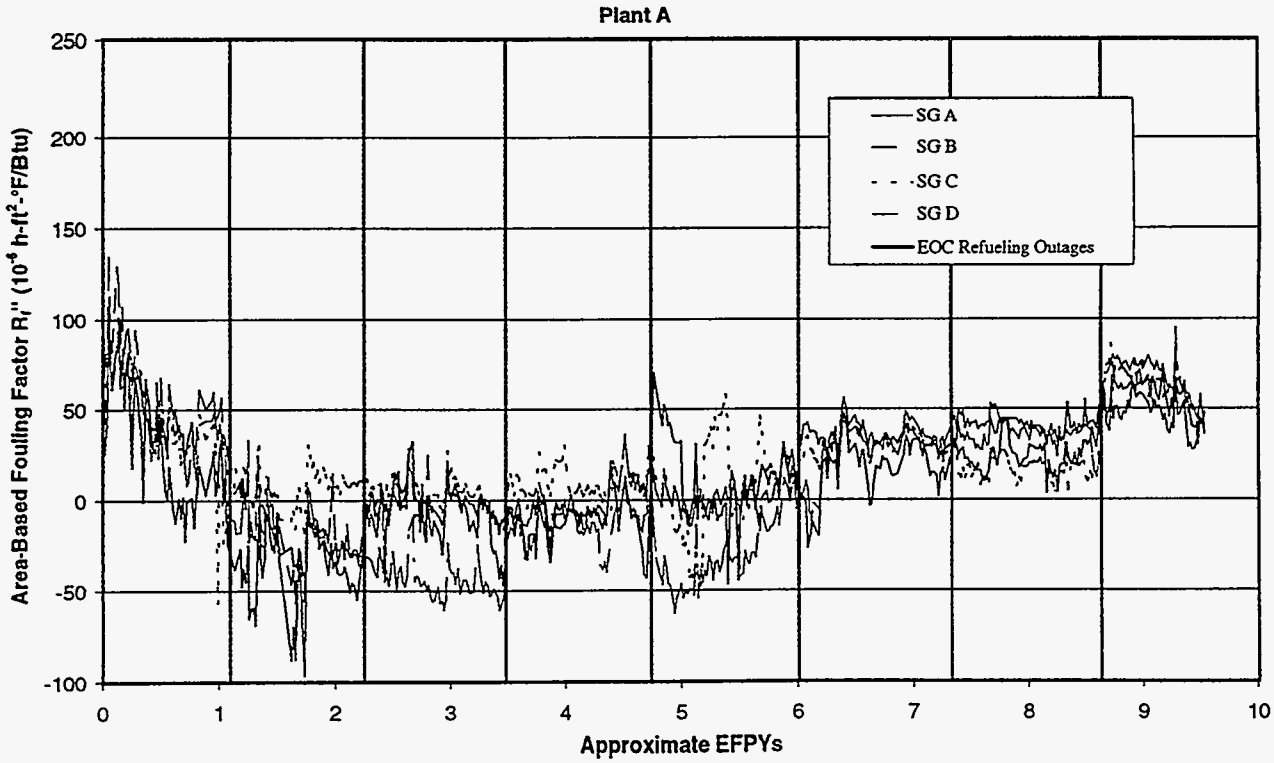

Figure IV-4. Historical SG Steam Pressure and Global Fouling Factor at Plant A

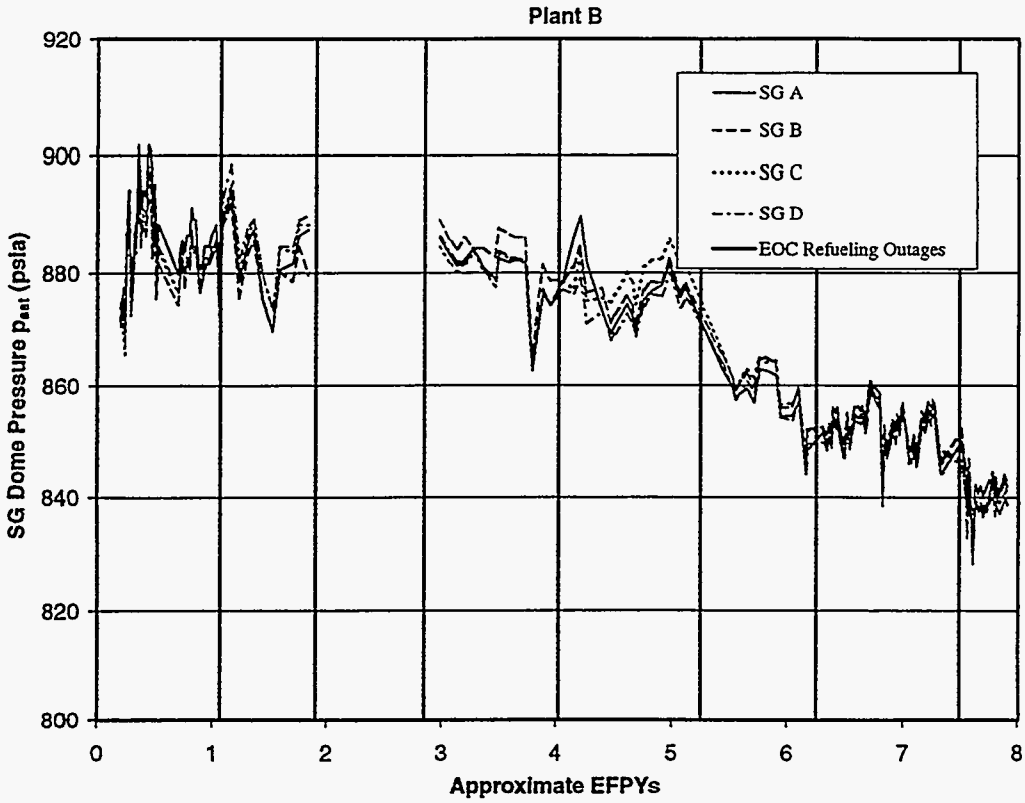

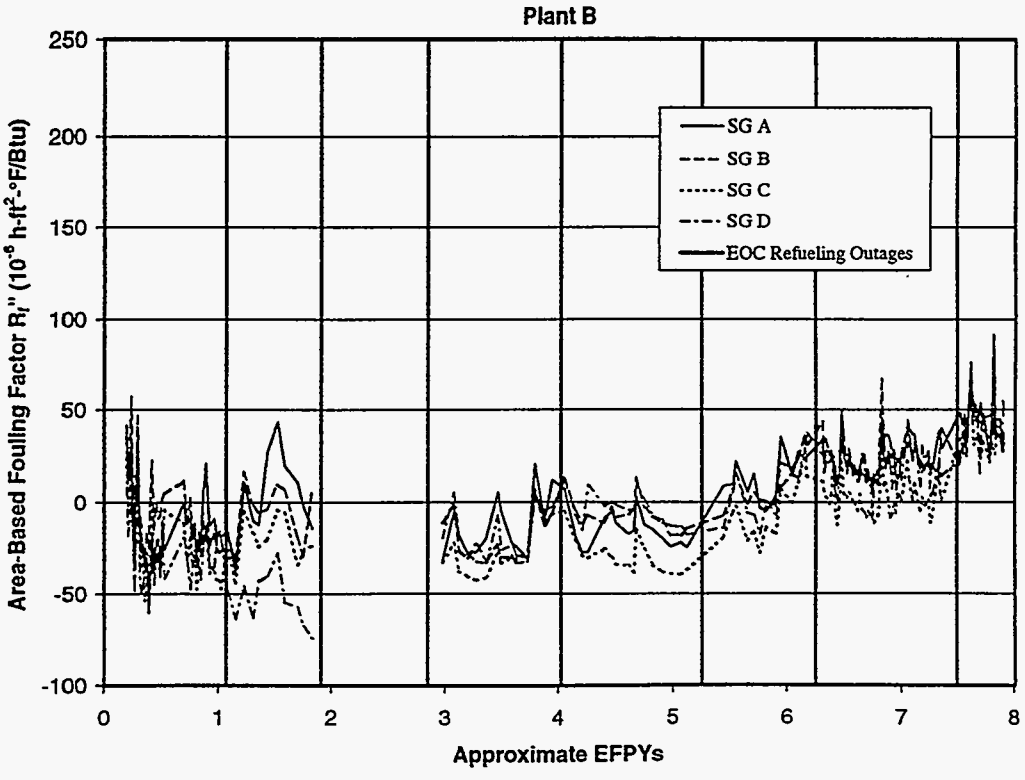

Figure IV-5. Historical SG Steam Pressure and Global Fouling Factor at Plant B

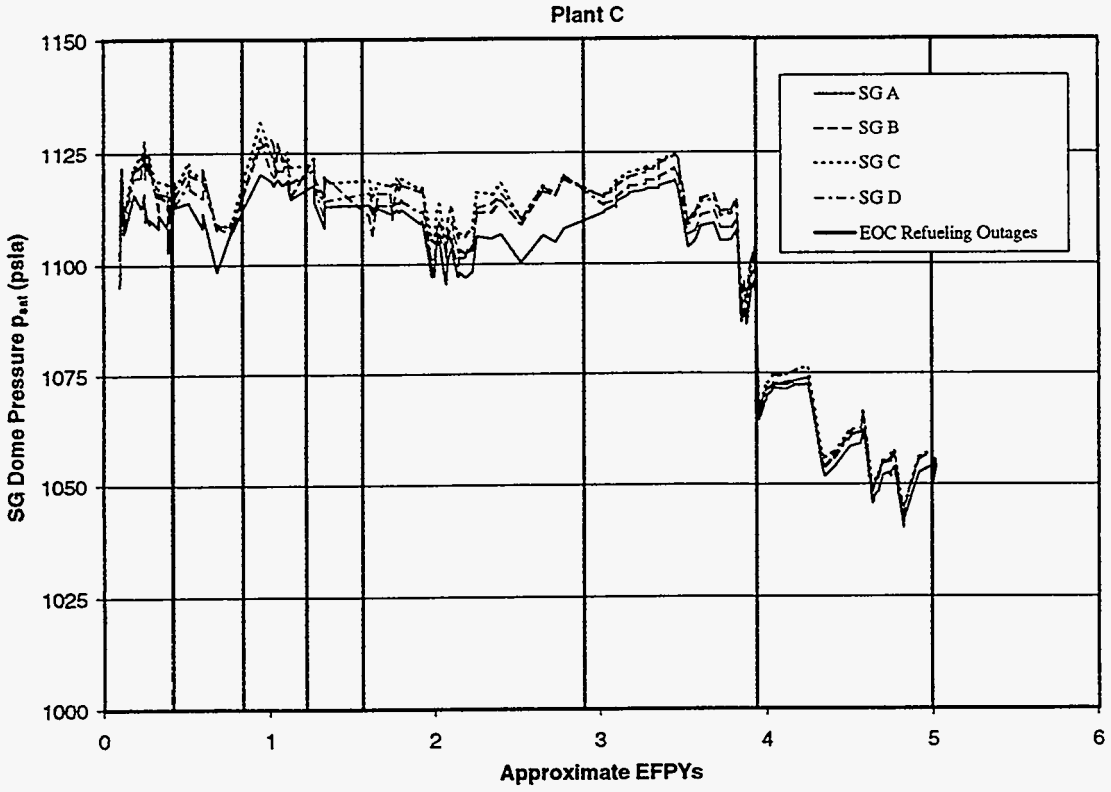

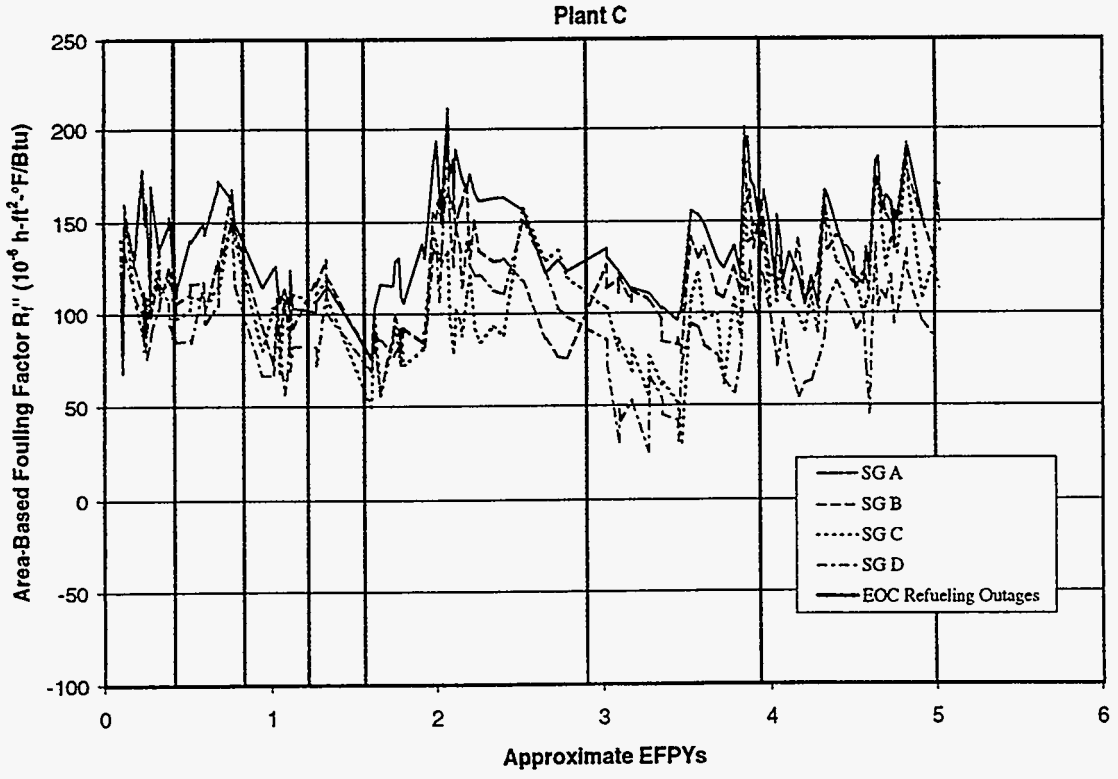

Figure IV-6. Historical SG Steam Pressure and Global Fouling Factor at Plant C

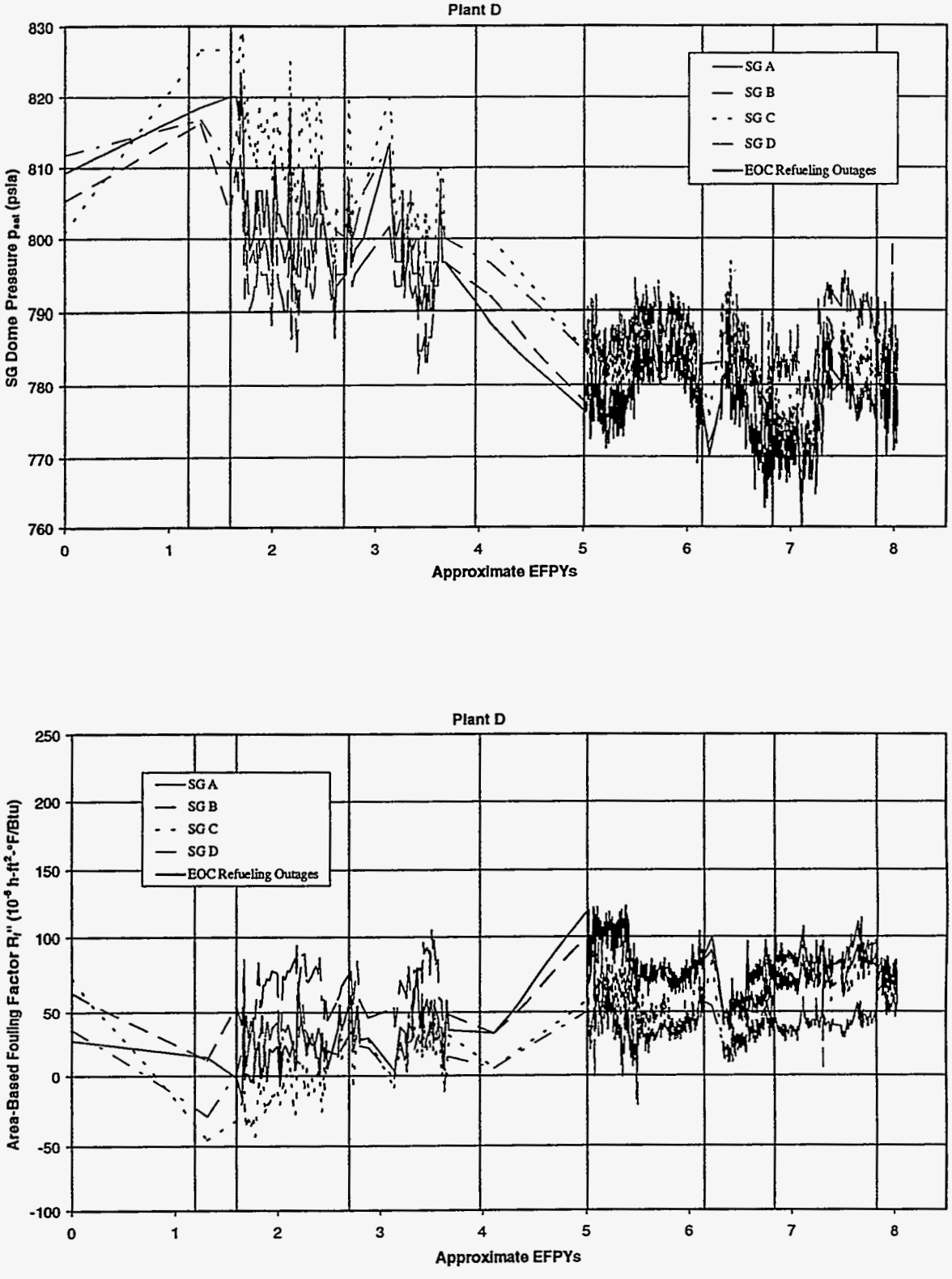

Figure IV-7. Historical SG Steam Pressure and Global Fouling Factor at Plant D

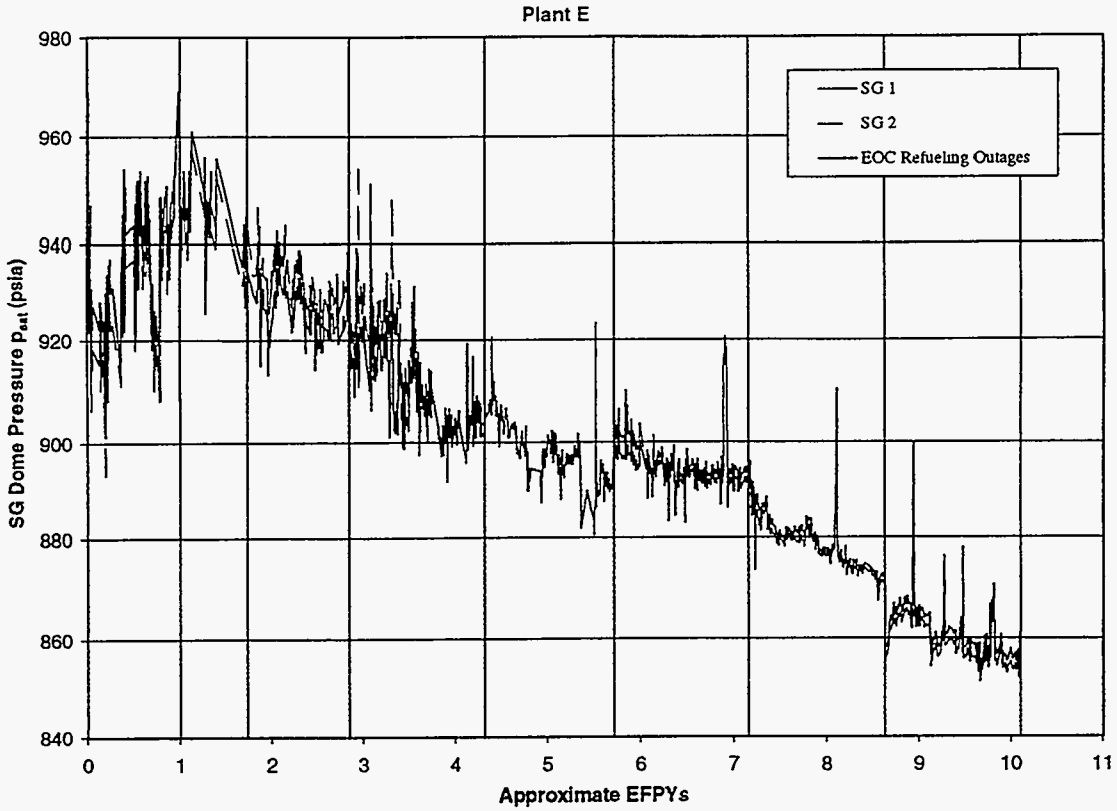

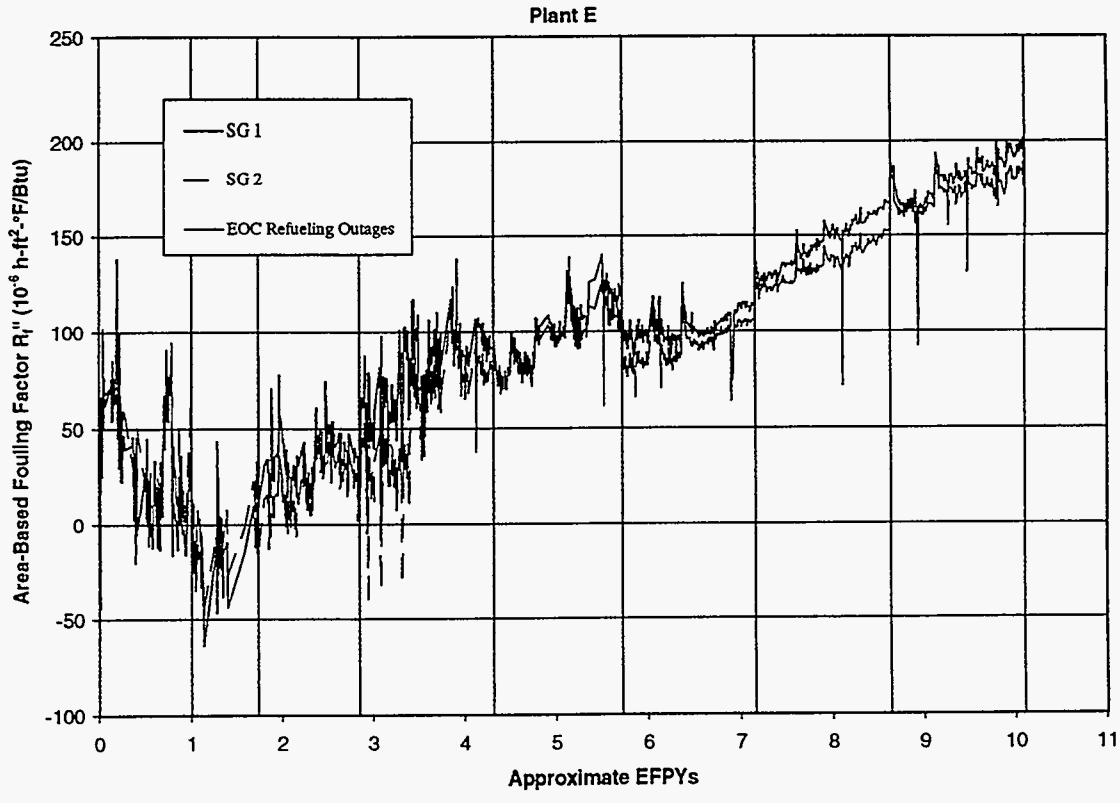

Figure IV-8. Historical SG Steam Pressure and Global Fouling Factor at Plant E

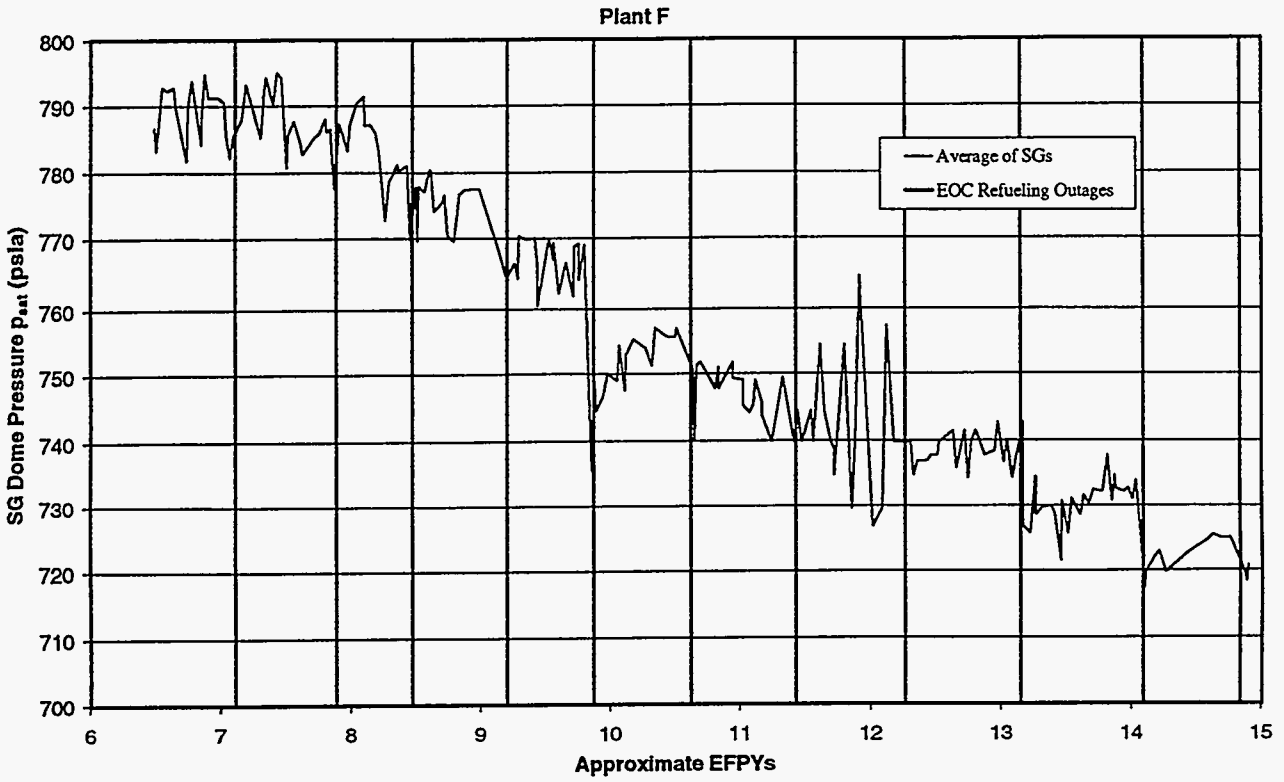

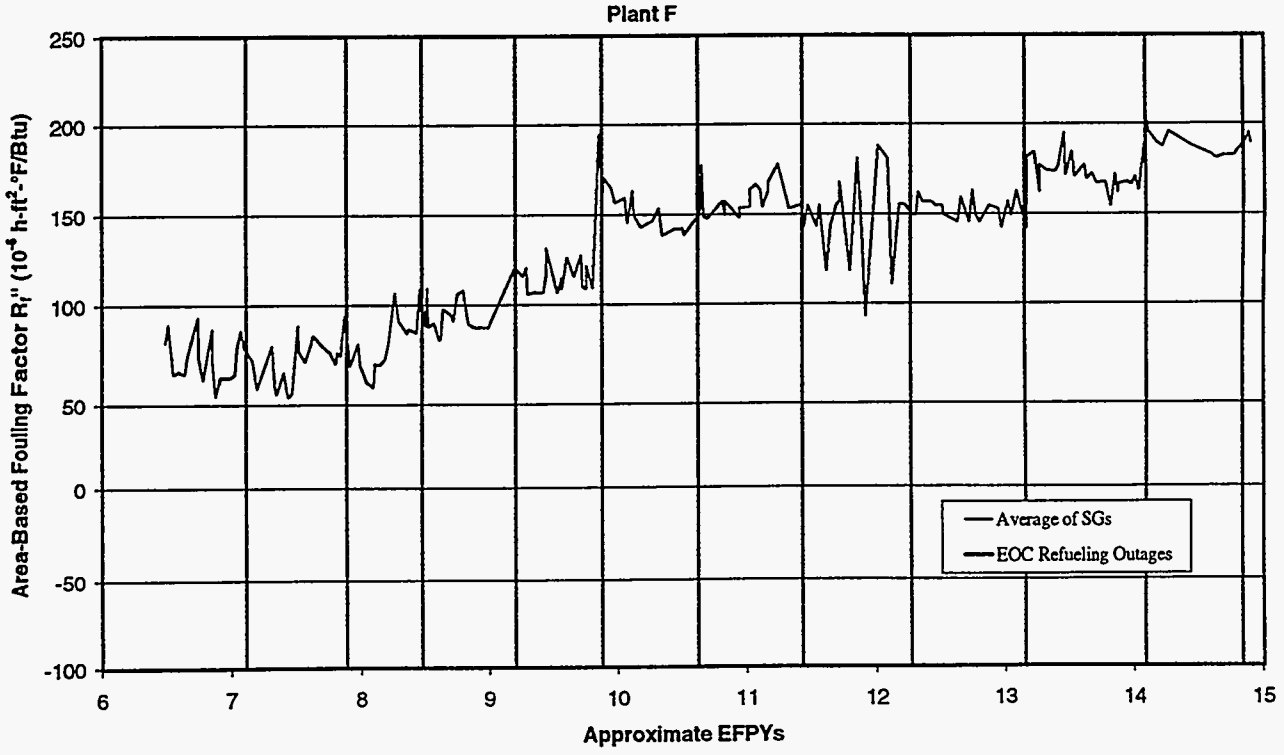

Figure IV-9. Historical SG Steam Pressure and Global Fouling Factor at Plant F

V. CAUSES OF SG STEAM PRESSURE LOSS IN FIVE US PLANTS

The fouling factor methodology detailed in Section IV adjusts for changes in primary temperatures, thermal power, and heat-transfer area (e.g., plugged tubes). In other words, changes in these variables, if they are known, will not contribute to an increasing (or decreasing) fouling factor.* However, there are numerous other possible causes of SG pressure loss which are not accounted for by the fouling factor. These other causes need to be evaluated before any calculated level of fouling can be attributed to secondary deposits. This section summarizes the results of these evaluations for the five plants examined in this study. A more complete discussion is provided in Appendix D.

Causes of pressure loss in SGs can be divided into five broad categories:

- *CHANGES IN FOULING FACTOR VARIABLES.* As indicated above, the fouling factor by its nature accounts for variations in T_{hot}, T_{cold}, A, and Q. Pressure losses caused by these changes are unrelated to primary or secondary tube fouling. The sensitivity of SG pressure to each variable for each plant in this study was calculated in order to attribute the proper amount of pressure decrease to changes in each variable. These sensitivities were computed with the aid of Eq. IV-7. The results are documented in Appendix D; see Tables D-1 through D-5 for a complete summary of the plant-specific numeric results. The most important pressure losses attributable to this category (compared to early operation) for the plants in this study are as follows (all are for recent operation).

  PLANT A
  - Primary temperature decrease: 3 psi
  - Power uprate of 4.5%: 15 psi

  PLANT B
  - Tube plugging: 4 psi before CC

  PLANT C
  - Primary temperature decrease: 52 psi

  PLANT D
  - Tube plugging: 10 psi
  - Primary temperature decrease: 6 psi

  PLANT E
  - Tube plugging: 12 psi
  - Primary temperature decrease: -5 psi (increase in temp.)

* Note, though, that the fouling factor methodology does not adjust for second-order effects such as those due to changes in fluid property values with temperature.

- *SOURCES THAT AFFECT INITIAL PERFORMANCE VS. IDEAL DESIGN PERFORMANCE.* These include pre-service tube plugging, variation in primary temperatures or primary fluid velocity compared to the design values, and variations of tube wall thickness and tube metal thermal conductivity from the nominal values. These causes cannot account for an observed pressure decrease during the operating history of the plant, although they can result in poor initial performance and can permanently reduce available steam pressure margin. See Appendix D for details.

- *SOURCES NOT DUE TO DEPOSITS WITHIN THE BUNDLE WHICH ARE CAPTURED BY THE FOULING FACTOR.* These can include the following; detailed plant-specific discussions are presented in Appendix D.

  - Uncertainty in SG pressure measurements. For the plants in this study, this quantity is about ±5 to ±8 psi.

  - Added pressure drop across moisture separators and dryers.

  - Error in applied primary temperature due to

    - T_{ave} measurement error.

    - Hot-leg streaming. This phenomenon can affect T_{ave}-controlled plants (e.g., Plants A through D). T_{cold}-controlled plants (e.g., Plant E) are not subject to hot-leg streaming because T_{hot} is not used in the primary temperature control scheme. Detailed discussions for each plant are provided in Appendix D.

    - Divider-plate leakage. This consists of primary coolant "short-circuiting" the SG by leaking through the divider separating the inlet and outlet sides of the primary channel head. Although noted in a number of Canadian heavy-water plants with bolted divider plates, this problem is not believed to be relevant to US plants which have welded connections.

- *MINOR CONTRIBUTORS.* These include

  - Changes in performance of other secondary-cycle equipment (turbines, condensers, moisture separator reheaters, feedwater heaters, etc.). This effect was empirically evaluated for the plants in this study by observing historical changes in feedwater temperature. In short, pressure loss due to this cause was determined to be small for all plants. See Appendix D for further details.

  - Turbine back-pressure. This can only be a factor if the plant is operating in the VWO condition (Plant A and Plant E prior to chemical cleaning). In this case, changes in the secondary system that cause a decrease in steam admission flow rate for a given high-pressure turbine inlet pressure would precipitate additional loss of electrical generating capacity. See Appendix D for further detail.

- *PRIMARY AND SECONDARY FOULING.* As discussed in Section III, corrosion deposits on SG tube surfaces, particularly the secondary side, can cause a wide range of effects on heat transfer. Depending on the composition and morphology of secondary deposits, anywhere from a slight enhancement in heat transfer to a large increase in thermal resistance can result.

Based on the analyses presented in this section (and in greater detail in Appendix D), the SG steam pressure losses attributable to each cause for Plants A through F since early operation are summarized in Table V-1 for one or more times in the plants' operating histories. The bottom of the table indicates how the sum of best-estimate losses for each individual cause for each plant compares with the actual observed total loss. The "balance" line reflects

- Any errors in the pressure losses listed in the table. All values are believed to be well known with relatively little associated uncertainty (i.e., less than ±2 psi) except for hot-leg streaming and additional separator/dryer pressure drop.* The added uncertainty associated with these causes is estimated to be about ±5 psi.
- The effects of primary and secondary tube deposits. As indicated in Section III and Appendix E, heat-transfer degradation due to primary deposits is expected to be very small for each plant.

Given the results in Table V-1, we can estimate the effects of secondary-side deposits on heat transfer. The results are presented in the top part of Table V-2, including both upper- and lower-bound estimates. Note that 1 psi is assumed to be caused by primary-side deposits in each plant. In the last row of Table V-2, the pressure loss estimates based on deposit characterization data reported in Table III-9 are repeated for comparative purposes. The inferred values and predicted values match reasonably well for all of the plants—particularly Plants A and E. Except for Plants B and F, all predicted values fall within the estimated bounds inferred from global fouling data (and even those estimates are not far from one of the bounds). Note that the predictions for Plant B suggest that the scale that formed after chemical cleaning (or was left in place following the cleaning) was less resistive than the scale present before the cleaning, while global fouling data suggest the opposite conclusion. However, the quantities being compared for Plant B are subject to uncertainties of the same order as the differences between them, so this disagreement should not be too heavily emphasized. In addition, note that the observed loss in the top row of Table V-2 for Plant F only captures the effects of operation between 1980 and 1990. Pressure decreases due to the growth of scale between 1970 and 1980 are not included in the 32-psi value.†

---

* For Plant F, the uncertainties are somewhat higher.

† Due to operation on phosphate water chemistry between 1970 and 1974 and the subsequent growth of a scale layer that included thermally resistive calcium hydroxyapatite, it is believed that in fact the pressure loss between 1970 and 1980 is likely to have been significant. In other words, the 32-psi observed loss between 1980 and 1990 is potentially consistent with the predicted pressure loss of 73 psi cited in Section III.

Table V-1. Pressure-Loss Breakdowns – Non-Deposit Causes

Unit	Plant A		Plant B				Plant C	Plant D	Plant E		Plant F†
Year	1995	1996	1989	1990	1995	1996	1996	1995	1995	1996	1990
Operating Time (EFPY)	8.6	9.5	3.0	3.9	7.5	7.8	5.0	8.0	8.6	10.1	9.1
Tube Plugging	1.2	1.6	1.2	1.2	3.6	6.9	1.5	9.6	10.9	11.7	19.3
Power Uprate	15.4	15.4	–	–	–	–	–	–	–	–	–
Primary Temperature Variation	0.8	3.3	-2.9	0.7	0.0	0.7	51.7	6.3	-4.5	-4.5	*2.0*
Hot-Leg Streaming	4.0	4.0	0.0	0.0	14.7	14.7	12.9	-3.1	–	–	0.0
Thermal Power Variation	-3.6	-2.7	-3.7	-3.7	-2.8	-1.9	-0.8	-3.6	-0.7	-0.7	0.0
FW Temperature Variations	-0.7	-3.4	0.0	0.0	0.0	0.0	0.0	0.0	-1.0	-1.4	0.0
Flow Maldistribution in PH	–	–	–	–	–	–	3.0	–	–	–	–
FW Venturi Fouling**	0.0	0.0	0.0	0.0	0.0	0.0	0.0	0.0	0.5	0.5	*10.0*
Additional Separator/Dryer ΔP	4.0	4.0	0.5	0.5	1.0	1.0	3.0	3.0	3.5	4.0	*3.0*
Total Estimated Loss	**21.1**	**22.2**	**-4.9**	**-1.3**	**16.5**	**21.4**	**71.3**	**12.2**	**8.7**	**9.6**	**34.3**
Total Observed Loss	**17.0**	**28.4**	**-4.6**	**0.6**	**25.2**	**36.3**	**62.5**	**30.4**	**60.1**	**77.1**	**67.0***
Balance	**-4.1**	**6.2**	**0.3**	**1.9**	**8.7**	**14.9**	**-8.8**	**18.2**	**51.4**	**67.5**	**32.7**

* Does not reflect any pressure loss due to deposits observed between 1970 and 1980.

** Includes an adjustment for blowdown flow (17).

† Plant-F italicized values per Reference (17).

Table V-2. Estimated Pressure Loss Due to Secondary Deposits Based on Other Causes

Unit	Plant A		Plant B				Plant C	Plant D	Plant E		Plant F
Time	3/95	4/96	1/89	3/90	9/95	5/96	6/96	6/95	2/95	11/96	3/91
Operating Time (EFPY)	8.6	9.5	3.0	3.9	7.5	7.8	5.0	8.0	8.6	10.1	9.1
Best Estimate (psi)	**-5**	**5**	**-1**	**1**	**8**	**14**	**-10**	**17**	**50**	**67**	**32***
Est. Tolerance (psi)	±5	±5	±7	±7	±7	±7	±10	±10	±5	±5	±20
Est. Upper Bound (psi)	0	10	6	8	15	21	0	27	55	72	52*
Est. Lower Bound (psi)	-10	0	-8	-6	1	7	-20	7	45	62	12*
Best-Estimates Based on Deposit Characterization (Table III-10)	**-5**	**4**	**–**	**–**	**16**	**3**	**0**	**22**	**–**	**72**	**73**

*Does not reflect any pressure loss due to deposits observed between 1970 and 1980.

VI. THERMAL-HYDRAULIC ANALYSES FOR FIVE US STEAM GENERATORS

Use of a thermal-hydraulic analysis tool can provide insight into how a spatially varying tube scale thickness distribution impacts SG thermal performance. EPRI provided its ATHOS thermal-hydraulic code for DEI to analyze the SG designs examined for this project. In addition to predicting the basic thermal-hydraulic conditions in the SG, the ATHOS code includes a sludge deposition prediction postprocessor module. This section includes a brief summary of this postprocessor, the thermal-hydraulic results generated for clean conditions at each of the five original SG designs included in this study (using values typical of recent operation), and the results of a sensitivity study investigating the effects of thermal resistance distribution on SG steam pressure.

ATHOS Sludge Deposition Postprocessor

As mentioned above, the ATHOS code used in this analysis includes a sludge potential model implemented as a postprocessor to the thermal-hydraulic code. After an SG flow-field solution is calculated by ATHOS, the resulting thermal-hydraulic parameters can be input to the sludge model. Using these thermal-hydraulic inputs, the sludge model computes a "sludge potential," which is the ratio of calculated deposition rate ($\dot{m}_g$) to calculated reentrainment rate ($\dot{m}_r$). Higher values of this ratio indicate thermal-hydraulic conditions predicted by the model to be favorable to tube scale formation.

The deposition model implemented in ATHOS is the same basic model developed by Beal and Chen (25) and later modified by Keefer (26) to allow a closed-form solution. The sludge deposition model incorporates mathematical descriptions of turbulent deposition, boiling-enhanced deposition, gravitational settling, and reentrainment of deposited particles. The model predicts that several thermal-hydraulic conditions are conducive to tube scale formation. Both high and low fluid velocities are predicted to favor turbulent deposition through particle momentum and diffusion mechanisms, respectively. Since deposition is assumed to take place only in the liquid phase and the model assumes a constant particle concentration for the entire SG (i.e., no spatial variation), areas of high void fraction will also favor deposition. Finally, areas of high heat flux are conducive to boiling-enhanced deposition and show higher sludge potential.

Several simplifying assumptions have been made by Keefer for the ATHOS implementation of the deposition model. First, steady-state values are used for both the sludge concentration in the liquid and the sludge mass deposited on each surface rather than solving for time-varying values of these quantities. Deposition and reentrainment rates are calculated in each ATHOS grid cell

based upon local (i.e., grid cell) thermal-hydraulic conditions. Particle growth and scale ripening effects are ignored. Finally, the primary model output is the sludge potential. If time variations are neglected, actual scale thickness can be approximated by multiplying this sludge potential by the mass fraction of particulates in the liquid. However, the primary purpose of the ATHOS model is the prediction of high sludge potential regions within the SG rather than calculation of a quantitative scale mass distribution.

Thermal-Hydraulic Inputs

In order to calibrate ATHOS for the SG geometries of interest, calculations were performed for each SG design using inputs typical of recent operation at each unit and zero fouling.* The inputs required in each case are

- Feedwater mass flow rate (including preheater flow as applicable)
- Feedwater inlet temperature
- Downcomer water level
- Steam carryunder
- Steam exit quality
- Primary mass flow rate
- Blowdown mass flow rate
- Primary inlet temperature (T_{hot})

These parameters are listed for each plant in Table VI-1 for each plant's SGs operating under typical recent full-power conditions.†

Steam pressure and primary outlet temperature (T_{cold}) are the key ATHOS outputs. Results are shown for each of the five SGs in the study in Figures VI-A1 through VI-E4. Note that the ATHOS model is for a 180° slice of the SG. All views are looking at the vertical mid-plane of the SG with the hot-leg side shown on the left.

Baseline Results for Clean Conditions

Figures VI-(A-E)1 show steam pressure, secondary-side temperature, and steam quality for each SG design. In general, steam pressure is relatively constant spatially through the SG, decreasing slightly from bottom to top due to gravitational head, friction, and two-phase acceleration effects.

---

* The Plant-B calculations employed inputs typical of early operation.

† Note that two sets of values are provided for Plant B—those characteristic of early operation and those typical of recent operation.

The steam pressure in Figure VI-C1 exhibits some circumferential variation due to the presence of a preheater (Model E2) in the lower-right (cold-leg) region. Similarly, secondary-side temperature is constant at the saturation pressure for most of the SGs. Figures VI-A1,-B1,-D1, and -E1 all show a small region of subcooled conditions in the vicinity of the tube sheet elevation. Figure VI-A1 (Model F) shows a smaller region of subcooled conditions on the hot-leg side of the tube sheet (compared to the other SG designs) due to the presence of a flow distribution baffle. The steam quality profile in each figure is similar for all five SGs. Steam quality is higher on the hot-leg side, reaching its maximum at the top of the U-bend region on the hot-leg side.

Figures VI-(A-E)2, VI-(A-E)3, and VI-(A-E)4 show the sludge potential calculated by the ATHOS sludge post-processor for each SG design along with the corresponding thermal-hydraulic parameters which affect relative scale deposition rate most strongly. Figures VI-(A-E)2 show sludge potential and fluid velocity. Higher sludge potentials (indicating areas predicted to be favorable for scale formation) exist in areas of low velocity near the tubesheet and especially in the preheater region of the Model E2 SG (Figure VI-C2). All SGs exhibit higher sludge potential in the upper tube regions due to the higher fluid velocities there. Figures VI-(A-E)3 show higher sludge potential in the upper hot-leg regions of each SG as void fraction reaches its maximum. Figures VI-(A-E)4 show that high heat flux areas also have relatively high sludge potential.

Use of ATHOS to Evaluate Spatially Varying Thermal Resistance

The ATHOS code includes an option for applying a uniform thermal resistance over the entire tube bundle. In order to facilitate investigation of the tube scale thickness distribution, a technique was developed to allow application of a spatially varying thermal resistance. This technique consists of the following steps, which can be applied for a given scale thickness distribution:

- Create a list of scale thicknesses which correspond on a one-to-one basis with the cells in the ATHOS model geometry. For scale distributions predicted using the ATHOS sludge deposition postprocessor, this list can be directly generated using ATHOS. For other distributions (e.g., those based on plant data), the list can be generated with the aid of a coarse discretization of the SG geometry and a Microsoft Excel spreadsheet.
- Convert the scale thickness values to corresponding local fouling factors. This conversion requires a postulated functional relationship between scale thickness and local fouling factor.

- Modify the ATHOS code to allow input of a localized heat transfer fouling resistance. (As indicated above, the standard ATHOS code only allows application of a uniform fouling resistance over the entire SG geometry.)
- For each cell, add the spatially varying fouling resistance to the secondary heat-transfer resistance calculated by ATHOS during its solution process using the other plant thermal-hydraulic inputs.

The first step in the above procedure can be carried out in two different ways: 1) using the scale thickness distribution analytically predicted by the ATHOS sludge deposition module, and 2) using the composite thickness distributions based on low-frequency ECT profiles discussed in Section III. Possible methods for applying these distributions are discussed below. Note that the second method was employed in performing a sensitivity study on spatially varying thermal resistance (see later part of this section).

APPLICATION OF ATHOS-PREDICTED SCALE DISTRIBUTIONS. Using the average thickness estimates discussed in Section III, the input concentration to the sludge potential code in ATHOS can be modified iteratively such that the average scale thickness predicted by ATHOS approximately matches the Section-III estimate for each plant.

APPLICATION OF COMPOSITE SCALE DISTRIBUTIONS BASED ON PLANT DATA. To evaluate how scale distributions based on plant data affect SG steam pressure loss, a simplified composite scale distribution model based on a coarse discretization of the SG geometry was created. Since all of the SG geometry grids used in the ATHOS code contain many nodes (>10,000), it was not feasible to generate a variable scale thickness for each node based on available plant ECT data. The main goal of the composite scale distribution model is a discretization of the SG geometry that includes sufficient resolution to capture the effects of variable scale distributions. Therefore, the heated area of the steam generator is divided into three radial regions, two circumferential regions (hot leg and cold leg), and five axial regions (including the U-bend area). This discretization of the SG yields 30 total regions as shown in Figure VI-1.

Since the scale distribution calculated using this model is directly input to the ATHOS code, the region boundaries in the composite model were set to match nodal boundaries of the applicable ATHOS geometric model. For each of the 30 regions, the total heated tube area (both vertical and horizontal) was calculated. For all regions excepting the U-bend area, nodal boundaries were set such that total heated tube areas in the regions are all approximately equal. The U-bend regions were defined as all nodes above the first presence of horizontal heated tube area (corresponding to the curved portions of the SG tubes).

The scale thickness applied within each of the 30 regions of the composite model is constant. To calculate the scale thickness in each region, the following procedure is used. First, total scale volume in the SG is computed from a specified average scale thickness (per Section III) and total heated tube area,

$$V_{total} = t_{average} A_{total} \quad \text{[VI-1]}$$

A three-dimensional distribution function is then used to specify the volume of scale in a particular region. The distribution function specifies the percentage of scale volume to be contained in each spatial dimension. For example, in the radial dimension the distribution function could be defined such that 40% of the tube-scale volume is contained in the inner region, 30% in the middle region, and 30% in the outer region, with the sum of the percentage distributions in each dimension totaling 100%. For a specific region, the percentage of total scale volume in the region is the product of the percentages for each dimension,

$$D_{region} = d_{radial} d_{circumferential} d_{axial} \quad \text{[VI-2]}$$

The scale volume in each region is then,

$$V_{region} = D_{region} V_{total} = D_{region} t_{average} A_{total} \quad \text{[VI-3]}$$

Finally, the constant scale thickness applied to the heat-transfer area in each region is given by

$$t_{region} = \frac{V_{region}}{A_{region}} = D_{region} t_{average} \left(\frac{A_{total}}{A_{region}} \right) \quad \text{[VI-4]}$$

With the scale thickness for each region calculated, a mapping of the thickness values in each region to the nodal geometry of the steam generator is generated, resulting in an input file of scale thicknesses corresponding to the cells in the ATHOS geometric grid. Pressure losses compared to clean conditions can then be calculated for spatially varying scale thicknesses or local fouling factors.

Comparison of Thickness Distributions

Table VI-2 compares the values of relative scale thickness (versus the bundle average) predicted by the ATHOS sludge deposition postprocessor with those values calculated based on plant ECT data for Plants A, B, D, and E. Each value is an average for one of the five axial slices discussed

earlier in this section (see Figure VI-1). The predicted distributions and the plant-data distributions both indicate significantly more mass on the hot-leg side and in general agree reasonably well except for the second cold-leg region.

Sensitivity of SG Steam Pressure to Thermal Resistance Distribution

With the discretization technique discussed earlier, a limited sensitivity analysis was conducted to evaluate the dependence of predicted steam pressure on axial scale distribution. Specifically, the effect on SG steam pressure of scale thermal resistance distributions (local fouling factors) that vary linearly from the tube sheet to the U-bend area was investigated for the Plant-E geometry and inputs. Figures VI-2 and VI-3 depict the cases examined for area-averaged thermal resistances of 60 10^{-6} h-ft^2-°F/BTU and 200 10^{-6} h-ft^2-°F/BTU, respectively. The slope of each line is listed on the left side of each plot. Note that the linear variation shown is approximated by applying piecewise constant thermal resistances to the five axial regions of the Plant-E SG geometry (illustrated for one case by the stepped line on Figure VI-2). Also note that these values of thermal resistance correspond respectively to scale thicknesses of about 5–6 mils (as evidenced by Plants B and D in Section IV) and 9–10 mils (Plants E and F).

The effect on SG steam pressure for each case is summarized graphically in Figure VI-4. The key conclusions suggested by this plot are

- Over the range of average thermal resistances examined, the total tube scale mass is predicted by ATHOS to have a greater impact on steam pressure than mass distribution. This is reflected by the fact that the 60 10^{-6} curve and the 200 10^{-6} curve are about 40 psi apart while variations from one end of each curve to the other are 10 psi or less.
- For both curves, the uniform distribution results in the highest pressure loss. This occurs because the various regions of the SG transfer heat roughly in parallel. As a consequence, more heat is transferred through regions with smaller thermal resistances.*
- The 60 10^{-6} curve is similar in shape to the 200 10^{-6} curve, indicating that the average thermal resistance level (at least up to 200 10^{-6}) does not greatly affect the character of the variation.

* This effect is roughly analogous to having two equal resistors (say 10 ohms) in parallel versus having unequal resistors with the same sum in parallel (e.g., 5 ohms and 15 ohms). The equivalent resistance of the unequal resistors in parallel is less than that for the equal resistors.

Table VI-1. ATHOS Input Parameters[1]

Quantity	*Plant A*	*Plant B (Early)*	*Plant B (Recent)*	*Plant C*	*Plant D*	*Plant E*
Steam Dome Pressure (Initial Guess)[2] (psia)	978.9	879.1	841.9	1050.1	776.58	861.01
Feedwater Flow Rate (Downcomer)[3] (lb_m/h)	1.976E+06	1.875E+06	1.905E+06	0	1.827E+06	3.601E+06
Feedwater Flow Rate (Economizer)[3] (lb_m/h)	0	0	0	2.135E+06	0	0
Feedwater Flow Rate (Lower Boundary)[3] (lb_m/h)	0	0	0	0	0	0
Feedwater Inlet Temperature (°F)	423.8	431.3	437.1	441.7	426.39	421.97
Downcomer Water Level (ft)	41.83	42.16	42.16	44.29	42.16	44.3
Carry Under	0	0	0	0	0	0
Steam Exit Quality (–)	0.9995	0.9991	0.9977	0.9975	0.9980	0.9980
Primary Fluid Flow Rate[3] (lb_m/h)	18.80E+06	18.22E+06	16.91E+06	18.53E+06	17.21E+06	40.92E+06
Fraction of Downcomer Feed Added to Hot Side (–)	54%	50%	50%	50%	50%	50%
Blowdown (% of FW flow rate)	0.64%	1.41%	1.30%	0.91%	1.03%	0.71%
Primary Fluid Inlet Temperature (°F)	618.4	607.4	609.5	621.0	598.74	605.92

NOTES

1. All values are typical of recent plant operation except as noted.
2. Steam pressure was chosen to be an ATHOS output; these values are initial guesses provided to facilitate iterative calculations.
3. Flow rates are for half of a steam generator.

Table VI-2. Comparison of ATHOS-Predicted and ECT Scale Thickness Distributions[1]

Location[2]	Plant A				Plant B				Plant D				Plant E			
	ATHOS		ECT		ATHOS		ECT		ATHOS		ECT		ATHOS		ECT[3]	
U-Bend	1.0		1.4		1.3		1.0		1.3		1.0		1.7		1.2	
HL4/CL4	1.3	0.7	1.8	0.6	1.7	1.0	1.2	0.8	1.7	1.0	1.2	0.8	1.4	0.8	1.5	0.7
HL3/CL3	1.1	0.8	1.9	0.6	1.3	0.6	1.3	0.8	1.2	0.6	1.3	0.8	1.2	0.6	1.6	0.7
HL2/CL2	0.8	1.2	1.4	0.5	1.0	1.5	1.4	0.8	0.9	1.7	1.4	0.8	1.0	0.6	1.4	0.6
HL1/CL1	1.1	0.8	0.7	0.2	0.4	0.1	1.3	0.5	0.4	0.1	1.3	0.5	0.3	0.1	1.0	0.3

NOTES

1. Values are relative scale thickness versus the bundle average (see Table III-7).
2. Axial *region per discussion in Section VIII.*
3. Based on a composite of the Plant A and Plant B scale thickness distributions.

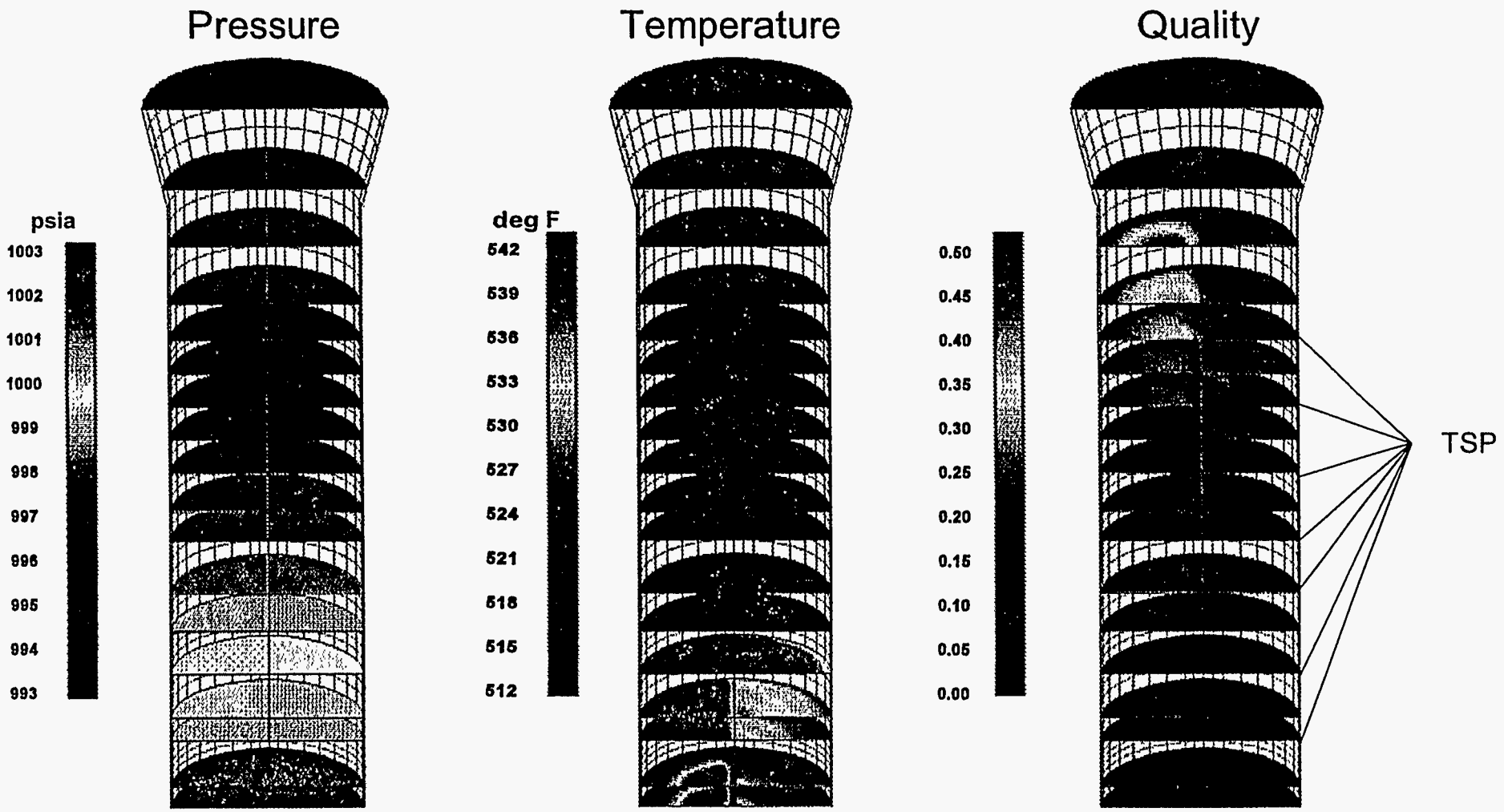

Figure VI-A1. ATHOS Steam Pressure, Temperature, and Quality for Plant A (Inputs Typical of Recent Operation)

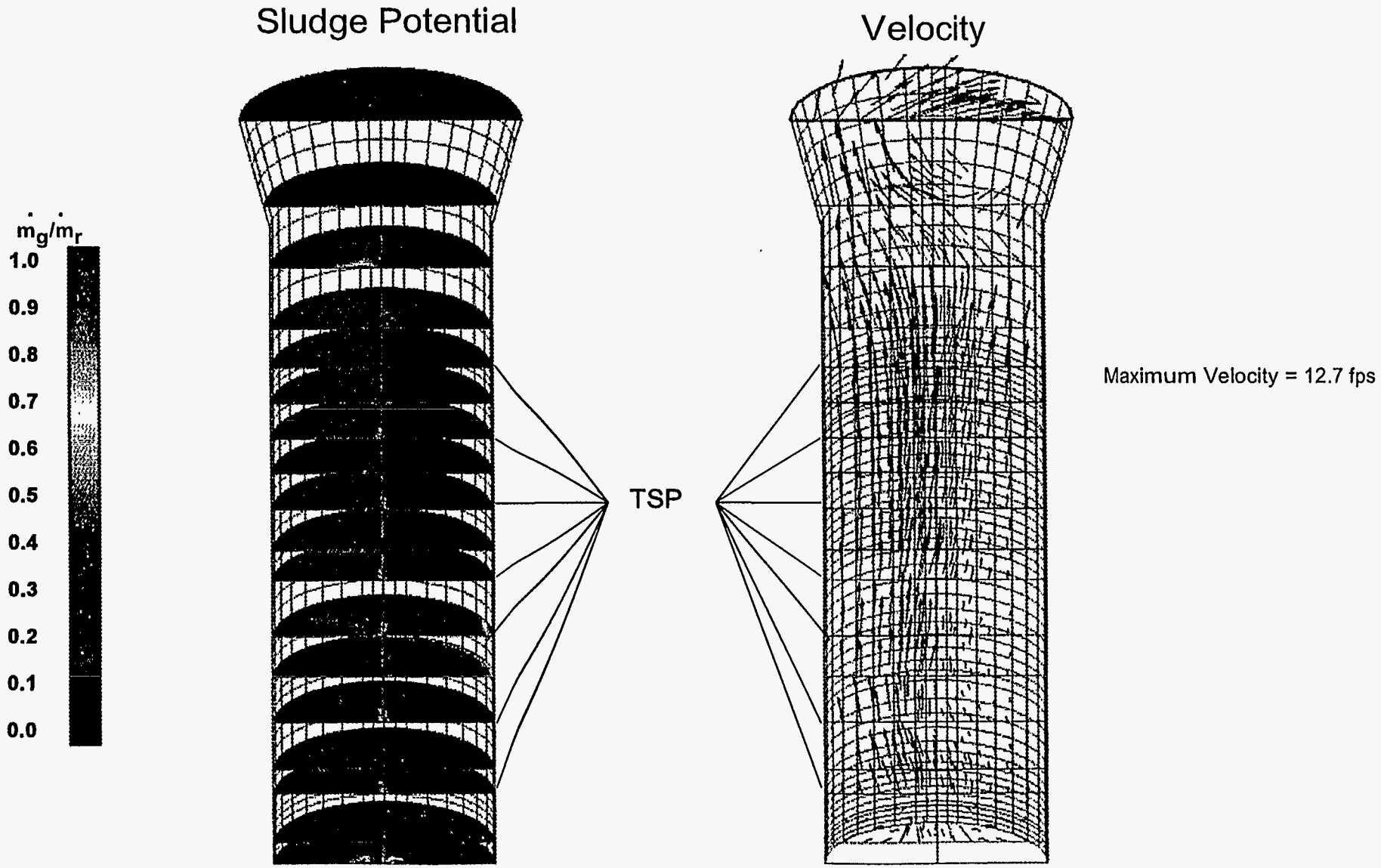

Figure VI-A2. ATHOS Sludge Potential and Velocity for Plant A (Inputs Typical of Recent Operation)

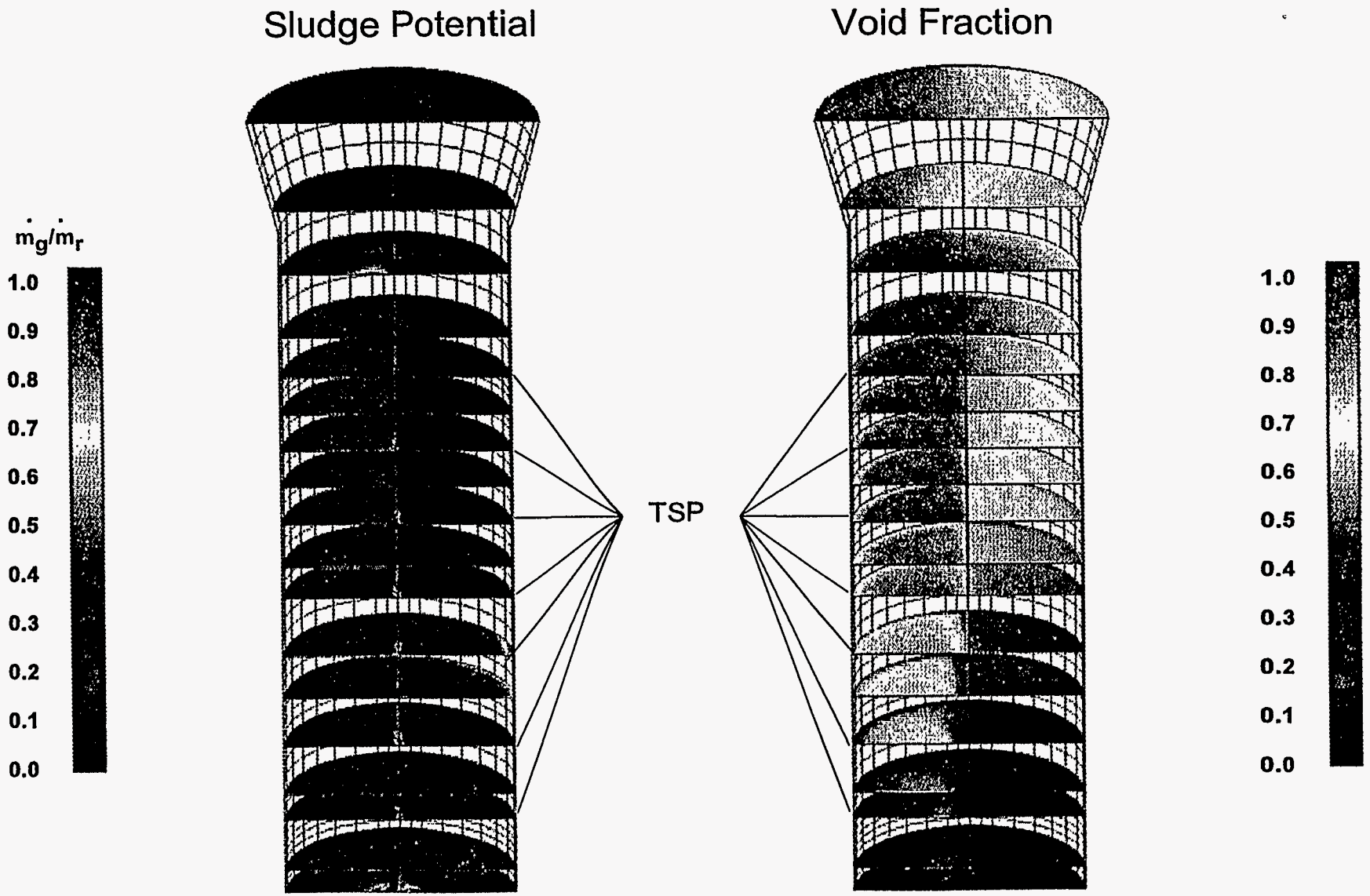

Figure VI-A3. ATHOS Sludge Potential and Void Fraction for Plant A (Inputs Typical of Recent Operation)

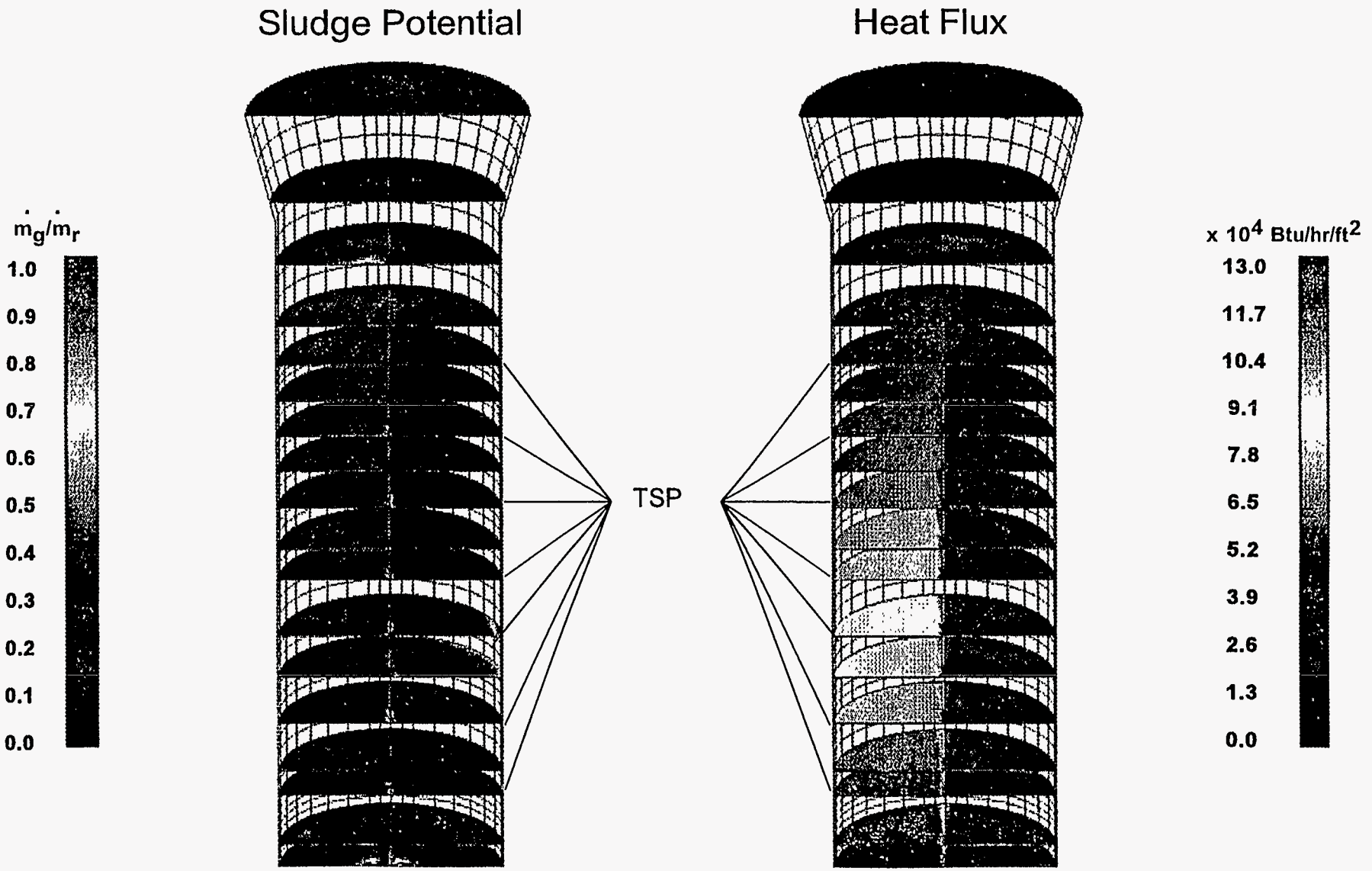

Figure VI-A4. ATHOS Sludge Potential and Heat Flux for Plant A (Inputs Typical of Recent Operation)

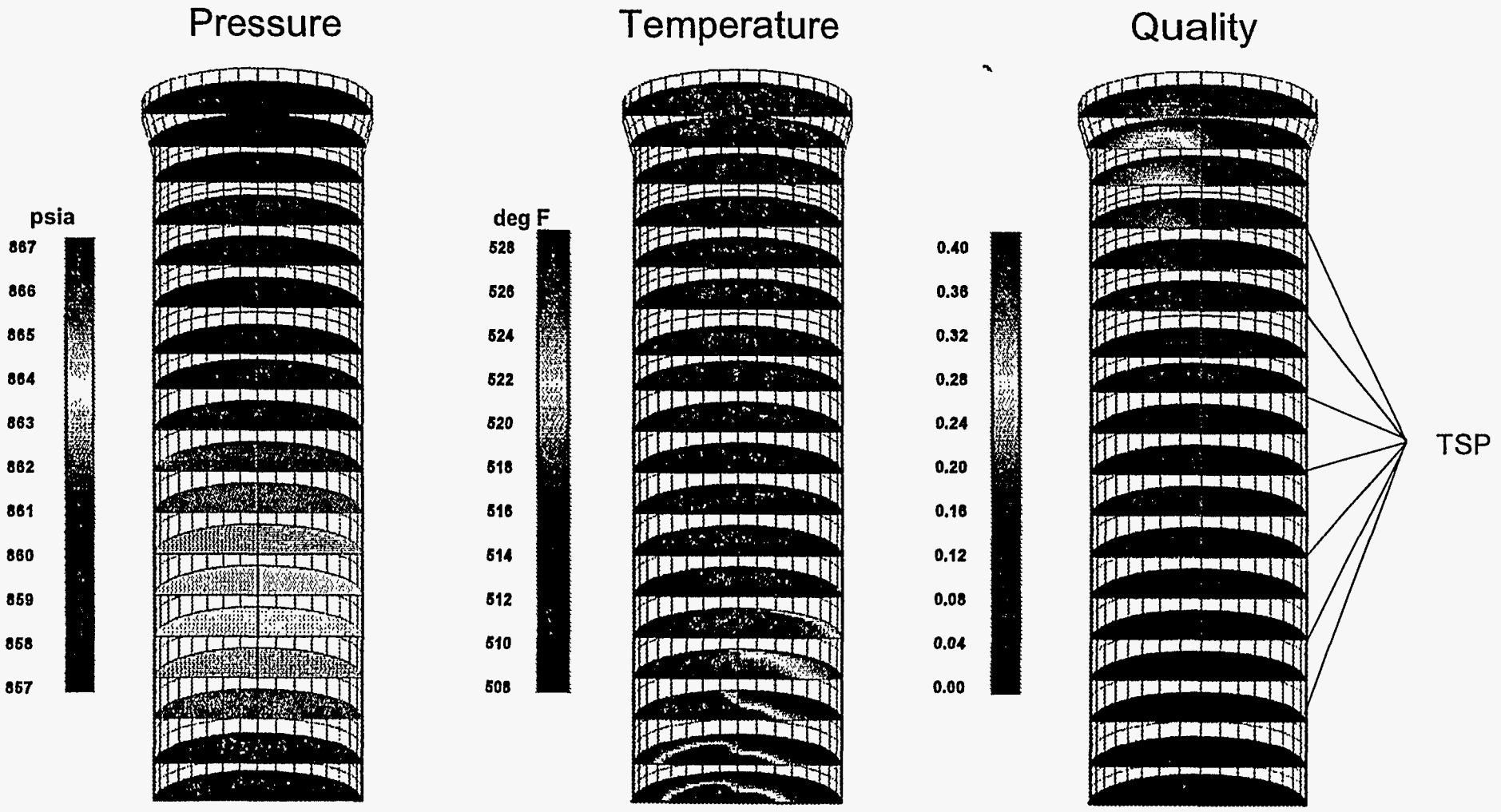

Figure VI-B1. ATHOS Steam Pressure, Temperature, and Quality for Plant B (Inputs Typical of Early Operation)

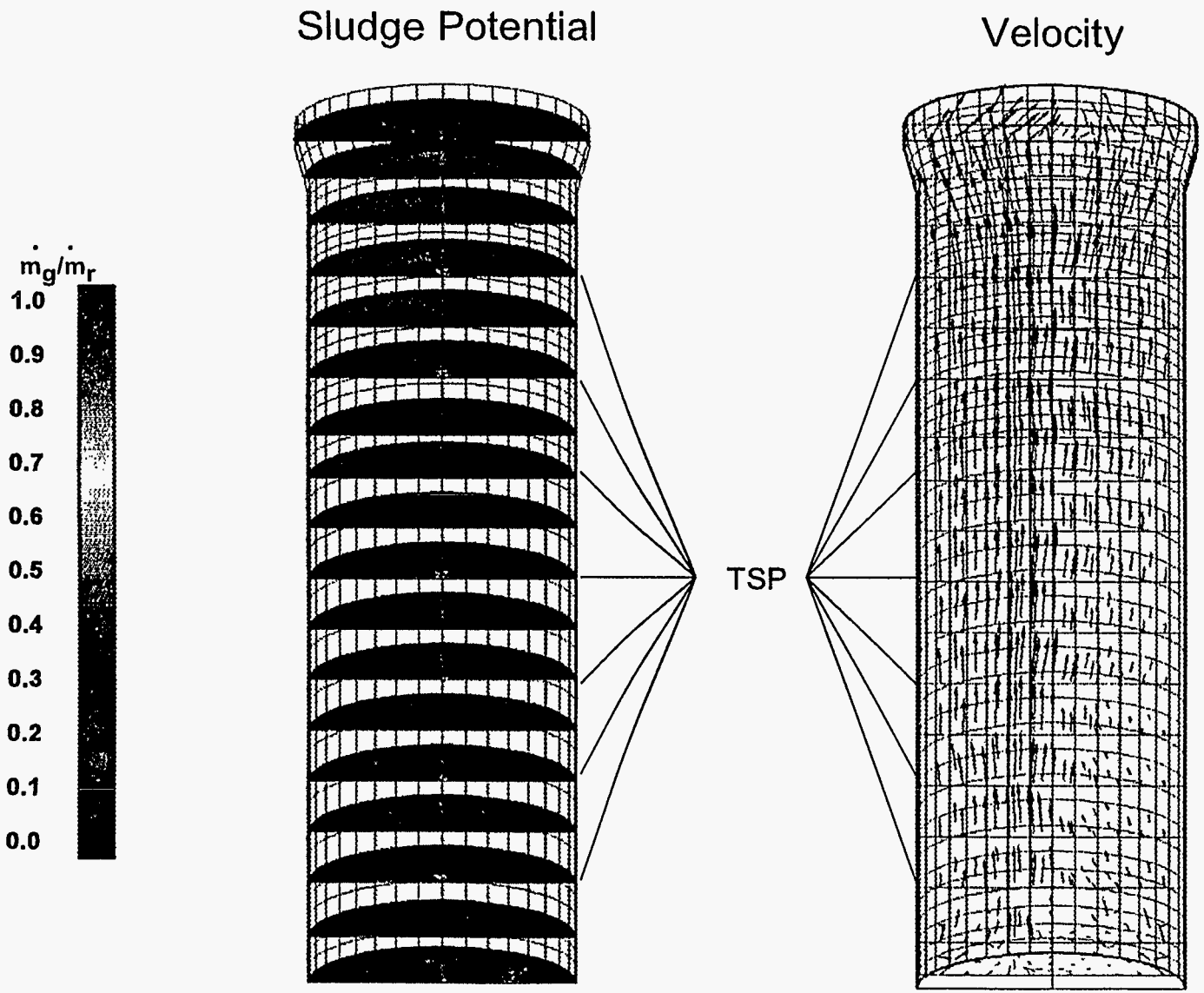

Figure VI-B2. ATHOS Sludge Potential and Velocity for Plant B (Inputs Typical of Early Operation)

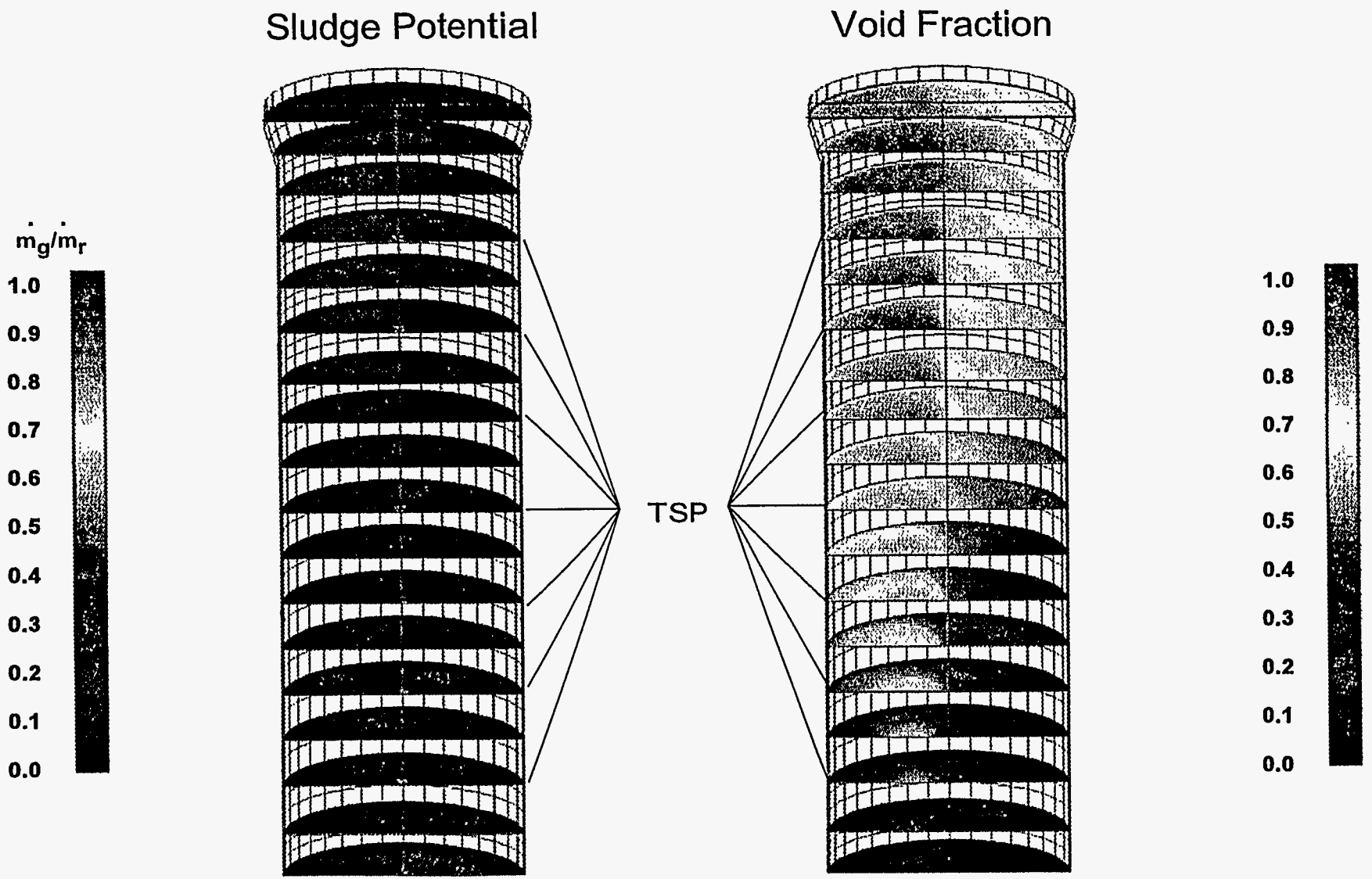

Figure VI-B3. ATHOS Sludge Potential and Void Fraction for Plant B (Inputs Typical of Early Operation)

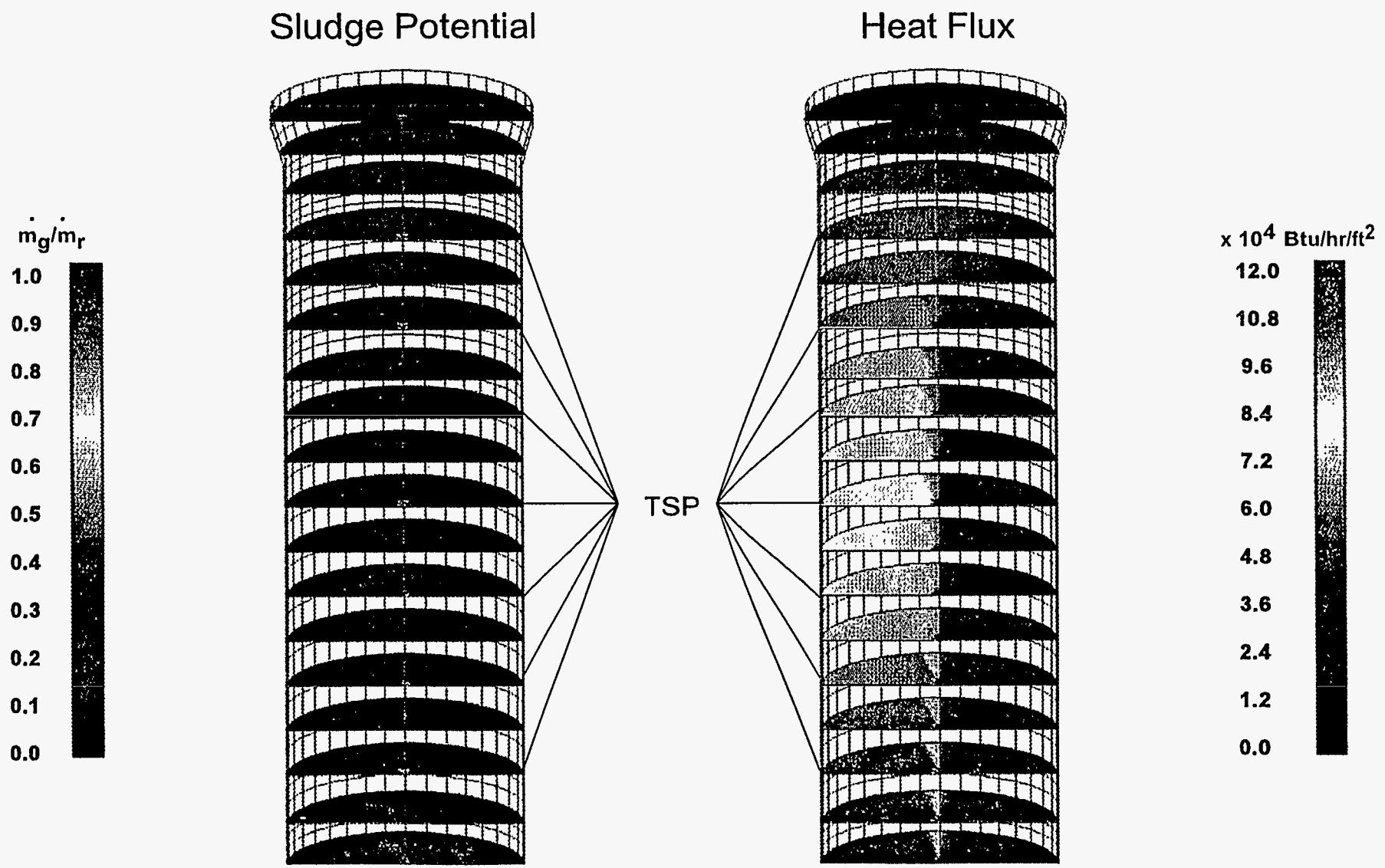

Figure VI-B4. ATHOS Sludge Potential and Heat Flux for Plant B (Inputs Typical of Early Operation)

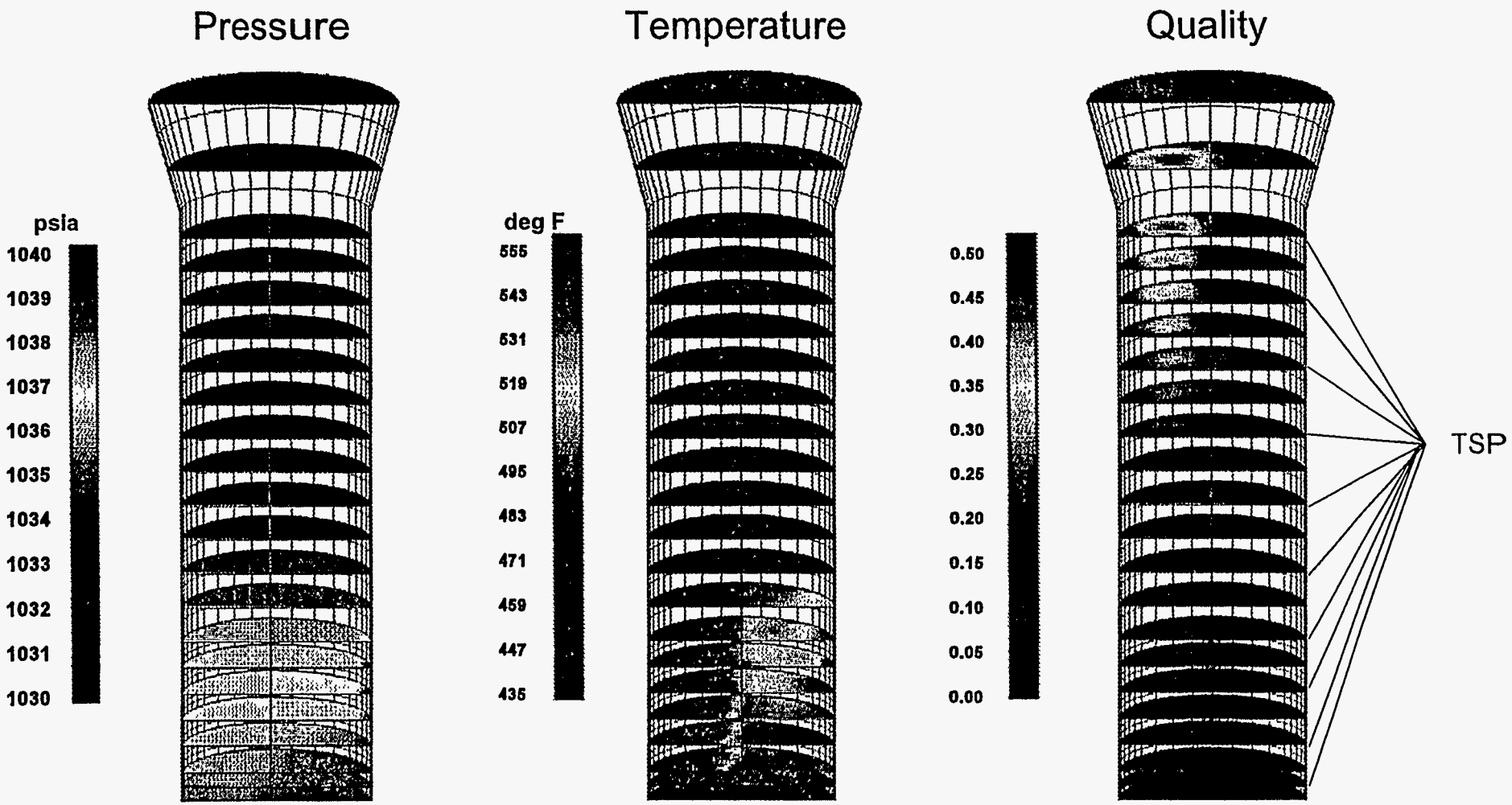

Figure VI-C1. ATHOS Steam Pressure, Temperature, and Quality for Plant C (Inputs Typical of Recent Operation)

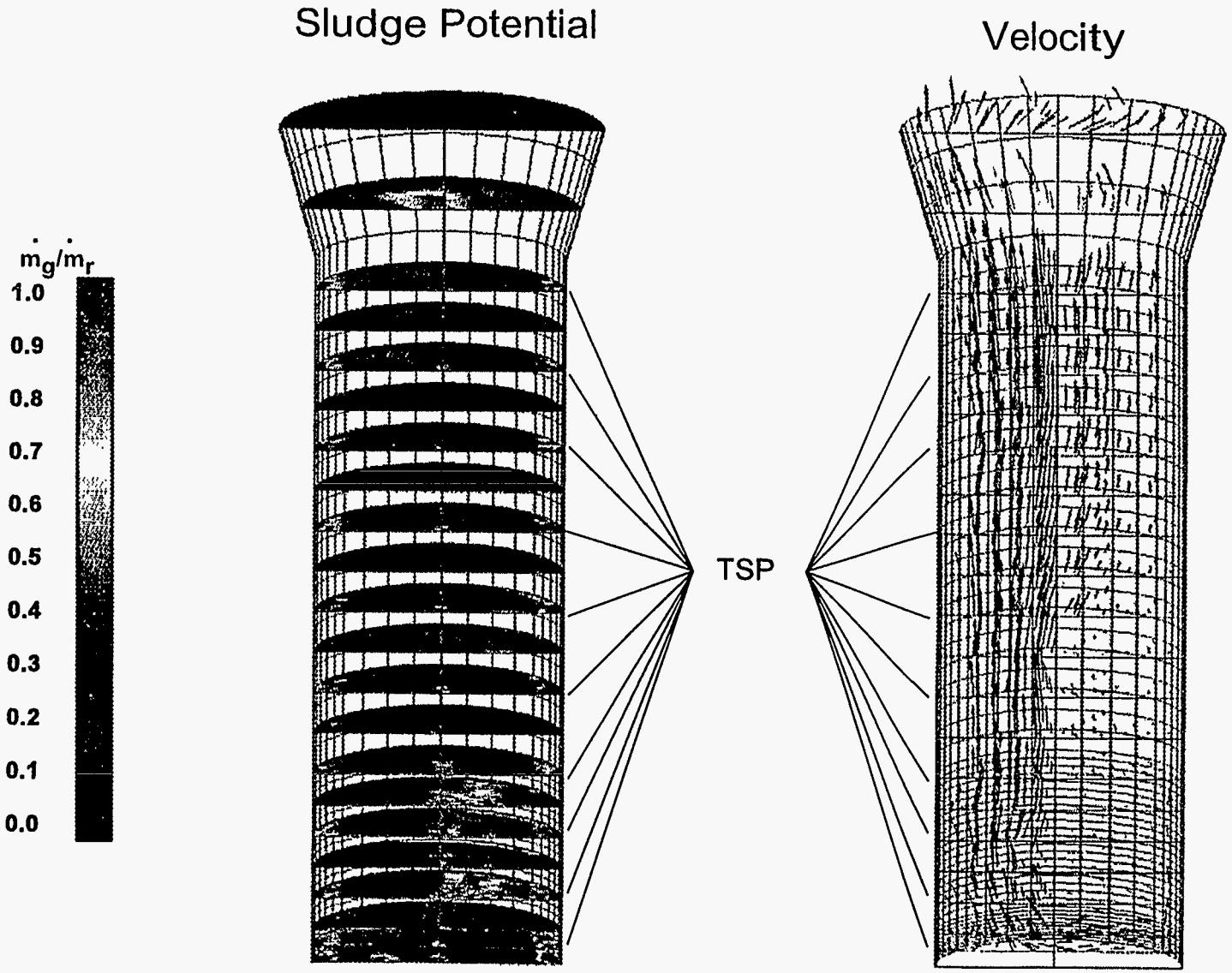

Figure VI-C2. ATHOS Sludge Potential and Velocity for Plant C (Inputs Typical of Recent Operation)

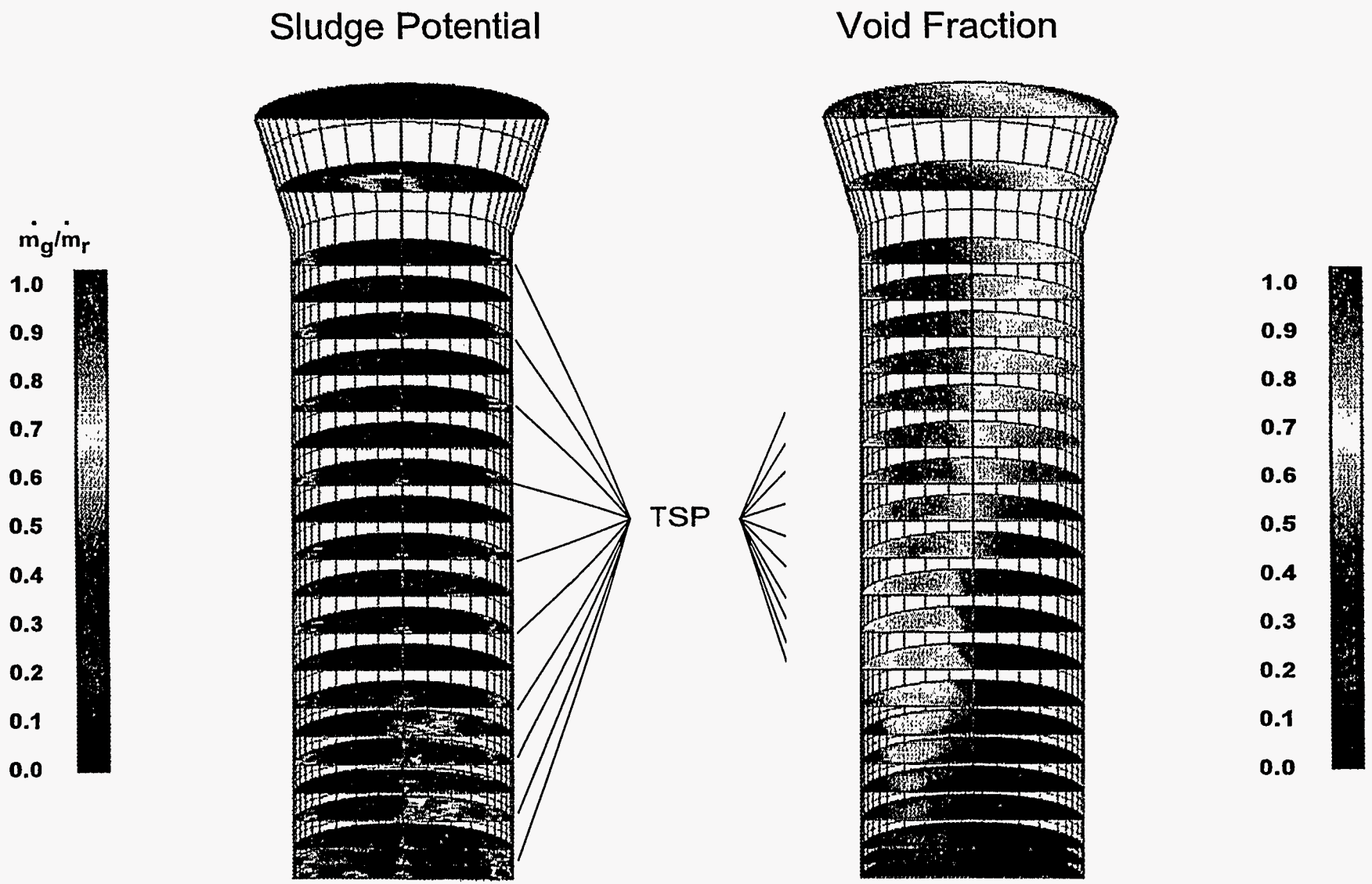

Figure VI-C3. ATHOS Sludge Potential and Void Fractionf or Plant C (Inputs Typical of Recent Operation)

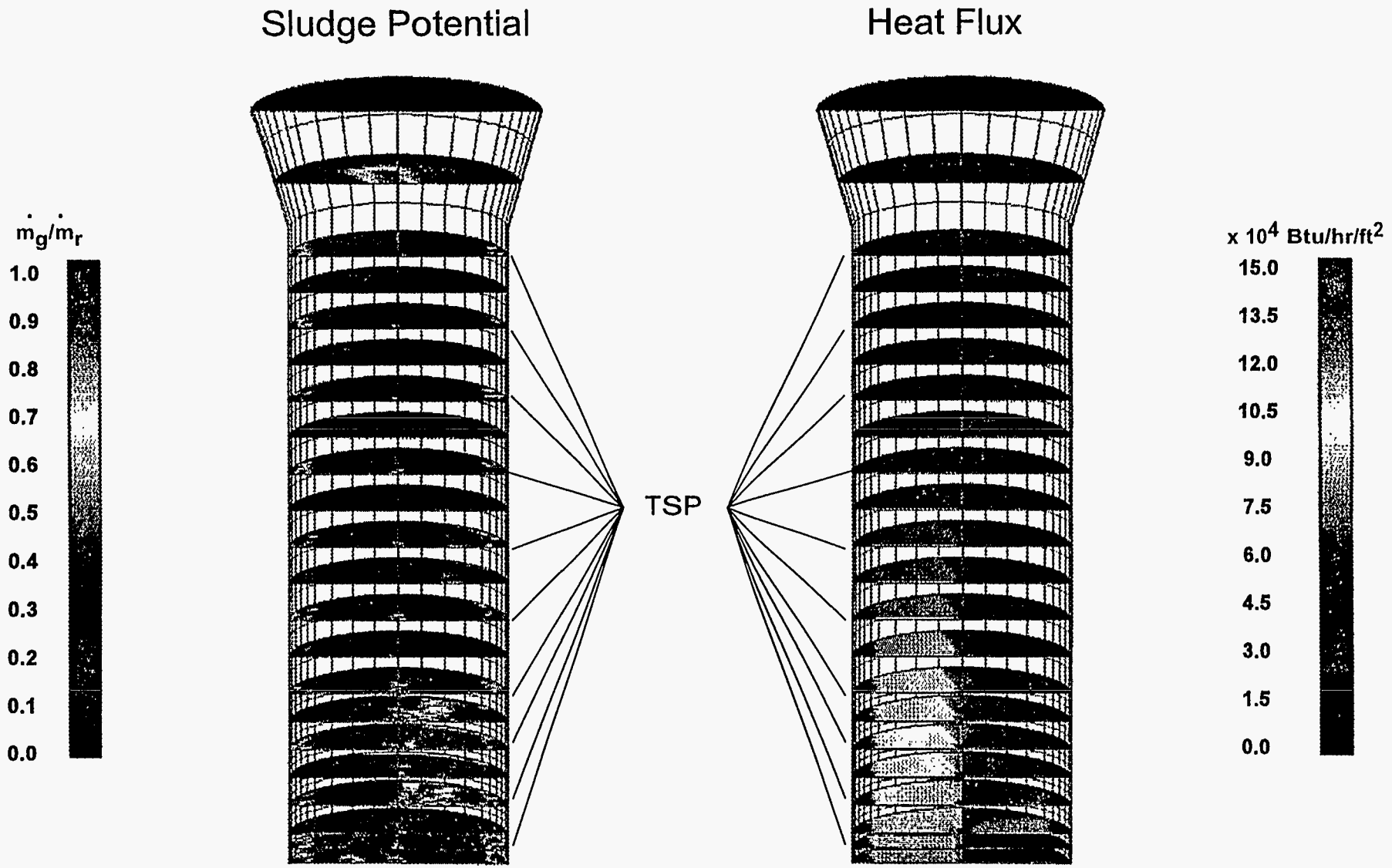

Figure VI-C4. ATHOS Sludge Potential and Heat Flux for Plant C (Inputs Typical of Recent Operation)

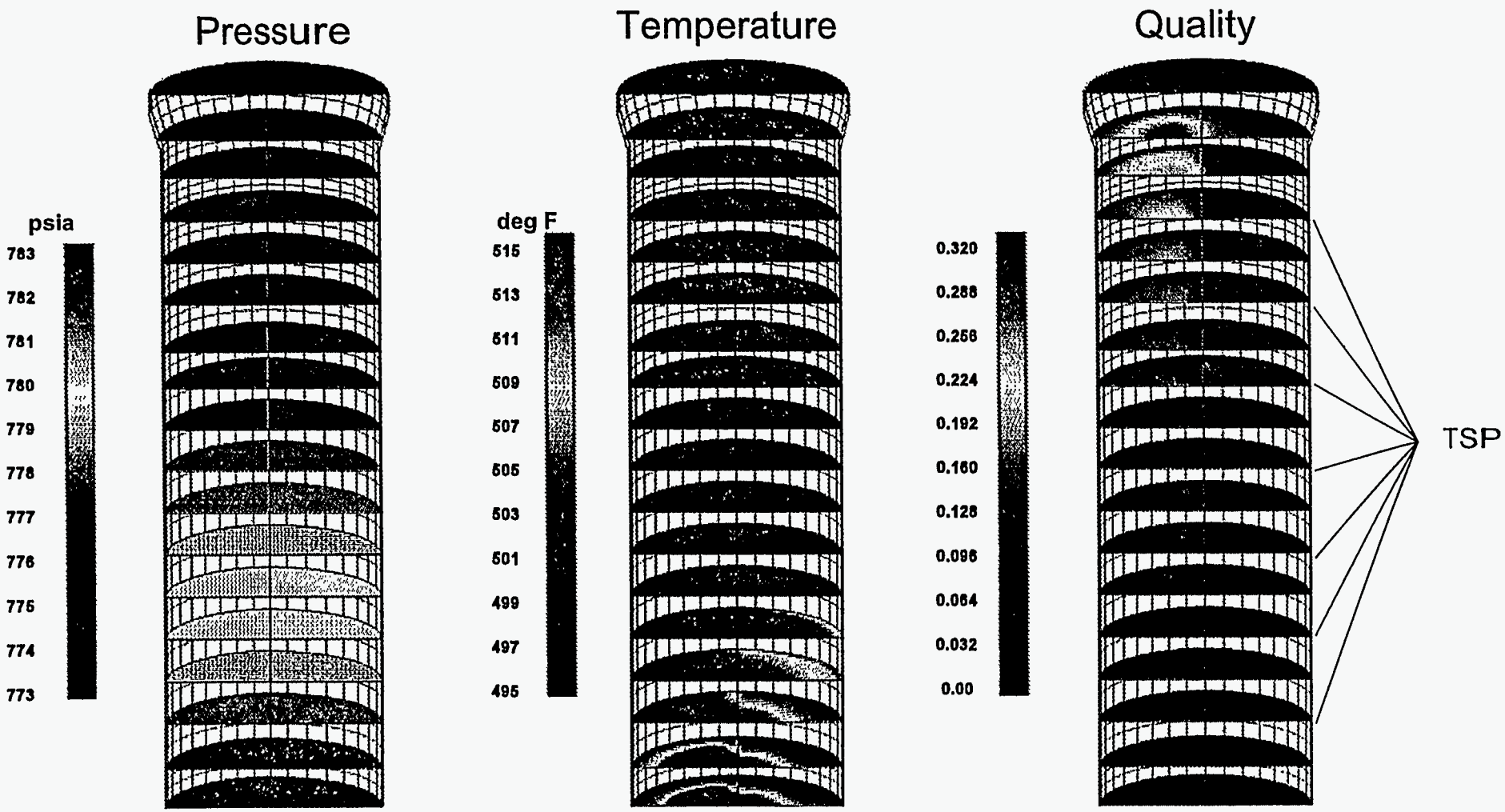

Figure VI-D1. ATHOS Steam Pressure, Temperature, and Quality for Plant D (Inputs Typical of Recent Operation)

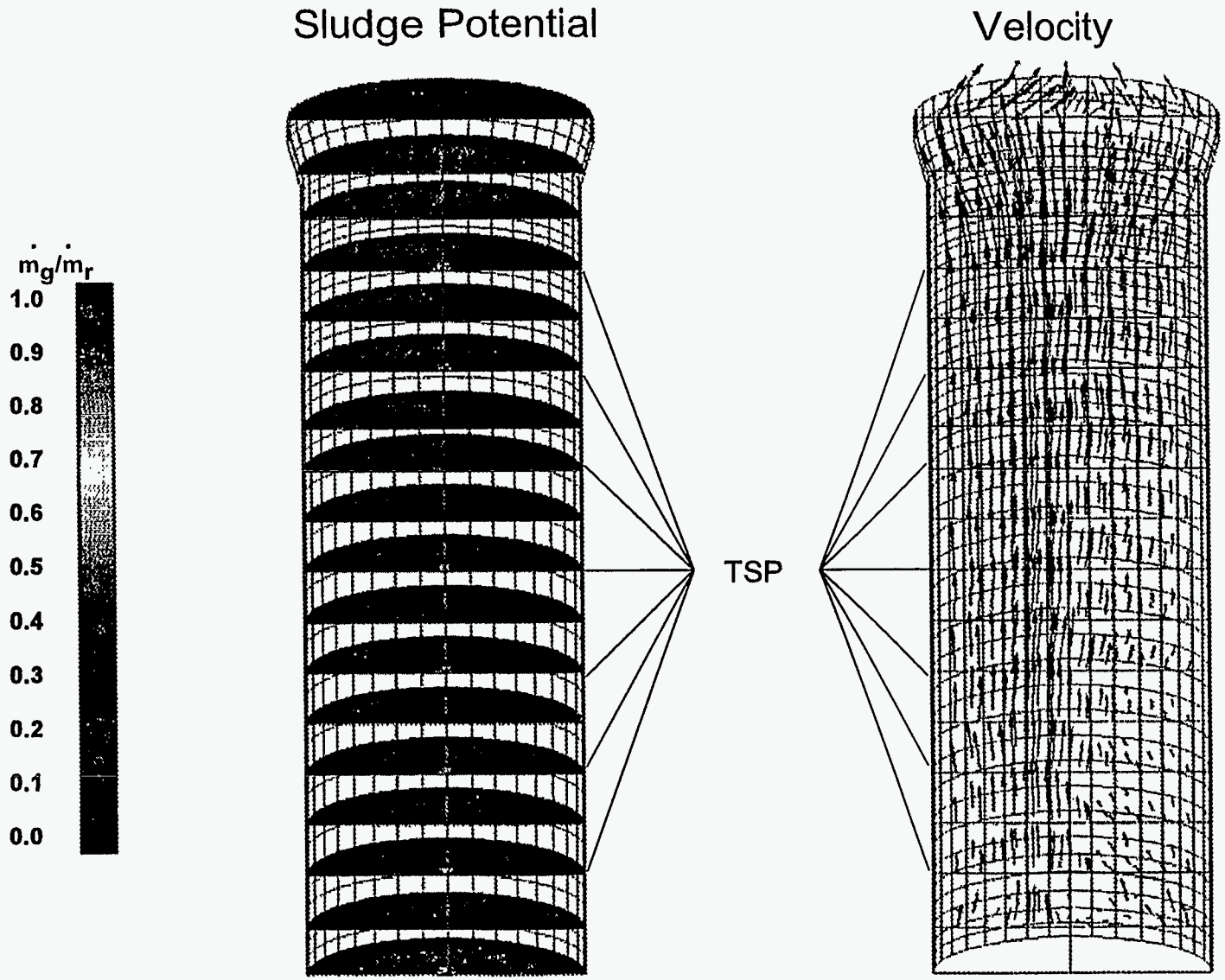

Figure VI-D2. ATHOS Sludge Potential and Velocity for Plant D (Inputs Typical of Recent Operation)

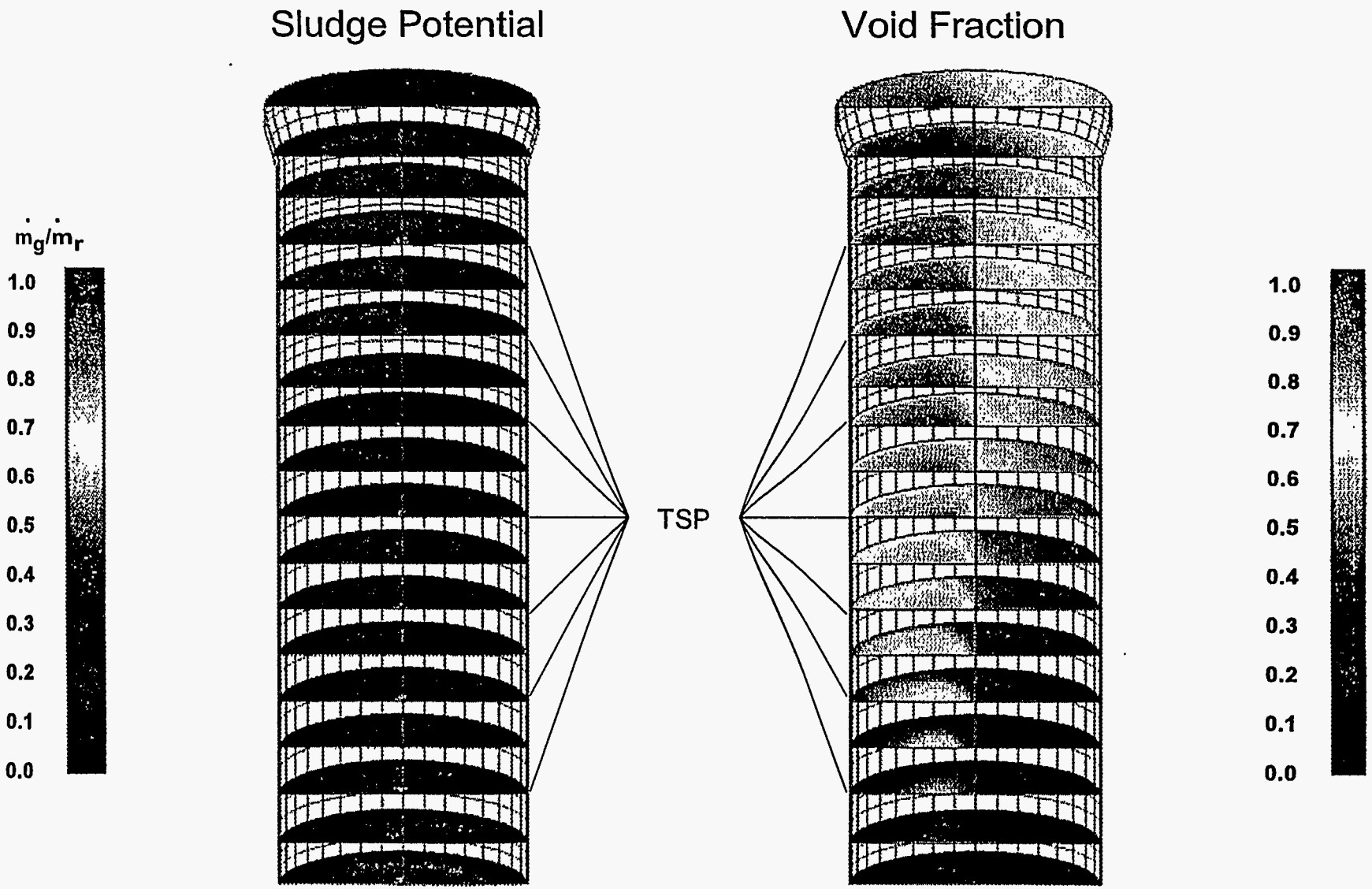

Figure VI-D3. ATHOS Sludge Potential and Void Fraction for Plant D (Inputs Typical of Recent Operation)

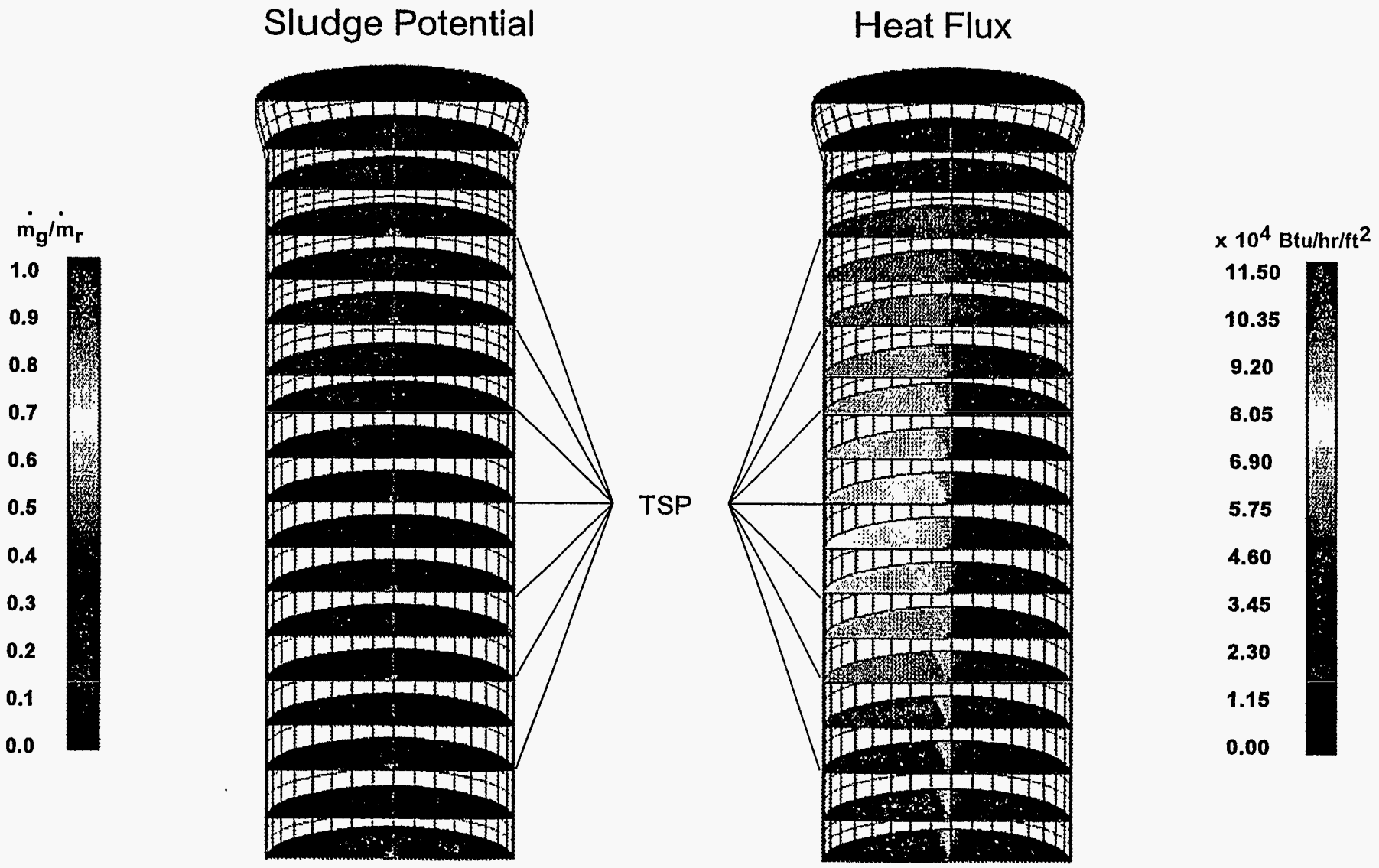

Figure VI-D4. ATHOS Sludge Potential and Heat Flux for Plant D (Inputs Typical of Recent Operation)

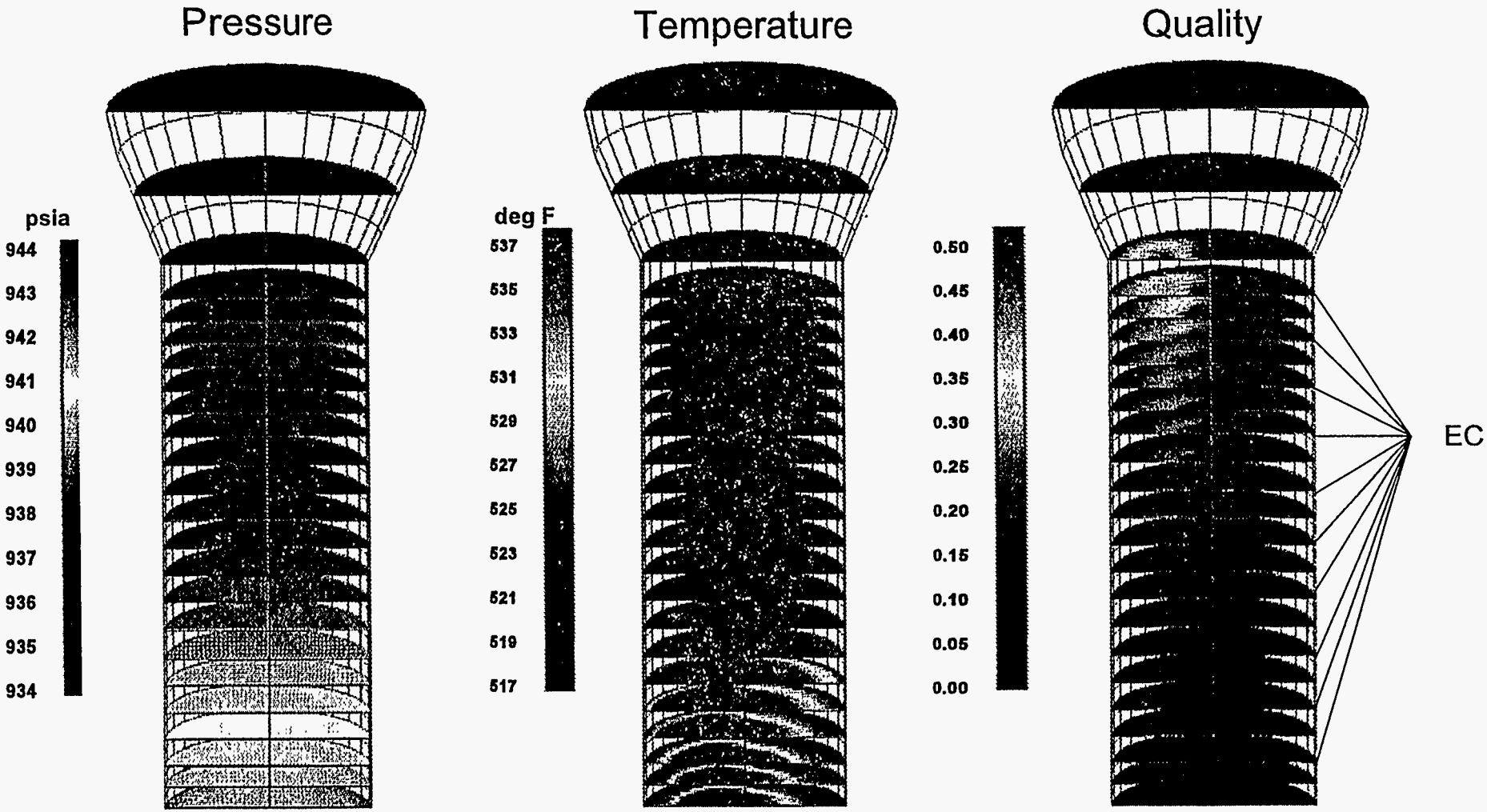

Figure VI-E1. ATHOS Steam Pressure, Temperature, and Quality for Plant E (Inputs Typical of Recent Operation)

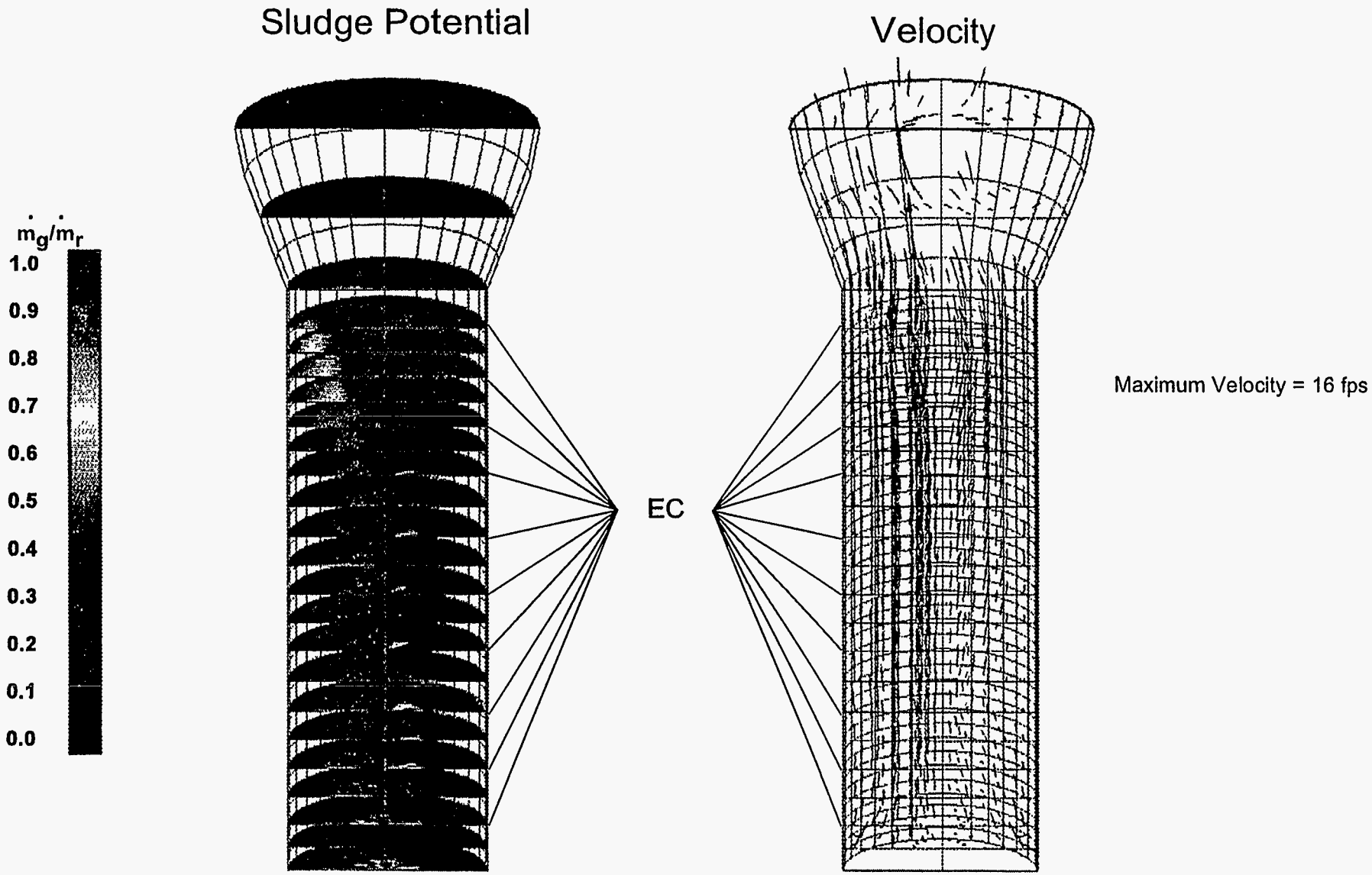

Figure VI-E2. ATHOS Sludge Potential and Velocity for Plant E (Inputs Typical of Recent Operation)

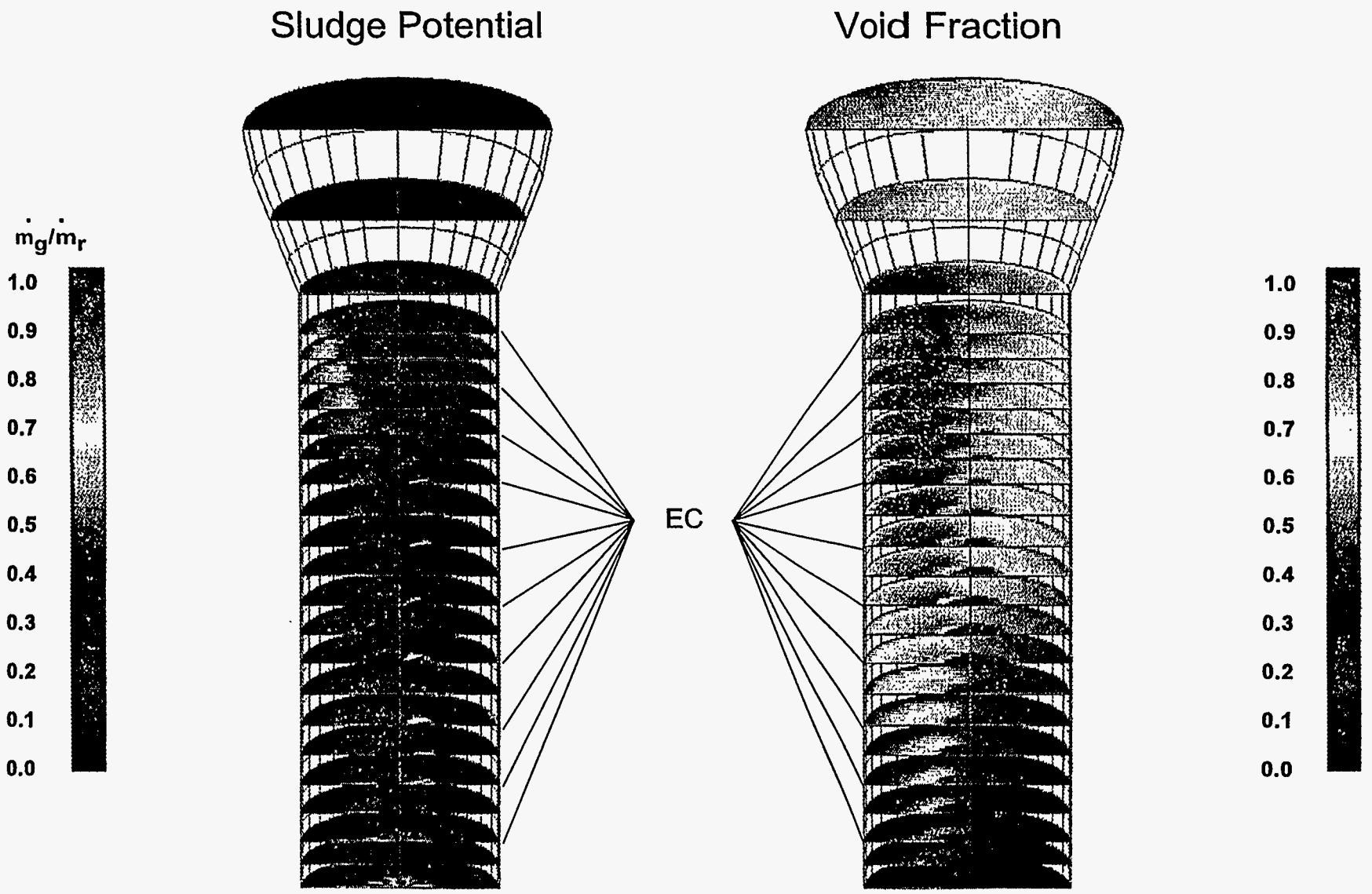

Figure VI-E3. ATHOS Sludge Potential and Void Fraction for Plant E (Inputs Typical of Recent Operation)

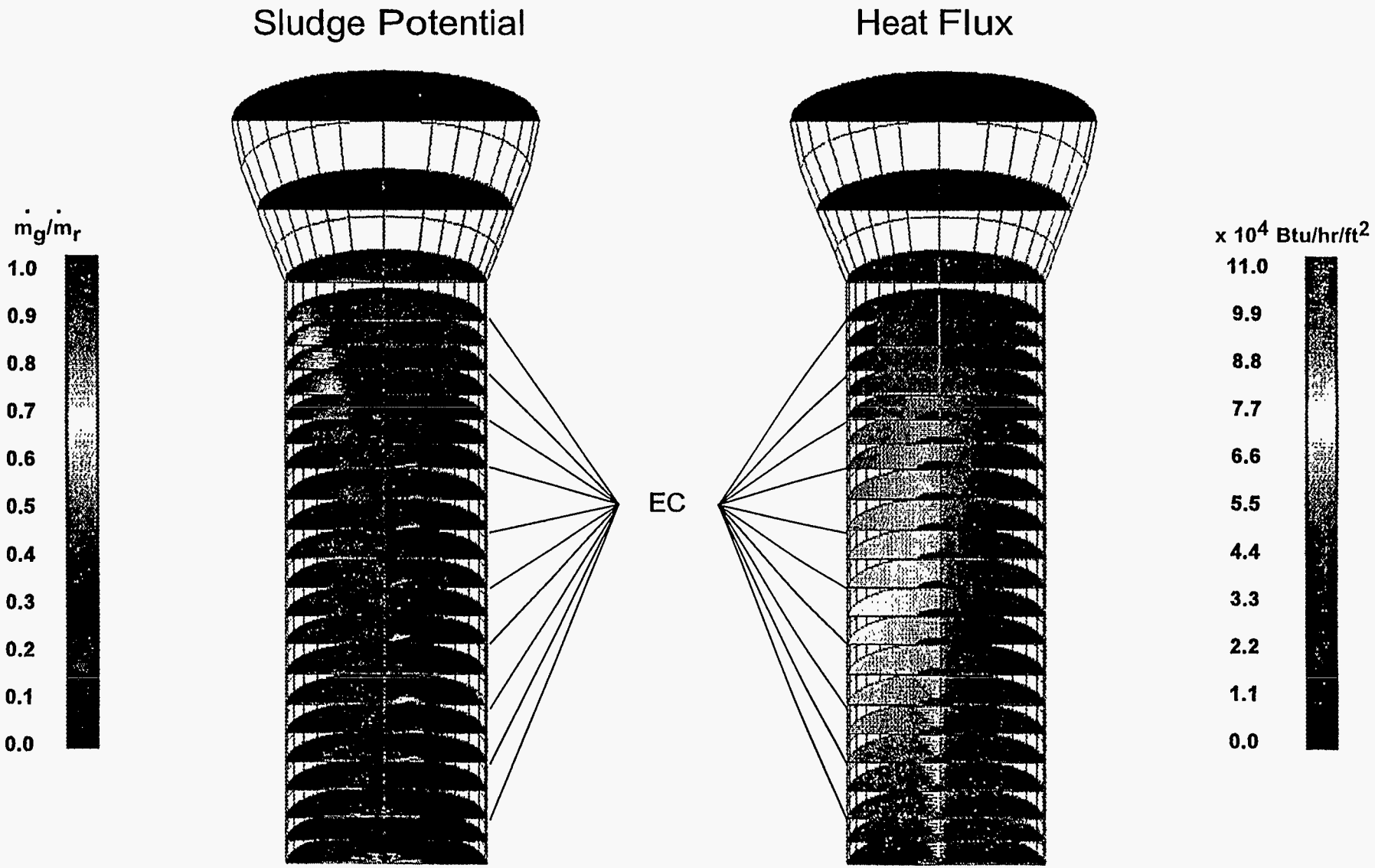

Figure VI-E4. ATHOS Sludge Potential and Heat Flux for Plant E (Inputs Typical of Recent Operation)

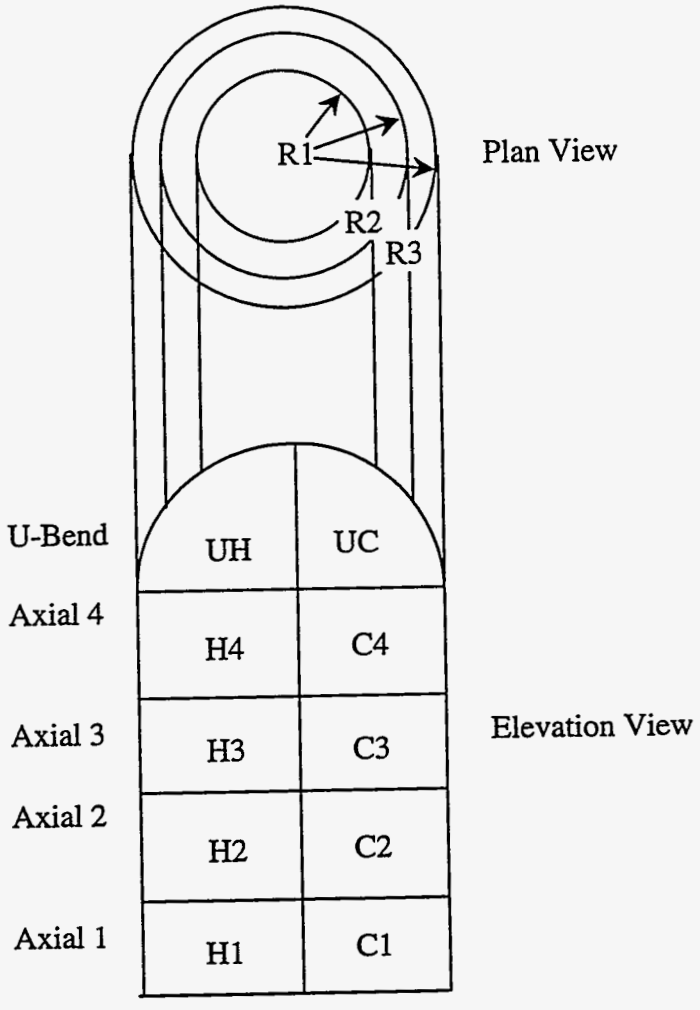

Cn = Cold-Leg Axial Region n
Hn = Hot-Leg Axial Region n
UC = Cold-Leg U-Bend Region
UH = Hot-Leg U-Bend Region

Figure VI-1. ATHOS Regions Used for Discretizing Scale Thickness Distributions

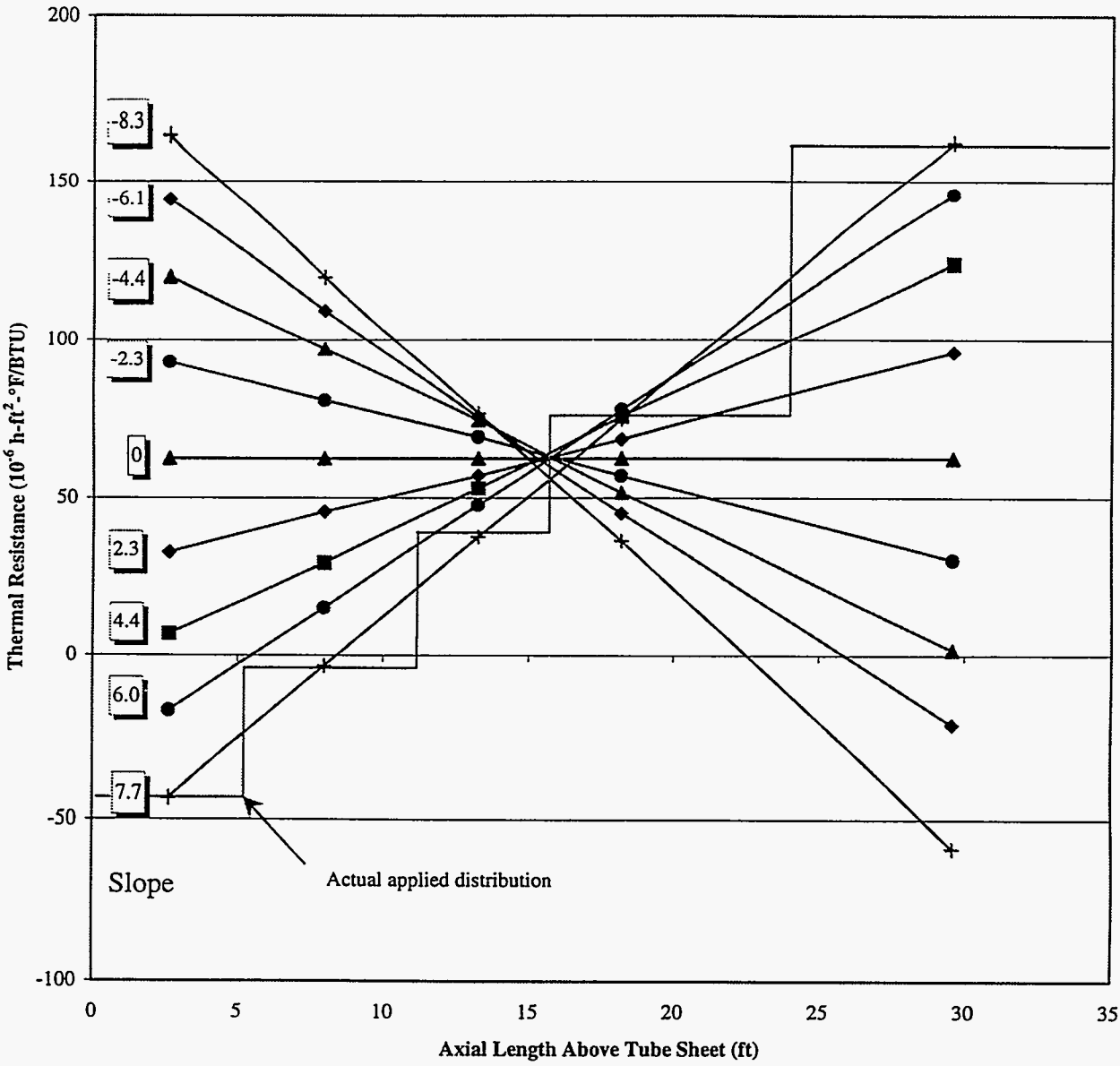

Figure VI-2. Linear Variation of Scale Thermal Resistance with Axial Position (60 10^{-6} Area-Averaged Thermal Resistance)

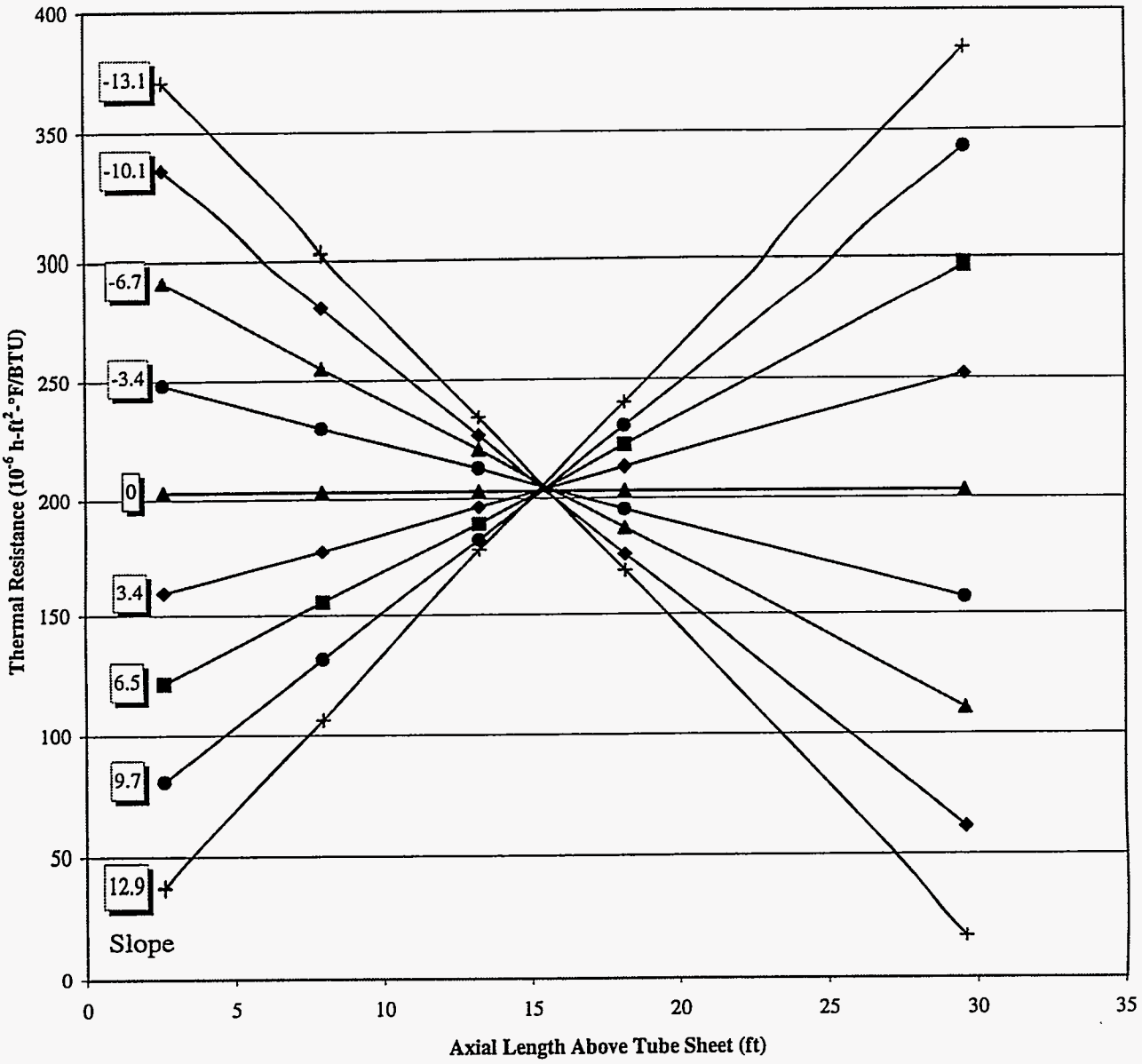

Figure VI-3. Linear Variation of Scale Thermal Resistance with Axial Position (200 10^{-6} Area-Averaged Thermal Resistance)

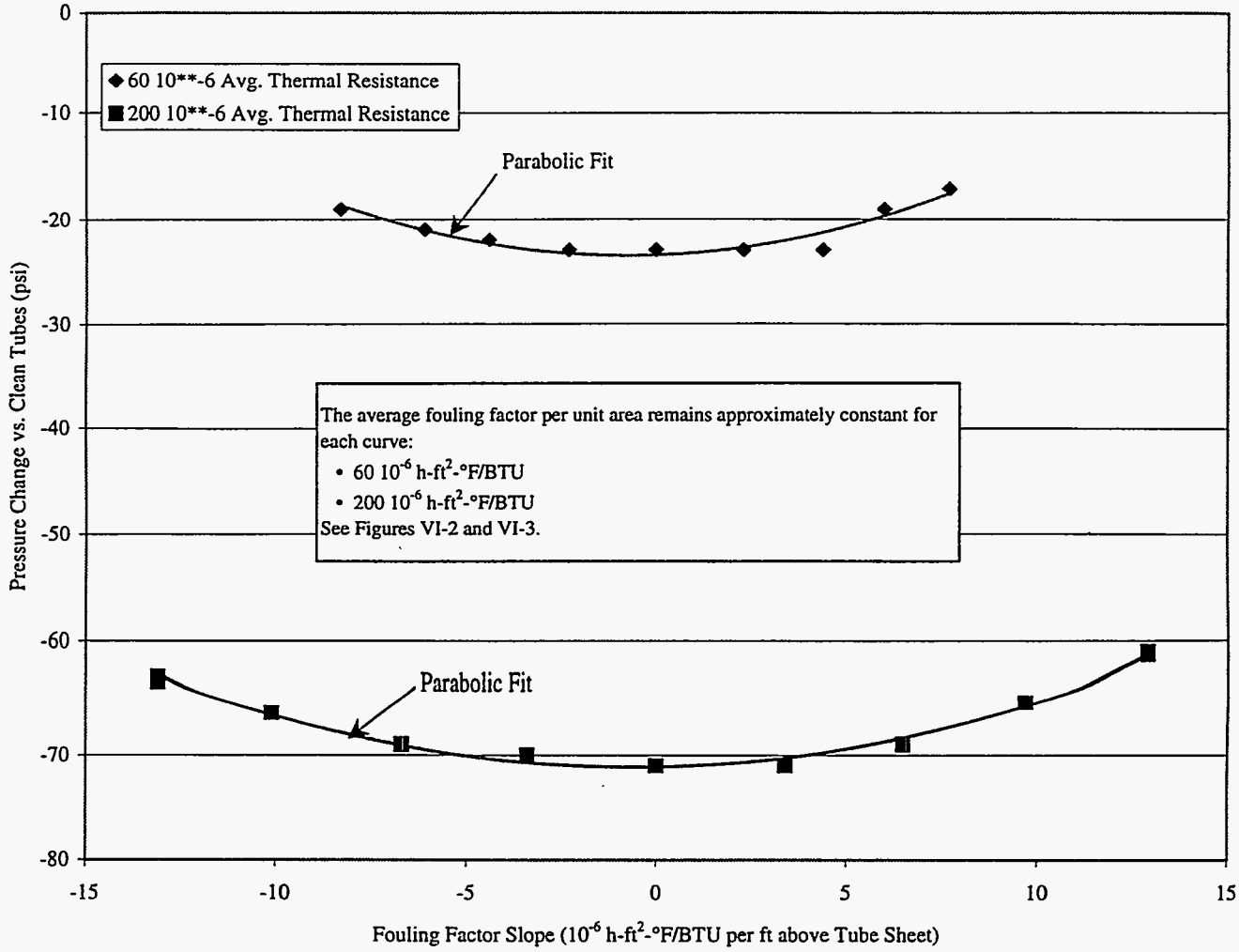

Figure VI-4. Sensitivity of Steam Pressure Loss to Secondary Scale Distribution at Plant E (Linear Variation of Thermal Resistance)

VII. REFERENCES

1. *Ginna Station Steam Generator U-Bend Tube Analysis for Chemical Cleaning Data*, Electric Power Research Institute Project S413-01, Final Report, EPRI TR-100866, July 1992.

2. *Characterization of PWR Steam Generator Deposits*, Electric Power Research Institute Project S523-01, Final Report, EPRI TR-106048, February 1996.

3. *Verification of the ATHOS3 Code Against Feedring and Preheat Steam Generator Test Data*, Electric Power Research Institute Project 1066-10, Final Report, EPRI NP-5728, May 1988.

4. *Thermal-Hydraulic Characteristics of a Westinghouse Model F Steam Generator*, Vol. 1, Electric Power Research Institute Project S129-1, Interim Report, EPRI NP-1719, March 1981.

5. "PWR Units – Steam Generator ID Oxide Layers' Thickness and Chemical Composition," [translated from French], Cattant, François, Electricité de France Doc. No. D.5004/CTT/RA.90.128, December 3, 1990.

6. *Examination of Three Steam Generator Tubes From the Ginna Nuclear Power Plant*, Electric Power Research Institute Project S138-2, Final Report, EPRI NP-2534-LD, August 1982.

7. *Evaluation of Steam Generator U-Bend Tubes from the Trojan Nuclear Power Plant*, Electric Power Research Institute Project S138-4, Final Report, EPRI NP-2629-LD, September 1982.

8. *Destructive Examination of Tube R31C66 From the Ginna Nuclear Plant Steam Generator*, Electric Power Research Institute Project S407-40, Final Report, EPRI NP-7371-M, June 1991.

9. *Metallurgical and Chemical Evaluation of Tubes R17C85, R28C32, and R26C50 From a Doel Unit 2 Steam Generator*, Electric Power Research Institute Project S304-3, Final Report, EPRI NP-5022-LD, December 1986.

10. *Examination of Tubes R3C41HL and R9C58HL of Steam Generator C, North Anna Unit 1*, Electric Power Research Institute Project S304-20, Final Report, EPRI NP-5420-LD, October 1987.

11. *The Oxide Handbook*, Second Edition, Samsonov, G.V., ed., IFI/Plenum Data Company, New York, 1982.

12. "Thermal Conductivity of Magnetite and Hematite," Malgaard, Journal of Applied Physics, Vol. 42, No. 9, pp. 3644-3647, August 1971.

13. Bruggeman, D.A.G., *Annalen der Physik* [in German], Vol. 24, pp. 636-679, 1935.

14. "Telecons with Charles Laire (Laborelec), François Cattant (EPRI/NMAC), and Kjell Norring (Studsvik Energy)," Internal DEI Memo M-3613-00-8, December 1, 1995 [attached].

15. "Using a Flow Correction Factor to Compensate for Feedwater Venturi Bias and Increase Plant Generation," Lestina, T. (MPR Associates) and Contard, C. (Niagara Mohawk Power

Corp.), paper presented at the EPRI Nuclear Plant Performance Improvement Seminar, Asheville, NC, September 3-4, 1996.

16. *Fundamentals of Heat and Mass Transfer*, Second Edition, Incropera, F. P., and DeWitt, D. P., John Wiley & Sons, New York, 1985.

17. *Steam Generator Performance Degradation*, Electric Power Research Institute Project S403-11, Final Report, EPRI NP-7524, September 1991.

18. *Thermal Analysis of Pressurized Water Reactors*, Third Edition, Tong, L. S. and Weisman, Joel, American Nuclear Society, 1996.

19. ASME Performance Test Code PTC 19.1-1985, American Society of Mechanical Engineers, 1985.

20. *Steam Pressure Trends at R. E. Ginna*, Electric Power Research Institute Project S401-1, Final Report, EPRI TR-100371, May 1992.

21. Reference deleted.

22. *The ASME Handbook on Water Technology for Thermal Power Systems*, Cohen, P., ed., The American Society of Mechanical Engineers, New York, 1989.

23. *Prairie Island Updated Final Safety Analysis Report*, Chapter 4 "Reactor Coolant System," available from the US Nuclear Regulatory Commission (NRC) Public Documents Room.

24. *Handbook of Heat Transfer Fundamentals,* Second Edition, Rohsenow, Warren M., ed., McGraw-Hill Book Co., New York, 1985.

25. "A Model of Sludge Behavior in Nuclear Plant Steam Generators," Beal, S. K., and Chen, J. H., Electric Power Research Institute, Technical Report EPRI NP-4620, Palo Alto, CA, 1986.

26. "An Analytical Model for Particle Deposition on Vertical Heat Transfer Surfaces in a Boiling Environment," Keefer, R. H., Rider, J. L., and Waldman, L. A., Proceedings of ADPA Predictive Technology Symposium, pp. 89-104, 1993.

27. T. F. Habib, P. A. Sherburne, J. F. Dunne, and C. L. Williams. 1992. Degradation in Ginna steam generator tube heat transfer due to secondary side fouling. In *Steam generator sludge deposition in recirculating and once through steam generator upper tube bundle and support plates,* edited by R. L. Baker and E. A. Harvego. New York: The American Society of Mechanical Engineers, NE - Vol. 8. (Presented at the 1992 International Joint Power Generation Conference, Atlanta, Georgia, October 18–22, 1992.)

28. K. R. Redmond, G. W. Geiken, J. M. Jevec, and J. Peter N. Paine. 1992. Ginna steam generator tube deposit characterization and chemical cleaning dissolution data. In *Steam generator sludge deposition in recirculating and once through steam generator upper tube bundle and support plates,* edited by R. L. Baker and E. A. Harvego. New York: The American Society of Mechanical Engineers, NE - Vol. 8. (Presented at the 1992 International Joint Power Generation Conference, Atlanta, Georgia, October 18–22, 1992.)

29. "Application of the ATHOS3 Code for Steam Generator Thermal Hydraulics and Fouling Analysis," Srikantiah, G. S., and Chappidi, P. R., International Conference on Nuclear Engineering, Vol. 5, 1996, pp. 373–390.

30. *PWR Secondary Water Chemistry Guidelines*, Electric Power Research Institute Special Report, EPRI NP-2704-SR, October 1982.

31. *PWR Secondary Water Chemistry Guidelines—Revision 4*, Electric Power Research Institute Final Report, EPRI TR-102134-R4, November 1996.

Additional Related Reference Materials

32. *Utility Experience with Steam Generator Chemical Cleaning*, Electric Power Research Institute Project S523-03, Final Report, EPRI TR-104553, December 1994.

33. Collier, J. G. and Thome, J. R. *Convective Boiling and Condensation,* Clarendon Press–Oxford, Third Edition 1994, pp. 259-64.

34. "Steam Generator Tube Fouling Characteristics and Mechanisms," Baum, A., SG-94-05-007, presented at the EPRI Sludge Management Workshop, May 10-12, 1994, Norfolk, VA.

APPENDIX A

ISSUES ASSOCIATED WITH FOULING OF STEAM GENERATORS WITH INTEGRAL PREHEATERS

This appendix addresses the key differences between feedring and preheater SGs with regard to the global fouling factor. These unique preheater issues must be considered before interpreting global fouling factor calculations made for preheater SGs.

Flow Distribution

All or most of the feedwater entering preheater SGs passes first through the preheater section before passing into the open portion of the tube bundle. For Plant C (a Model E2), the flow is directed to the bottom portion of the preheater where most of it makes 5 or 6 passes through a counterflow arrangement before exiting the preheater at the top. A fraction of the flow exits the preheater at the bottom (see Figure A-1). This design is termed a counterflow preheater. Commercial plants also use split flow and axial flow designs.

For optimal performance of the preheater, the ratio of the flow through the counterflow portion of the preheater to the flow into the mixing region must be maintained at a certain value. If the flow holes in the baffle plates become clogged or partly obstructed due to fouling, this ratio can change, potentially reducing the efficiency of the SG as a whole.* This phenomenon cannot be captured with the global fouling factor methodology outlined in Section IV.

Log-Mean Temperature Difference

For feedring SGs, the use of T_{sat} for both the inlet and outlet secondary fluid temperature in Eq. [IV-7] reflects neglect of the subcooling of the feedwater entering the feedring. As was shown in Figure IV-1, this error is usually moderately small and is the best approximation available if a single global fouling factor is to be employed. For preheater SGs this error is larger because the degree of subcooling is significantly larger. Even more importantly, the presence of the preheater allows the steam temperature T_{sat} to approach the cold-leg temperature T_{cold}. This is because the feedwater reaches saturation at a relatively high elevation on the cold-leg side in a preheater tube bundle compared to a feedring tube bundle. The primary-side temperature at that elevation is significantly higher than the outlet temperature (T_{cold}). This permits T_{sat} to be higher than in a feedring unit, in which T_{sat} is limited to T_{cold} because saturation is reached at an elevation just above the tube sheet where the primary temperature is very close to T_{cold}. This phenomenon is illustrated in Figure A-2 (adapted from Reference (18)), which shows how the primary and secondary temperatures vary along the length of the SG tubes. Note that feedwater exits the preheater at a point some distance from the cold-leg end, meaning that the subcooled feedwater

* This effect is distinct from that caused by reduced heat transfer coefficient within the preheater due to tube surface fouling, which can itself lower the efficiency of the preheater and hence the SG.

can acquire heat from the primary fluid when it is significantly warmer than T_{cold}. This point is illustrated graphically in Figure A-2 via the pinch point (closest approach between primary and secondary fluid temperatures), which moves from P_1 to P_2 due to the presence of the preheater. As a consequence, the final exit temperature at the top of the preheater (i.e., the boiling temperature) can closely approach the cold-leg temperature. The result is that preheater SGs can produce higher steam pressures than feedring SGs given the same inlet conditions (i.e., they are more efficient).

The significance of this characteristic is that the calculated LMTD (as expressed in Eq. [IV-7]) and hence the calculated fouling factor are much more sensitive to changes in the cold-leg temperature than is the case for feedring SGs. It is possible that for preheaters, a modified LMTD could be defined using an estimated primary temperature at the location where the secondary fluid exits the preheater in place of T_{cold}. In spite of the added limitations of Eq. [IV-7] when applied to preheater SGs, it is believed that the global fouling factor captures the essence of fouling behavior just as it does for feedring SGs, although with a greater degree of uncertainty.

Multiple Fouling Factors

Because the geometry and mode of heat-transfer inside the preheater are fundamentally different from the remainder of the SG, a more accurate global analysis might include two or more fouling factors with distinct LMTDs (e.g., one for the hot-leg side, one for the cold-leg side, one for the preheater, and one for the mixing region). This technique would be capable of revealing fouling in specific regions of the SG (e.g., in the preheater). However, use of a more detailed method like this requires fluid temperature measurements at more locations than just the hot-leg inlet and the cold-leg outlet. Such measurements are generally not available for the operating history of the plant, making the method difficult to apply. Use of this technique may require several assumptions including flow rate distributions.

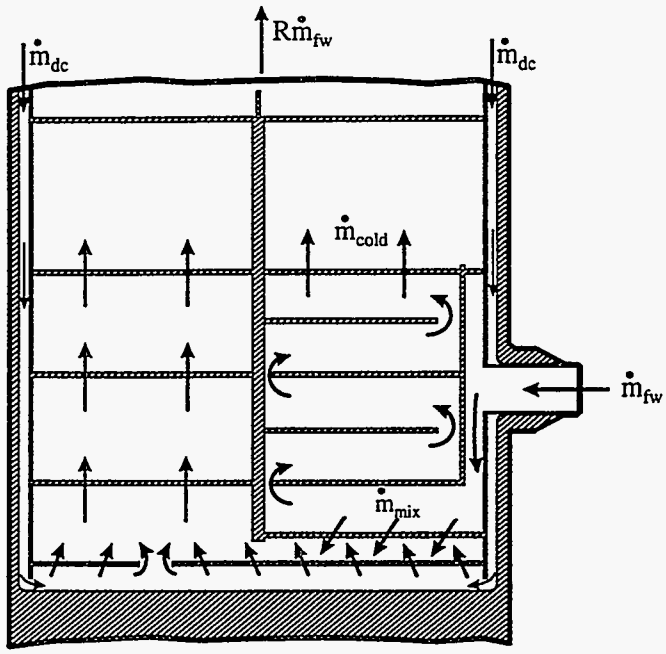

Figure A-1. Schematic of a Steam Generator with Counterflow Preheater

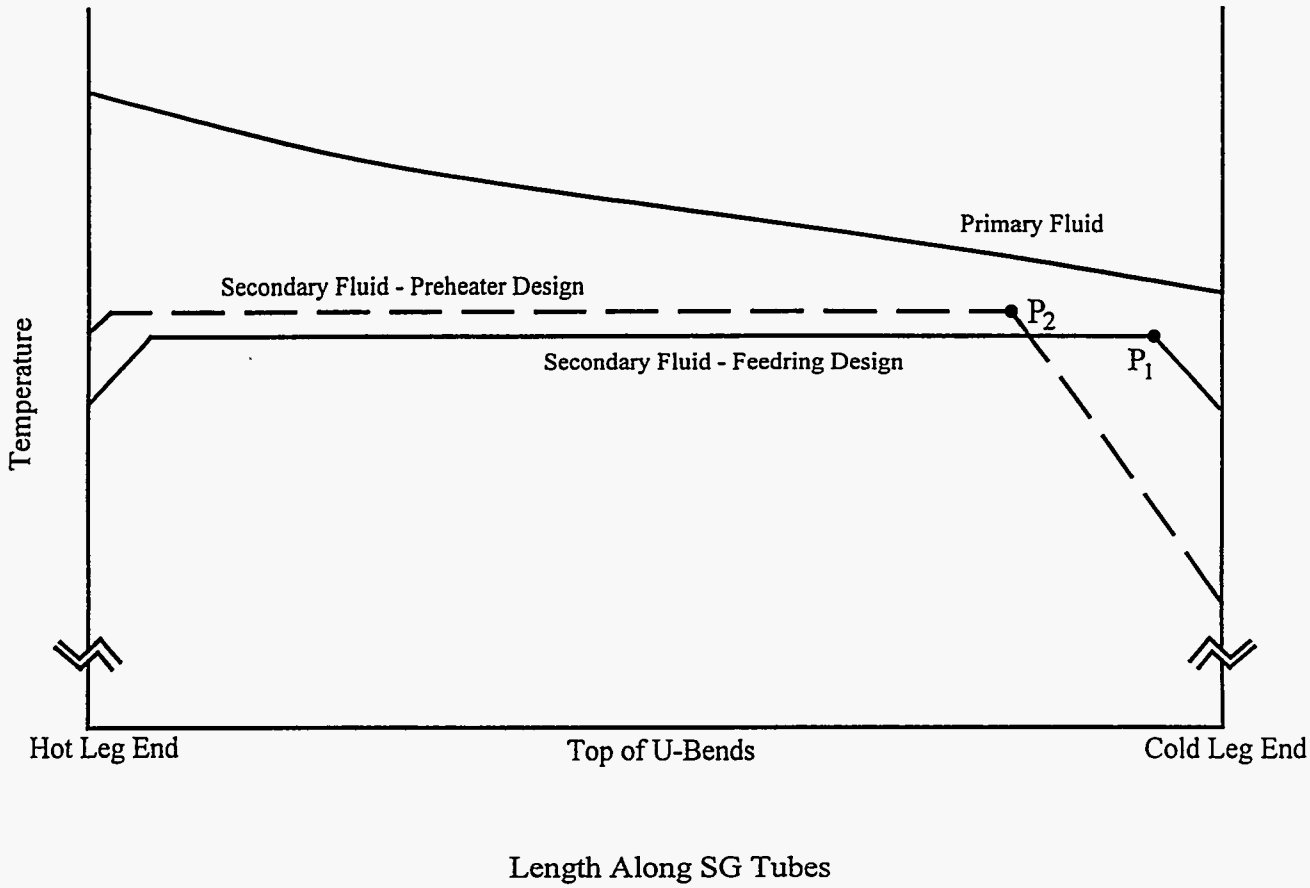

Figure A-2. Fluid Temperature vs. Tube Position for Preheater and Feedring SGs

Adapted from "Thermal Analysis of Pressurized Water Reactors,"
Third Edition, Tong, L. S. and Weisman, Joel, American Nuclear Society, 1996.

APPENDIX B

MEASURED PLANT OPERATING DATA

This appendix provides details on the measured plant data used as the basis for the fouling factor calculations for each of the five original plants included in this study. A brief discussion of the data used for a sixth plant (F) is also included at the end of the appendix.

General Information

Data for full-power operation were provided by each of the participating utilities. Data for Plant A spanned the time period from initial operation in 1984 until April 1996. On average, about one set of measurements per operating week was provided; the largest single gap between measurements was 0.1 EFPY (36 EFPD). All data were provided in electronic form except for some of the Cycle 1 measurements.

For Plant B, data were provided in electronic spreadsheet form for dates between initial commercial operation in 1981 until May 1996. Data were provided on average once per month over the entire period. However, three large gaps are present: January to May 1982 (0.3 EFPY), November 1983 to January 1989 (1.3 EFPY, including all of Cycle 3) and August 1991 to March 1992 (0.3 EFPY). For the remaining periods of operation, data were available on average about once every 2½ weeks of operating time (about once per week during Cycles 1, 7, and 8). Note that values reported prior to March 1992 (i.e., for Cycles 1-5) reflect instantaneous measurements recorded at a specific time on the day in question. Data from Cycles 6-8 comprise time-averaged values (time averaging performed by Plant B over an unspecified length of time—perhaps one or two hours).

For Plant C, electronic data were provided covering the period from initial commercial operation in 1988 until June 1996. As with Plant B, the overall average frequency was approximately once per month. However, there are two sizable gaps between available data points (i.e., greater than 0.2 EFPY): August 1990 to April 1991 (0.27 EFPY) and August 1992 to April 1994 (0.24 EFPY). Over the remaining periods, measurements were provided about once every two weeks of operating time. Note that Plant C reported data averaged once per hour for the days on which measurements were provided. For each such day, one of these averages that reflected near-100% power operation was selected for the fouling factor calculations.

For Plant D, full-power data were provided on average approximately 3 times per operating month from May 1985 up to April 1988 (hard copies) and about 5 times per operating month between August 1990 and May 1995 (electronic spreadsheet files). With the exception of several

state-point data records, no data were available for operation during Cycles 1, 2, and 5 (August 1981 to October 1984 and April 1988 to August 1990).

For Plant E, electronic data were provided approximately 2 times per week over the operating life of the plant with no gaps longer than 0.2 EFPY.

Listed below are the items used in fouling factor calculations for each plant:

Outage Dates and EFPY

For each plant, the start and end dates of major outages (i.e., refueling outages, planned in-service inspections, and any forced outages lasting more than about three weeks) were compiled. The effective full-power years (EFPY) of operation at the start of each refueling outage were provided by the utilities or were taken from DEI databases. The EFPY value at the start of each major forced outage is estimated based on the date of the outage.* (Note that these EFPY estimates do take into account shorter outages not explicitly considered.)

Number of Plugged Tubes

The entire tube plugging history is included in the calculations for each plant. That is, the number of tubes plugged in each SG during each outage is an explicit part of the computation of available heat-transfer surface area for subsequent plant operation. (None of the five plants in this study have experienced any reduction in effective heat-transfer area due to the sleeving method of tube repair.)

Primary Temperatures

Plant A: For each date, T_{hot}, T_{cold}, and T_{ave} were reported by Plant A for each SG. However, because the T_{hot} values were wide-band measurements subject to significant uncertainty, the T_{ave} and T_{cold} values were used to back-calculate T_{hot} for the purposes of the fouling factor calculations.

Plant B: For all dates on which measurements were provided, T_{ave} was reported by Plant B for each SG. In addition, for Cycles 1, 2, and 6-8 the primary temperature difference ΔT (T_{hot} - T_{cold}) was used to calculate T_{hot} and T_{cold}. For Cycles 4 and 5, only the average ΔT for all four loops was available. Thus, T_{cold} for each SG is taken as the average value. T_{hot} for each loop during these two cycles is calculated based on the actual T_{ave} and the average T_{cold}. In a couple of cases, ΔT was not available; in these cases the primary temperatures were estimated as the average of the preceding and the succeeding values.

Plant C: Both T_{hot} and T_{cold} measurements were directly provided by Plant C. Note, however, that these measurements are wide range and therefore are not as accurate as narrow-range values.

Plant D: Single measurements of T_{hot}, T_{cold}, or T_{ave} were provided by Plant D. Between May 1985 and April 1988 (Cycles 3 and 4), T_{ave} and ΔT (i.e., T_{hot}-T_{cold}) were provided, allowing direct calculation of T_{hot} and T_{cold}. For the period between August 1990 and October 1994

* This was not necessary for Plant A, which has not experienced a forced outage longer than about 2 weeks.

(Cycles 6-8), only T_{ave} was provided; T_{hot} and T_{cold} for this period are estimated based on a primary-side heat balance calculation using thermal power and primary temperatures recorded during Cycles 3, 4, and 9.* Measurements of all three quantities (T_{hot}, T_{cold}, and T_{ave}) were provided only for Cycle 9.

Plant E: In general, single measurements of T_{hot} and T_{cold} were provided for only one loop. Absent additional data, the other loop is assumed to have the same primary temperatures.† Note, however, that primary temperature measurements for both loops were available for 25 dates early in the life of the plant; they are incorporated in the calculations.

Feedwater Temperature

Single measurements were reported for each SG at each plant; all values are incorporated in the fouling factor calculations. (Note that for Plant A prior to March 1991, only the temperature at the feedwater header, which supplies all four loops, was provided. This temperature is used for each loop.)

Feedwater Pressure

Single measurements of feedwater pressure were provided for each loop at Plants B, C and E, but not for Plant A or Plant D. These values were incorporated into the fouling factor calculations. (For Plants A and D, the design value of the pressure drop between the feedwater inlet and the SG outlet is used to estimate the actual feedwater pressure for each data point. This estimate is reasonable, particularly since the fouling factor calculation is not sensitive to the feedwater pressure.)

Feedwater Mass Flow Rate

Plant A: Single feedwater flow rates were provided for each loop.

Plant B: Single measurements for each loop were provided for Cycles 1 and 2, and two measurements were provided for each loop for Cycles 4 through 8. In all cases, the average measured rate is used in the fouling factor calculations.

Plant C: Three measurements were provided for each loop on most dates while one or two measurements were provided on the remaining dates. In all cases, the average measured rate is used in the fouling factor calculations.

Plant D: Single measurements were reported for Cycles 3-4 and 6-9. However, beginning with Cycle 7, it is believed that an ingress of river water into the secondary cycle resulted in bypass flow in the venturi meters used to measure feedwater flow rate. Unlike venturi fouling, bypass flow causes the meter reading to be lower than the actual flow rate. It is believed that the error induced in the measurements was approximately 4.5% at the time it was corrected after Cycle 8. No information is known on the progress of this error (i.e., whether it occurred all at once or slowly increased). However, it is believed that one of the circumferential welds that secure the venturi corroded, allowing bypass flow through the

---

* This calculation is performed using the equation $Q = \dot{m}_{prim} c_{p,prim} (T_{hot} - T_{cold})$. The average calculated primary flow rate for all data points in Cycles 3, 4, and 9 is used to compute T_{hot} and T_{cold}.

† Note that Plant E is a T_{cold}-controlled plant not subject to steam pressure variations induced by hot-leg streaming. As a consequence, this assumption is not as potentially significant as it would be for a T_{ave}-controlled plant.

annulus. Until the crack reached 100% through-wall around the circumference, it is believed that bypass flow was minimal. Afterwards, it is postulated that bypass flow reached its maximum value essentially all at once. Thus, for the purposes of the fouling factor calculations, it is assumed that the bypass error represents a single event that occurred at the beginning of Cycle 7. Bypass flow is assumed to have remained constant at 4.5% of the nominal flow rate until the end of Cycle 8 when the problem was corrected.

Plant E: Single feedwater flow rates were provided for each loop.

Steam Mass Flow Rate

Although not necessary for computing the fouling factor, independent steam mass flow rate measurements (adjusted for blowdown flow) can be used as an alternative to the feedwater flow rate. The alternate calculation can be used to check for consistency between feedwater and steam flow measurements. Note, however, that the feedwater flow rate measurement is generally more accurate than the steam flow rate measurement.

Plant A: Single steam flow rates were provided for each loop.

Plant B: Single measurements for each loop were provided for Cycles 1 and 2, and two measurements were provided for Cycles 4 through 8. In all cases, the average measured rate is used in the fouling factor calculations.

Plant C: Two measurements were provided for each loop for all cycles except Cycle 1. In all cases, the average measured rate is used in the fouling factor calculations. Note that a correction for variations in density was applied by the authors to the raw data supplied by Plant C.

Plant D: No steam mass flow rate measurements were provided.

Plant E: Except for about 25 data points provided for one SG during a three-month period early in plant life, steam mass flow rate was only reported for operation since mid-1995 (single measurement for each loop).

Blowdown Flow Rate

Plant A: Total blowdown flow for all four loops was reported by Plant A. For the fouling factor calculations, it is assumed that this total flow is evenly distributed among the four loops.

Plant B: Regular total blowdown measurements were provided by Plant B for operation after 1992 (i.e., Cycles 6-8). As with Plant A, blowdown is assumed to be evenly distributed among the four loops. Prior to Cycle 6, blowdown is estimated using the average value for total blowdown recorded during Cycles 6-8.*

Plant C: Individual loop measurements were reported by Plant C; each is incorporated in the fouling factor calculations.

Plant D: Single measurements were provided for Cycles 3-4 and 6-9; all are incorporated in the fouling factor calculations.

---

* Note that the fouling factor is relatively insensitive to changes in the blowdown flow rate because the feedwater flow rate is so much larger. As a result, this approximation is judged reasonable.

Plant E: Single measurements were provided for each loop in gpm; each is converted to lb_m/h and incorporated in the fouling factor calculations.

Steam Pressure

In most cases, secondary steam pressure is measured downstream of the SG outlets. However, tube bundle performance is reflected by the average pressure located within the tube bundle rather than the pressure at some location downstream. Therefore, the measured values must be corrected for the pressure drop from the tube bundle to the location of the measurement. (Note that all measurements reported as gage pressures (psig) are converted to absolute pressures (psia) for the purposes of the fouling factor calculations.)

Plant A: The main steam pressure recorded by instrumentation is converted to the pressure at the middle of the tube bundle (i.e., average tube bundle pressure) by applying the following corrections:

1. The loss due to flow through the piping between the SG outlet and the pressure transducers. This pressure drop is calculated using a modified Darcy Equation (corrected for the effects of changing density). Prior to July 1992, this correction is made explicitly in the fouling factor calculations. After July 1992, the pressure measurements reported by Plant A already incorporate this correction.

2. Postulated additional separator/dryer pressure drop. Plant A performed measurements in February 1996 that indicate a total pressure drop of 6.4 to 7.4 psi across the separators and dryers. This is compared to an original design value. When computing the mid-bundle pressure, a fraction of this difference is added to the main-steam pressure measurements according to the time of the measurement (i.e., the correction increases linearly from zero at initial startup to the maximum value by February 1996).

3. Pressure drop between the middle of the tube bundle and the SG outlet nozzle. This is estimated to be 11.5 psi based on published literature for Model F steam generators (p. E-104 of Reference (3) and pp. 7-16 and 7-17 of Reference (4)).

4. For operation prior to March 1985, an added pressure drop of 20 psi is included to reflect the presence of start-up strainers on the main steam line. This value was chosen to smooth the fouling factor trend in Cycle 1.

Plant B: Like Plant A, steam pressure at Plant B is measured downstream of the SG outlet. For Cycles 1-2, a single measurement (or perhaps an average measurement) was reported for each loop. For Cycles 4-8, three separate measurements were reported for each loop. In all instances, the average value is used in the fouling factor calculations. For the Plant-B measurements, the pipe-loss correction between the SG outlet and the measurement location is about 5 psi. The additional pressure drop between the average bundle pressure and the SG outlet at Plant B is roughly 10 psi according to Plant B. No direct measurements have been made concerning moisture separator and dryer pressure drop at Plant B. However, ΔP measurements between top of the tube bundle and the main steam line, which include the drop across the dryers and separators, show little or no increase since 1991. As a result, no corrections were made for additional separator pressure drop in the fouling factor calculations.

Plant C: Steam pressure at Plant C is also measured downstream of the SG outlets. Three measurements for each loop were recorded; the average values were used in the fouling factor calculations. In this case, the required corrections from the measurements to the average bundle pressure are

1. Pressure drop between the middle of the tube bundle and the SG outlet nozzle. Per Plant C, this differential is between 5 and 10 psi.
2. The loss due to flow through the piping between the SG outlet and the pressure transducers. According to Plant C, this pressure loss is about 10 psi to the downstream side of the outlet nozzle.

Plant D: Three pressure transducers record the steam pressure at a location downstream of each SG outlet. For some dates, all three measurements were provided; for the others only the average value was reported. In all cases, the average steam pressure is used in the fouling factor calculations. As for Plant C, the main steam pressure is converted to an approximate average tube bundle pressure with the aid of two corrections:

1. The pressure drop between the middle of the tube bundle and the SG outlet. This is roughly 10 psi based on information for Model 51 SGs.
2. The pressure drop between the SG outlet and the measurement location. This is computed to be 5 psi per DEI calculations using utility drawings of the plant layout.

Plant E: Unlike the other four plants, Plant E has four pressure transducers that record the steam pressure for each loop located in the steam dome (i.e., just upstream of the SG outlets). The average pressure for each loop is used in the fouling factor calculations. In this case, the only correction required is for the pressure drop between the middle of the tube bundle and the measurement location. No plant-specific data or design values are available for this pressure drop at Plant E; other industry data and engineering judgment were used to estimate a 10 psi pressure drop for the large SG.

Calorimetric Thermal Power

Plant-computed thermal power measurements were provided for Plants A, B, D, and E but not for Plant C.* This quantity can be used as an alternate basis for computing the fouling factor. Such an alternate computation may be useful for discerning the effects of measurements errors.

Graphical presentations of the key variables discussed above are provided at the end of this appendix. A summary listing follows for each plant.

Plant A

Figure B-A1. Historical Steam Generator Outlet Steam Pressure at Plant A

Figure B-A2a. Historical Hot and Cold Leg Temperatures at Plant A

* Plants A and B provided calculated power values from the beginning of plant operation, Plant D provided values for Cycles 3-4 and 6-9, and Plant E provided values after 1988.

---

* The steam flow rate is calculated from reported feedwater and blowdown flow rates (i.e., $\dot{m}_s = \dot{m}_{FW} - \dot{m}_{BD}$). A ratio greater than 1 most likely indicates either a too-high feedwater measurement or a too-low steam flow measurement. A ratio less than 1 indicates the reverse.

Addition of Plant F

Due to the low degree of fouling and thin deposits present at Plant C (see Sections III and IV), the thermal performance of the SGs at a sixth plant were also analyzed. However, the detailed thermal-hydraulic data that were used for Plants A through E were not available. Instead, the following items were used to calculate an approximate fouling factor history for Plant F:

- Average SG steam pressure between 1980 and 1990 (6.5 EFPY to 15 EFPY). Values were available on average twice per operating month.
- Outage dates, plugged and sleeved tubes, and operating times for the same time span. Note that sleeved tubes were treated as the equivalent of $\frac{1}{30}$ of a plugged tube with regard to lost heat-transfer area.
- Design values of all other thermal-hydraulic inputs.

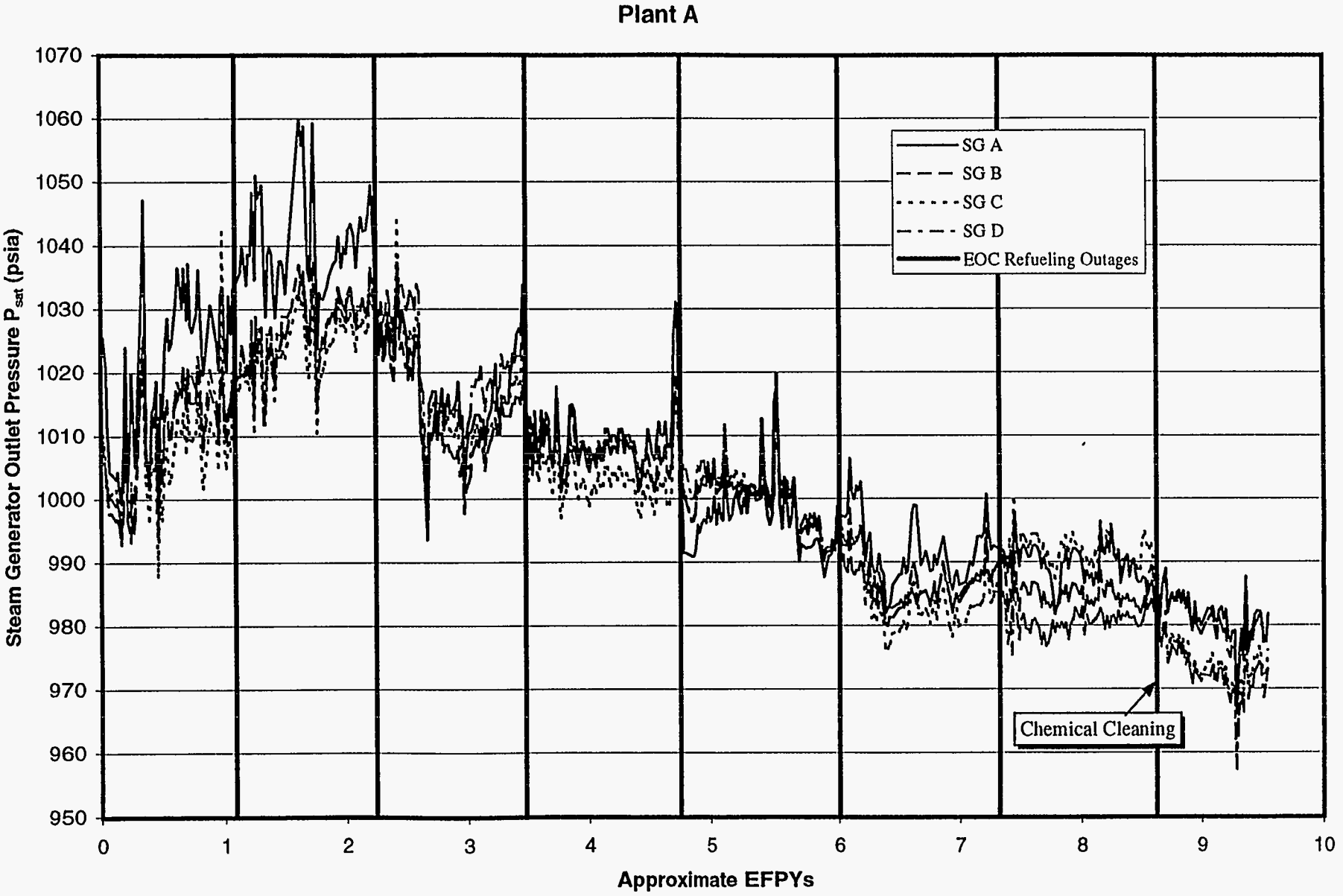

Figure B-A1. Historical Steam Generator Outlet Steam Pressure at Plant A

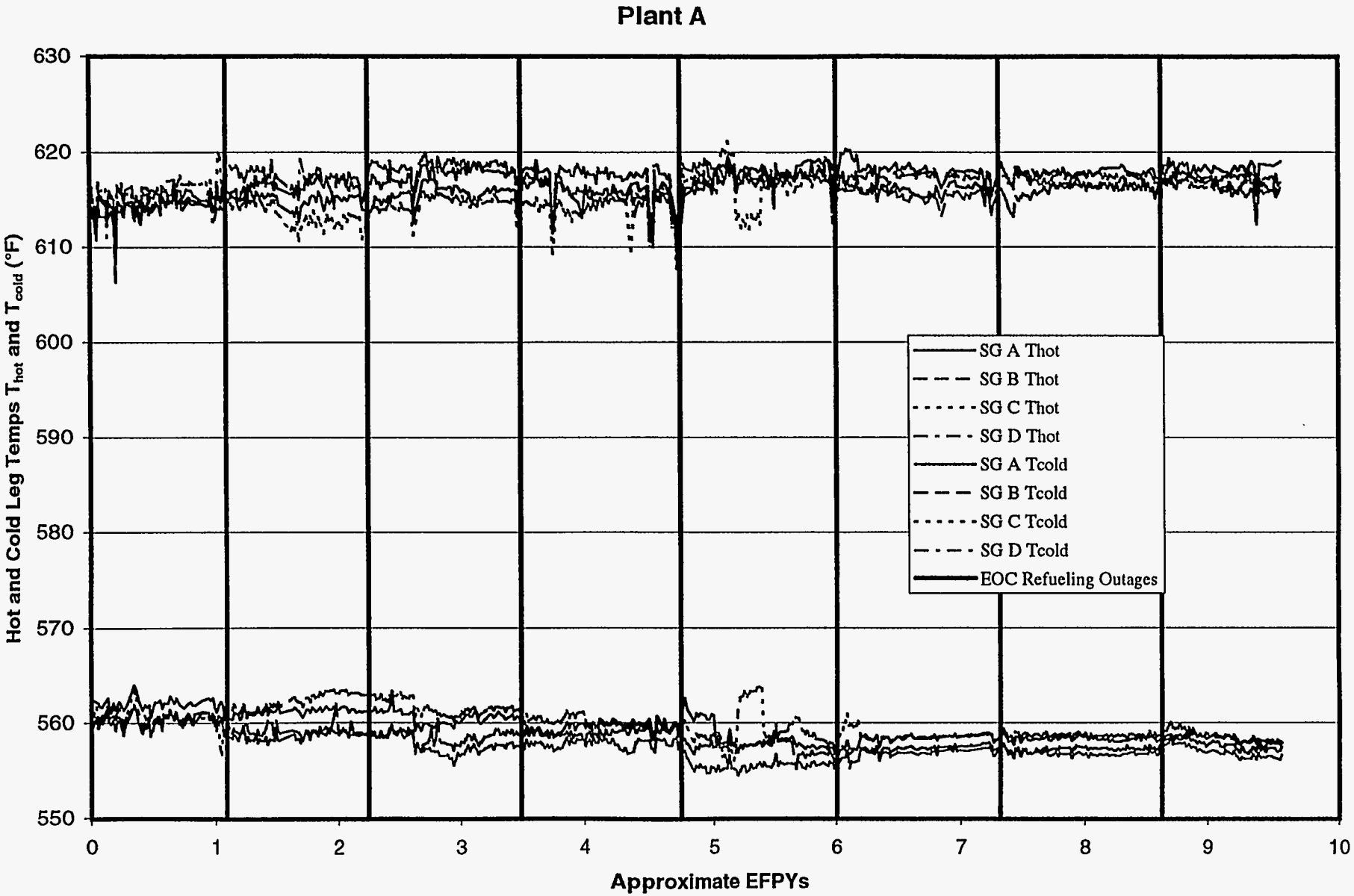

Figure B-A2a. Historical Hot and Cold Leg Temperatures at Plant A

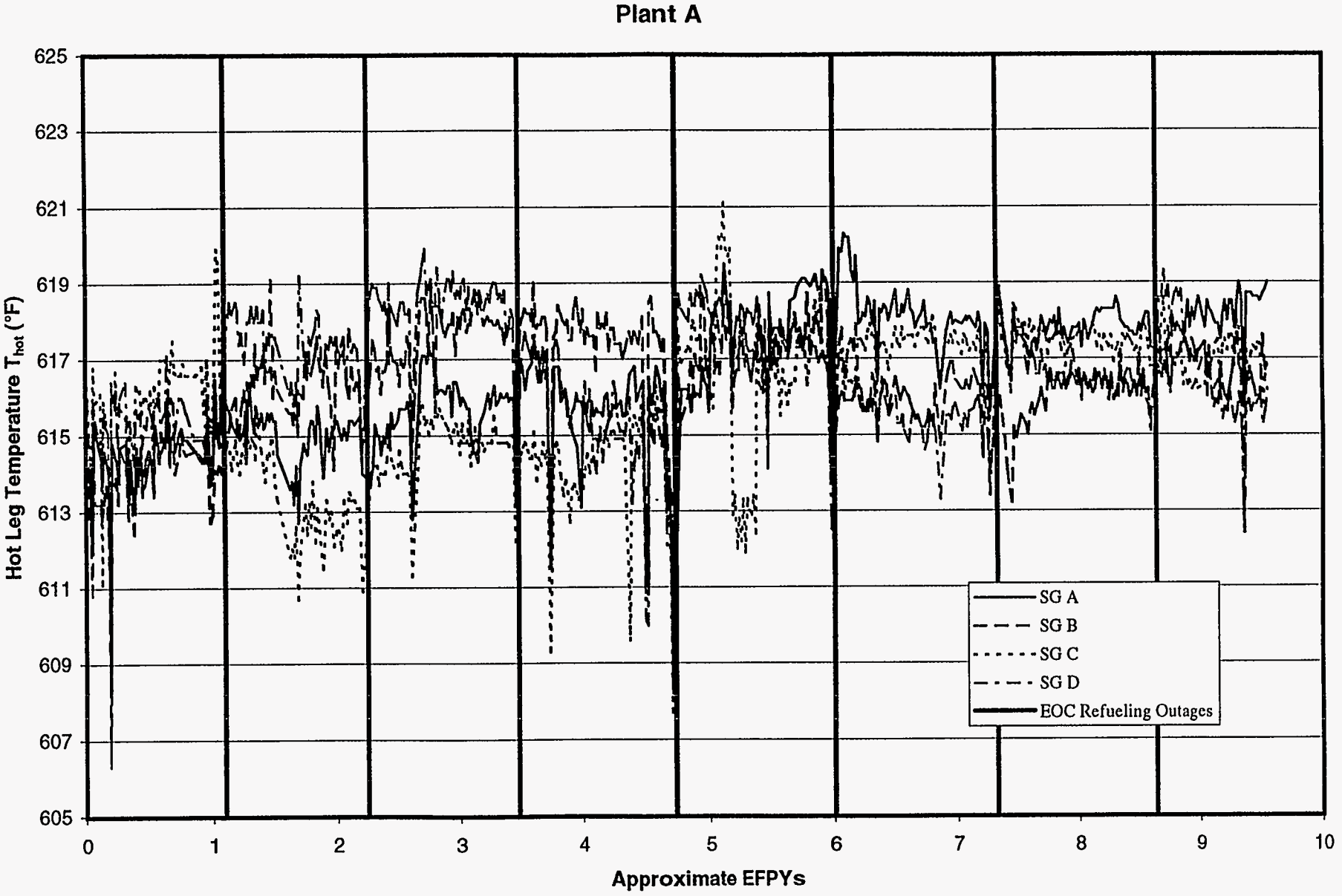

Figure B-A2b. Historical Hot Leg Temperature at Plant A

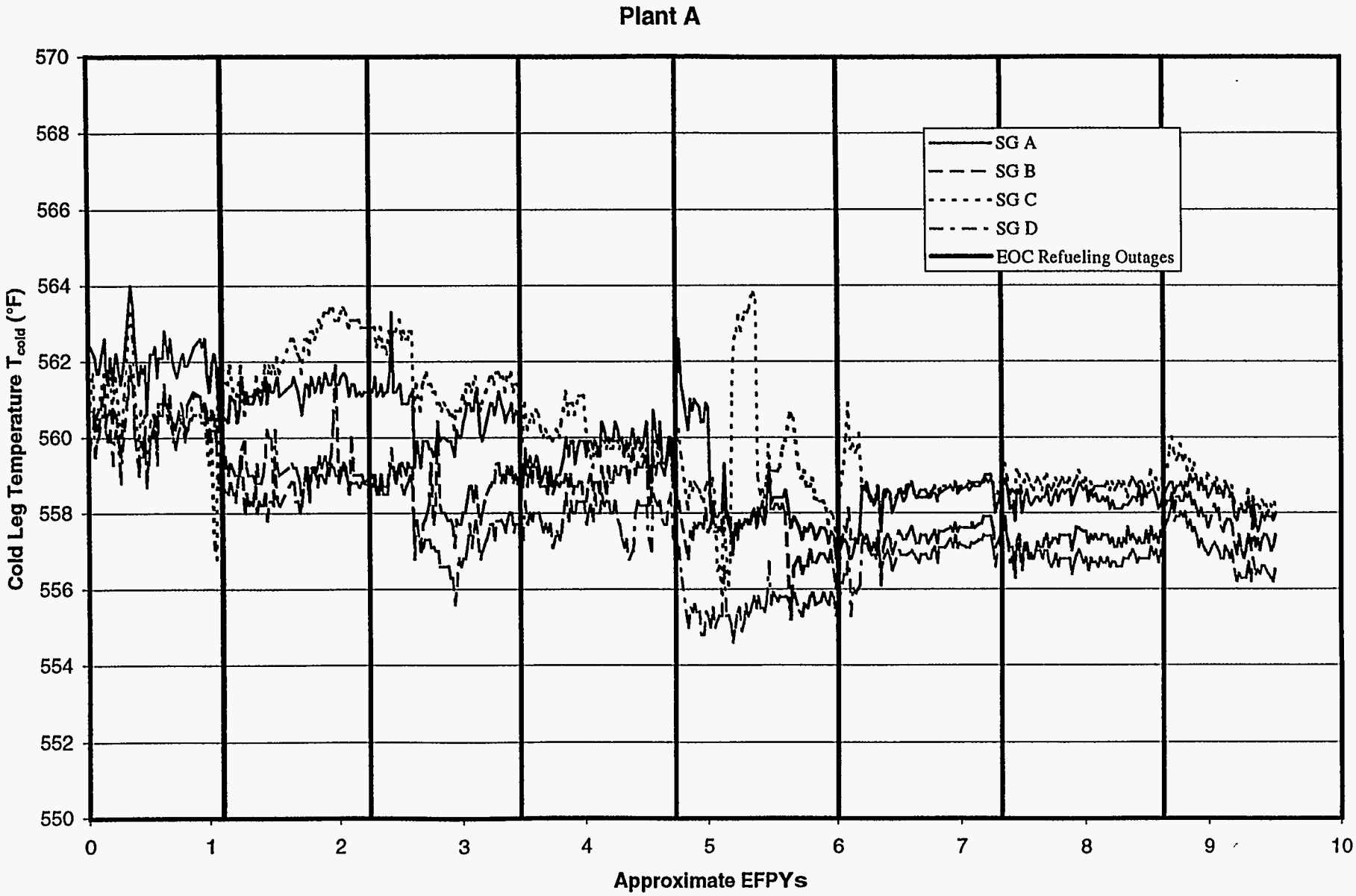

Figure B-A2c. Historical Cold Leg Temperature at Plant A

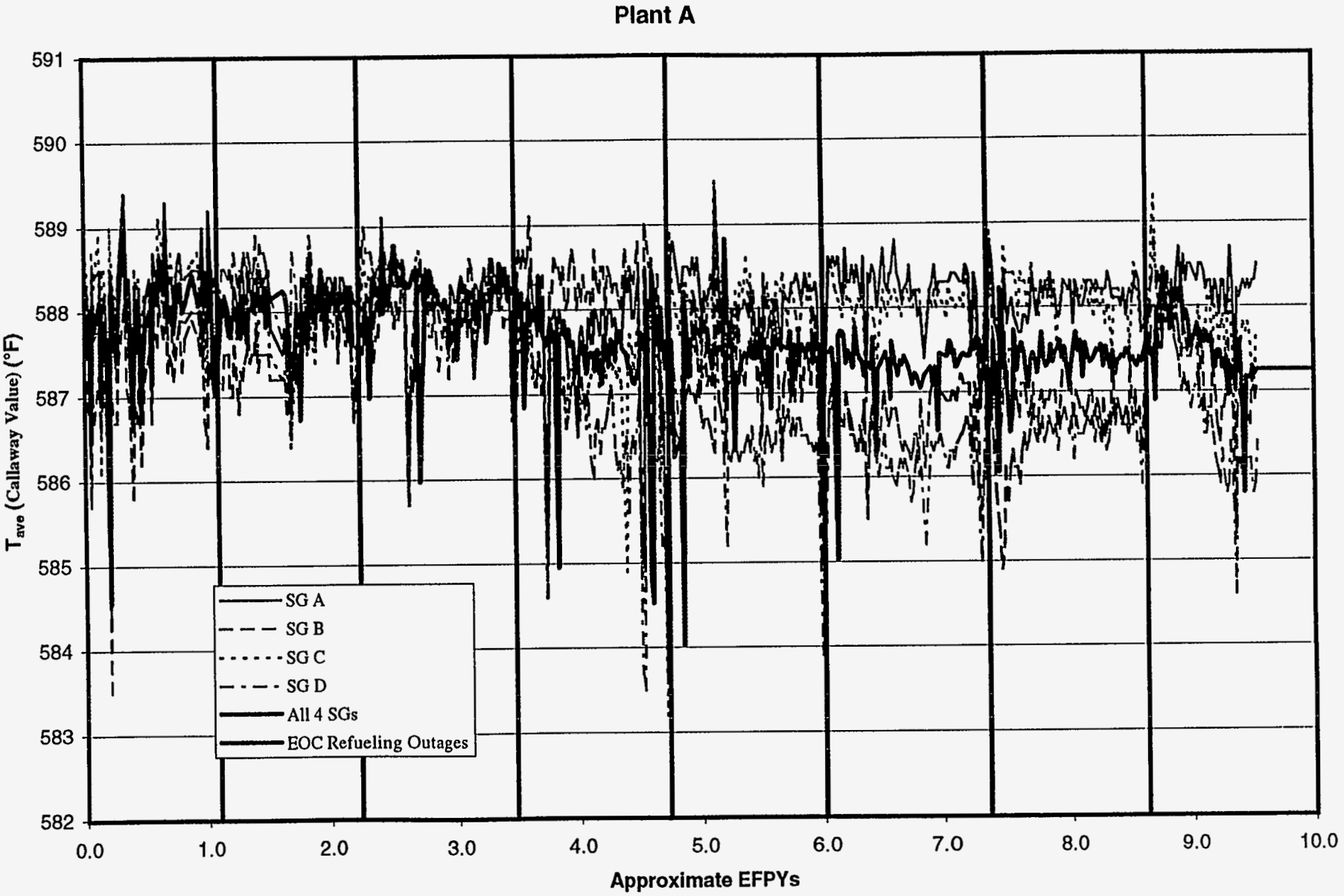

Figure B-A3. Historical Plant-A T_{ave}

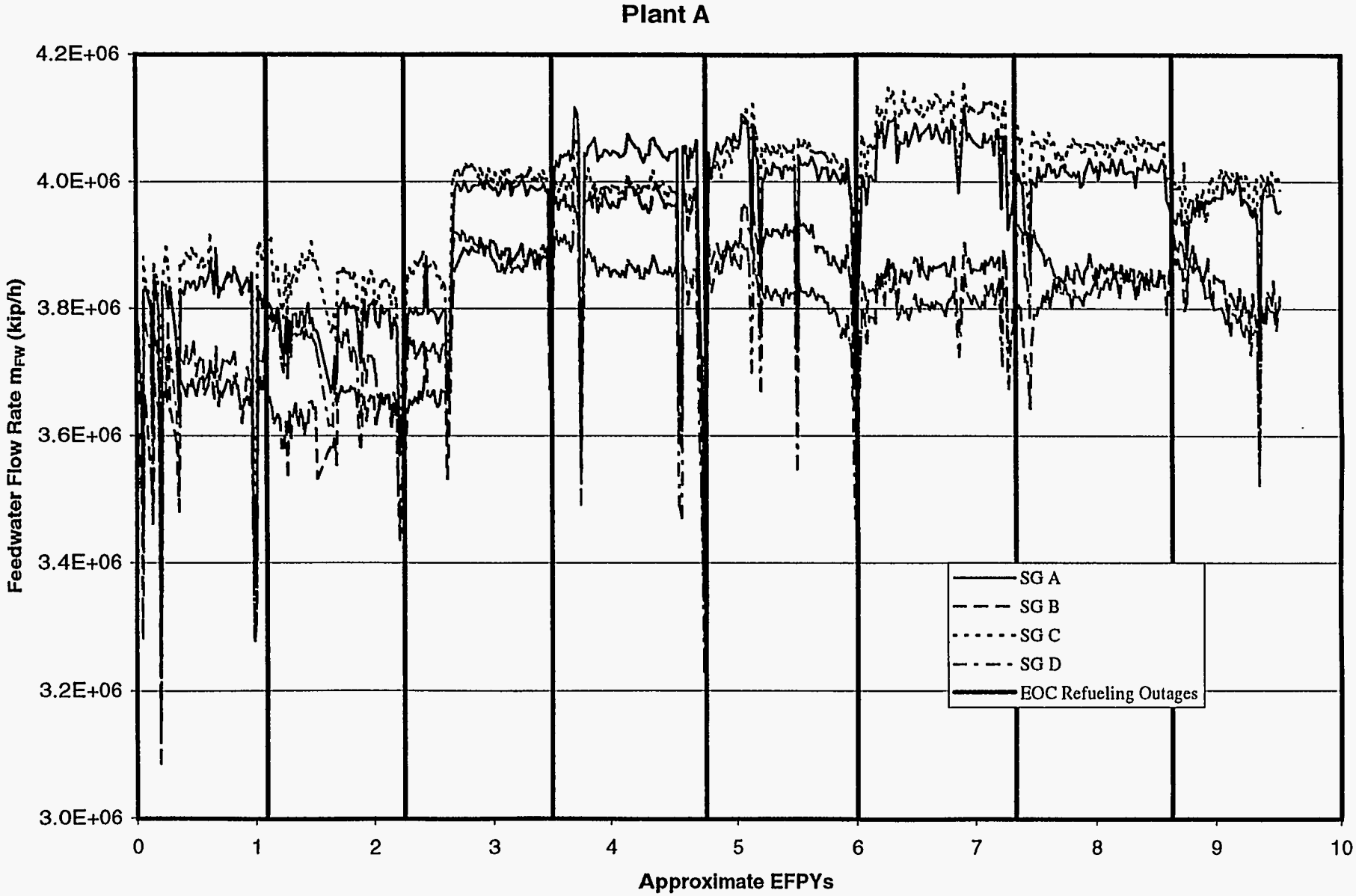

Figure B-A4a. Historical Feedwater Mass Flow Rate at Plant A

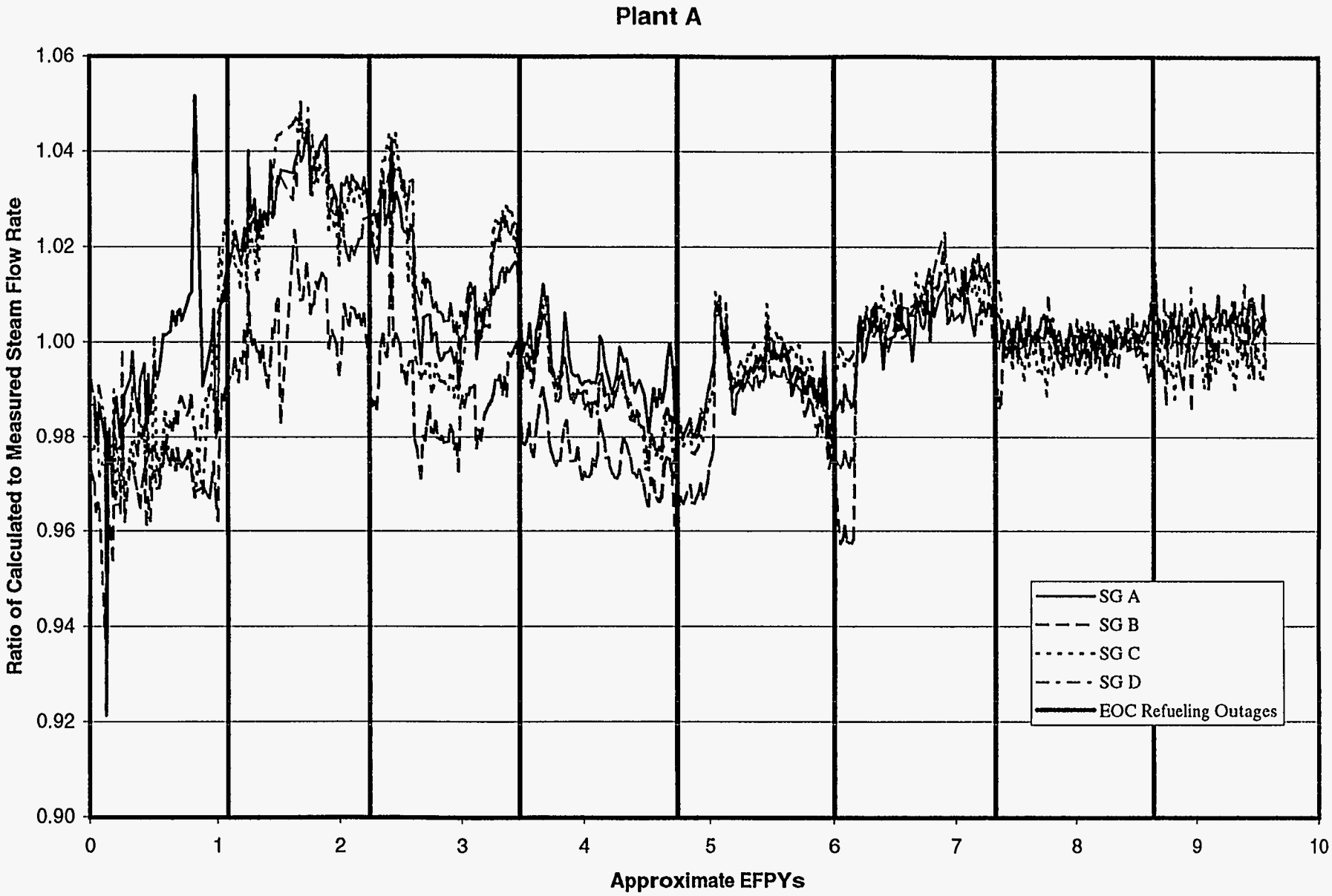

Figure B-A4b. Historical Ratio of Calculated to Measured Steam Flow Rate at Plant A

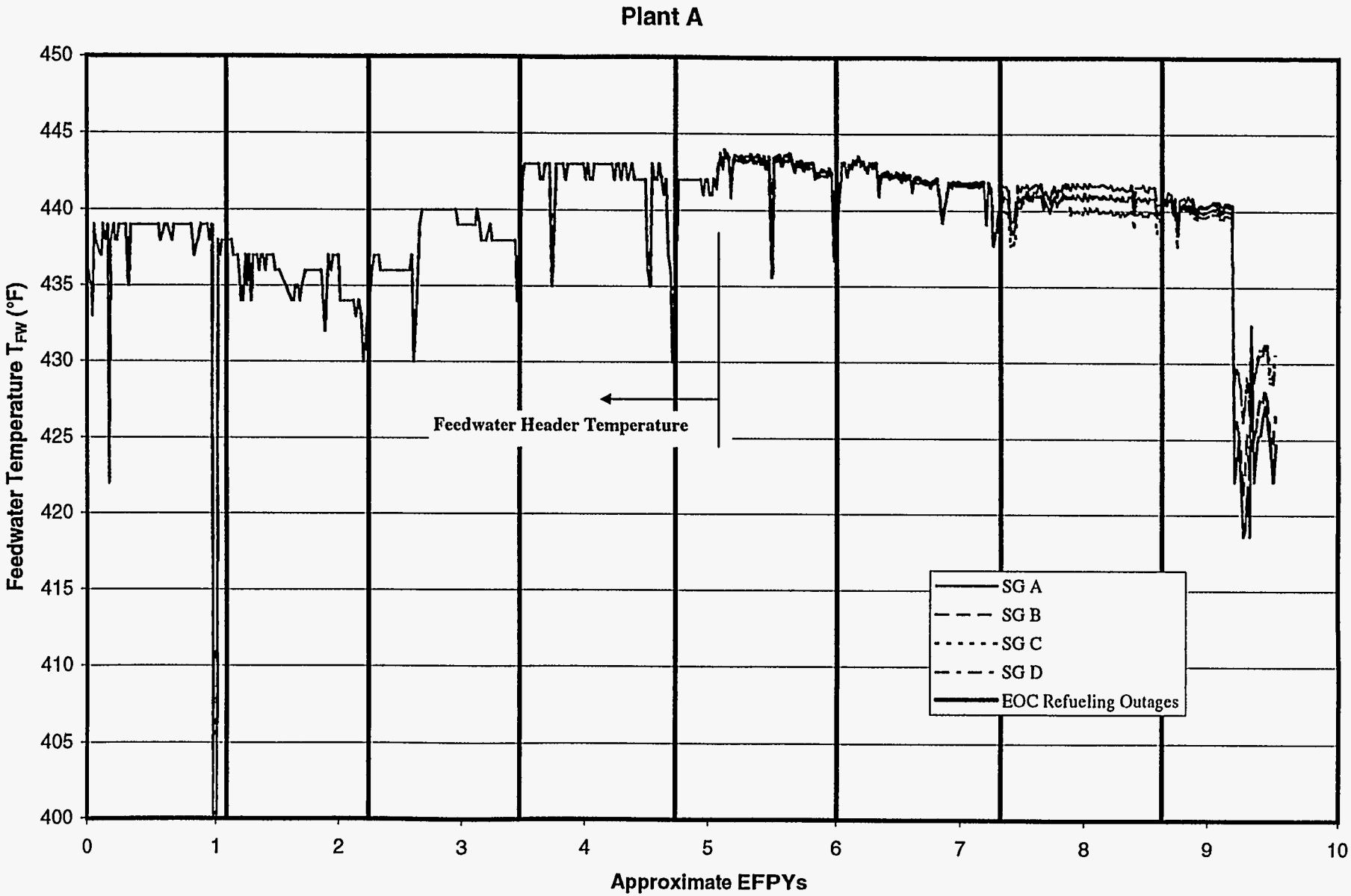

Figure B-A5. Historical Feedwater Temperature at Plant A

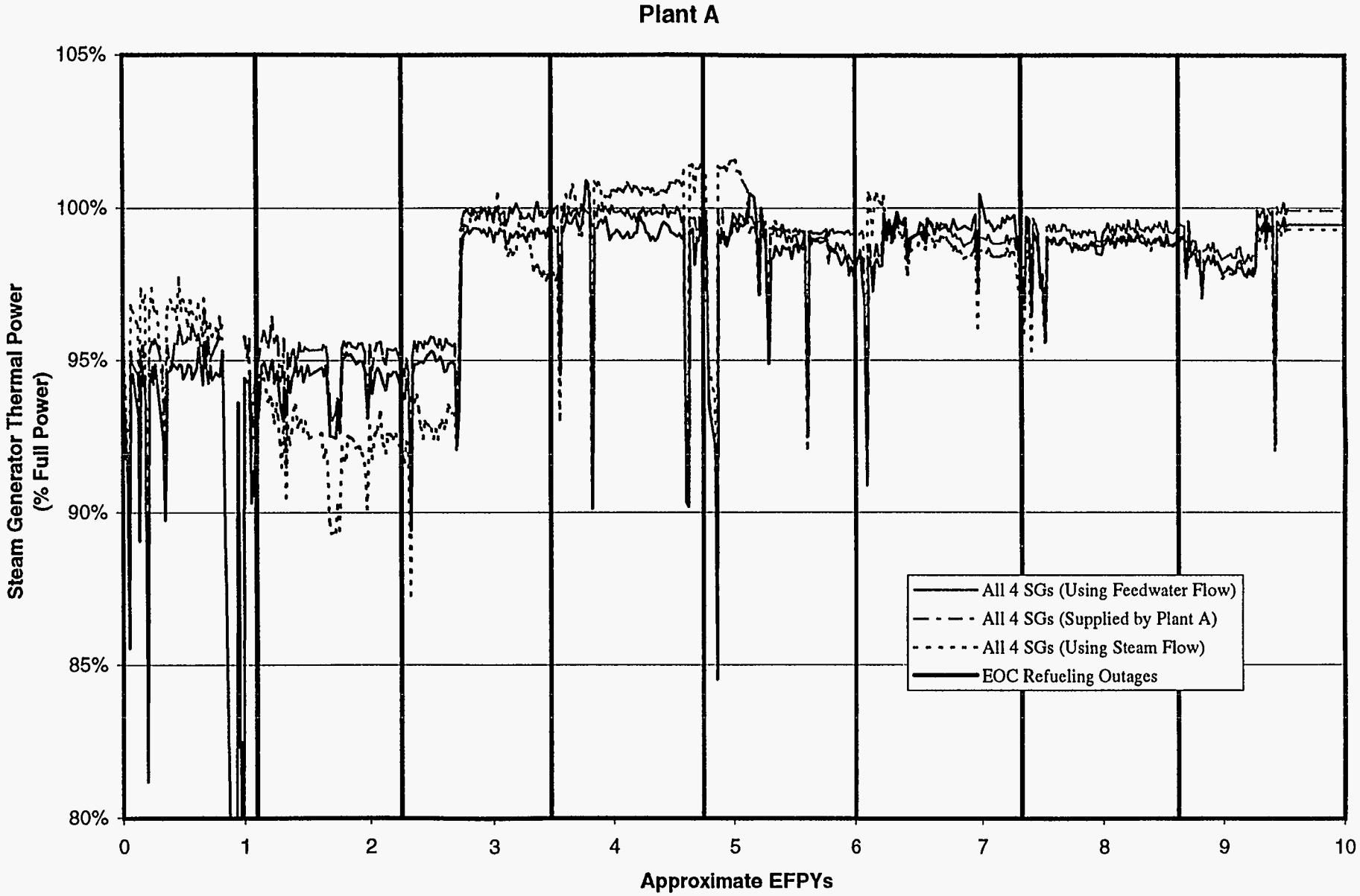

Figure B-A6. Historical Thermal Power Per Steam Generator at Plant A

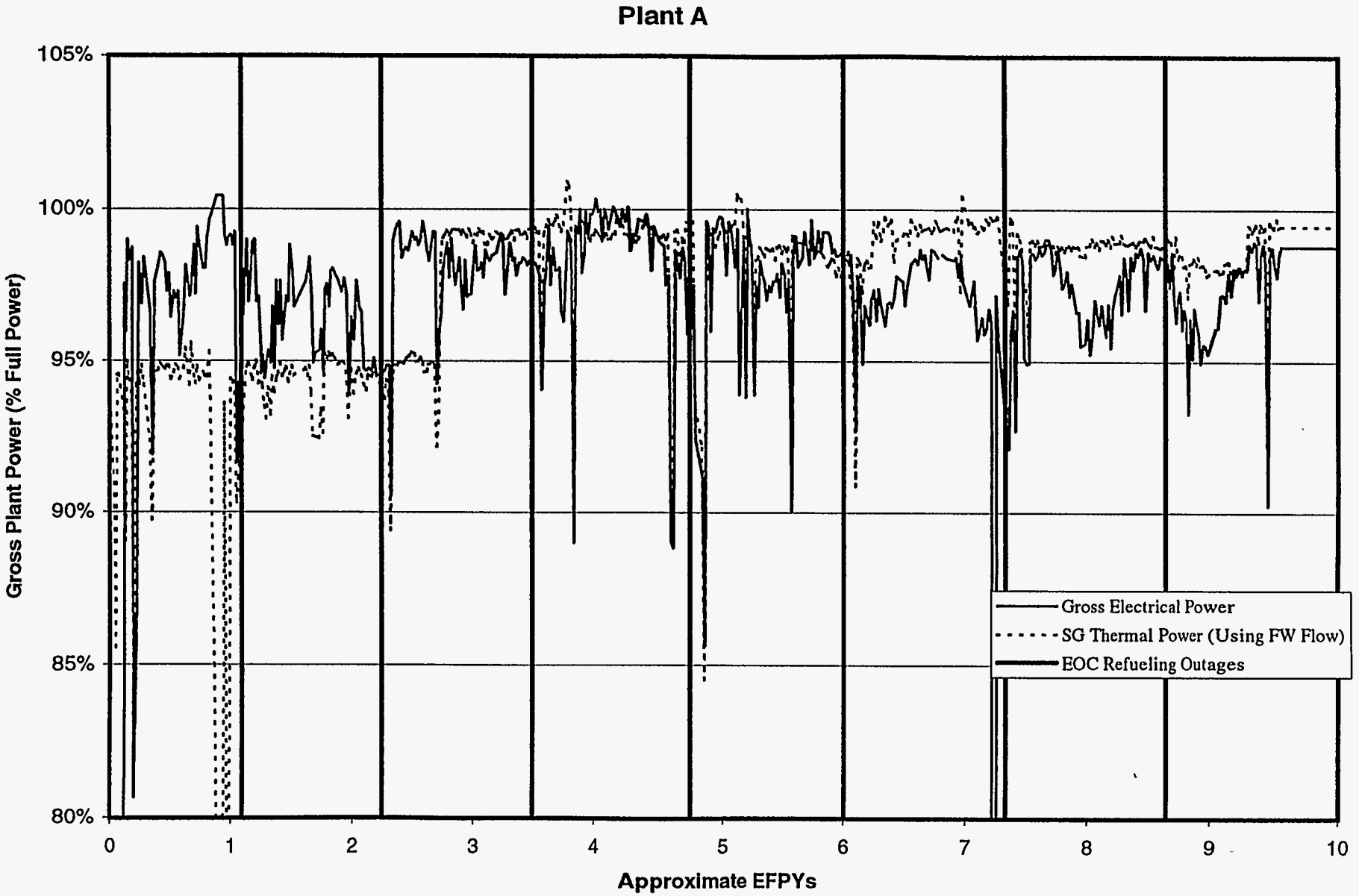

Figure B-A7. Historical Gross Thermal and Electrical Power Output at Plant A

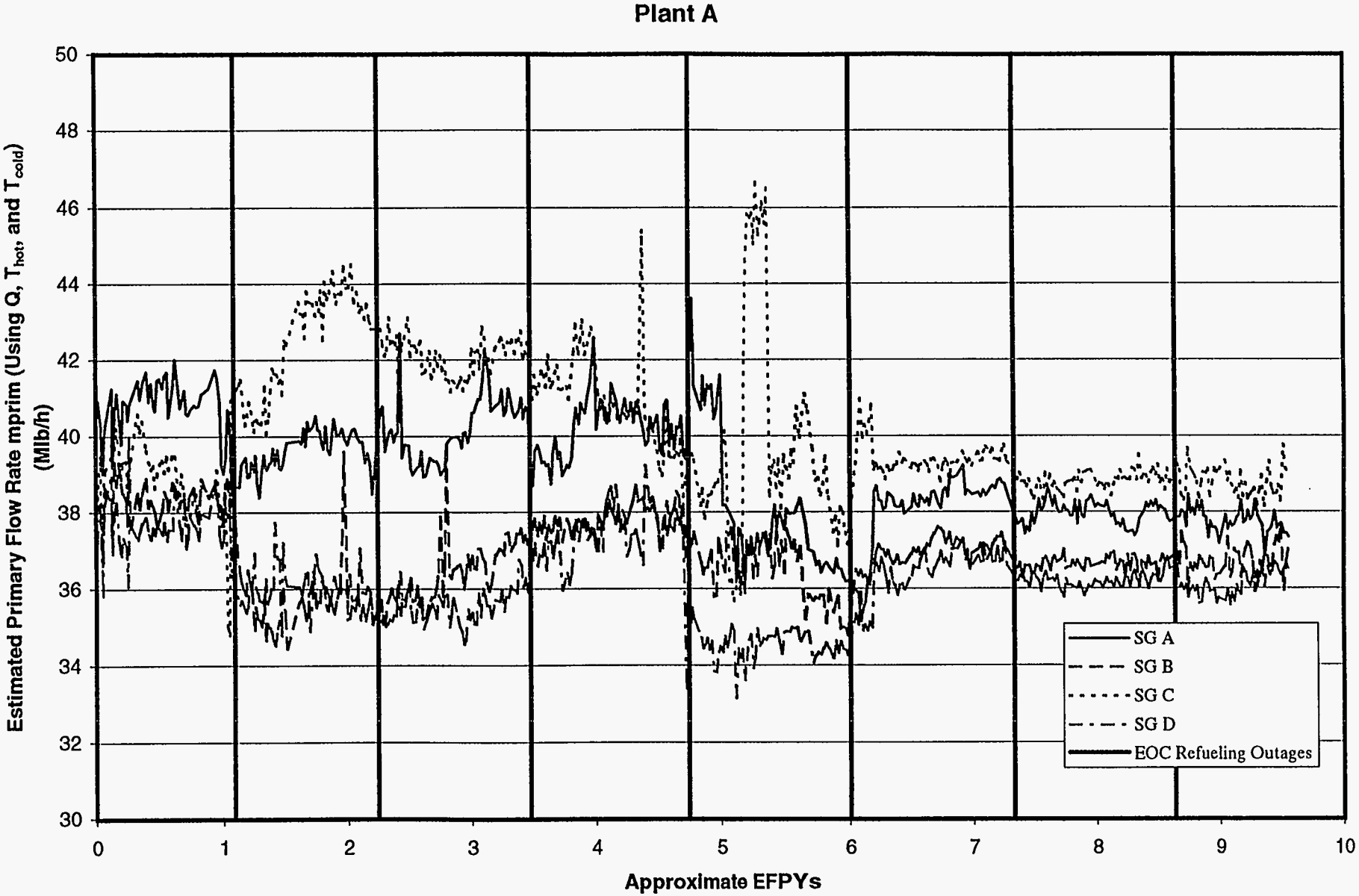

Figure B-A8. Historical Estimated Primary Mass Flow Rate at Plant A

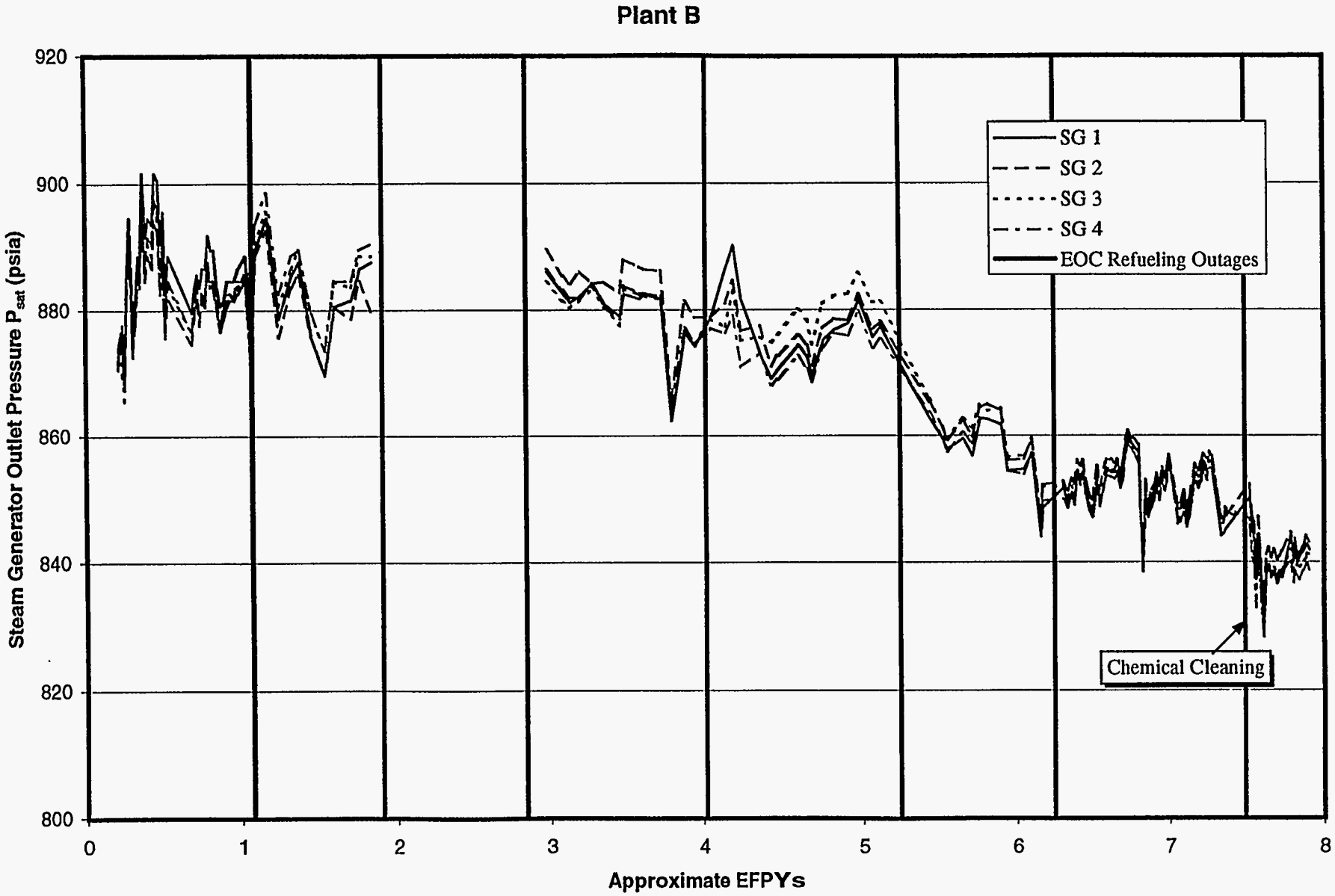

Figure B-B1. Historical Steam Generator Outlet Steam Pressure at Plant B

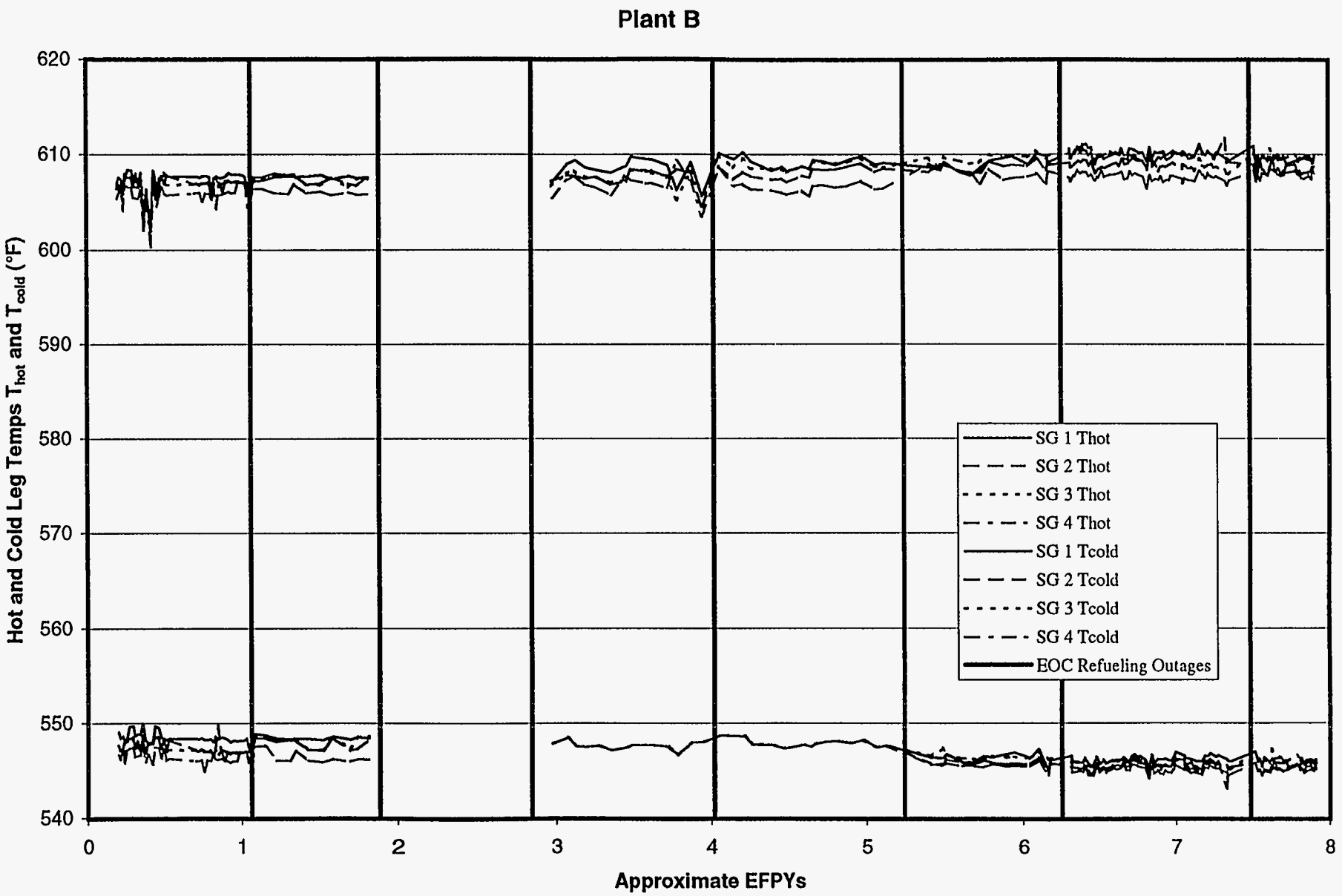

Figure B-B2a. Historical Hot and Cold Leg Temperatures at Plant B (As Measured)

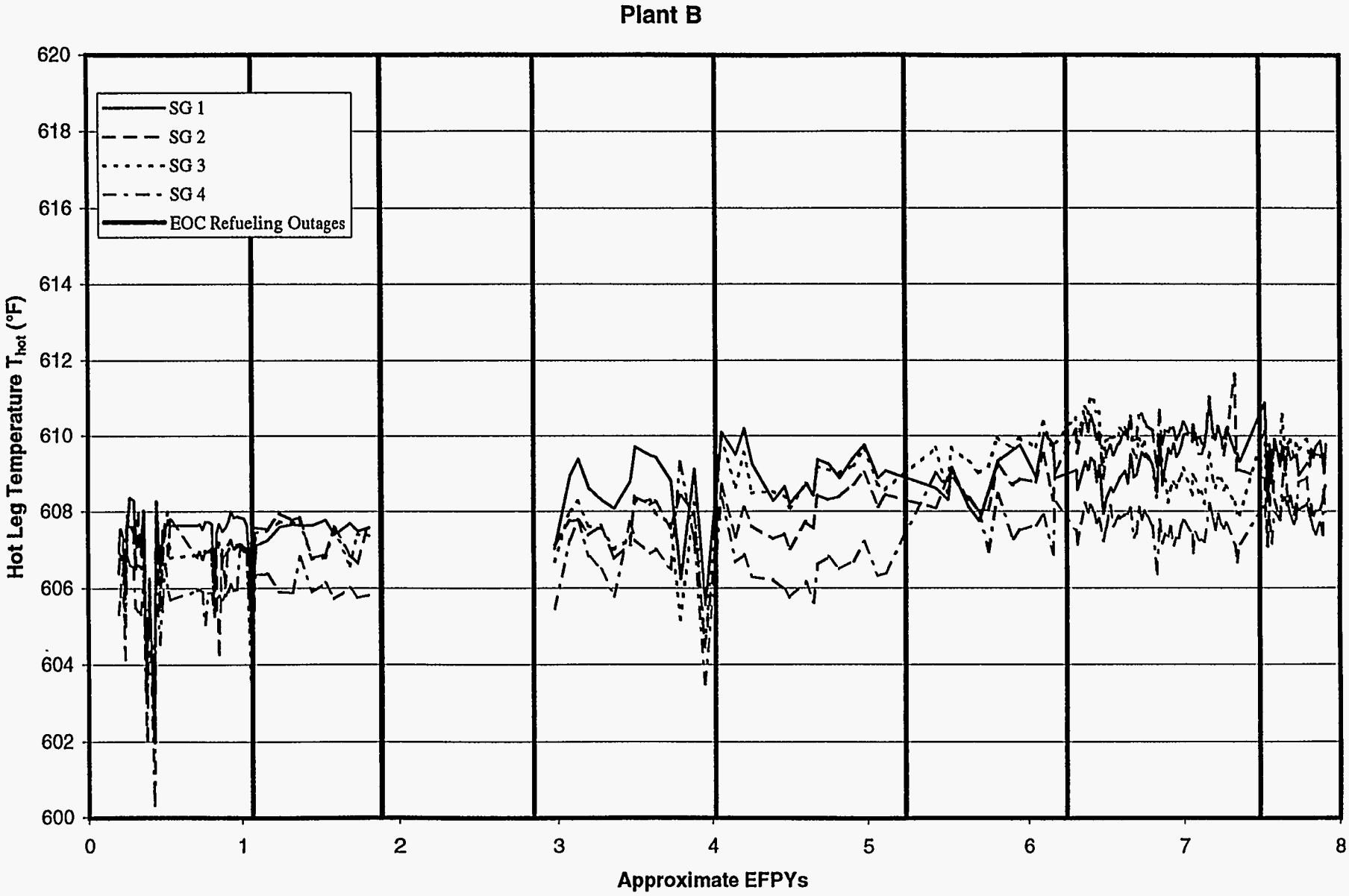

Figure B-B2b. Historical Hot Leg Temperature at Plant B (As Measured)

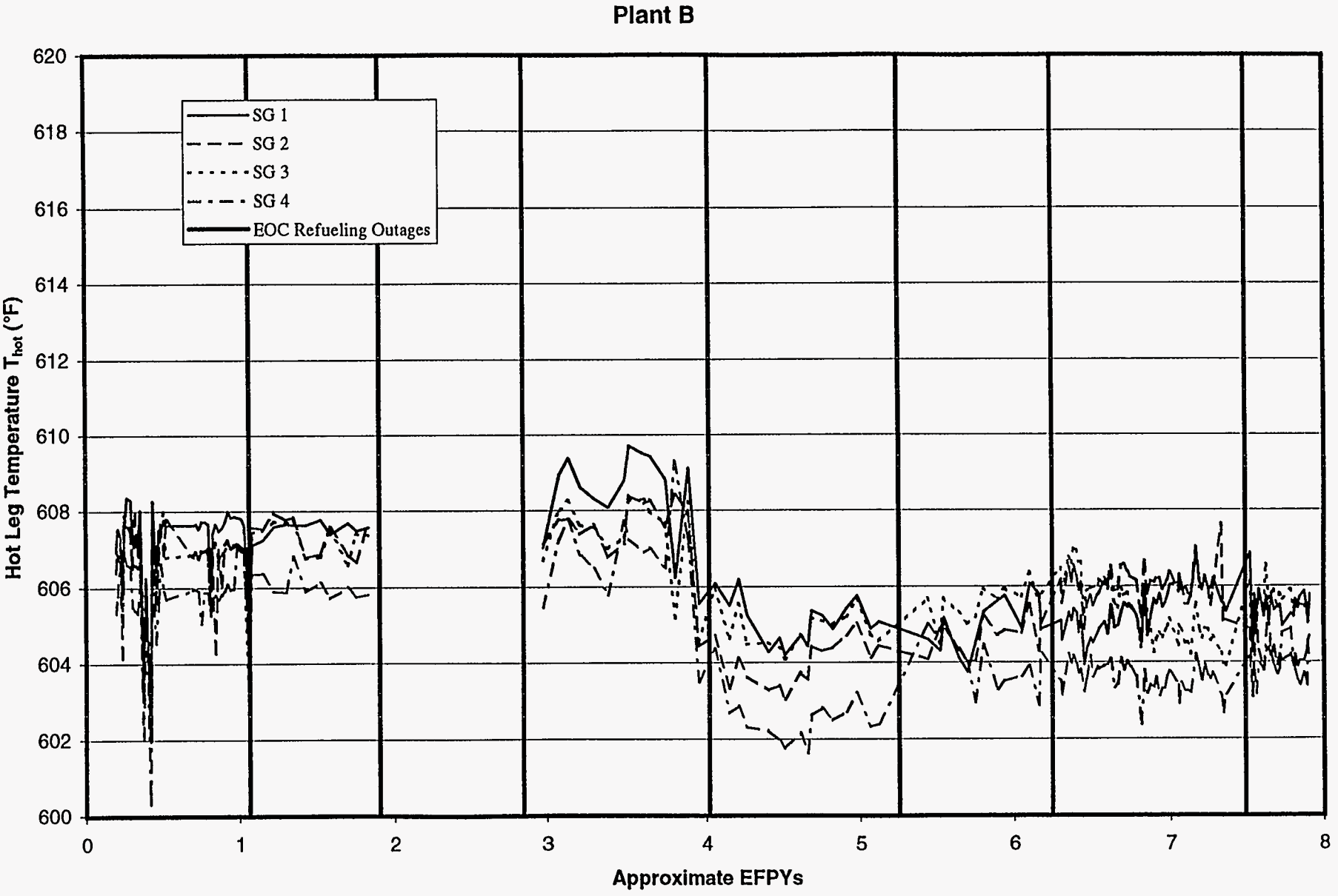

Figure B-B2c. Historical Hot Leg Temperature at Plant B (Corrected for HL Streaming)

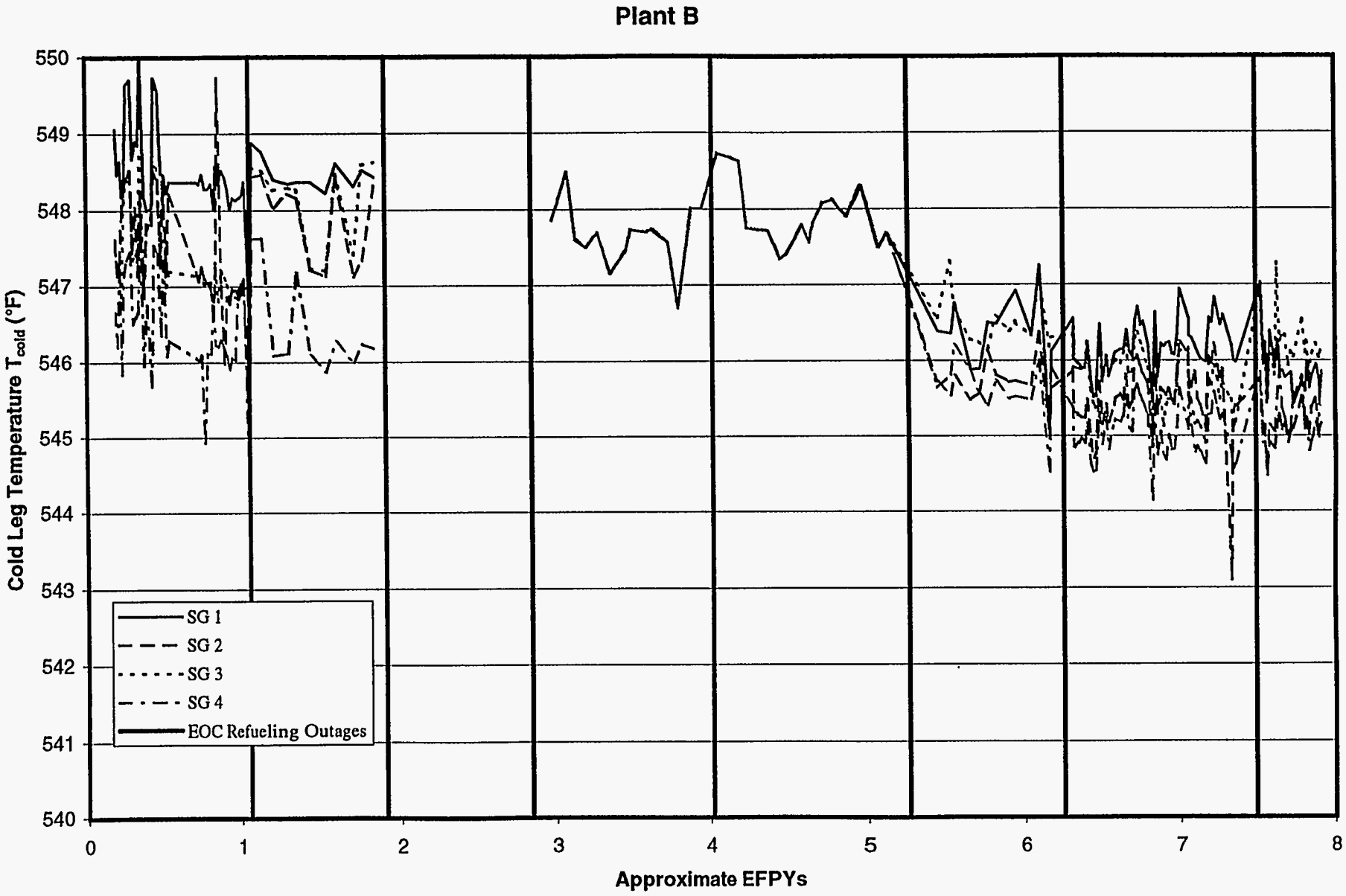

Figure B-B2d. Historical Cold Leg Temperature at Plant B

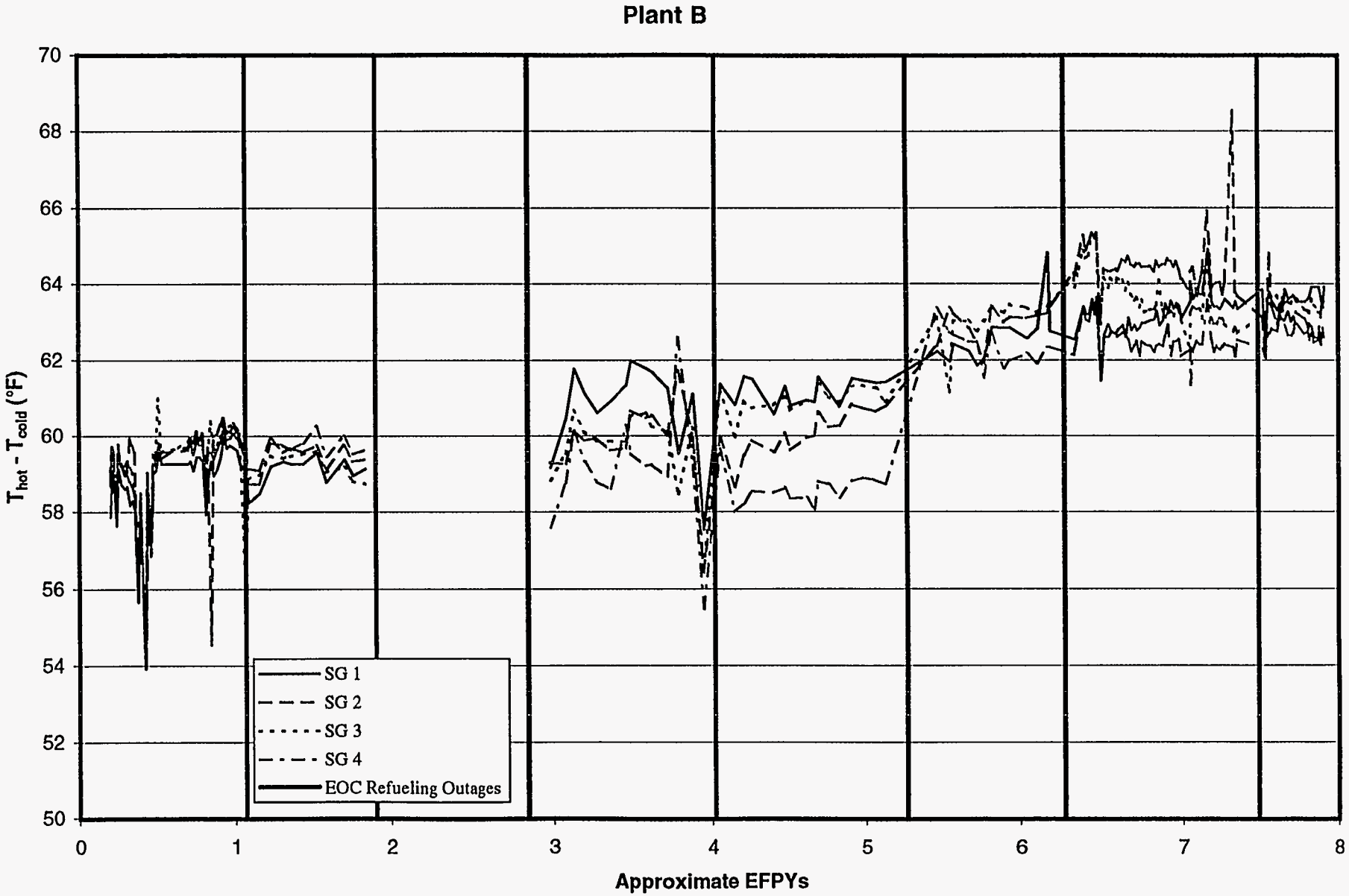

Figure B-B3. Historical Primary Temperature Difference at Plant B

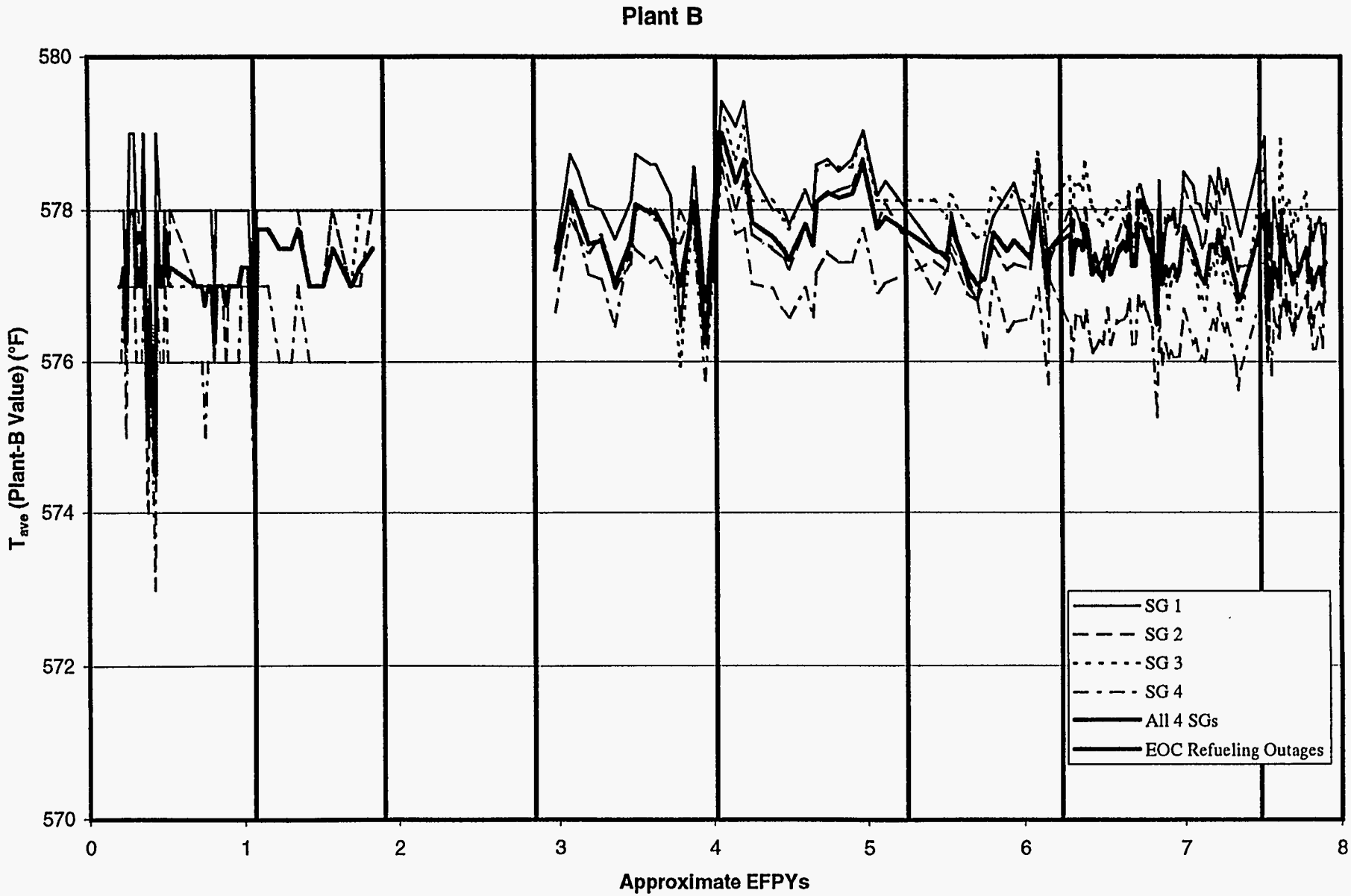

Figure B-B4. Historical Plant-B T_{ave}

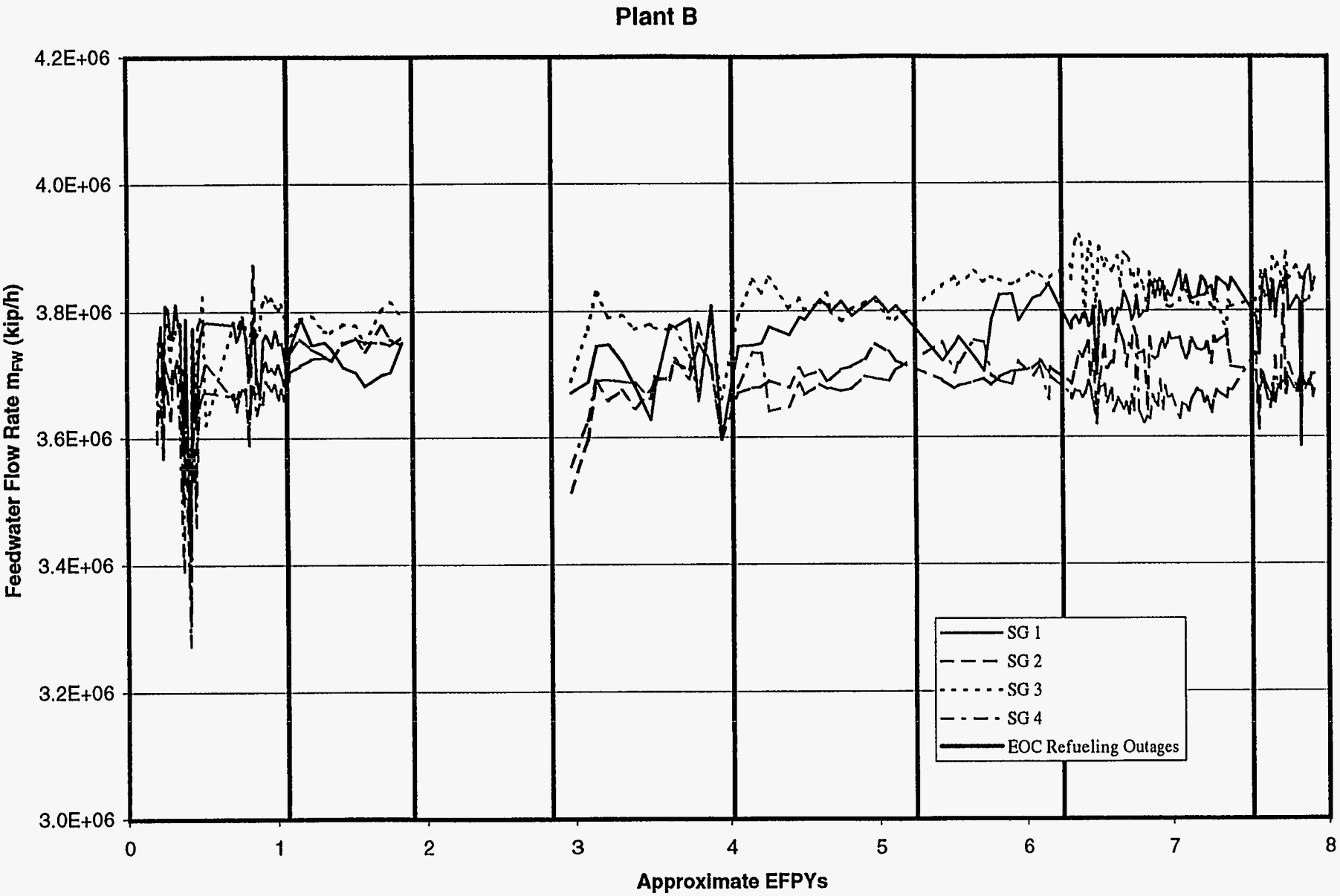

Figure B-B5a. Historical Feedwater Mass Flow Rate at Plant B

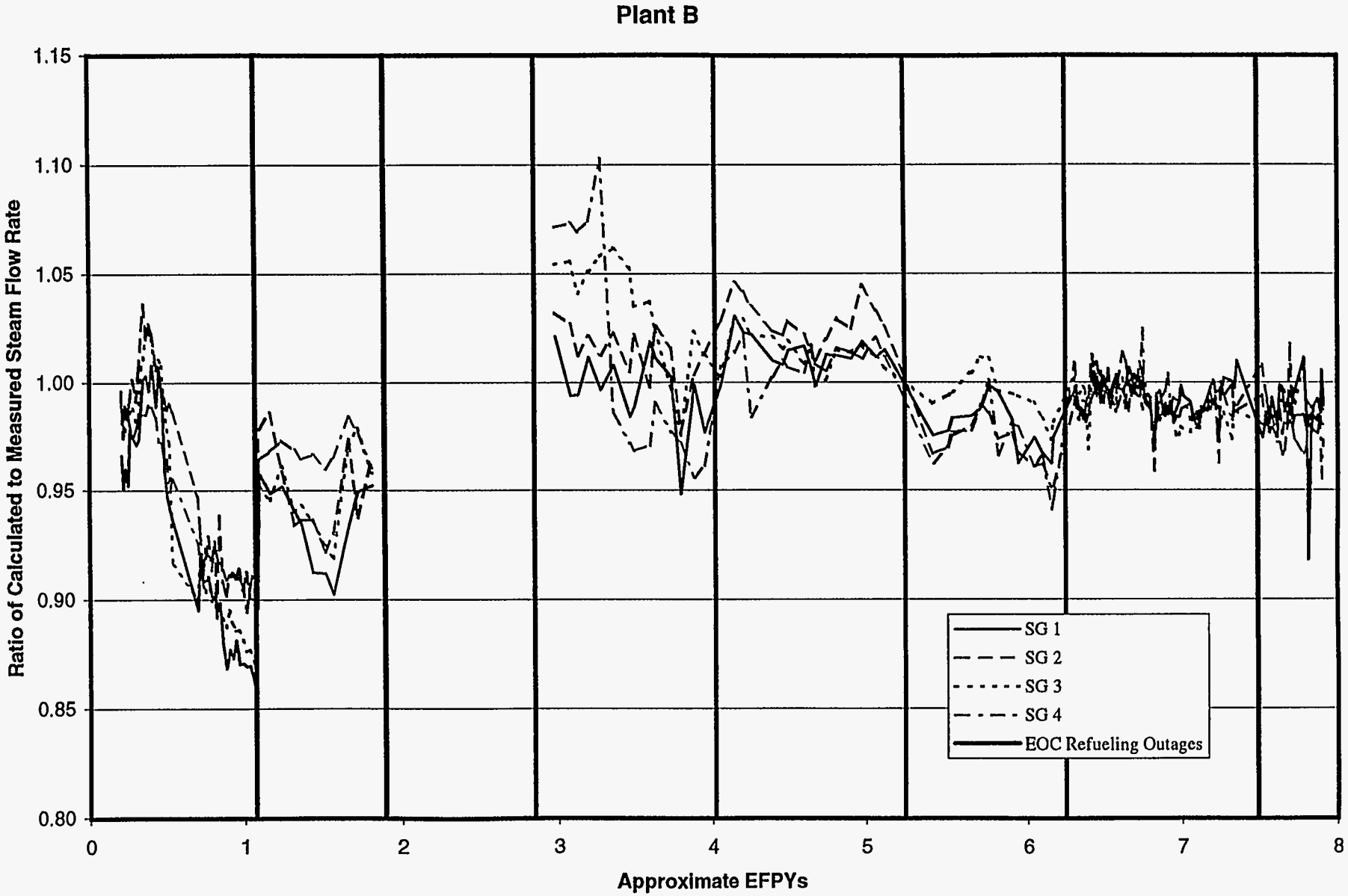

Figure B-B5b. Historical Ratio of Calculated to Measured Steam Flow Rate at Plant B

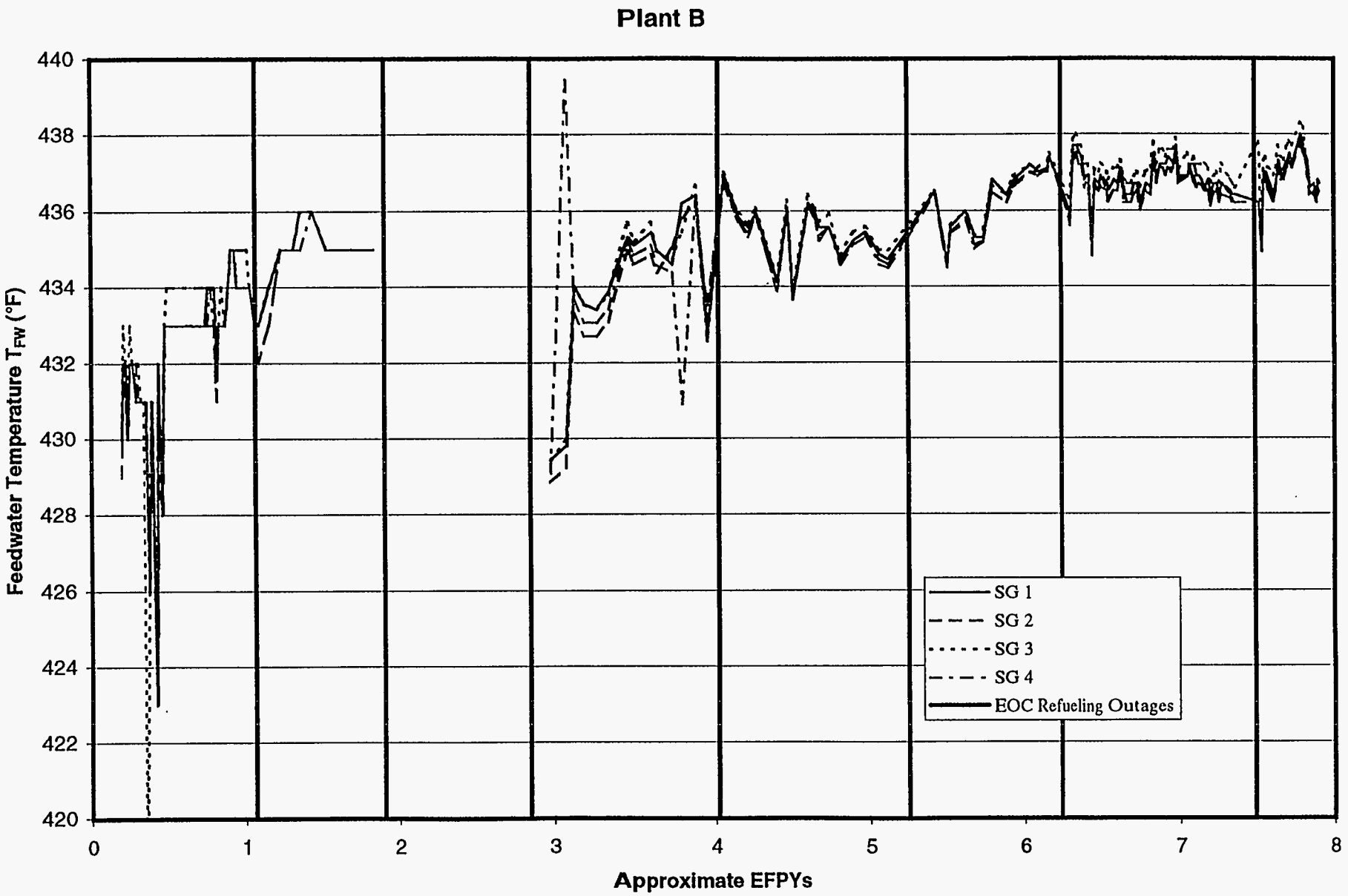

Figure B-B6. Historical Feedwater Temperature at Plant B

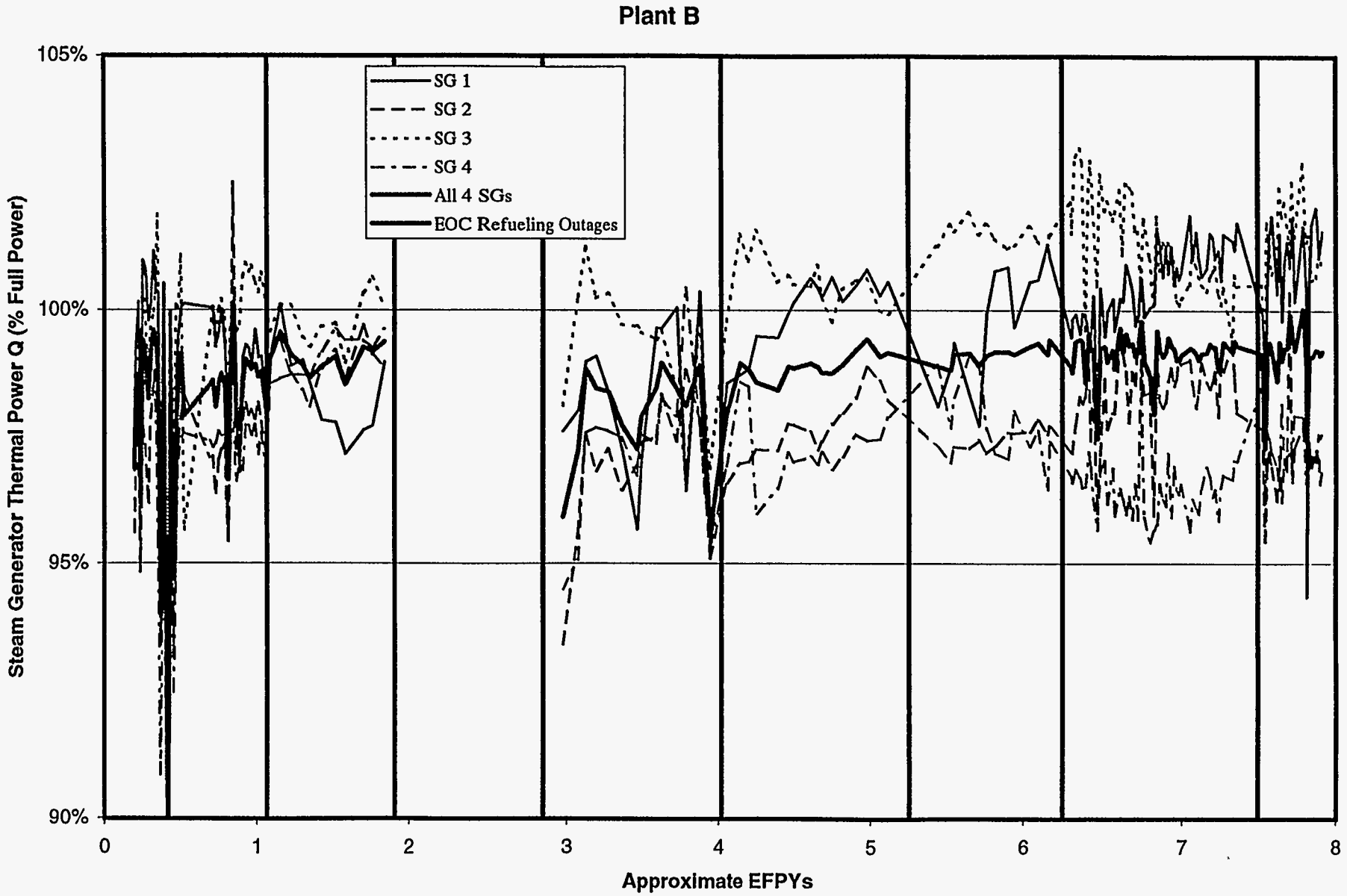

Figure B-B7. Historical Thermal Power Per Steam Generator at Plant B

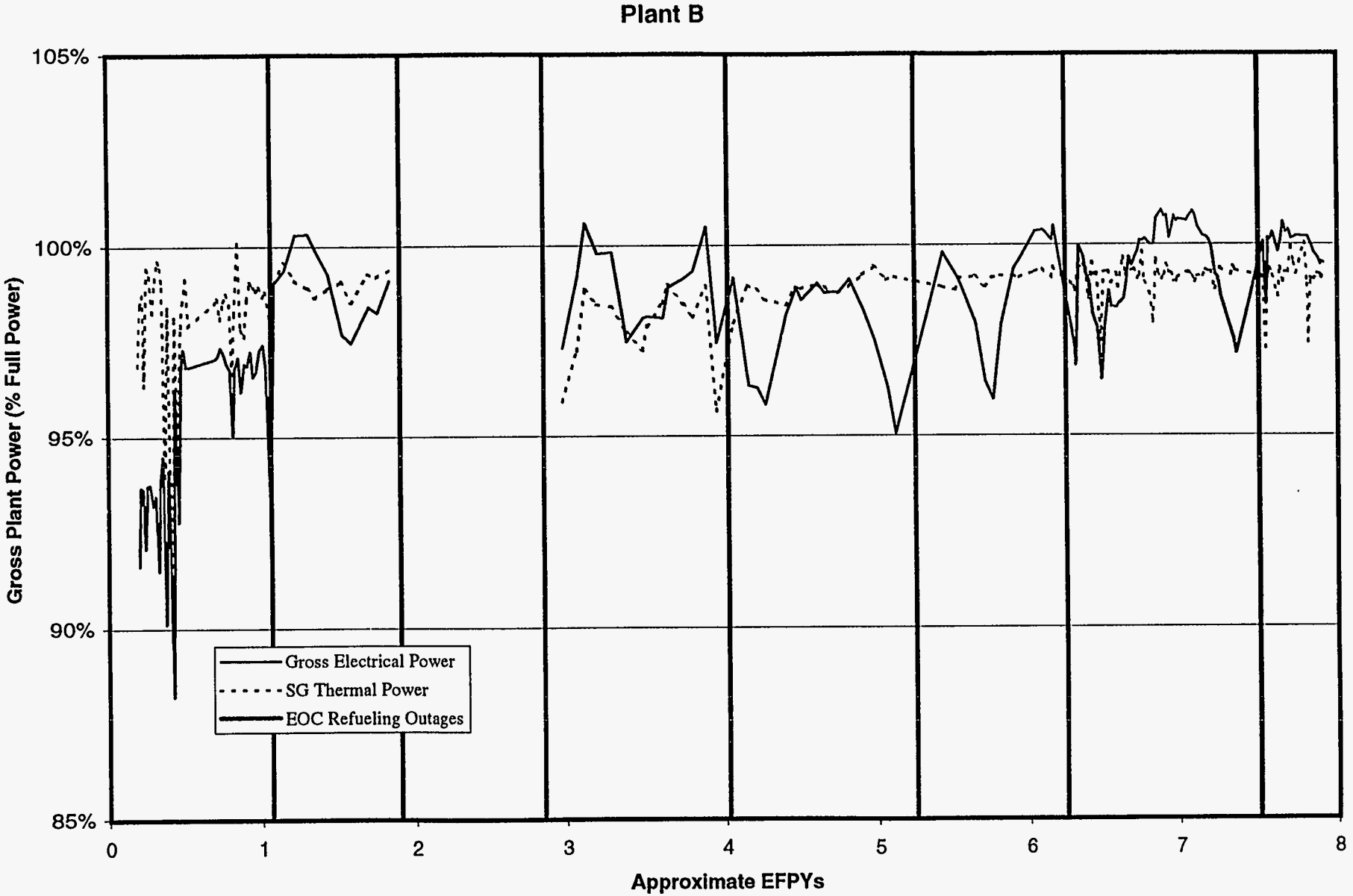

Figure B-B8. Historical Gross Thermal and Electrical Power Output at Plant B

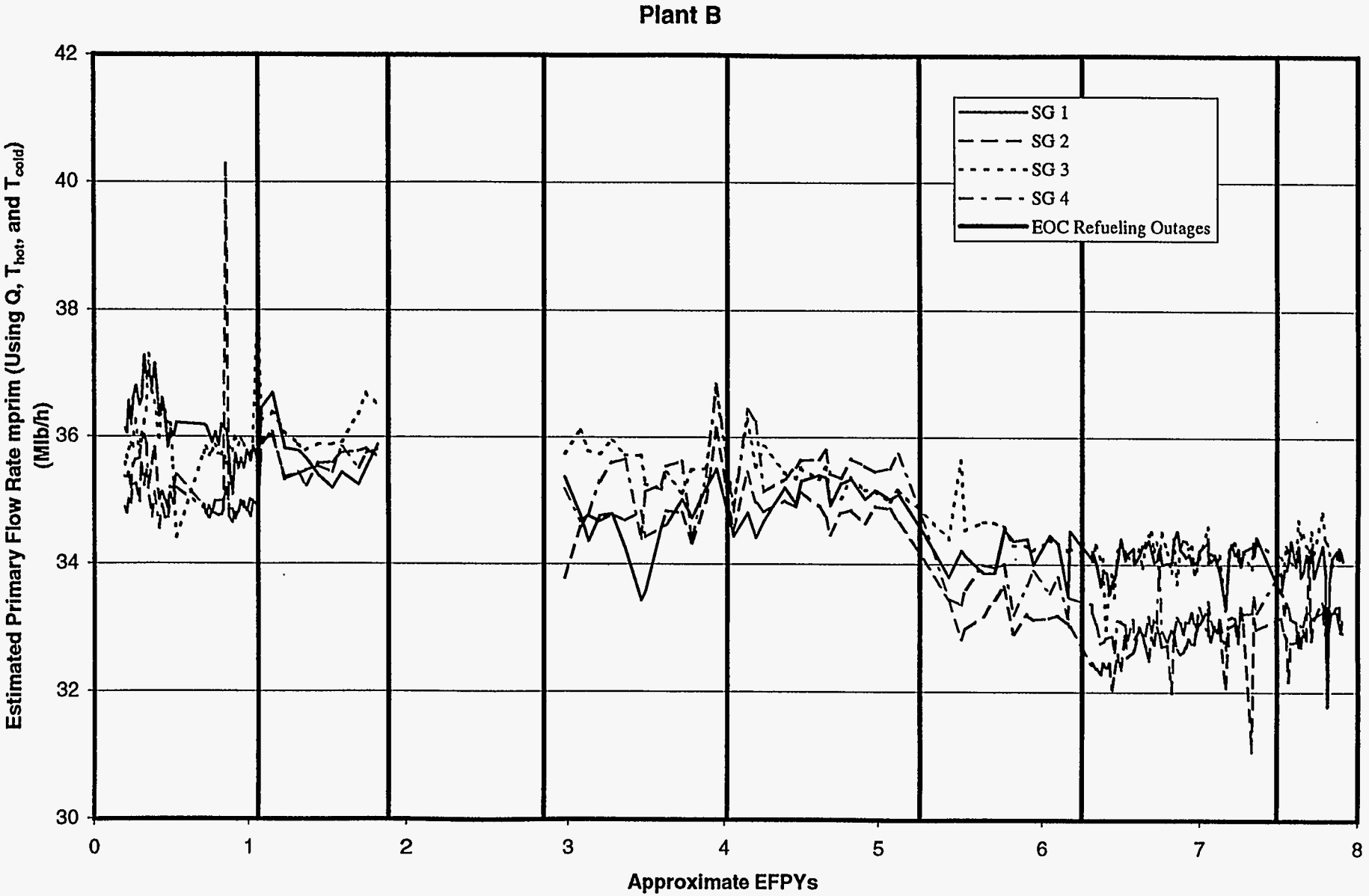

Figure B-B9. Historical Estimated Primary Mass Flow Rate at Plant B

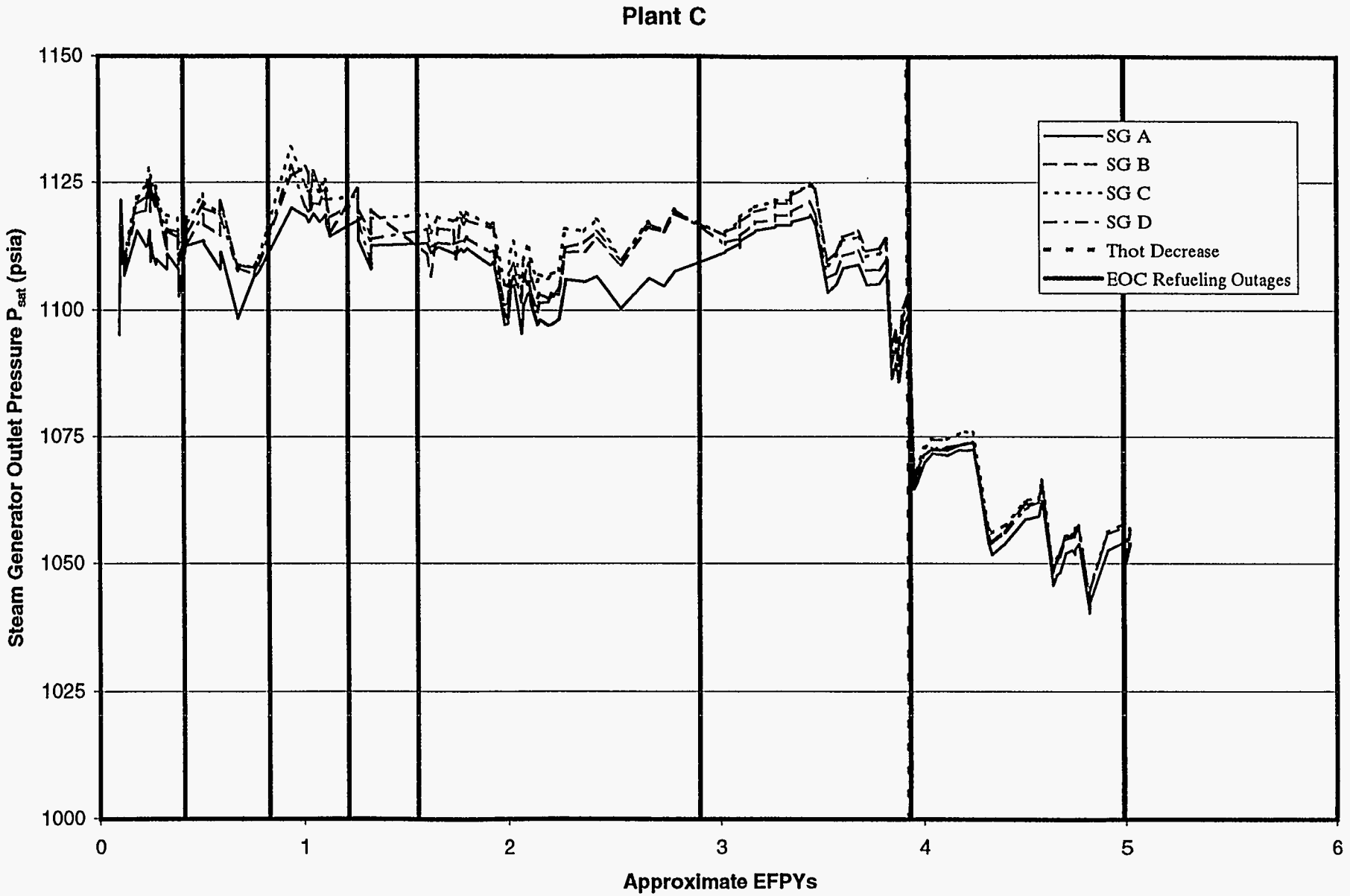

Figure B-C1. Historical Steam Generator Outlet Steam Pressure at Plant C

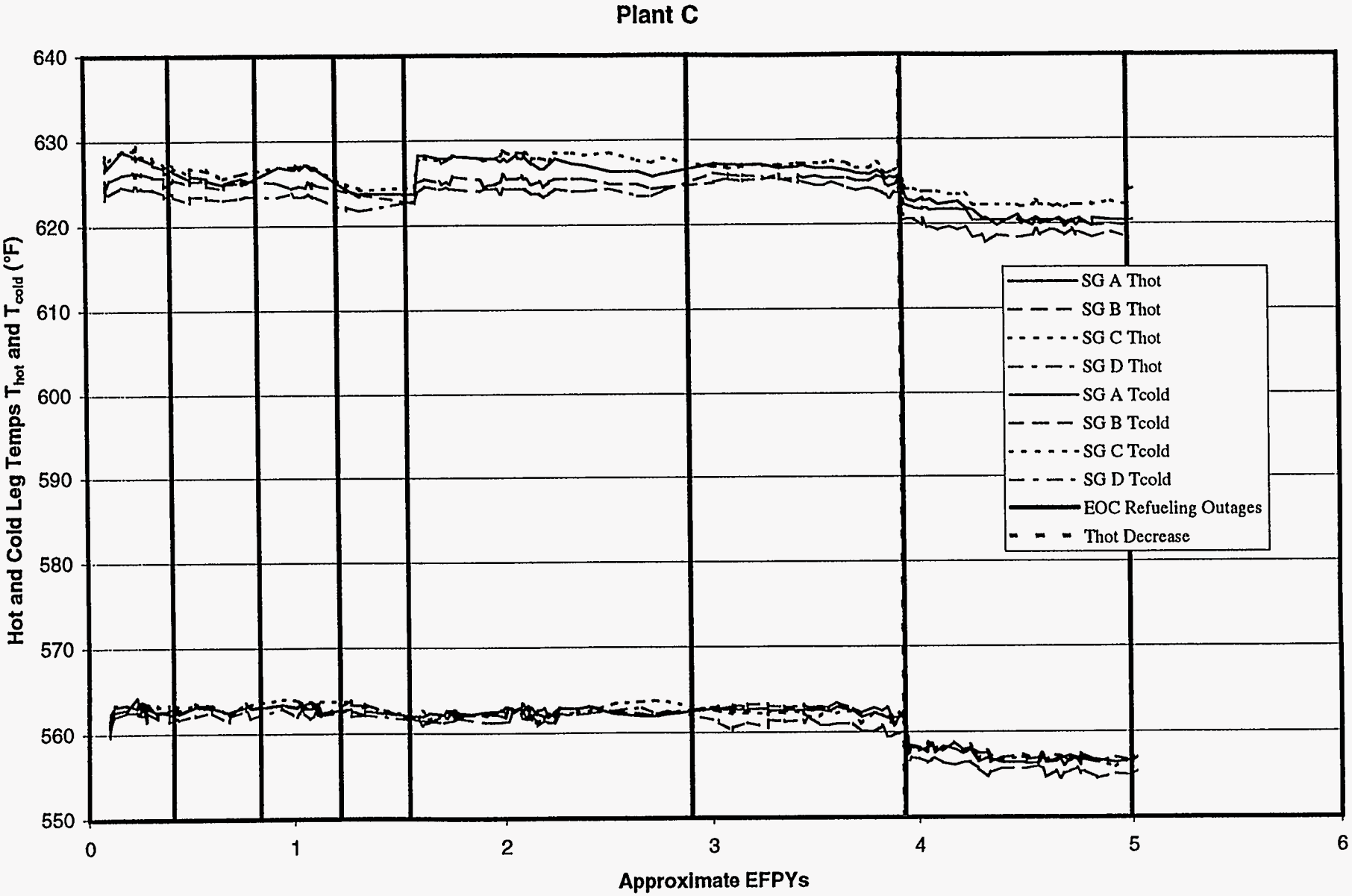

Figure B-C2a. Historical Hot and Cold Leg Temperatures at Plant C

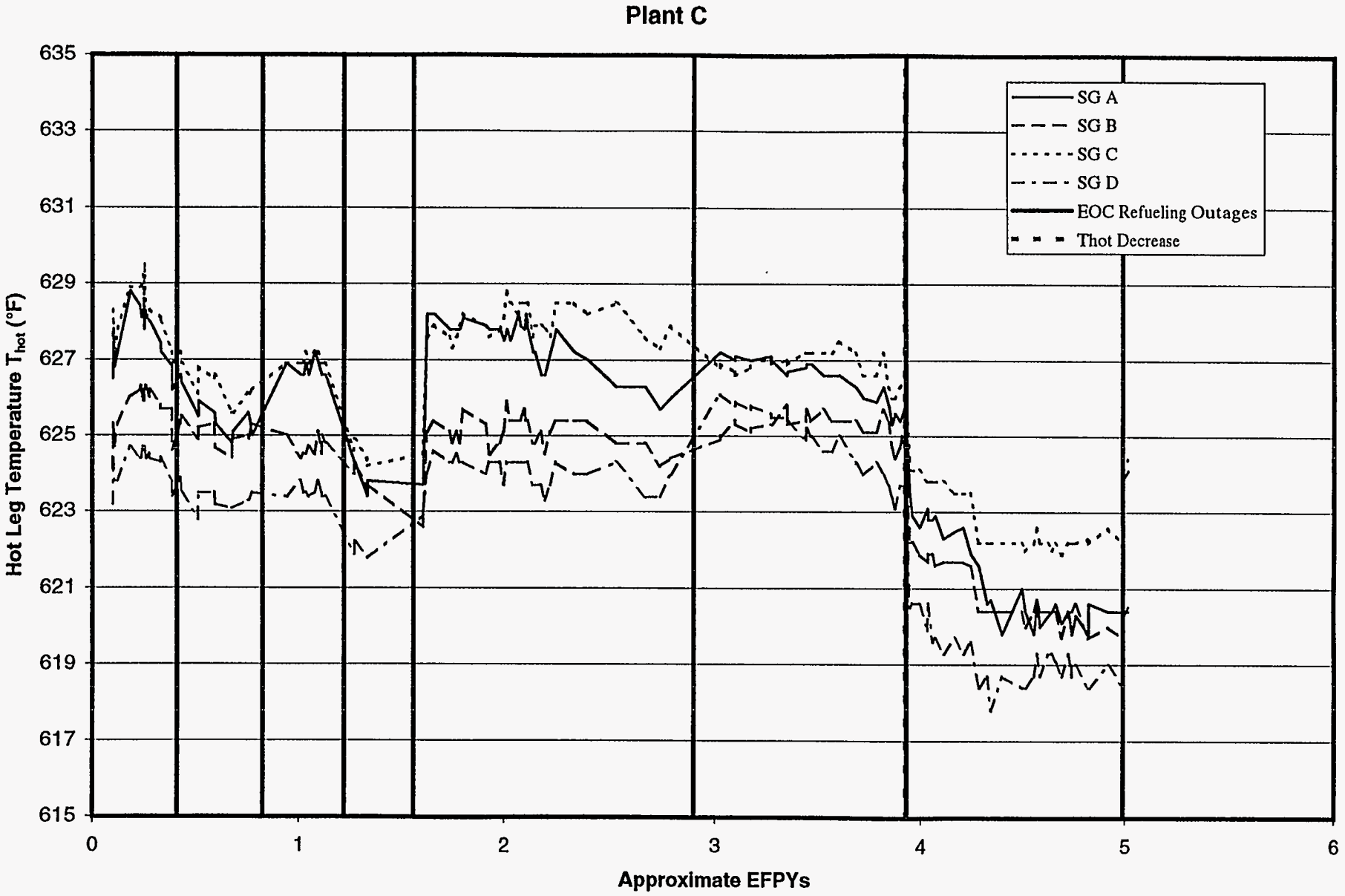

Figure B-C2b. Historical Hot Leg Temperature at Plant C

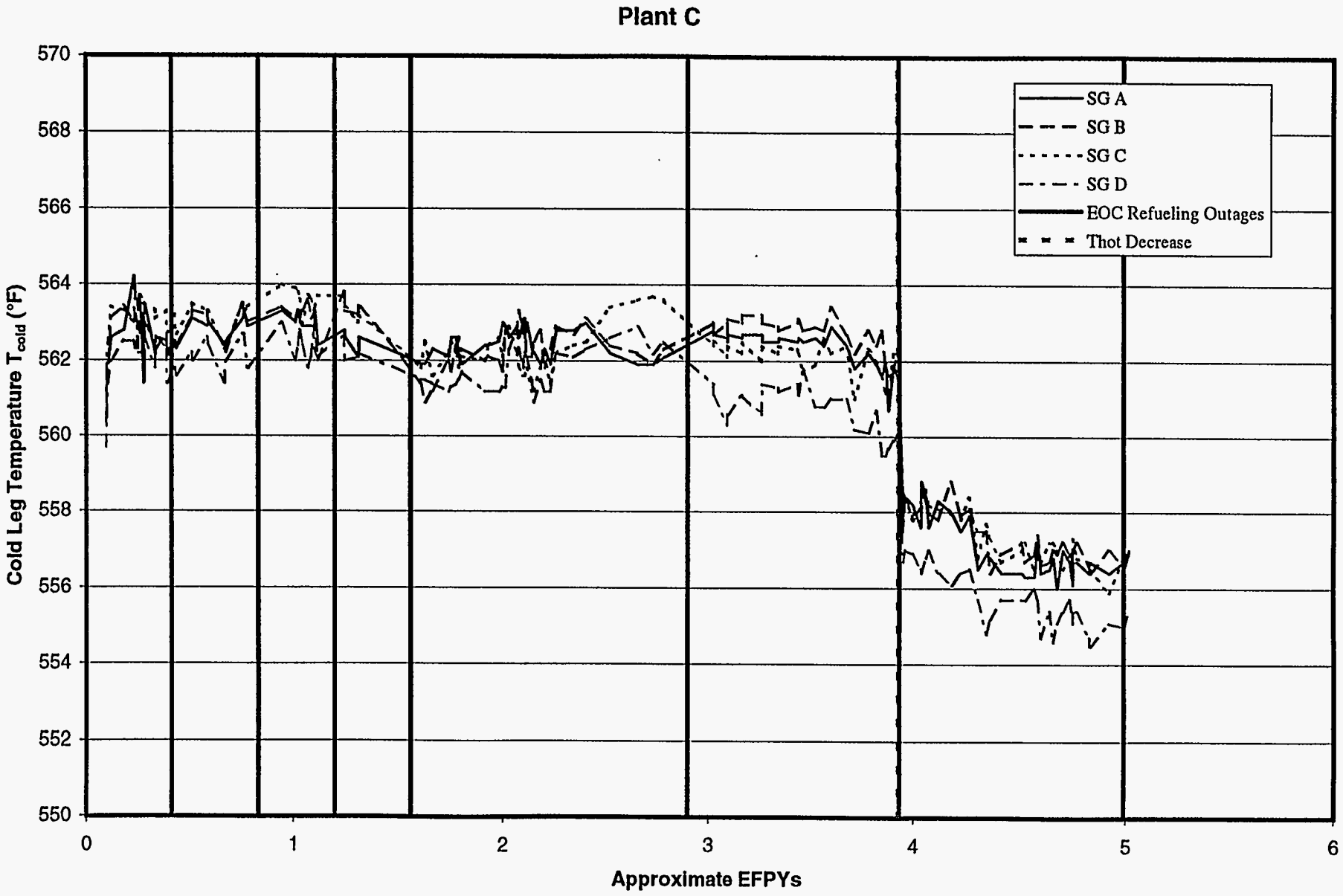

Figure B-C2c. Historical Cold Leg Temperature at Plant C

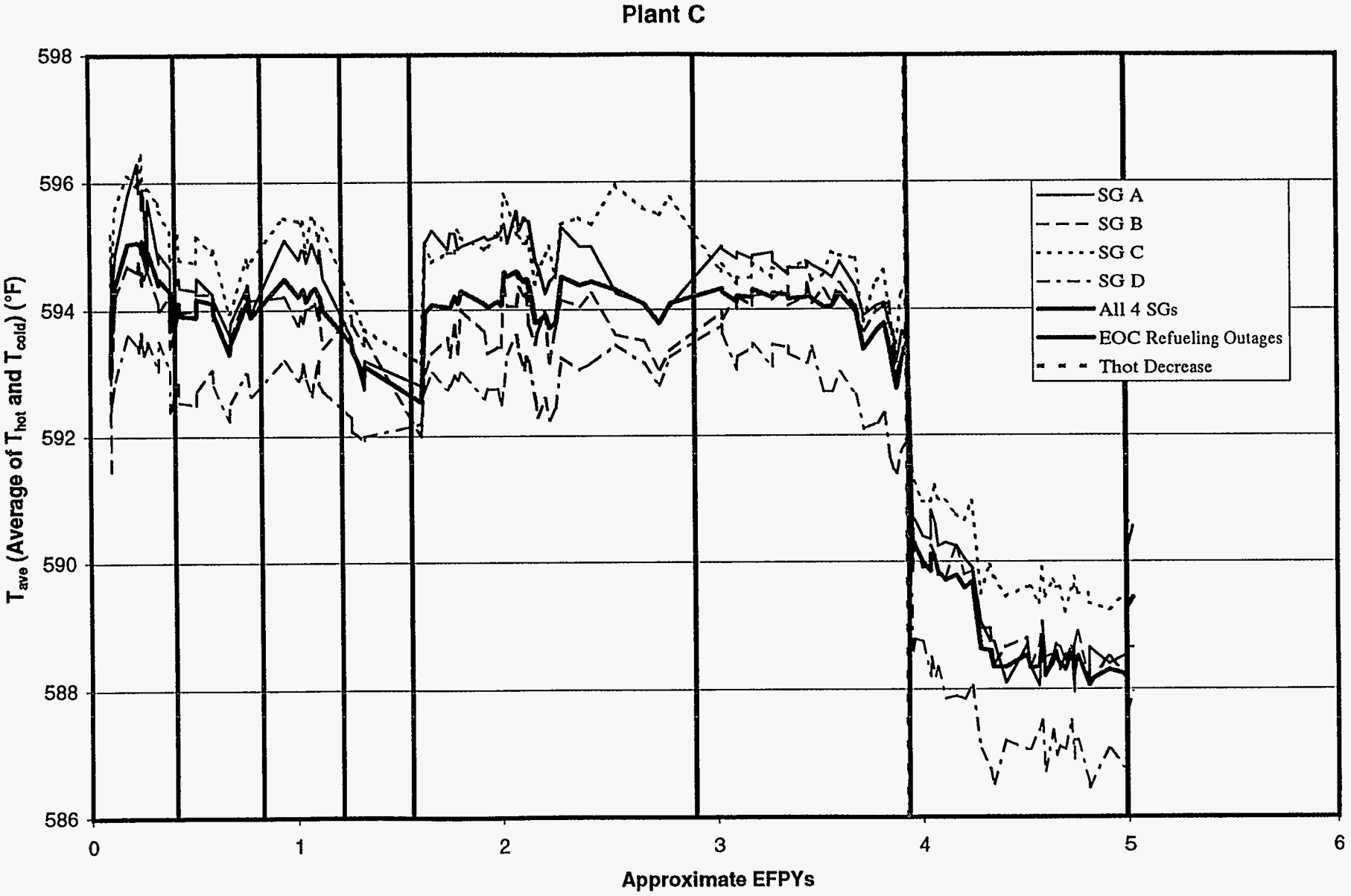

Figure B-C3. Historical Average of Hot and Cold Leg Temperatures (T_{ave}) at Plant C

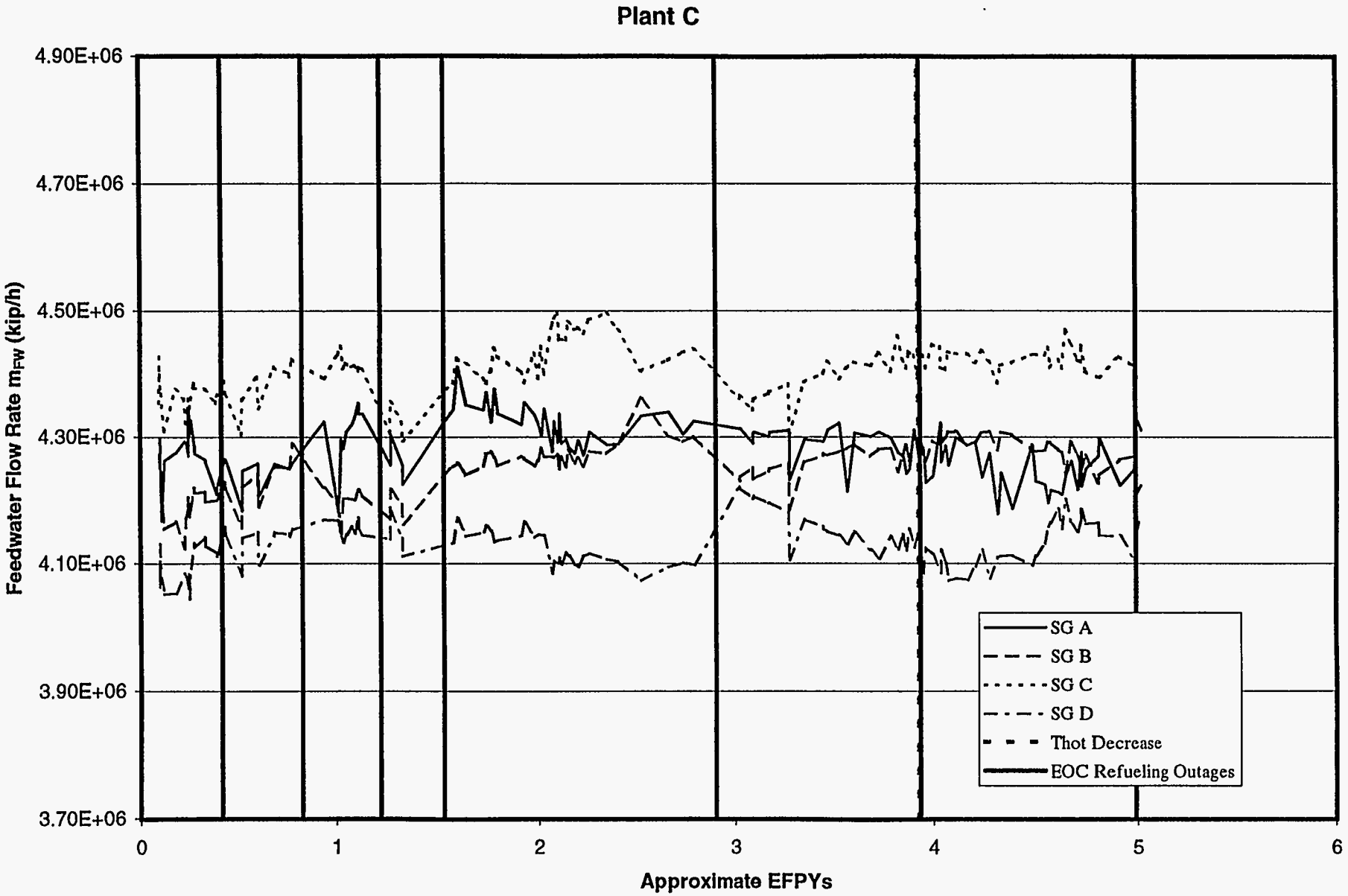

Figure B-C4a. Historical Feedwater Mass Flow Rate at Plant C

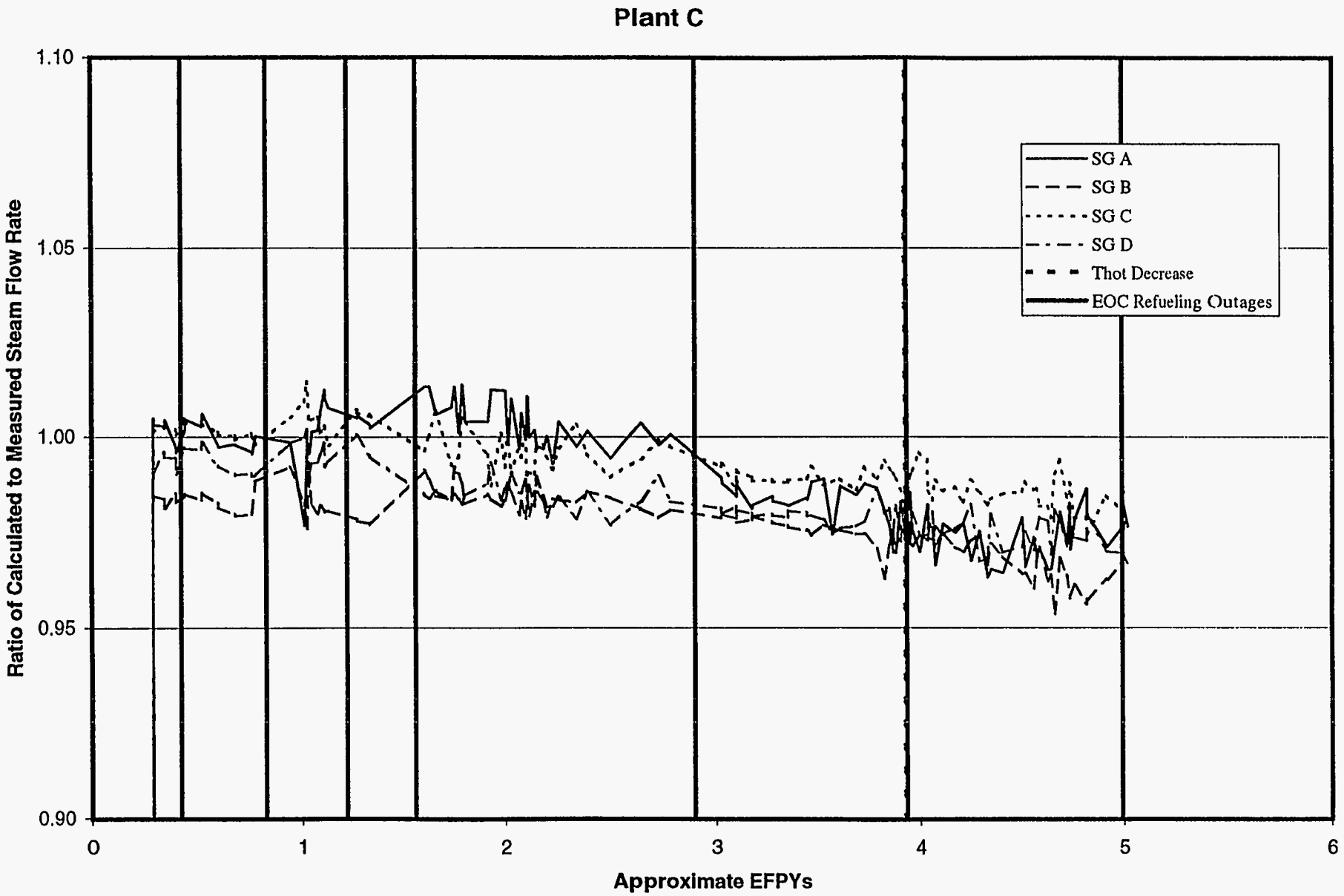

Figure B-C4b. Historical Ratio of Calculated to Measured Steam Flow Rate at Plant C

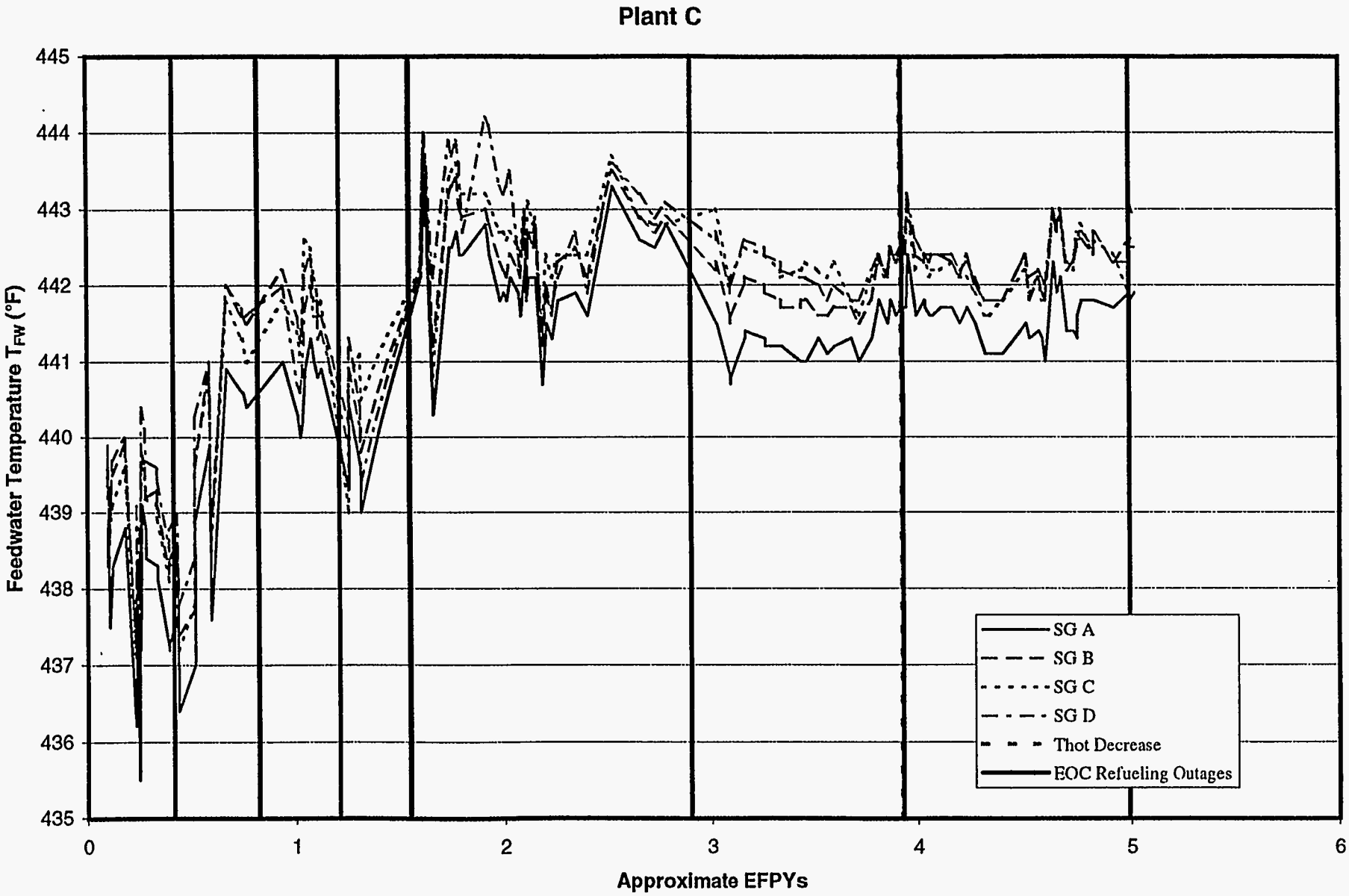

Figure B-C5. Historical Feedwater Temperature at Plant C

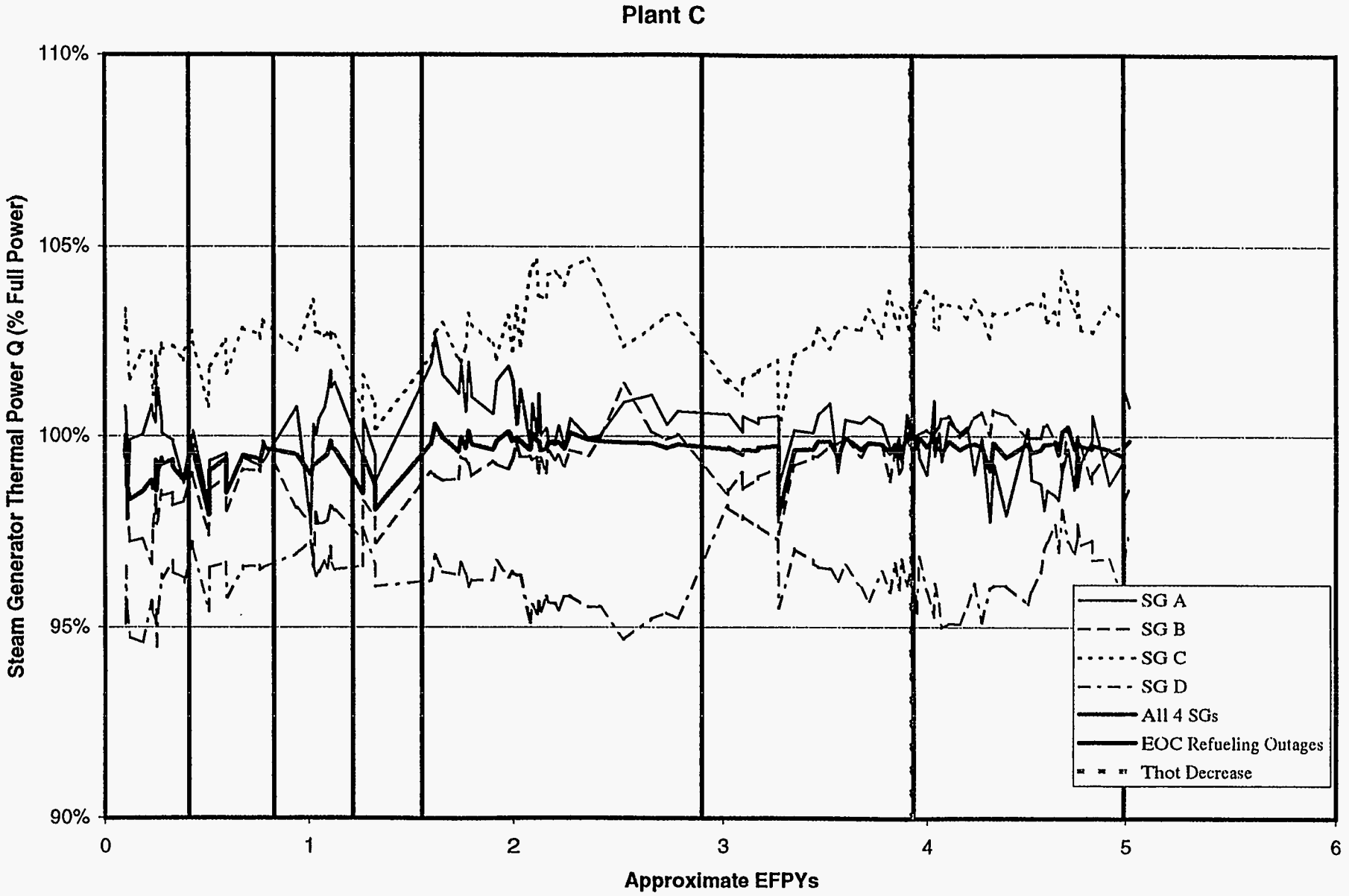

Figure B-C6. Historical Thermal Power Per Steam Generator at Plant C (Based on FW Flow Rate)

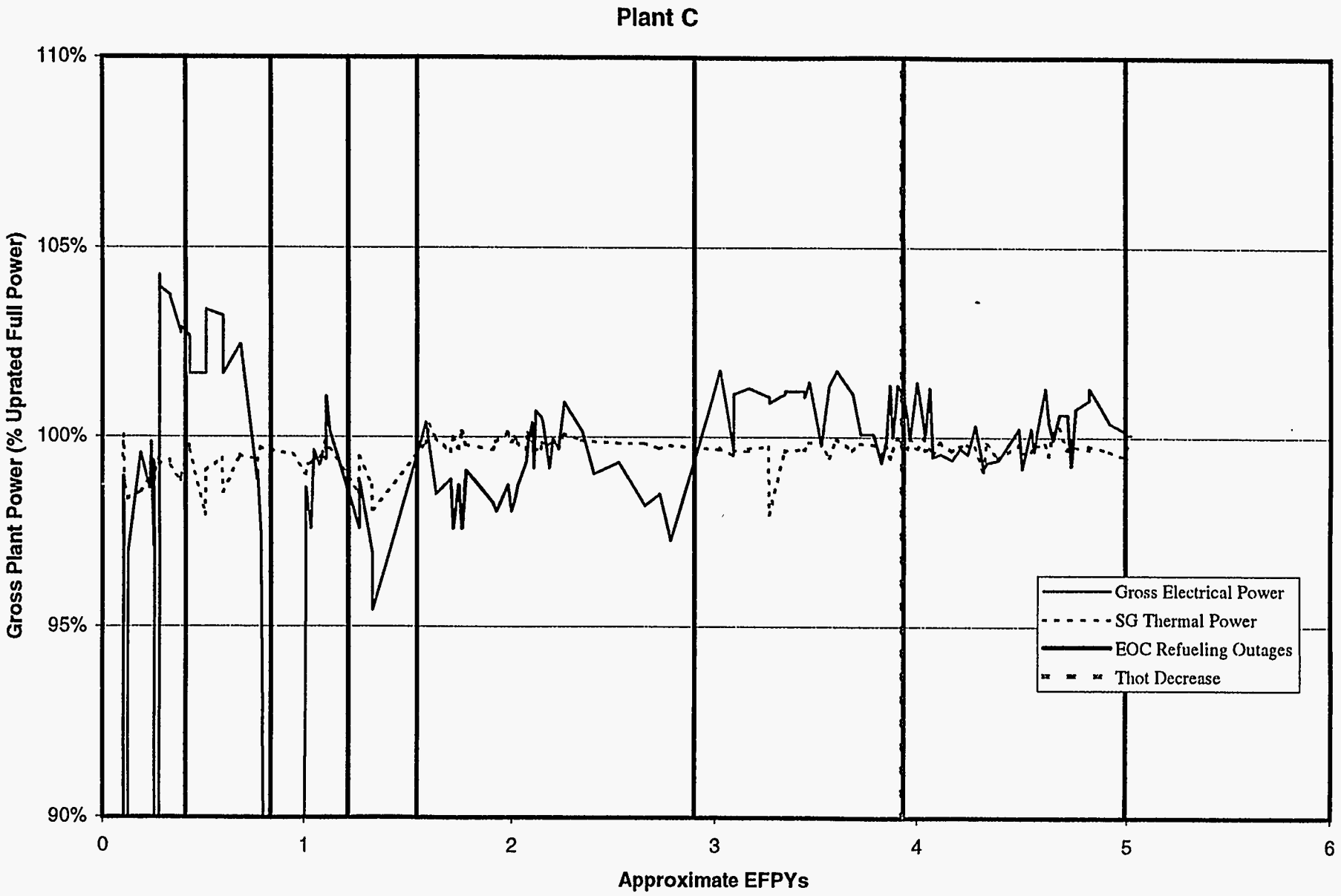

Figure B-C7. Historical Gross Thermal and Electrical Power Output at Plant C

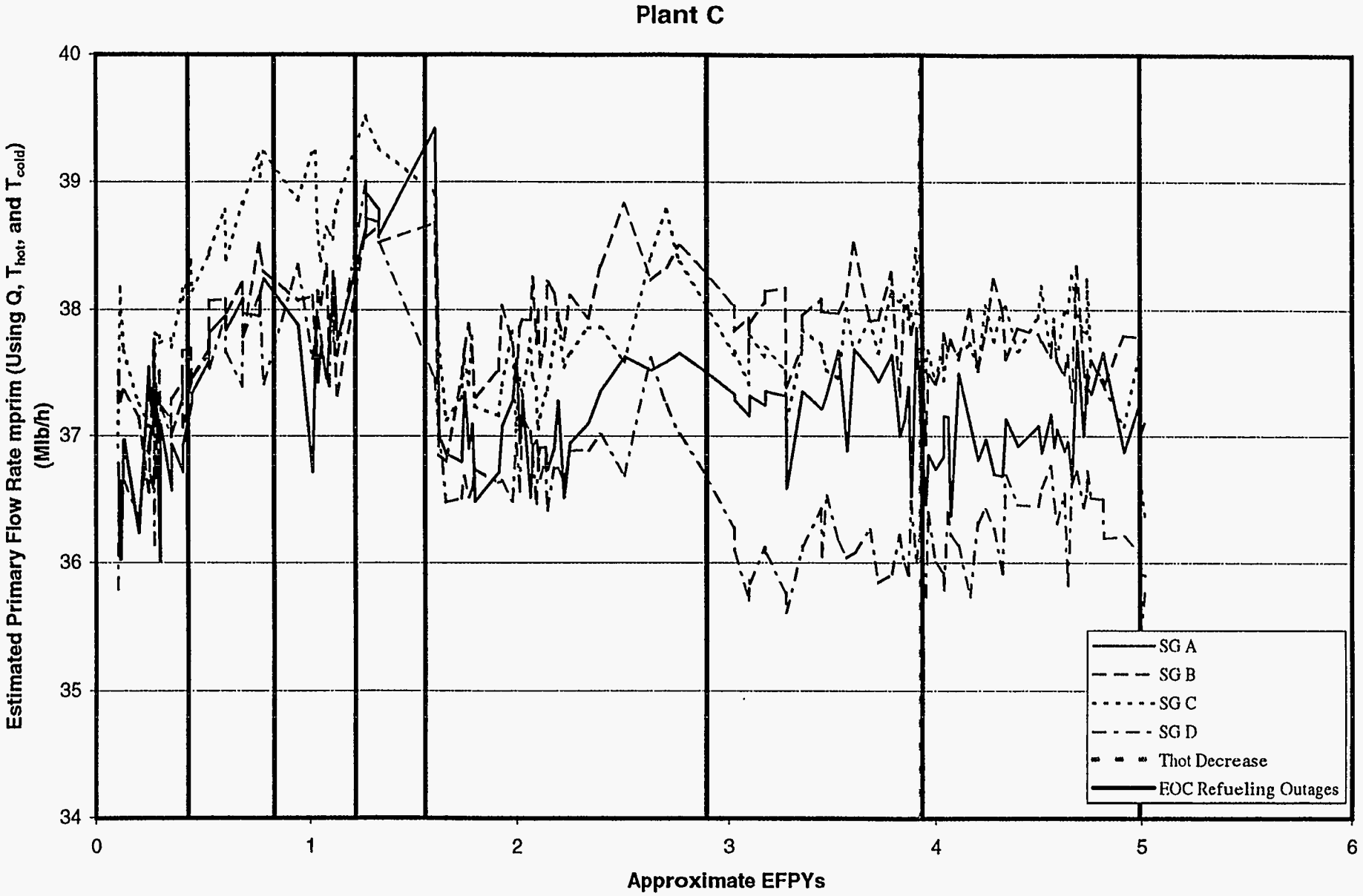

Figure B-C8. Historical Estimated Primary Mass Flow Rate at Plant C

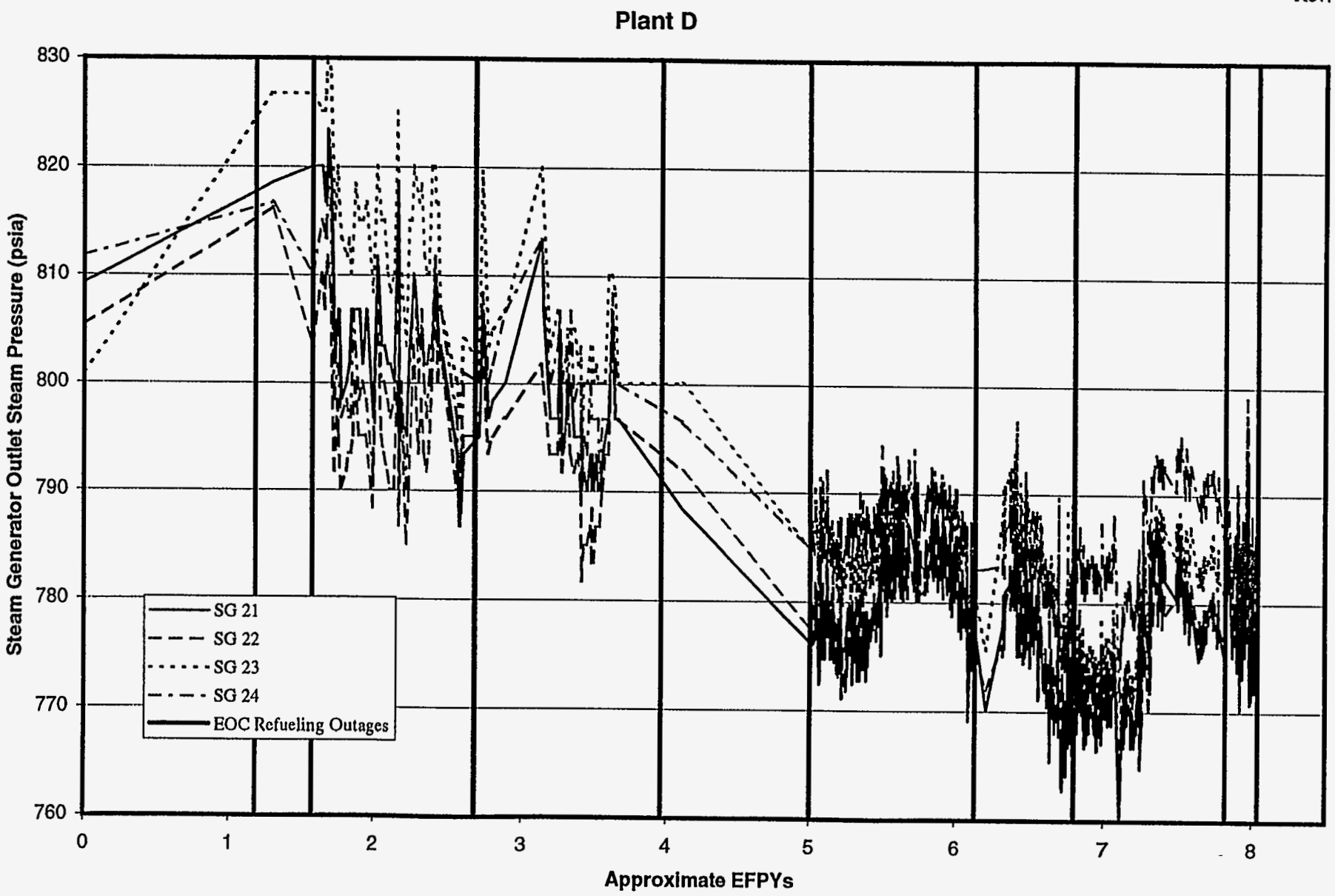

Figure B-D1. Historical Steam Generator Outlet Steam Pressure at Plant D

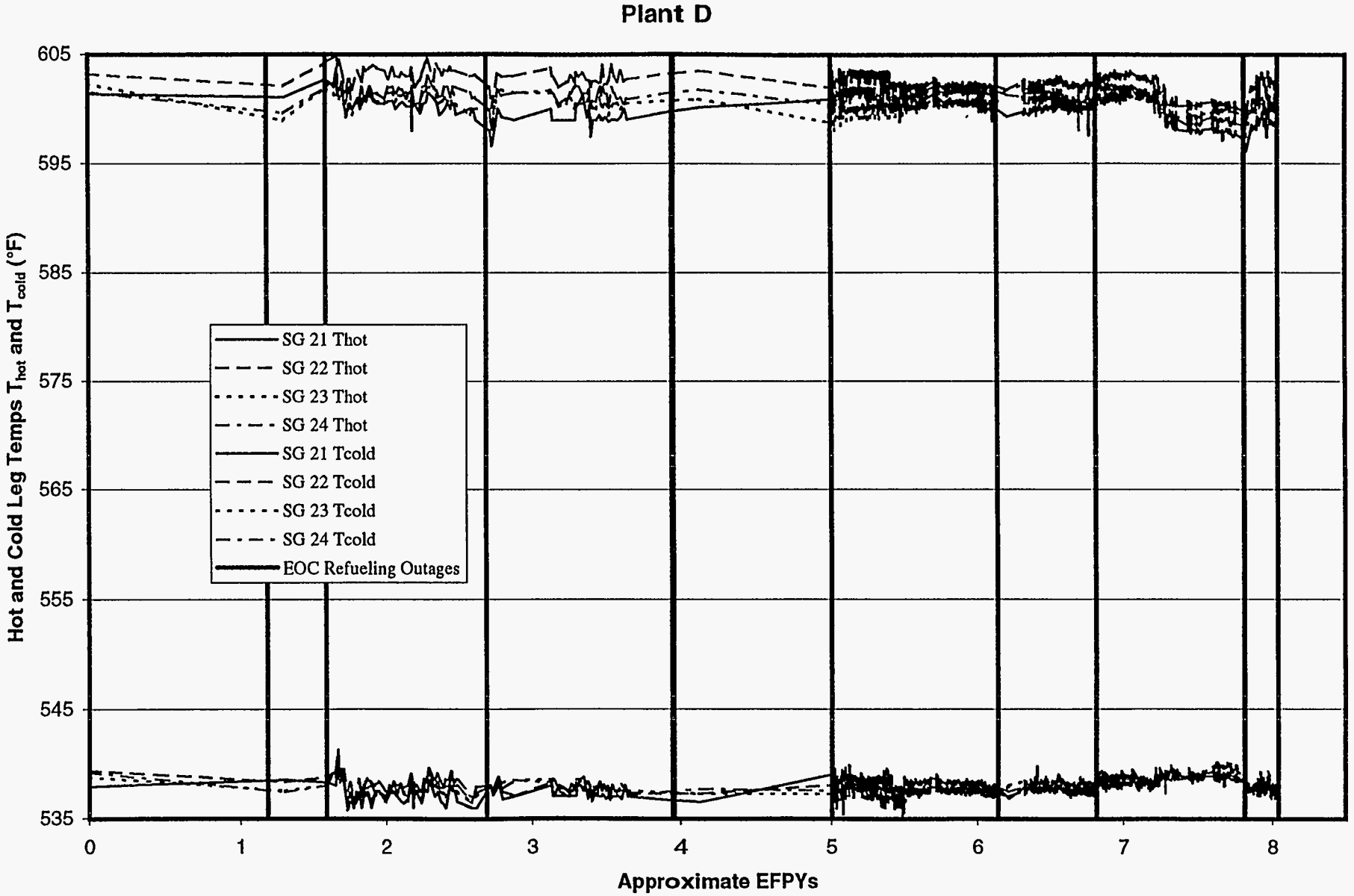

Figure B-D2a. Historical Hot and Cold Leg Temperatures at Plant D

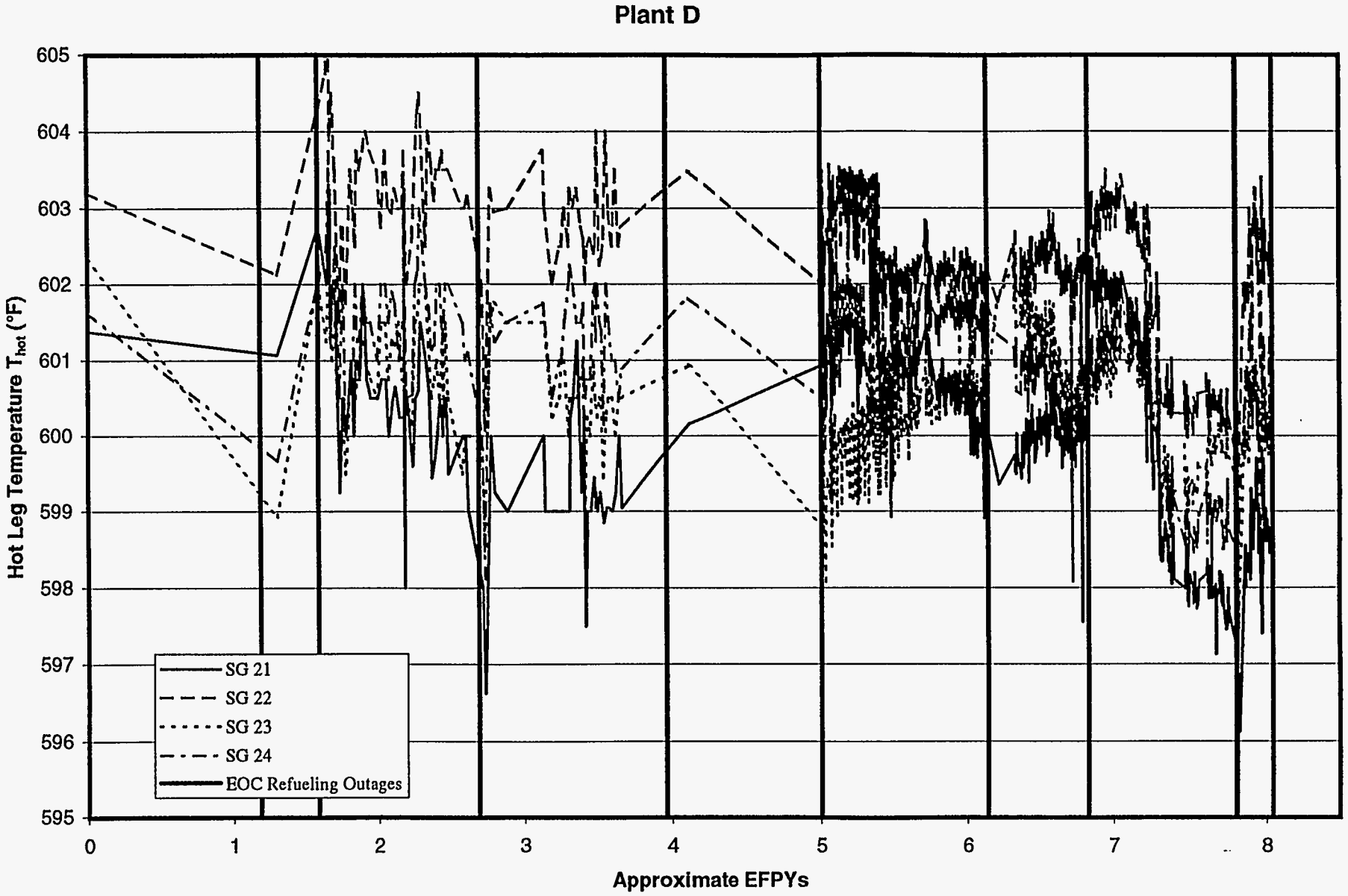

Figure B-D2b. Historical Hot Leg Temperature at Plant D

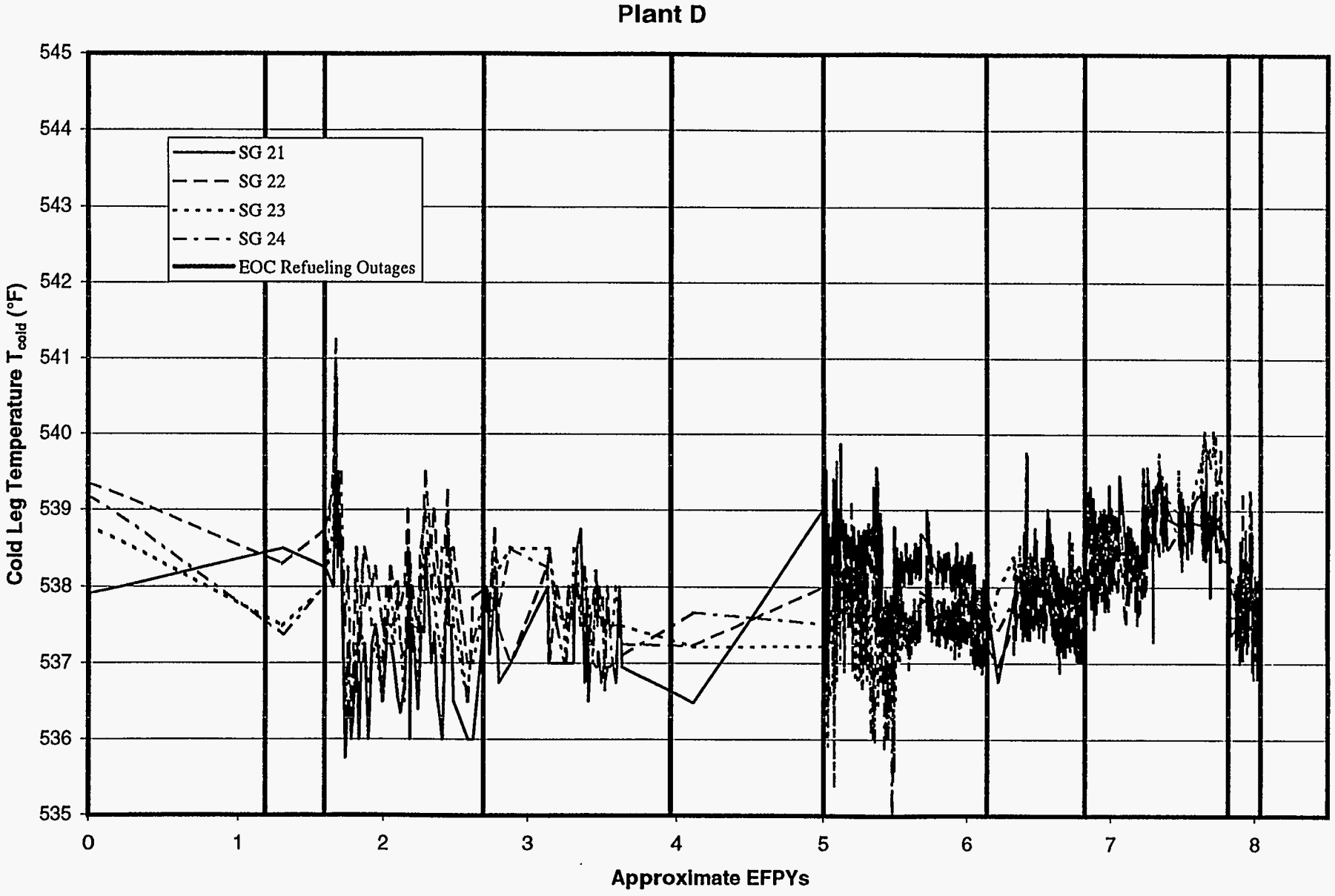

Figure B-D2c. Historical Cold Leg Temperature at Plant D

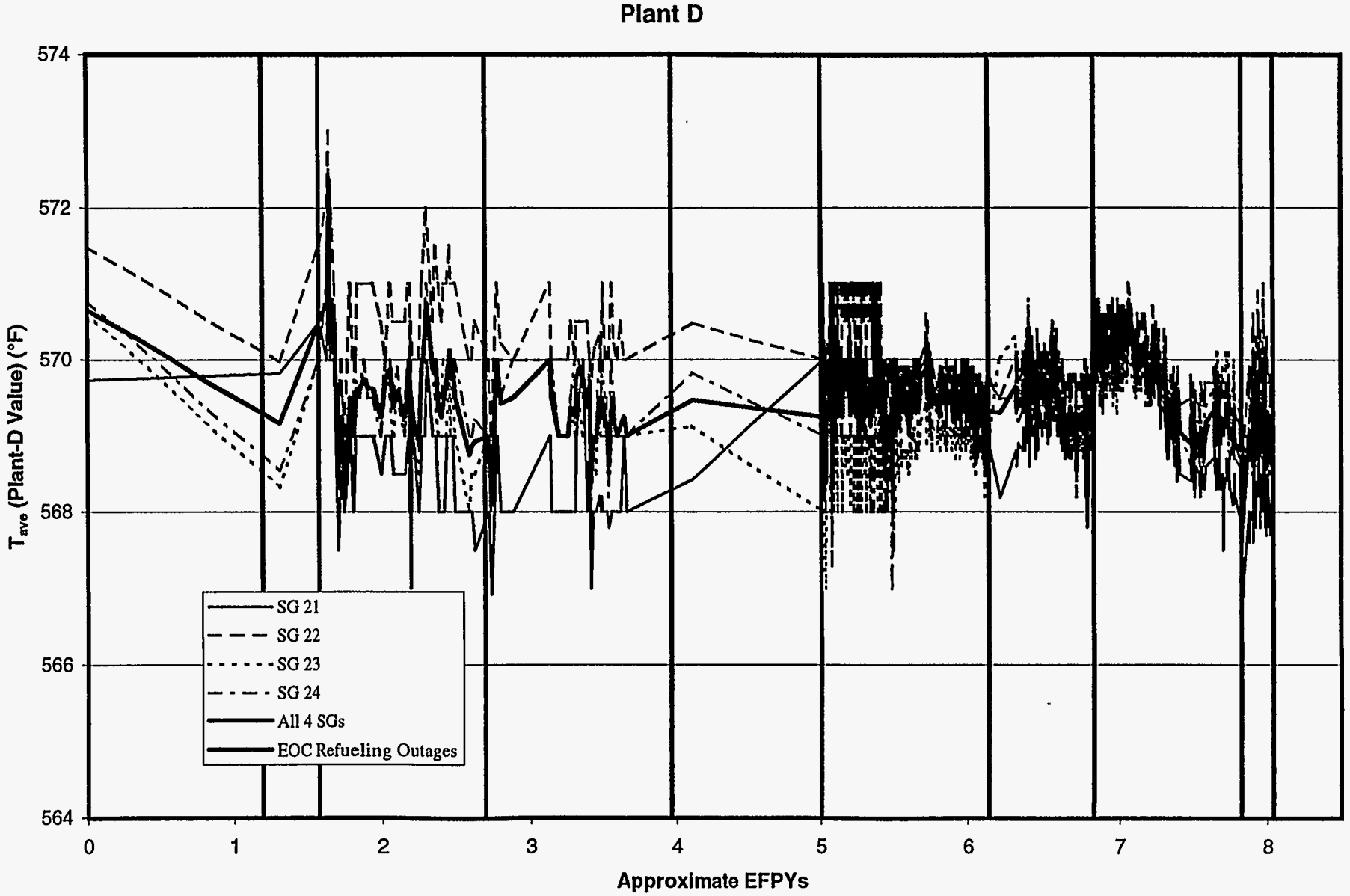

Figure B-D3. Historical Plant-D T_{ave}

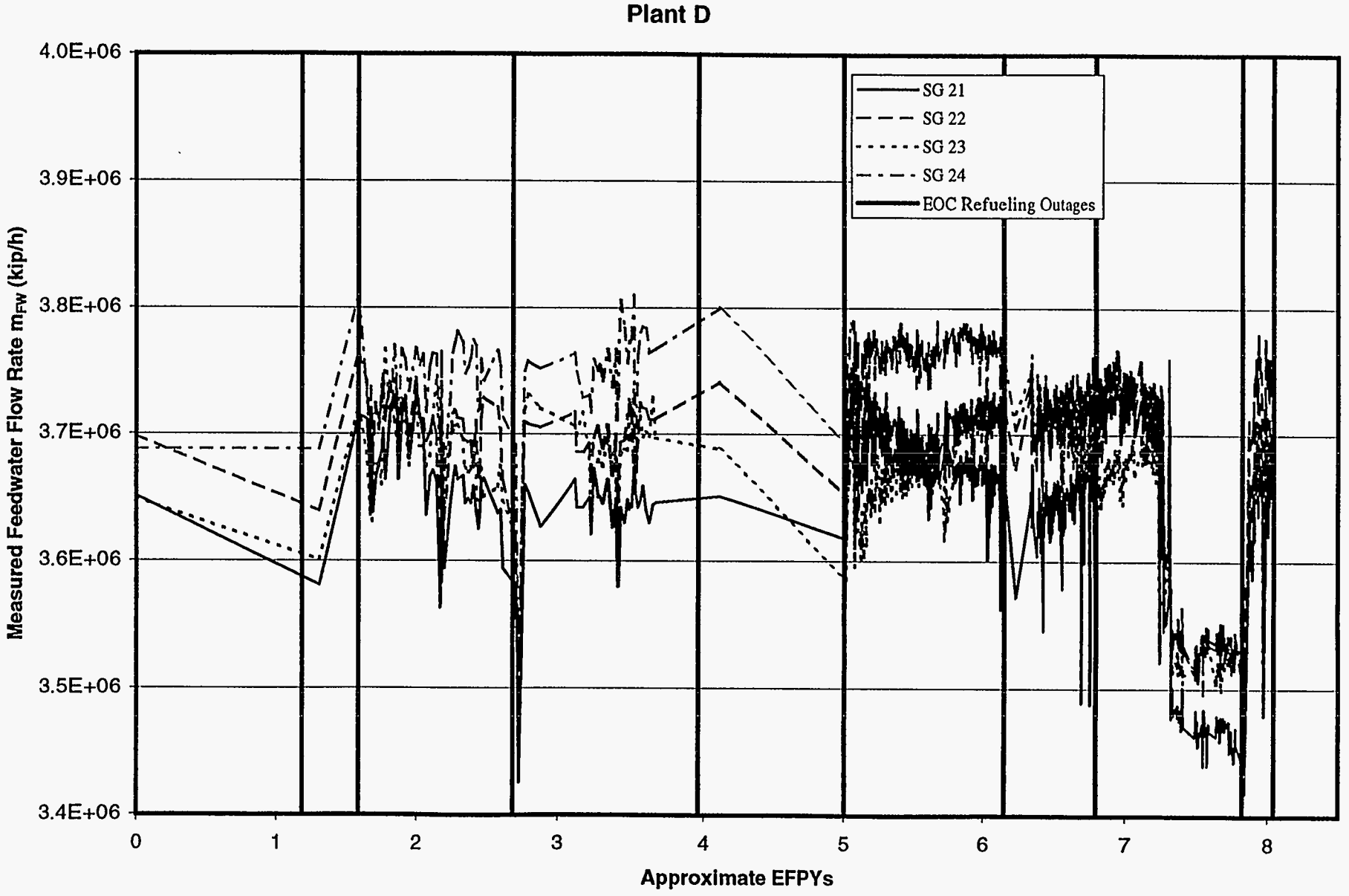

Figure B-D4a. Historical Feedwater Mass Flow Rate at Plant D (Raw Data)

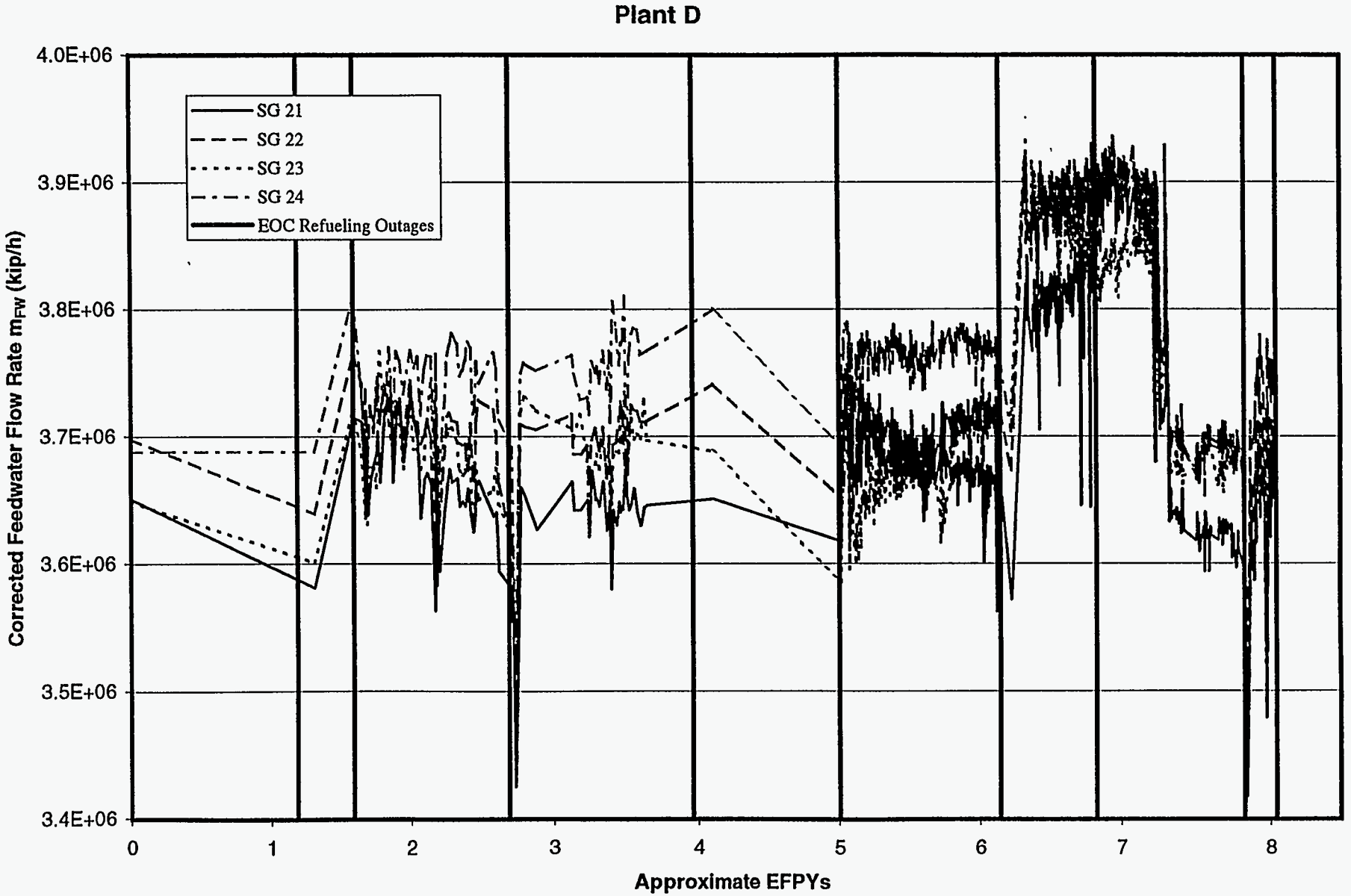

Figure B-D4b. Historical Feedwater Mass Flow Rate at Plant D (Corrected for Venturi Bypass Error)

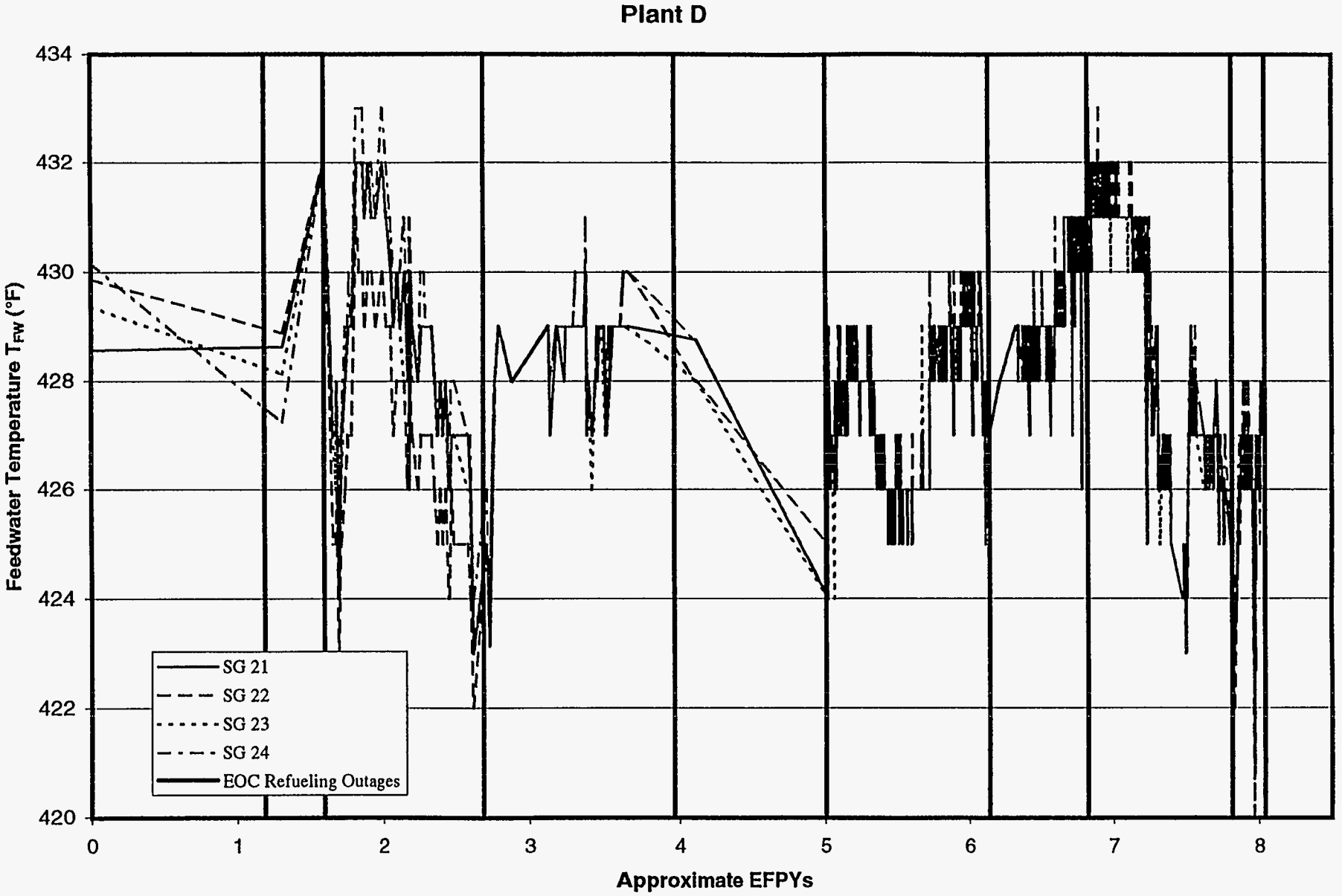

Figure B-D5. Historical Feedwater Temperature at Plant D

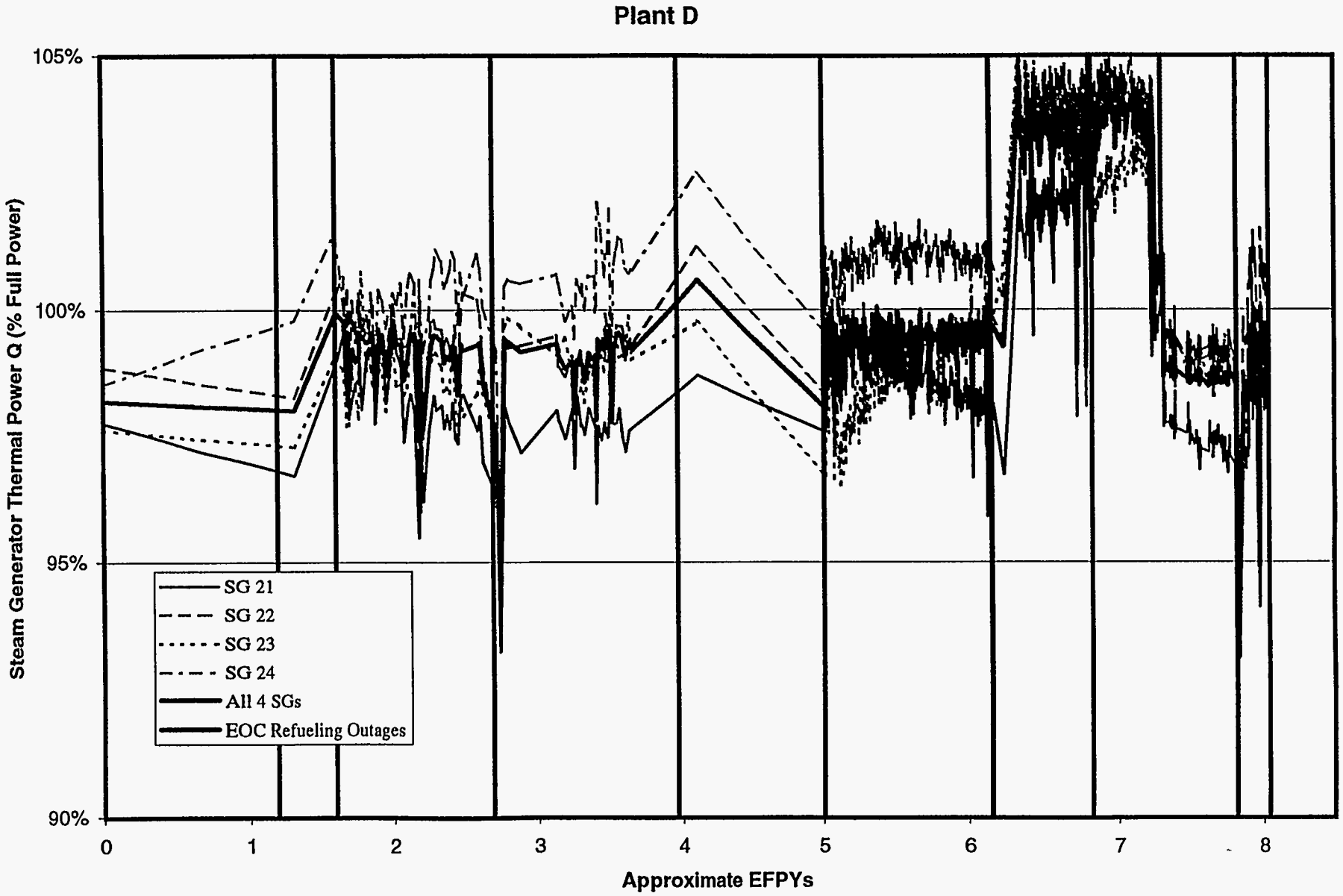

Figure B-D6. Historical Thermal Power Per Steam Generator at Plant D (Based on FW Flow Rate)

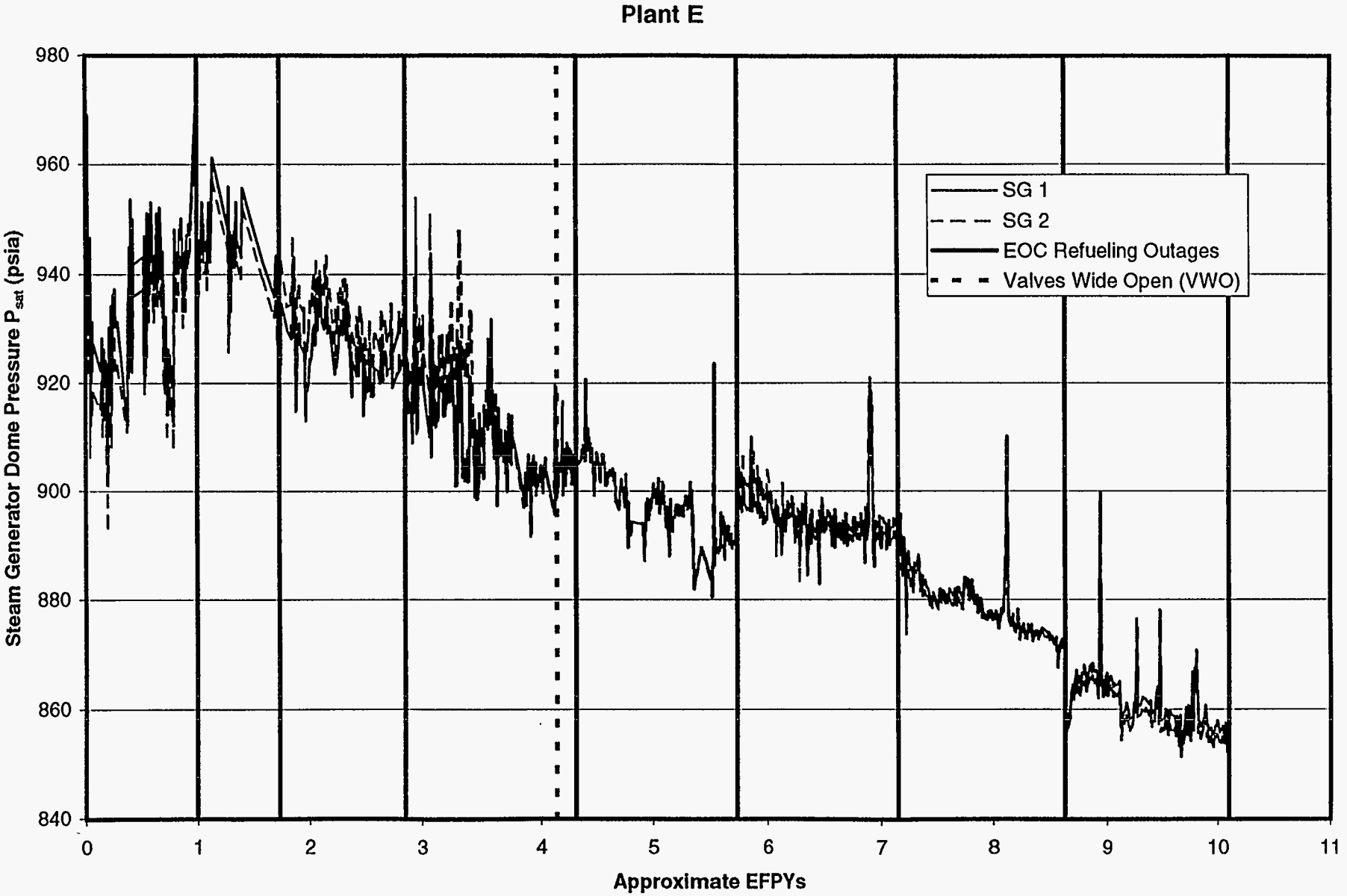

Figure B-E1. Historical Steam Generator Dome Pressure at Plant E

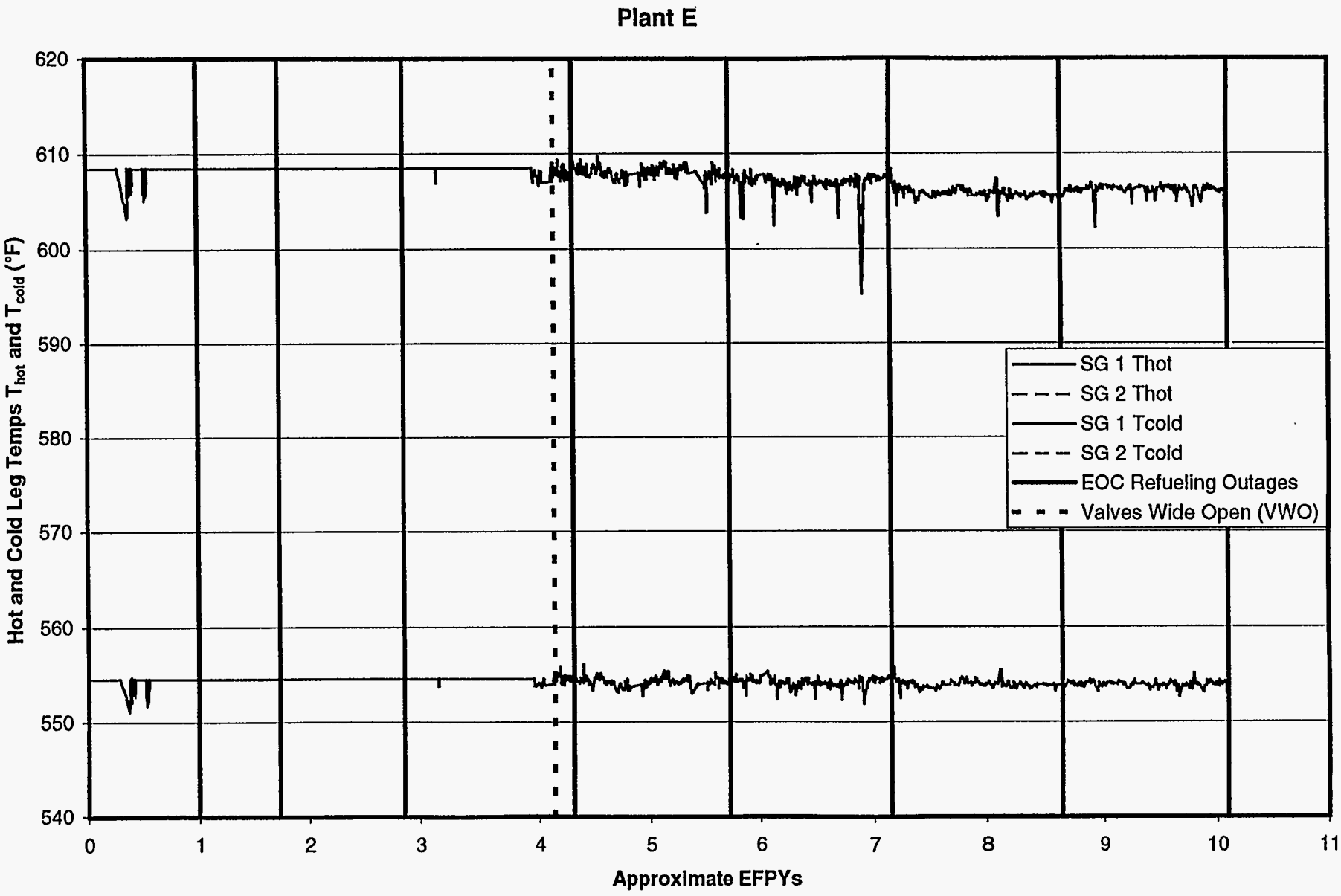

Figure B-E2a. Historical Hot and Cold Leg Temperatures at Plant E

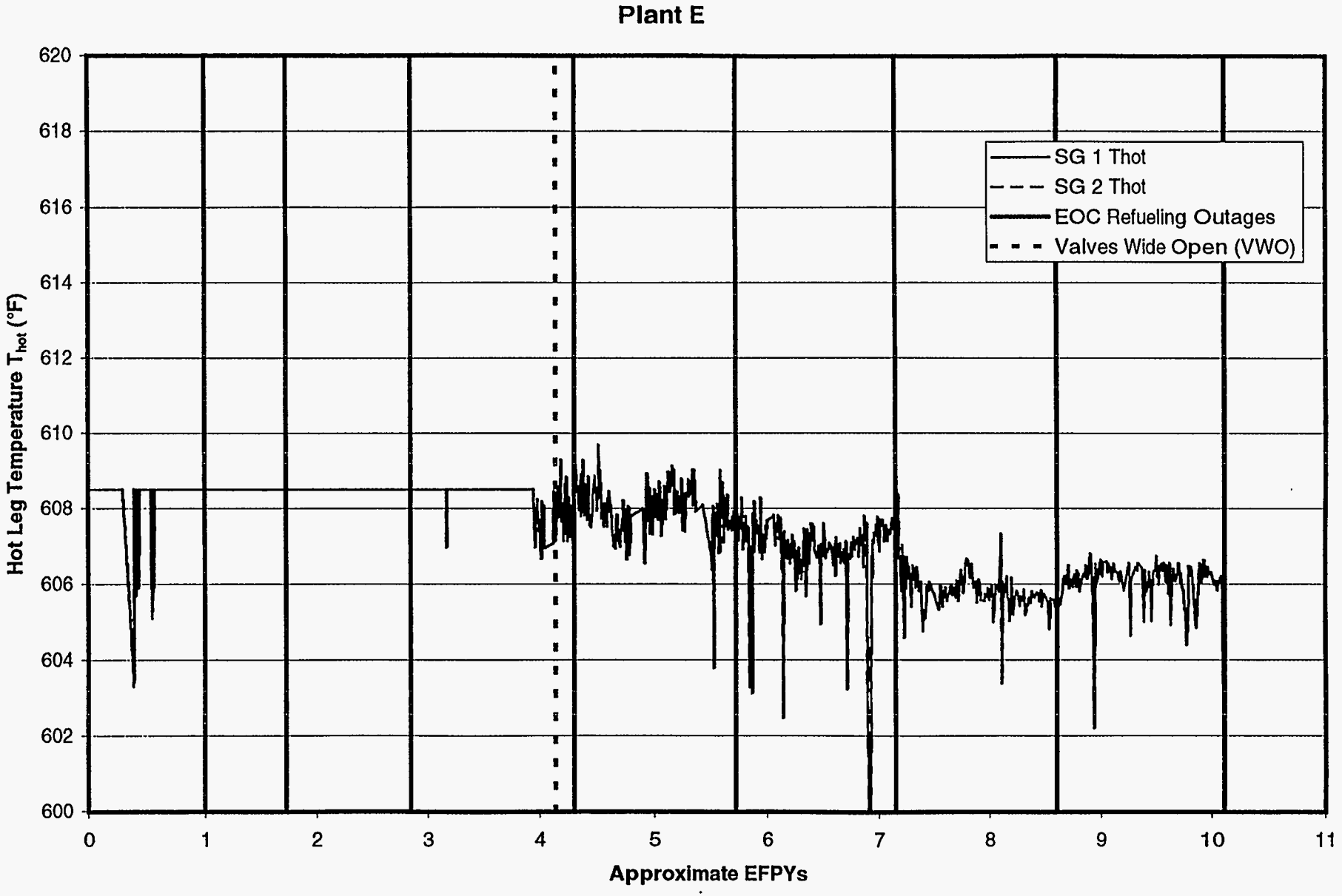

Figure B-E2b. Historical Hot Leg Temperature at Plant E

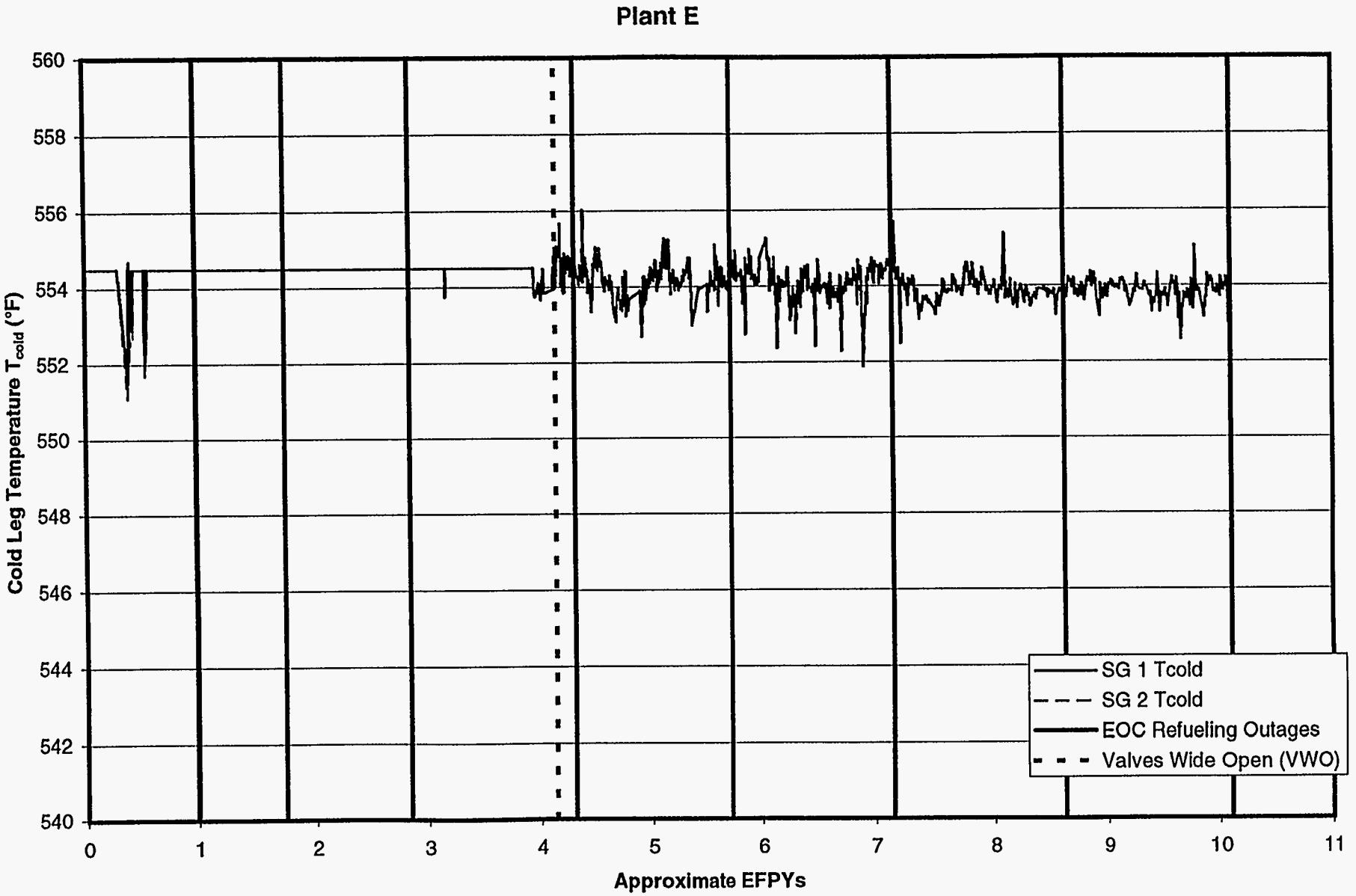

Figure B-E2c. Historical Cold Leg Temperature at Plant E

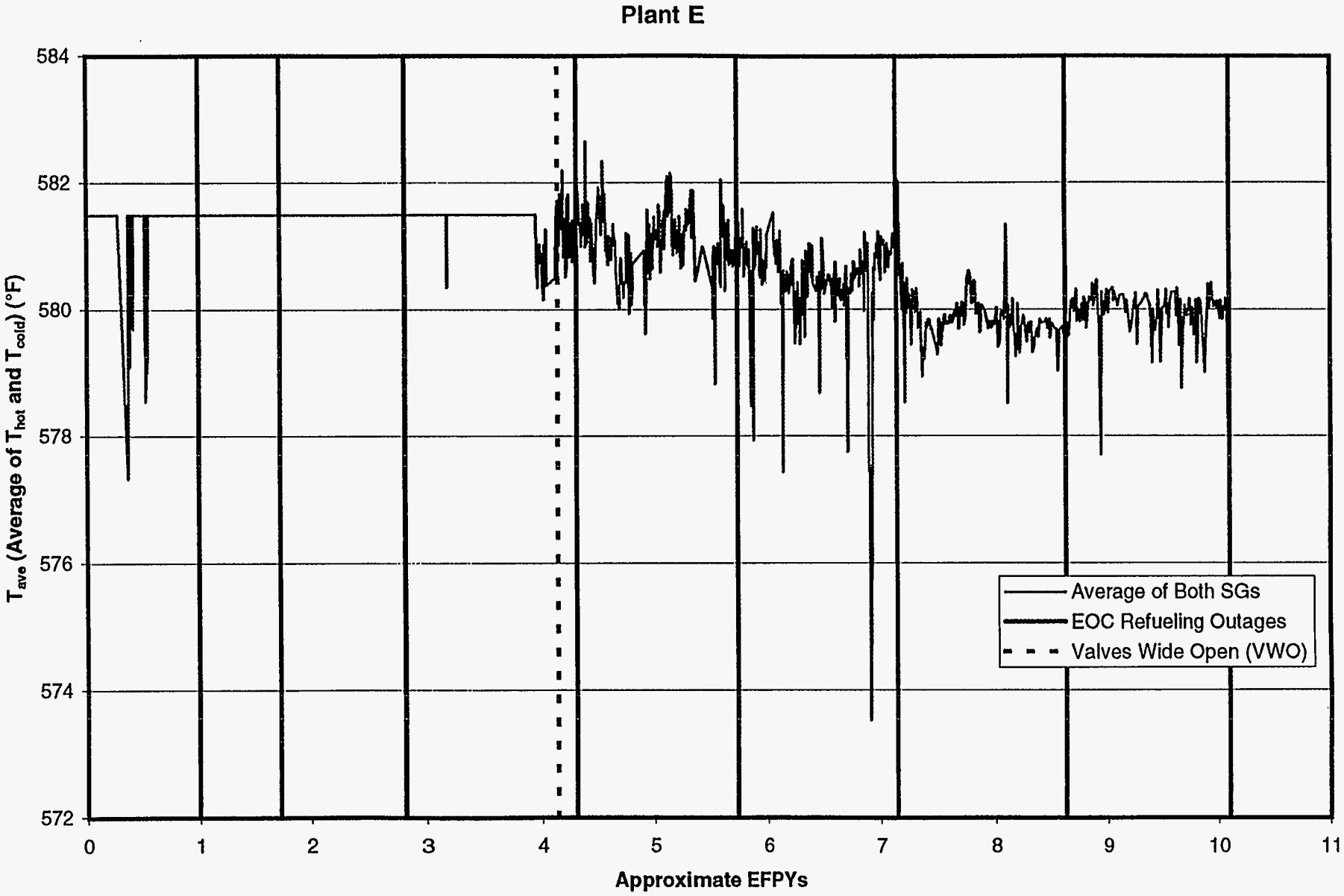

Figure B-E3. Historical Average of Hot and Cold Leg Temperatures at Plant E

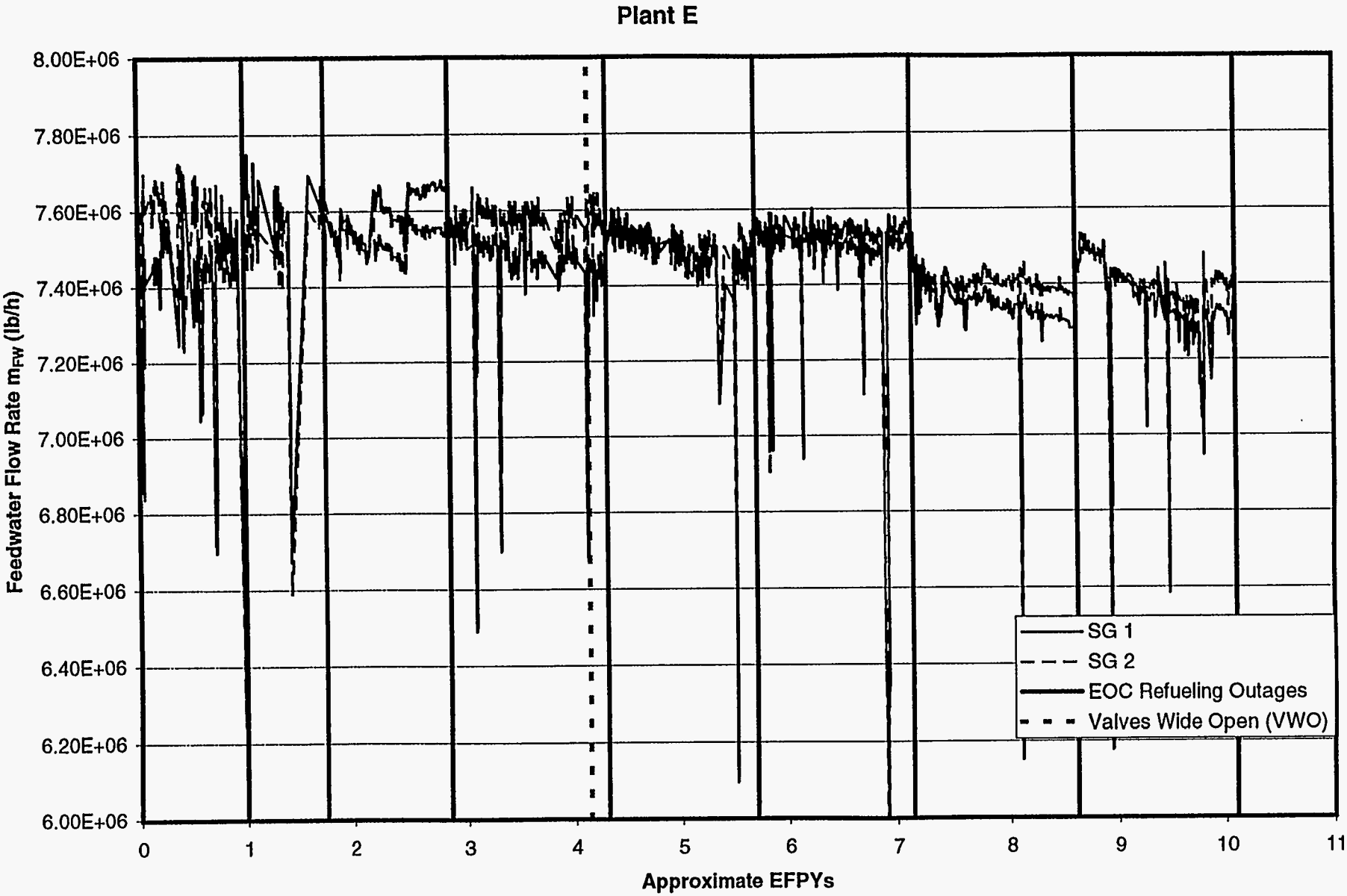

Figure B-E4. Historical Feedwater Mass Flow Rate at Plant E

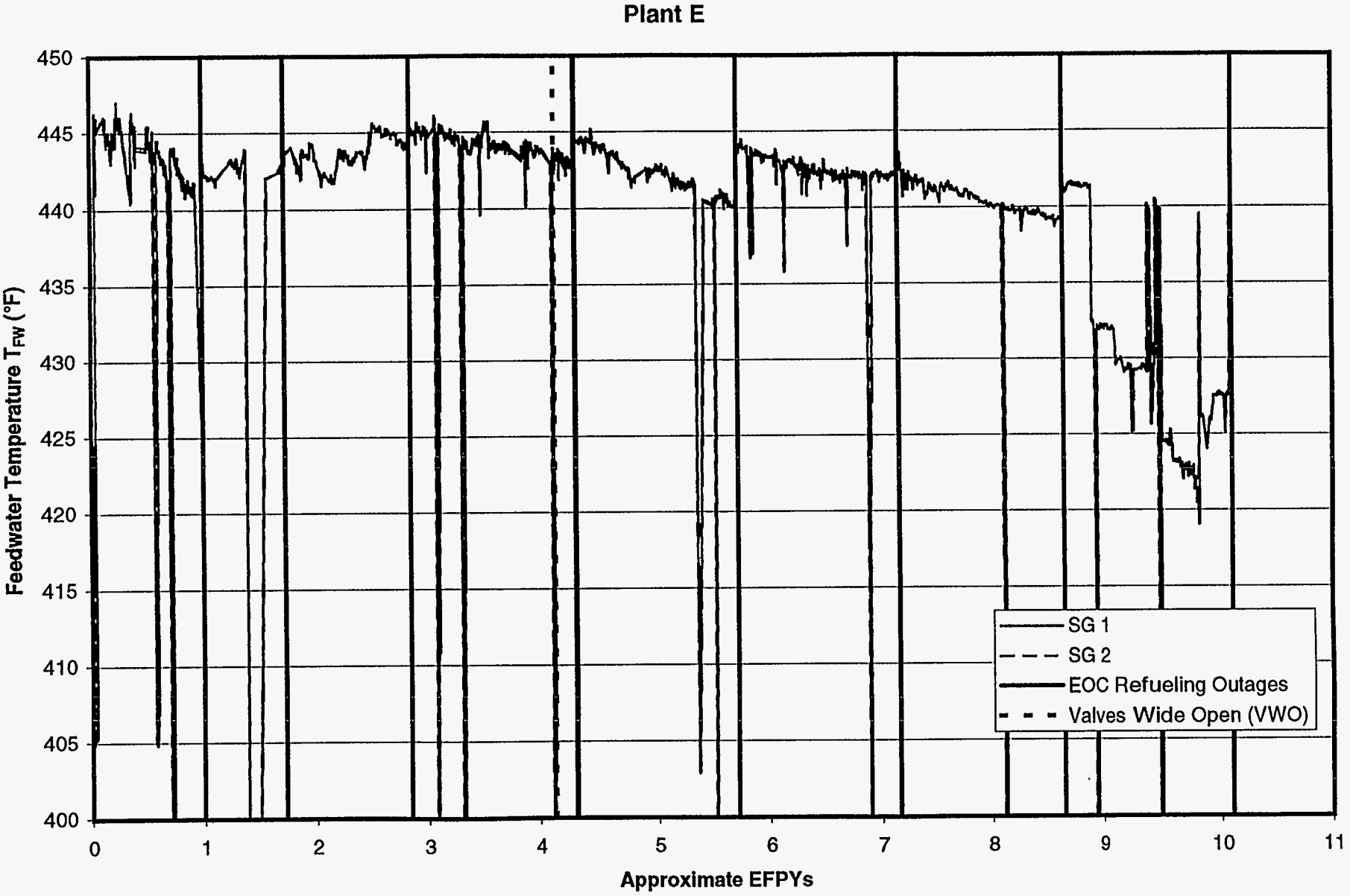

Figure B-E5. Historical Feedwater Temperature at Plant E

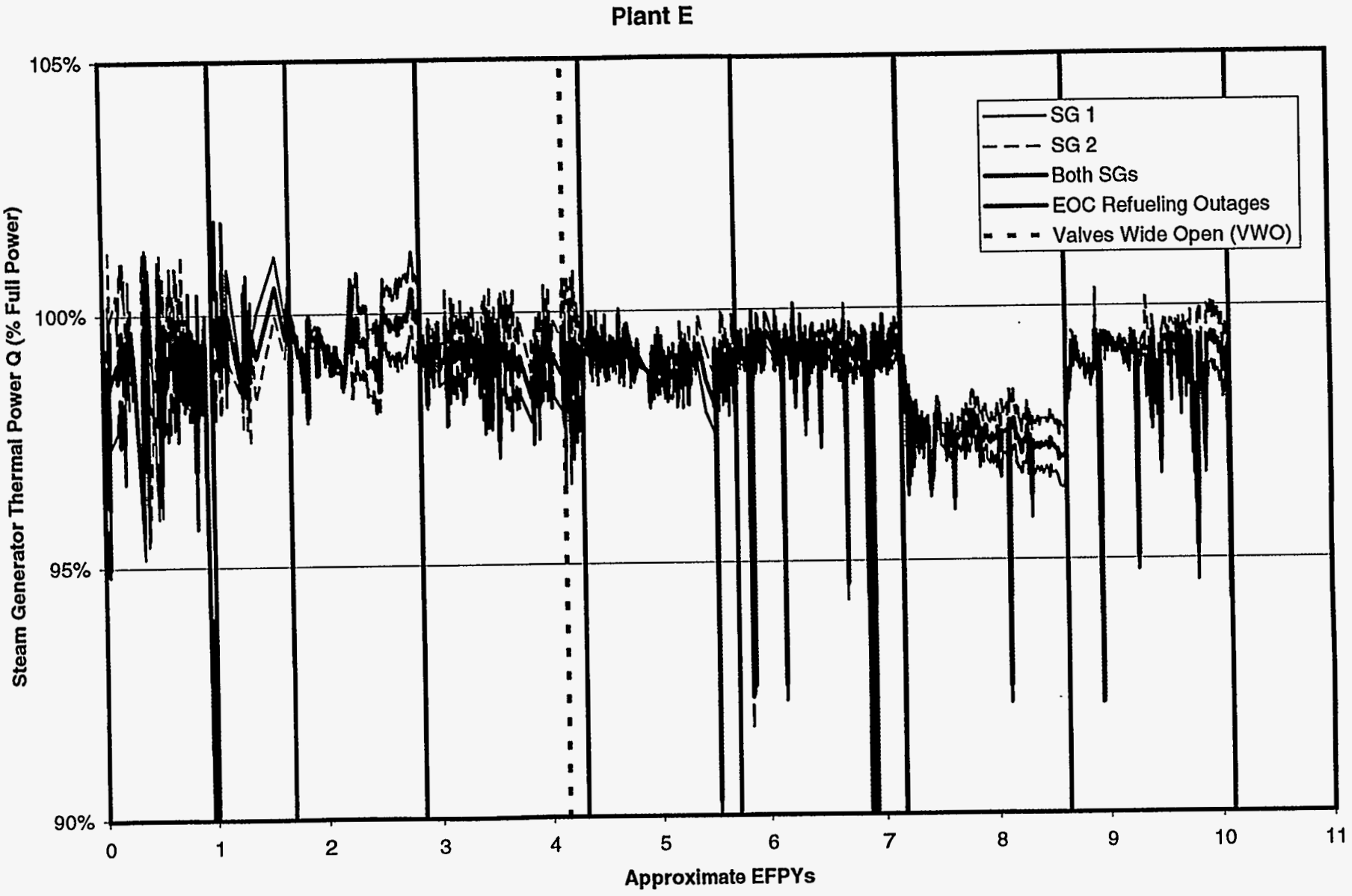

Figure B-E6. Historical Thermal Power Per Steam Generator at Plant E (Based on FW Flow Rate)

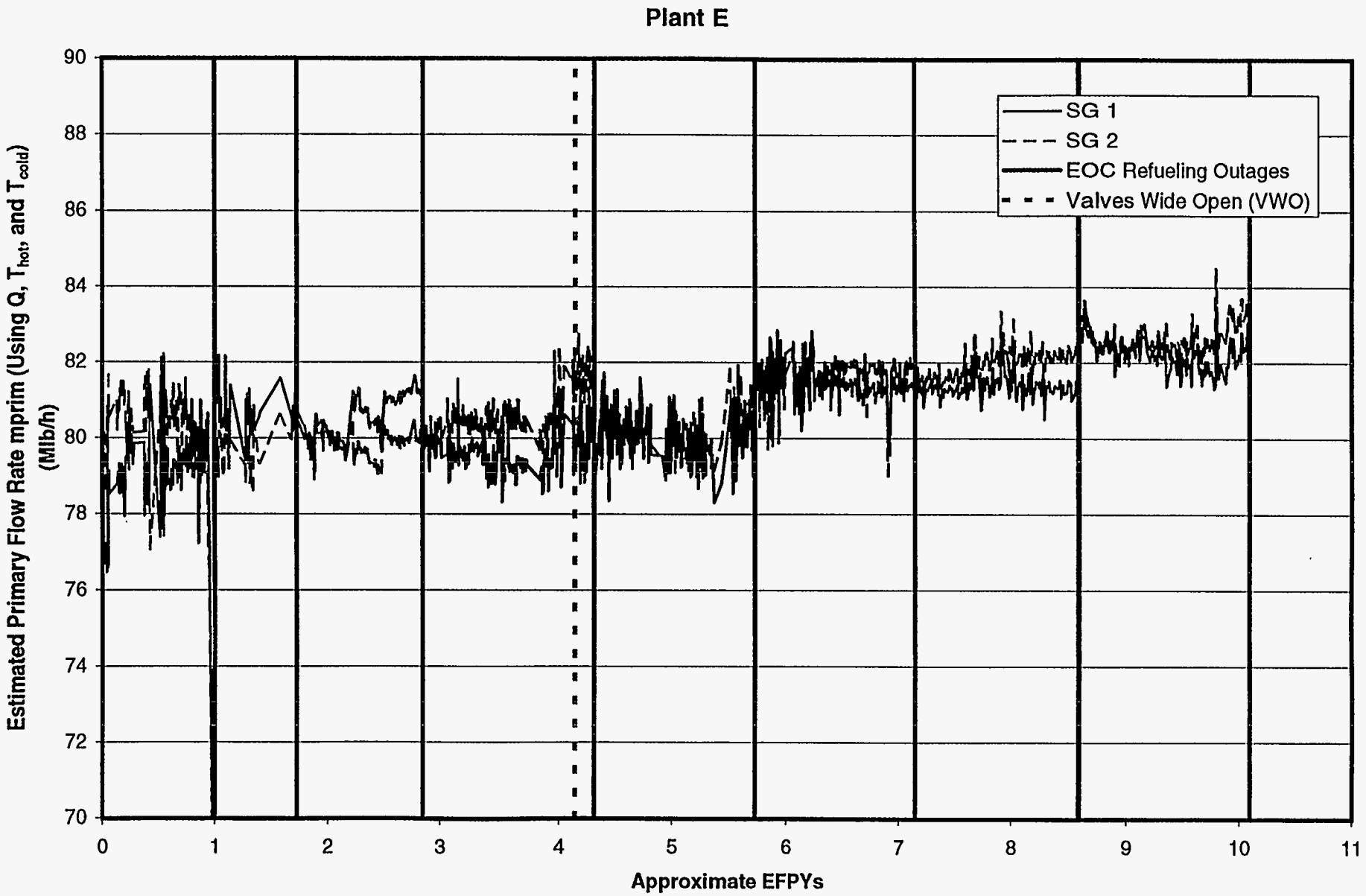

Figure B-E7. Historical Estimated Primary Mass Flow Rate at Plant E

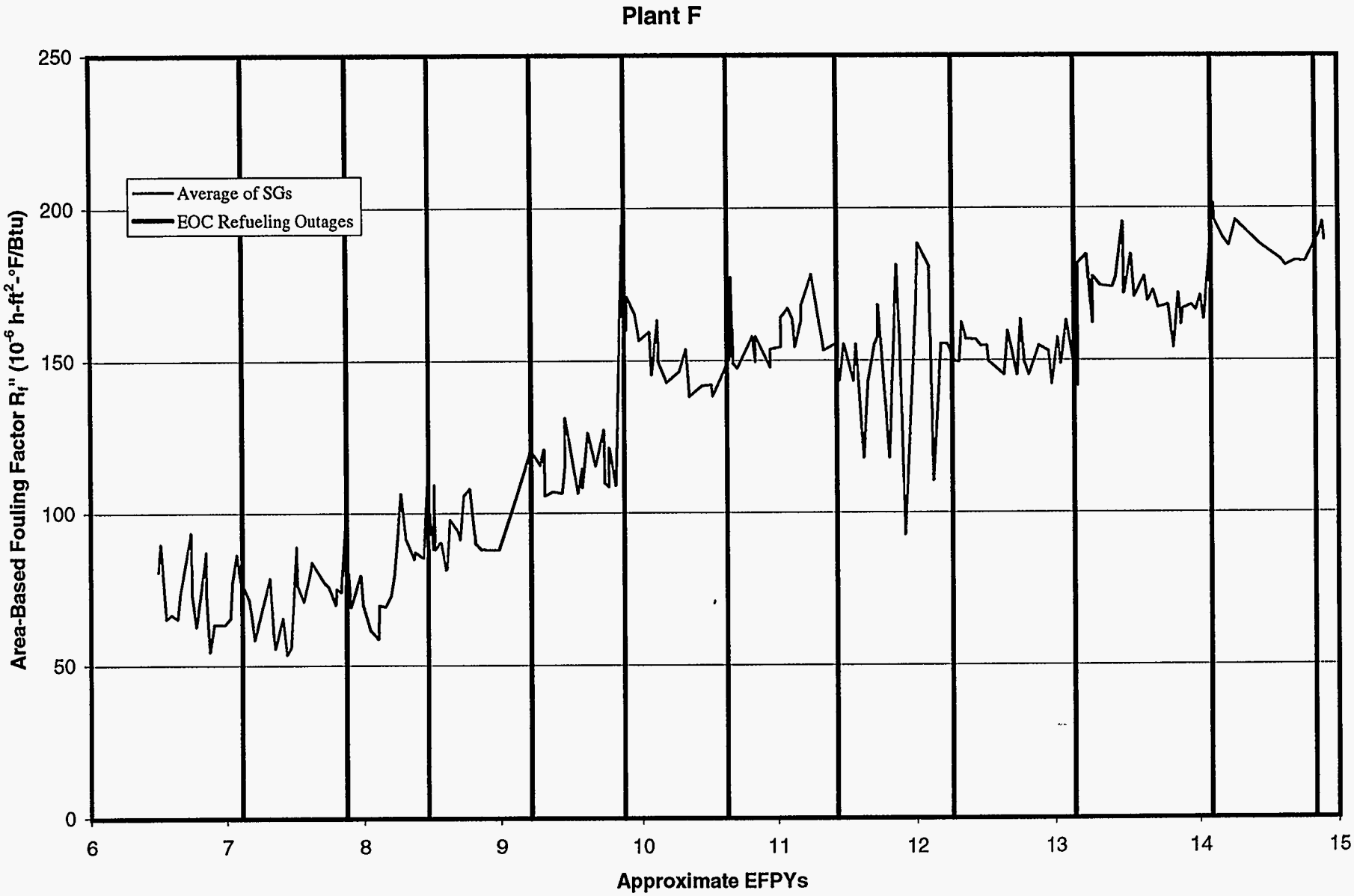

Figure C-F1. Historical Fouling Factor at Plant F

APPENDIX C

DETAILS OF FOULING FACTOR CALCULATIONS AND UNCERTAINTY ANALYSES

Fouling Factor Calculations

With the data described in Appendix B, the fouling factor is calculated for the operating history of Plants A, B, C, D, E, and F.* Note that the secondary-side thermal-hydraulic values are used to calculate the thermal power (Q in Eq. [IV-7]), which is used in place of the plant-calculated thermal power.† Unless otherwise noted, the fouling factor is computed relative to the design value for the "clean" resistance $R_0^{"}$. For some plants, the fouling factor is calculated more than one way (e.g., using feedwater flow rate and using steam flow rate). The results for each plant are discussed below.

Plant A

Figure C-A1. Historical Fouling Factor at Plant A (Using Feedwater Flow Measurements)

Figure C-A2. Historical Fouling Factor at Plant A (Using Steam Flow Measurements)

Figure C-A3. Historical Fouling Factor at Plant A (Using Plant A-Supplied Power)

The three figures do not differ significantly, indicating that feedwater flow measurements, steam flow measurements, and Plant A-calculated thermal power are all fairly consistent. Since Plant A experienced some fouling of its feedwater venturis (particularly early in life), Figure C-A2 is chosen as the basis for discussion regarding the Plant-A fouling factor. There are several noteworthy features on this graph:

- The fouling factor decreases sharply during the first cycle of operation. This may reflect the development of heat-transfer-enhancing deposits on the secondary side of the SG tubes.
- After the early decrease, the fouling factor remains near zero, or even slightly negative, during Cycles 2-4. During this time, the Plant-A power rating was increased by 4.5%, thereby reducing the available margin against fouling and tube plugging.
- During startup after the EOC 4 outage, the VWO condition was reached, resulting in a decrease in electrical generating capacity. Note that there is no sharp increase in the average fouling factor marking this occasion. In fact, the fouling factor is only slightly positive at the beginning of Cycle 5.
- During Cycles 5 and 6, the fouling factor increased steadily until the institution of ETA in the feedwater. Coincident with this change, the fouling factor appears to level off.

---

* For Plant F, the fouling factor is calculated for the time span between 1980 and 1990 (6.5 EFPY to 15 EFPY). The data required to calculate the fouling factor were unavailable for earlier operation.

† In some cases, plant-calculated values were unavailable, requiring independent calculation using the inputs discussed in Appendix B.

- During the EOC 7 outage, a chemical cleaning of the SG secondary side was performed in each of the four SGs. Upon restart in Cycle 8, the fouling factor exhibits a step increase. This suggests that the deposits removed by the chemical cleaning were in fact beneficial to heat transfer (i.e., responsible for a decrease in the fouling factor). Thin deposits (<3 to 4 mils) have been known to cause this behavior in a number of cases.

- The net change in fouling factor (according to Figure C-A2) between early operation and recent operation is -5 10^{-6} h-ft^2-°F/BTU. The net change just prior to chemical cleaning was -28 10^{-6}.

Plant B

Figure C-B1. Historical Fouling Factor at Plant B (Using Feedwater Flow Measurements)

Figure C-B2. Historical Fouling Factor at Plant B (Using Steam Flow Measurements)

Figure C-B3. Historical Fouling Factor at Plant B (Using Plant B-Supplied Power)

Figure C-B4. Historical Fouling Factor at Plant B (Using Feedwater Flow and Corrected T_{hot})

Figures C-B1 and C-B2 are noticeably different, suggesting that feedwater and steam flow measurements are not in good agreement. This is confirmed in Figure B-B5b, which indicates substantial disagreement in Cycles 1, 4, and 5. Figure C-B3 is in good agreement with C-B1, which is expected because Plant B uses feedwater flow rate to calculate thermal power. Figure C-B4 is identical to C-B1 except that the former also reflects a correction for 2°F of hot-leg streaming beginning in Cycle 5. Streaming most likely became a factor at Plant B at this time due to

- Institution of a low-leakage reactor core, begun in 1990.
- Removal of RTD bypass loops present on all four loops, also in 1990. Bypass loops increase thermal mixing dramatically, making hot-leg streaming much less severe or nonexistent.

Note from the figures that this correction reduces the calculated fouling factor by about 23 10^{-6} h-ft^2-°F/BTU. Also, the overall change in fouling factor since early operation suggested by Figure C-B4 is about 42 10^{-6} (21 10^{-6} just prior to chemical cleaning).

Plant C

Figure C-C1. Historical Fouling Factor at Plant C (Using Feedwater Flow Measurements)

Figure C-C2. Historical Fouling Factor at Plant C (Using Steam Flow Measurements)

Except for Cycle 1 (for which no steam flow rate measurements were available), these two figures are in fairly close agreement. From Figure C-C1, the fouling factor increase between early and recent operation is about 30 10^{-6} h-ft^2-°F/BTU.

Plant D

Figure C-D1. Historical Fouling Factor at Plant D (Using Feedwater Flow Measurements)

Figure C-D2. Historical Fouling Factor at Plant D (Relative to Initial Performance)

Figure C-D3. Historical Fouling Factor at Plant D (Using Plant-D Power)

The first of these figures shows the fouling factor calculated relative to the design thermal resistance for Plant D. Figure C-D2 reflects the fouling factor calculated relative to the initial thermal resistance actually recorded for each SG (i.e., state-point data taken in 1981). Both of these figures also reflect DEI-calculated thermal power based on other measurements (temperatures and flow rates). Figure C-D3 is identical to C-D1 except that Plant D-reported thermal power is used instead of the DEI-calculated thermal power. Note the increase in fouling factor during Cycles 7 and 8 in Figure C-D3 compared to C-D1. This is a direct result of the bypass flow in the feedwater flow venturi meters. The bypass flow caused the measured flow to be lower than the actual flow, resulting in an erroneously low thermal power calculated by the Plant-D computer and consequently an erroneously high fouling factor. Thus, it is believed that Figure C-D1 is a more accurate representation of the fouling factor than C-D3.

For the purpose of considering the effects of possible secondary-side corrosion deposits, the change in fouling factor over the life of the plant R_f" is more important than the initial or current thermal resistance value. Thus, we seek to determine R_f" for Plant D starting with Figure C-D1. The initial value R_{f0}" is clearly uncertain due to the dearth of early data (only two state-point runs are available for the period of operation between initial startup and 1.3 EFPY), and also due to the scatter of the data that is present. The best estimate for R_{f0}" is obtained as follows:

- Average the fouling factor for the first two state-point runs for all 4 SGs, resulting in a value of 19 10^{-6} h-ft^2-°F/BTU.
- Average the fouling factor for all four SGs for the first three months for which regular data are available (May to July of 1985). This results in a value of 16 10^{-6} h-ft^2-°F/BTU. Since this agrees well with the above number, it is used as the best estimate for R_{f0}" relative to the design values. It is important to note that this estimate could deviate significantly from the true value due to the absence of early data (e.g., -15 10^{-6} and 45 10^{-6} are both possible).

The current value $R_{f\text{-current}}$" is subject to less uncertainty due to the frequency and smaller scatter of available data. For May 1995, the average fouling factor for all four SGs is 67 10^{-6} h-ft^2-°F/BTU.

Therefore, the best-estimate increase in fouling factor over the life of Plant D is 51 10^{-6} h-ft^2-°F/BTU.

Plant E

Figure C-E1. Historical Fouling Factor at Plant E (Using Feedwater Flow Measurements)

This figure shows the calculated fouling factor relative to the design thermal resistance using feedwater flow rate measurements to calculate thermal power. Note that the scatter in the data drops considerably starting at about Cycle 5, reflecting more complete and consistent instrument measurements. Examination of Figure C-E1 indicates that the fouling factor increase between early operation and operation just prior to the 1996 chemical cleaning is approximately 172 10^{-6} h-ft^2-°F/BTU.

Plant F

Figure C-F1. Historical Fouling Factor at Plant F

This figure shows the calculated fouling factor relative to the design thermal resistance using measured values of SG steam pressure and design values of all other thermal-hydraulic parameters. In spite of the scatter in the data, the figure clearly shows four or five transient increases in fouling factor accompanied by concomitant decreases in SG steam pressure. According to the figure, the approximate change in calculated global fouling factor over the period 1980 to 1990 was 117 10^{-6} h-ft^2-°F/BTU. In order to compare directly with Plant E, we also note that for the period between 1980 and 1984 (6.5 EFPY to 10 EFPY), the fouling factor increase at Plant F was approximately 87 10^{-6} h-ft^2-°F/BTU. For the same period of operation (6.5 EFPY to 10 EFPY), the fouling factor increase at Plant E was about 93 10^{-6} h-ft^2-°F/BTU, suggesting similar effects on heat transfer at the two plants for the same period of operation.

Fouling Factor Uncertainty Analyses

There are potentially significant uncertainties in the plant instrument data required as inputs to the fouling factor calculation. As a result, a statistical uncertainty analysis is warranted when reporting the fouling factor calculations. The standard engineering approximation for calculating the uncertainty tolerance of a computed quantity uses the following equation:

$$\Delta_{statistical}(F) = \sqrt{\sum_{i=1}^{n}\left(\frac{\partial F}{\partial x_i}\right)^2 \Delta^2(x_i)} \qquad [C\text{-}1]$$

where F is a function of x_1 through x_n and $\Delta(x_i)$ is the engineering estimate of the uncertainty in the measured quantity x_i. The worst case uncertainty in the calculated quantity F is given by

$$\Delta_{worst\ case}(F) = \sum_{i=1}^{n} \left| \left(\frac{\partial F}{\partial x_i} \right) \Delta(x_i) \right| \qquad [C\text{-}2]$$

However, this quantity is considered overly conservative for the fouling factor calculation. More detailed discussion of the issues involved in calculating uncertainties is provided in ASME Performance Test Code PTC 19.1-1985 (19), including such topics as precision and bias errors and sensitivity calculations. Page 3-8 of Reference (3) comprises a discussion of measurement uncertainty issues specific to nuclear plants.

Uncertainty Inputs

In order to perform the calculation suggested by Eq. [C-1], values for each of the $\Delta(x_i)$ must be determined. These include uncertainties for the following parameters:

- Primary temperatures T_{hot} and T_{cold}
- Feedwater temperature
- Feedwater mass flow rate
- Blowdown flow rate
- Feedwater pressure
- SG steam pressure
- Steam quality
- Heat-transfer area

The input values and the results of the uncertainty analysis for each plant are discussed below. No uncertainty calculations were performed for Plant F due to a lack of the above inputs.

Plant A

Measurement tolerances are indicated in Table C-1. Note that Table 3-2 of Reference (3) applies explicitly to another Model F plant. However, both plants are examples of the standardized nuclear unit power plant system (SNUPPS) design. Hence, these measurement tolerances are believed to be applicable to Plant A also. The tolerances marked "estimate" in Table C-1 are based on engineering judgment. The results of the uncertainty analysis are shown in Table C-2. Note that the total statistical uncertainty in the fouling factor ($\pm 25\ 10^{-6}$ h-ft^2-°F/BTU) is larger in magnitude than the previously calculated fouling factor change over the life of the plant ($-5\ 10^{-6}$).

From the lower portion of Table C-2, it is apparent that the uncertainty in SG steam pressure dominates the fouling factor uncertainty, while T_{cold}, T_{hot}, and feedwater flow rate play lesser roles. The remaining variables contribute very little to the total uncertainty. The fouling factor for Plant A (in 1996) is thus given by

$$R''_{f-Plant\ A} = -5 \pm 25\,10^{-6}\, h-ft^2-{}^\circ F/BTU \qquad [C\text{-}3]$$

Plant B

Measurement tolerances are listed in Table C-1, and the associated uncertainty analysis is shown in Table C-3. In this case, the uncertainties in T_{cold} and SG steam pressure are dominant, while T_{hot} has a minor contribution. The other variables contribute little to the fouling factor uncertainty. The calculated fouling factor may be completely reported for Plant B (in 1996) as

$$R''_{f-Plant\ B} = 42 \pm 24\,10^{-6}\, h-ft^2-{}^\circ F/BTU \qquad [C\text{-}4]$$

Plant C

Measurement tolerances specific to Plant C are shown in Table C-1; the values are based on conversations with utility personnel or are best estimates based on engineering judgment and industry data. The associated uncertainty analysis is shown in Table C-4. Note that the uncertainties in T_{cold} and SG pressure are the primary contributors to the fouling factor uncertainty. In view of the uncertainty analysis, the calculated fouling factor may be completely reported for Plant C (in 1996) as:

$$R''_{f-Plant\ C} = 30 \pm 96\,10^{-6}\, h-ft^2-{}^\circ F/BTU \qquad [C\text{-}5]$$

Plant D

Measurement tolerances specific to Plant D are shown in Table C-1; the values are based on conversations with utility personnel or are best estimates based on engineering judgment and industry data. The associated uncertainty analysis is shown in Table C-5. Note that the uncertainty in T_{cold} is the primary contributor to the fouling factor uncertainty with T_{hot} and SG pressure playing lesser roles. Also note that an extra ±30 10^{-6} h-ft^2-°F/BTU (not shown in Table C-5) has been explicitly added to the uncertainty for Plant D due to the dearth of early-cycle data. In view of the uncertainty analysis, the calculated fouling factor may be completely reported for Plant D (in 1995) as:

$$R''_{f-Plant\ D} = 51 \pm 89\,10^{-6}\, h-ft^2-{}^\circ F/BTU \qquad [C\text{-}6]$$

Plant E

Measurement tolerances specific to Plant E are shown in Table C-1; the values are based on conversations with utility personnel or are best estimates based on engineering judgment and industry data. The associated uncertainty analysis is shown in Table C-6; the T_{cold} uncertainty is the major cause while T_{hot}, SG pressure, and feedwater flow each have a minor contribution. In view of the uncertainty analysis, the calculated fouling factor may be completely reported for Plant E (in 1996) as:

$$R''_{f-Plant\ E} = 172 \pm 48\, 10^{-6}\, h - ft^2 - °F / BTU \qquad [C\text{-}7]$$

Table C-1. Plant Measurement Uncertainties

Symbol	Quantity	Tolerance	Source
Plant A			
T_{hot}	Hot-Leg Temperature	±1.0°F	Table 3-2 of EPRI NP-5728
T_{cold}	Cold-Leg Temperature	±0.5°F	Table 3-2 of EPRI NP-5728
p_{sat}	SG Steam Pressure	±0.5% FS (±6.5 psi)	Table 3-2 of EPRI NP-5728
m_{FW}	Feedwater Flow Rate	±2.7% FS (±129,600 lb_m/h)	Table 3-2 of EPRI NP-5728 & Utility Calibration Procedure
T_{FW}	Feedwater Temperature	±1.0°F	Estimate
Q_{BD}	Blowdown Flow Rate	±1% (312 lb_m/h)	Estimate
p_{FW}	Feedwater Pressure	±8 psi	Estimate
x	Steam Quality	±0.15%	Estimate
A	Heat-Transfer Area[1]	0.2% (±110 ft^2)	Estimate
Plant B			
T_{hot}	Hot-Leg Temperature	±1.2°F	Utility Personnel
T_{cold}	Cold-Leg Temperature	±1.2°F	Utility Personnel
p_{sat}	SG Steam Pressure[1]	±0.4% FS (±4.8 psi)	Utility Personnel
m_{FW}	Feedwater Flow Rate[2]	±0.5% FS (±2.25 10^4 lb_m/h)	Utility Personnel
T_{FW}	Feedwater Temperature	±1.5°F	Utility Personnel
Q_{BD}	Blowdown Flow Rate	±10% (2000 lb_m/h)	Utiltity Information
p_{FW}	Feedwater Pressure	±30 psi	Utility Personnel
x	Steam Quality	±0.15%	Estimate
A	Heat-Transfer Area[3]	0.3% (±155 ft^2)	Estimate
Plant C			
T_{hot}	Hot-Leg Temperature	±2°F	Utility Personnel
T_{cold}	Cold-Leg Temperature	±2°F	Utility Personnel
p_{sat}	SG Steam Pressure	±0.5% FS (±7.5 psi)	Best Estimate
m_{FW}	Feedwater Flow Rate	±0.5% FS (±2.12 10^4 lb_m/h)	Best Estimate
T_{FW}	Feedwater Temperature	±1°F	Utility Personnel
Q_{BD}	Blowdown Flow Rate	±10% (3900 lb_m/h)	Bounding Estimate
p_{FW}	Feedwater Pressure	±30 psi	Bounding Estimate
x	Steam Quality	±0.15%	Bounding Estimate
A	Heat-Transfer Area[1]	0.25% (±170 ft^2)	Bounding Estimate
Plant D			
T_{hot}	Hot-Leg Temperature	±4°F	Best Estimate
T_{cold}	Cold-Leg Temperature	±4°F	Best Estimate
p_{sat}	SG Steam Pressure	±0.45% FS (±5.4 psi)	Instrument Specifications
m_{FW}	Feedwater Flow Rate	±0.5% FS (±1.85 10^4 lb_m/h)	Calibration Procedure & Best Estimate
T_{FW}	Feedwater Temperature	±1°F	Best Estimate
Q_{BD}	Blowdown Flow Rate	±10% (3900 lb_m/h)	Bounding Estimate
p_{FW}	Feedwater Pressure	±30 psi	Bounding Estimate
x	Steam Quality	±0.15%	Bounding Estimate
A	Heat-Transfer Area[1]	0.25% (±129 ft^2)	Bounding Estimate
Plant E			
T_{hot}	Hot-Leg Temperature	±3°F	Utility Personnel
T_{cold}	Cold-Leg Temperature	±3°F	Utility Personnel
p_{sat}	SG Steam Pressure	±6 psi	Best Estimate
m_{FW}	Feedwater Flow Rate	±1.5% FS (±1.14 10^5 lb_m/h)	Best Estimate
T_{FW}	Feedwater Temperature	±1°F	Utility Personnel
Q_{BD}	Blowdown Flow Rate	±10% (7500 lb_m/h)	Bounding Estimate
p_{FW}	Feedwater Pressure	±30 psi	Bounding Estimate
x	Steam Quality	±0.15%	Bounding Estimate
A	Heat-Transfer Area[1]	0.5% (±473 ft^2)	Bounding Estimate

NOTES

1. This tolerance reflects the possibility that plugged tubes may be longer or shorter on average than the average-length tube in the whole bundle.
2. This error is believed to be applicable for operation since 1992. Earlier data may be subject to an error as large as 2.8% (1.8% per utiltity scaling and set point document plus 1% for venturi fouling).
3. This tolerance reflects the possibility that plugged tubes may be longer or shorter on average than the average-length tube in the whole bundle.

Table C-2. Fouling Factor Uncertainty Analysis for Plant A

Quantity	Description	Units	Design Value (VWO)	Bilateral Tolerance	Δx
measured quantities					
T_{hot}	hot leg temperature	°F	620.0	1.0	1.0
T_{cold}	cold leg temperature	°F	557.0	0.5	0.5
T_{FW}	feedwater temperature	°F	446.0	1.0	1.0
m_{FW}	feedwater flow rate[1]	lb/h	3.963E+06	2.7% of FS	129,600
Q_{BD}	blowdown volumetric flow rate	gpm	84	1.0%	1
p_{FW}	feedwater pressure	psia	1025	8	8
p_{sat}	steam generator dome pressure[2]	psia	1000	0.5% of FS	6.5
x	steam quality	%	99.75	0.15	0.15
A	heated outside-tube surface area	ft^2	46,750	0.2%	110
intermediate quantities					
$T_{sat,out}$	outlet saturation temperature	°F	544.58		
p_{bundle}	mid-bundle pressure	psia	1011.5		
T_{sat}	bundle saturation temperature	°F	545.97		
ΔT_{lm}	log-mean temperature difference	°F	33.09		
v_f	saturated liquid specific volume	ft^3/lb	0.02163		
m_{BD}	blowdown mass flow rate	lb/h	31,250		
m_{steam}	steam flow rate	lb/h	3.931E+06		
h_f	saturated liquid specific enthalpy	Btu/lb	542.6		
h_g	saturated vapor specific enthalpy	Btu/lb	1192.9		
$h_f(T_{FW})$	feedwater saturated spec. enthalpy	Btu/lb	425.6		
$v_f(T_{FW})$	feedwater saturated spec. volume	ft^3/lb	0.01936		
$p_{sat}(T_{FW})$	saturation pressure at feedwater T	psia	405.7		
h_{FW}	feedwater specific enthalpy	Btu/lb	427.9		
Q	steam generator heat transfer rate	Btu/h	3.005E+09		
R	global resistance to heat transfer	h-°F/Btu	1.101E-08		
U	global heat transfer coefficient	Btu/h-ft^2-°F	1942.8		
calculated quantity					
R"	global area-based resistance	10^{-6} h-ft^2-°F/Btu	514.7		
other quantities required for partial derivatives					
$c_{p,FW}$	feedwater specific heat	Btu/lb-°F	1.109		
v_{FW}	feedwater specific volume	ft^3/lb	0.01936		
h_{fg}	latent heat of vaporization at p_{sat}	Btu/lb	650.4		
v_g	saturated vapor specific volume	ft^3/lb	0.4404		
v_{fg}	specific volume change upon vap.	ft^3/lb	0.41881		
$\partial h_g/\partial p_{sat}$	partial derivative of vapor enthalpy	(Btu/lb)/psi	-0.03659		
$\partial h_f/\partial p_{sat}$	partial derivative of liquid enthalpy	(Btu/lb)/psi	0.1532		
$\partial(h_{fg}/v_f)/\partial p_{sat}$	partial derivative of h_{fg}/v_f ratio	(Btu/ft^3)/psi	-13.856		
$\partial Q/\partial p_{sat}$	partial derivative of thermal power	(Btu/h)/psi	-133,785		

Table C-2. Fouling Factor Uncertainty Analysis for Plant A

partial derivatives of area-based resistance		Units for $\partial R''/\partial x$	$\partial R''/\partial x$	$\Delta(x)$	$(\partial R''/\partial x)\Delta(x)$
$\partial R''/\partial T_{hot}$	partial deriv. wrt hot leg temp.	$(10^{-6}$ h-ft^2-°F/Btu)/°F	4.518	1.0	4.52
$\partial R''/\partial T_{cold}$	partial deriv. wrt cold leg temp.	$(10^{-6}$ h-ft^2-°F/Btu)/°F	16.345	0.5	8.17
$\partial R''/\partial T_{FW}$	partial deriv. wrt feedwater temp.	$(10^{-6}$ h-ft^2-°F/Btu)/°F	0.752	1.0	0.75
$\partial R''/\partial m_{FW}$	partial deriv. wrt feedwater flow	$(10^{-6}$ h-ft^2-°F/Btu)/(lb/h)	-1.308E-04	1.296E+05	-16.95
$\partial R''/Q_{BD}$	partial deriv. wrt blowdown flow	$(10^{-6}$ h-ft^2-°F/Btu)/gpm	0.041	1	0.03
$\partial R''/\partial p_{FW}$	partial deriv. wrt feedwater press.	$(10^{-6}$ h-ft^2-°F/Btu)/psi	0.002	8	0.02
$\partial R''/\partial p_{sat}$	partial deriv. wrt steam gen. press.	$(10^{-6}$ h-ft^2-°F/Btu)/psi	-2.477	6.5	-16.10
$\partial R''/\partial x$	partial deriv. wrt outlet quality	$(10^{-6}$ h-ft^2-°F/Btu)/%	-4.380	0.15	-0.66
$\partial R''/A$	partial deriv. wrt heated area	$(10^{-6}$ h-ft^2-°F/Btu)/ft^2	0.011	110	1.21
				$\Sigma\,(\partial R''/\partial x)\Delta(x)$	48.42
				$\Sigma[(\partial R''/\partial x)\Delta(x)]^2$	636.17
				$\{\Sigma[(\partial R''/\partial x)\Delta(x)]^2\}^{1/2}$	25.22
final results of error analysis			Design	$\Delta_{worst\ case}(R'')$	$\Delta_{statistical}(R'')$
R''	global area-based resistance	10^{-6} h-ft^2-°F/Btu	514.7	48.4	25.2

Notes

1. The full scale for feedwater flow measurement is 4.8 x 10^6 lb_m/h
2. The full scale for SG pressure measurement is 1300 psi.

Table C-3. Fouling Factor Uncertainty Analysis for Plant B

Quantity	Description	Units	Design Value (VWO)	Bilateral Tolerance	Δx
Measured quantities					
T_{hot}	hot leg temperature	°F	609.7	1.1	1.1
T_{cold}	cold leg temperature	°F	546.7	1.1	1.1
T_{FW}	feedwater temperature	°F	434.5	1.5	1.5
m_{FW}	feedwater flow rate	lb/h	3.749E+06	0.5%	2.250E+04
Q_{BD}	blowdown volumetric flow rate	gpm	53	10%	5
p_{FW}	feedwater pressure	psia	876	30	30
p_{sat}	steam generator dome pressure	psia	857	4.8	4.8
x	steam quality	%	99.75	0.15	0.15
A	heated outside-tube surface area	ft^2	51,500	0.3%	155
Intermediate quantities					
$T_{sat,out}$	outlet saturation temperature	°F	526.19		
p_{bundle}	mid-bundle pressure	psia	865		
T_{sat}	bundle saturation temperature	°F	527.27		
ΔT_{lm}	log-mean temperature difference	°F	43.60		
v_f	saturated liquid specific volume	ft^3/lb	0.02111		
m_{BD}	blowdown mass flow rate	lb/h	20,000		
m_{steam}	steam flow rate	lb/h	3.729E+06		
h_f	saturated liquid specific enthalpy	Btu/lb	520.9		
h_g	saturated vapor specific enthalpy	Btu/lb	1197.4		
$h_f(T_{FW})$	feedwater saturated spec. enthalpy	Btu/lb	412.9		
$v_f(T_{FW})$	feedwater saturated spec. volume	ft^3/lb	0.01917		
$p_{sat}(T_{FW})$	saturation pressure at feedwater T	psia	360.4		
h_{FW}	feedwater specific enthalpy	Btu/lb	414.7		
Q	steam generator heat transfer rate	Btu/h	2.915E+09		
R	global resistance to heat transfer	h-°F/Btu	1.496E-08		
U	global heat transfer coefficient	Btu/h-ft^2-°F	1298		
Calculated quantity					
R"	global area-based resistance	10^{-6} h-ft^2-°F/Btu	770.4		
Other quantities required for partial derivatives					
$c_{p,FW}$	feedwater specific heat	Btu/lb-°F	1.098		
v_{FW}	feedwater specific volume	ft^3/lb	0.01917		
h_{fg}	latent heat of vaporization at p_{sat}	Btu/lb	676.5		
v_g	saturated vapor specific volume	ft^3/lb	0.5233		
v_{fg}	specific volume change upon vap.	ft^3/lb	0.5022		
$\partial h_g/\partial p_{sat}$	partial derivative of vapor enthalpy	(Btu/lb)/psi	-0.03106		
$\partial h_f/\partial p_{sat}$	partial derivative of liquid enthalpy	(Btu/lb)/psi	0.1653		
$\partial(h_{fg}/v_f)/\partial p_{sat}$	partial derivative of h_{fg}/v_f ratio	(Btu/ft^3)/psi	-14.74		
$\partial Q/\partial p_{sat}$	partial derivative of thermal power	(Btu/h)/psi	-108,391		

Table C-3. Fouling Factor Uncertainty Analysis for Plant B

Partial derivatives of area-based resistance		Units for $\partial R''/\partial x$	$\partial R''/\partial x$	$\Delta(x)$	$(\partial R''/\partial x)\Delta(x)$
$\partial R''/\partial T_{hot}$	partial deriv. wrt hot leg temp.	$(10^{-6}$ h-ft^2-°F/Btu)/°F	5.761	1.1	6.57
$\partial R''/\partial T_{cold}$	partial deriv. wrt cold leg temp.	$(10^{-6}$ h-ft^2-°F/Btu)/°F	15.206	1.1	17.33
$\partial R''/\partial T_{FW}$	partial deriv. wrt feedwater temp.	$(10^{-6}$ h-ft^2-°F/Btu)/°F	1.088	1.5	1.63
$\partial R''/\partial m_{FW}$	partial deriv. wrt feedwater flow	$(10^{-6}$ h-ft^2-°F/Btu)/(lb/h)	-2.065E-04	2.250E+04	-4.65
$\partial R''/Q_{BD}$	partial deriv. wrt blowdown flow	$(10^{-6}$ h-ft^2-°F/Btu)/gpm	0.068	5	0.36
$\partial R''/\partial p_{FW}$	partial deriv. wrt feedwater press.	$(10^{-6}$ h-ft^2-°F/Btu)/psi	0.004	30	0.11
$\partial R''/\partial p_{sat}$	partial deriv. wrt steam gen. press.	$(10^{-6}$ h-ft^2-°F/Btu)/psi	-2.814	5	-13.51
$\partial R''/\partial x$	partial deriv. wrt outlet quality	$(10^{-6}$ h-ft^2-°F/Btu)/%	-6.668	0.15	-1.00
$\partial R''/A$	partial deriv. wrt heated area	$(10^{-6}$ h-ft^2-°F/Btu)/ft^2	0.015	155	2.31
				$\Sigma\,(\partial R''/\partial x)\Delta(x)$	47.46
				$\Sigma[(\partial R''/\partial x)\Delta(x)]^2$	556.74
				$\{\Sigma[(\partial R''/\partial x)\Delta(x)]^2\}^{1/2}$	23.60
Final results of error analysis			Design	$\Delta_{worst\ case}(R'')$	$\Delta_{statistical}(R'')$
R''	global area-based resistance	10^{-6} h-ft^2-°F/Btu	770.4	47.5	23.6

Table C-4. Fouling Factor Uncertainty Analysis for Plant C

Quantity	Description	Units	Design Value (VWO)	Bilateral Tolerance	Δx
Measured quantities					
T_{hot}	hot leg temperature	°F	626.1	2.0	2.0
T_{cold}	cold leg temperature	°F	559.7	2.0	2.0
T_{FW}	feedwater temperature	°F	440	1.0	1.0
m_{FW}	feedwater flow rate	lb/h	4.240E+06	0.5%	2.120E+04
Q_{BD}	blowdown volumetric flow rate	gpm	107	10%	11
p_{FW}	feedwater pressure	psia	1129	30	30
p_{sat}	steam generator dome pressure	psia	1100	7.5	7.5
x	steam quality	%	99.75	0.15	0.15
A	heated outside-tube surface area	ft^2	68,000	0.25%	170
Intermediate quantities					
$T_{sat,out}$	outlet saturation temperature	°F	556.27		
p_{bundle}	mid-bundle pressure	psia	1107		
T_{sat}	bundle saturation temperature	°F	557.06		
ΔT_{lm}	log-mean temperature difference	°F	20.34		
v_f	saturated liquid specific volume	ft^3/lb	0.02197		
m_{BD}	blowdown mass flow rate[1]	lb/h	39,000		
m_{steam}	steam flow rate	lb/h	4.201E+06		
h_f	saturated liquid specific enthalpy	Btu/lb	558.6		
h_g	saturated vapor specific enthalpy	Btu/lb	1188.8		
$h_f(T_{FW})$	feedwater saturated spec. enthalpy	Btu/lb	419.0		
$v_f(T_{FW})$	feedwater saturated spec. volume	ft^3/lb	0.01926		
$p_{sat}(T_{FW})$	saturation pressure at feedwater T	psia	381.54		
h_{FW}	feedwater specific enthalpy	Btu/lb	421.6		
Q	steam generator heat transfer rate	Btu/h	3.222E+09		
R	global resistance to heat transfer	h-°F/Btu	6.313E-09		
U	global heat transfer coefficient	Btu/h-ft^2-°F	2330		
Calculated quantity					
R"	global area-based resistance	10^{-6} h-ft^2-°F/Btu	429.3		
Other quantities required for partial derivatives					
$c_{p,FW}$	feedwater specific heat	Btu/lb-°F	1.103		
v_{FW}	feedwater specific volume	ft^3/lb	0.01926		
h_{fg}	latent heat of vaporization at p_{sat}	Btu/lb	630.3		
v_g	saturated vapor specific volume	ft^3/lb	0.3978		
v_{fg}	specific volume change upon vap.	ft^3/lb	0.3758		
$\partial h_g/\partial p_{sat}$	partial derivative of vapor enthalpy	(Btu/lb)/psi	-0.03818		
$\partial h_f/\partial p_{sat}$	partial derivative of liquid enthalpy	(Btu/lb)/psi	0.1448		
$\partial(h_{fg}/v_f)/\partial p_{sat}$	partial derivative of h_{fg}/v_f ratio	(Btu/ft^3)/psi	-13.36		
$\partial Q/\partial p_{sat}$	partial derivative of thermal power	(Btu/h)/psi	-148,516		

Table C-4. Fouling Factor Uncertainty Analysis for Plant C

Partial derivatives of area-based resistance		Units for $\partial R''/\partial x$	$\partial R''/\partial x$	$\Delta(x)$	$(\partial R''/\partial x)\Delta(x)$
$\partial R''/\partial T_{hot}$	partial deriv. wrt hot leg temp.	$(10^{-6}$ h-ft^2-°F/Btu)/°F	4.560	2.0	9.12
$\partial R''/\partial T_{cold}$	partial deriv. wrt cold leg temp.	$(10^{-6}$ h-ft^2-°F/Btu)/°F	43.386	2.0	86.77
$\partial R''/\partial T_{FW}$	partial deriv. wrt feedwater temp.	$(10^{-6}$ h-ft^2-°F/Btu)/°F	0.623	1.0	0.62
$\partial R''/\partial m_{FW}$	partial deriv. wrt feedwater flow	$(10^{-6}$ h-ft^2-°F/Btu)/(lb/h)	-1.020E-04	2.120E+04	-2.16
$\partial R''/Q_{BD}$	partial deriv. wrt blowdown flow	$(10^{-6}$ h-ft^2-°F/Btu)/gpm	0.031	11	0.33
$\partial R''/\partial p_{FW}$	partial deriv. wrt feedwater press.	$(10^{-6}$ h-ft^2-°F/Btu)/psi	0.002	30	0.06
$\partial R''/\partial p_{sat}$	partial deriv. wrt steam gen. press.	$(10^{-6}$ h-ft^2-°F/Btu)/psi	-5.359	8	-40.19
$\partial R''/\partial x$	partial deriv. wrt outlet quality	$(10^{-6}$ h-ft^2-°F/Btu)/%	-3.528	0.15	-0.53
$\partial R''/A$	partial deriv. wrt heated area	$(10^{-6}$ h-ft^2-°F/Btu)/ft^2	0.006	170	1.07
			$\Sigma\,(\partial R''/\partial x)\Delta(x)$		140.86
			$\Sigma[(\partial R''/\partial x)\Delta(x)]^2$		9234.61
			$\{\Sigma[(\partial R''/\partial x)\Delta(x)]^2\}^{1/2}$		96.10
Final results of error analysis			Design	$\Delta_{worst\ case}(R'')$	$\Delta_{statistical}(R'')$
R"	global area-based resistance	10^{-6} h-ft^2-°F/Btu	429.3	140.9	96.1

Notes

1. The average reported blowdown flow rate is used in the absence of a design value.

Table C-5. Fouling Factor Uncertainty Analysis for Plant D

Quantity	Description	Units	Design Value (VWO)	Bilateral Tolerance	Δx
measured quantities					
T_{hot}	hot leg temperature	°F	610.8	4.0	4.0
T_{cold}	cold leg temperature	°F	544.7	4.0	4.0
T_{FW}	feedwater temperature	°F	432.8	1.0	1.0
m_{FW}	feedwater flow rate[1]	lb/h	3.709E+06	0.5%	1.855E+04
Q_{BD}	blowdown volumetric flow rate	gpm	0	10%	0
p_{FW}	feedwater pressure	psia	836	30	30
p_{sat}	steam generator dome pressure[2]	psia	815	0.45%	5.4
x	steam quality	%	99.80	0.15	0.15
A	heated outside-tube surface area	ft^2	46,350	0.25%	116
intermediate quantities					
$T_{sat,out}$	outlet saturation temperature	°F	520.4		
p_{bundle}	mid-bundle pressure	psia	823.0		
T_{sat}	bundle saturation temperature	°F	521.6		
ΔT_{lm}	log-mean temperature difference	°F	48.97		
v_f	saturated liquid specific volume	ft^3/lb	0.02096		
m_{BD}	blowdown mass flow rate	lb/h	0		
m_{steam}	steam flow rate	lb/h	3.709E+06		
h_f	saturated liquid specific enthalpy	Btu/lb	513.8		
h_g	saturated vapor specific enthalpy	Btu/lb	1198.7		
$h_f(T_{FW})$	feedwater saturated spec. enthalpy	Btu/lb	411.0		
$v_f(T_{FW})$	feedwater saturated spec. volume	ft^3/lb	0.01914		
$p_{sat}(T_{FW})$	saturation pressure at feedwater T	psia	354.0		
h_{FW}	feedwater specific enthalpy	Btu/lb	412.7		
Q	steam generator heat transfer rate	Btu/h	2.910E+09		
R	global resistance to heat transfer	h-°F/Btu	1.683E-08		
U	global heat transfer coefficient	Btu/h-ft^2-°F	1282.3		
calculated quantity					
R"	global area-based resistance	10^{-6} h-ft^2-°F/Btu	779.8		
other quantities required for partial derivatives					
$c_{p,FW}$	feedwater specific heat	Btu/lb-°F	1.096		
v_{FW}	feedwater specific volume	ft^3/lb	0.01914		
h_{fg}	latent heat of vaporization at p_{sat}	Btu/lb	684.9		
v_g	saturated vapor specific volume	ft^3/lb	0.5522		
v_{fg}	specific volume change upon vap.	ft^3/lb	0.53124		
$\partial h_g/\partial p_{sat}$	partial derivative of vapor enthalpy	(Btu/lb)/psi	-0.02860		
$\partial h_f/\partial p_{sat}$	partial derivative of liquid enthalpy	(Btu/lb)/psi	0.17167		
$\partial(h_{fg}/v_f)/\partial p_{sat}$	partial derivative of h_{fg}/v_f ratio	(Btu/ft^3)/psi	-15.199		
$\partial Q/\partial p_{sat}$	partial derivative of thermal power	(Btu/h)/psi	-104,594		

Table C-5. Fouling Factor Uncertainty Analysis for Plant D

partial derivatives of area-based resistance		Units for $\partial R''/\partial x$	$\partial R''/\partial x$	$\Delta(x)$	$(\partial R''/\partial x)\Delta(x)$
$\partial R''/\partial T_{hot}$	partial deriv. wrt hot leg temp.	$(10^{-6}$ h-ft^2-°F/Btu)/°F	5.324	4.0	21.30
$\partial R''/\partial T_{cold}$	partial deriv. wrt cold leg temp.	$(10^{-6}$ h-ft^2-°F/Btu)/°F	13.172	4.0	52.69
$\partial R''/\partial T_{FW}$	partial deriv. wrt feedwater temp.	$(10^{-6}$ h-ft^2-°F/Btu)/°F	1.090	1.0	1.09
$\partial R''/\partial m_{FW}$	partial deriv. wrt feedwater flow	$(10^{-6}$ h-ft^2-°F/Btu)/(lb/h)	-2.103E-04	1.855E+04	-3.90
$\partial R''/Q_{BD}$	partial deriv. wrt blowdown flow	$(10^{-6}$ h-ft^2-°F/Btu)/gpm	0.070	0	0.00
$\partial R''/\partial p_{FW}$	partial deriv. wrt feedwater press.	$(10^{-6}$ h-ft^2-°F/Btu)/psi	0.004	30	0.11
$\partial R''/\partial p_{sat}$	partial deriv. wrt steam gen. press.	$(10^{-6}$ h-ft^2-°F/Btu)/psi	-2.577	5.4	-13.92
$\partial R''/\partial x$	partial deriv. wrt outlet quality	$(10^{-6}$ h-ft^2-°F/Btu)/%	-6.807	0.15	-1.02
$\partial R''/A$	partial deriv. wrt heated area	$(10^{-6}$ h-ft^2-°F/Btu)/ft^2	0.017	116	1.95
			Σ	$(\partial R''/\partial x)\Delta(x)$	95.97
			$\Sigma[(\partial R''/\partial x)\Delta(x)]^2$		3444.68
			$\{\Sigma[(\partial R''/\partial x)\Delta(x)]^2\}^{1/2}$		58.69
final results of error analysis			Design	$\Delta_{worst\ case}(R'')$	$\Delta_{statistical}(R'')$
R"	global area-based resistance	10^{-6} h-ft^2-°F/Btu	779.8	96.0	58.7

Notes

1. The full scale for feedwater flow measurement is 4.8 x 10^6 lb_m/h
2. The full scale for SG pressure measurement is 1300 psi.

Table C-6. Fouling Factor Uncertainty Analysis for Plant E

Quantity	Description	Units	Design Value (VWO)	Bilateral Tolerance	Δx
measured quantities					
T_{hot}	hot leg temperature	°F	611.0	3.0	3.0
T_{cold}	cold leg temperature	°F	553.0	3.0	3.0
T_{FW}	feedwater temperature	°F	445.0	1.0	1.0
m_{FW}	feedwater flow rate[1]	lb/h	7.619E+06	1.5%	1.143E+05
Q_{BD}	blowdown volumetric flow rate	gpm	200	10%	20
p_{FW}	feedwater pressure	psia	936	30	30
p_{sat}	steam generator dome pressure[2]	psia	900	6	6
x	steam quality	%	99.79	0.15	0.15
A	heated outside-tube surface area	ft^2	94,664	0.5%	473
intermediate quantities					
$T_{sat,out}$	outlet saturation temperature	°F	532.0		
p_{bundle}	mid-bundle pressure	psia	910.0		
T_{sat}	bundle saturation temperature	°F	533.4		
ΔT_{lm}	log-mean temperature difference	°F	42.21		
v_f	saturated liquid specific volume	ft^3/lb	0.02127		
m_{BD}	blowdown mass flow rate	lb/h	75,369		
m_{steam}	steam flow rate	lb/h	7.544E+06		
h_f	saturated liquid specific enthalpy	Btu/lb	526.5		
h_g	saturated vapor specific enthalpy	Btu/lb	1195.9		
$h_f(T_{FW})$	feedwater saturated spec. enthalpy	Btu/lb	424.5		
$v_f(T_{FW})$	feedwater saturated spec. volume	ft^3/lb	0.01935		
$p_{sat}(T_{FW})$	saturation pressure at feedwater T	psia	401.6		
h_{FW}	feedwater specific enthalpy	Btu/lb	426.4		
Q	steam generator heat transfer rate	Btu/h	5.802E+09		
R	global resistance to heat transfer	h-°F/Btu	7.275E-09		
U	global heat transfer coefficient	Btu/h-ft^2-°F	1452.0		
calculated quantity					
R"	global area-based resistance	10^{-6} h-ft^2-°F/Btu	688.7		
other quantities required for partial derivatives					
$c_{p,FW}$	feedwater specific heat	Btu/lb-°F	1.108		
v_{FW}	feedwater specific volume	ft^3/lb	0.01935		
h_{fg}	latent heat of vaporization at p_{sat}	Btu/lb	669.4		
v_g	saturated vapor specific volume	ft^3/lb	0.4951		
v_{fg}	specific volume change upon vap.	ft^3/lb	0.47384		
$\partial h_g/\partial p_{sat}$	partial derivative of vapor enthalpy	(Btu/lb)/psi	-0.03451		
$\partial h_f/\partial p_{sat}$	partial derivative of liquid enthalpy	(Btu/lb)/psi	0.16201		
$\partial(h_{fg}/v_f)/\partial p_{sat}$	partial derivative of h_{fg}/v_f ratio	(Btu/ft^3)/psi	-14.539		
$\partial Q/\partial p_{sat}$	partial derivative of thermal power	(Btu/h)/psi	-236,514		

Table C-6. Fouling Factor Uncertainty Analysis for Plant E

partial derivatives of area-based resistance		Units for $\partial R''/\partial x$	$\partial R''/\partial x$	$\Delta(x)$	$(\partial R''/\partial x)\Delta(x)$
$\partial R''/\partial T_{hot}$	partial deriv. wrt hot leg temp.	$(10^{-6}$ h-ft^2-°F/Btu)/°F	5.420	3.0	16.26
$\partial R''/\partial T_{cold}$	partial deriv. wrt cold leg temp.	$(10^{-6}$ h-ft^2-°F/Btu)/°F	13.632	3.0	40.89
$\partial R''/\partial T_{FW}$	partial deriv. wrt feedwater temp.	$(10^{-6}$ h-ft^2-°F/Btu)/°F	1.002	1.0	1.00
$\partial R''/\partial m_{FW}$	partial deriv. wrt feedwater flow	$(10^{-6}$ h-ft^2-°F/Btu)/(lb/h)	-9.117E-05	1.143E+05	-10.42
$\partial R''/Q_{BD}$	partial deriv. wrt blowdown flow	$(10^{-6}$ h-ft^2-°F/Btu)/gpm	0.030	20	0.60
$\partial R''/\partial p_{FW}$	partial deriv. wrt feedwater press.	$(10^{-6}$ h-ft^2-°F/Btu)/psi	0.003	30	0.10
$\partial R''/\partial p_{sat}$	partial deriv. wrt steam gen. press.	$(10^{-6}$ h-ft^2-°F/Btu)/psi	-2.450	6.0	-14.70
$\partial R''/\partial x$	partial deriv. wrt outlet quality	$(10^{-6}$ h-ft^2-°F/Btu)/%	-5.994	0.15	-0.90
$\partial R''/A$	partial deriv. wrt heated area	$(10^{-6}$ h-ft^2-°F/Btu)/ft^2	0.007	473	3.44
				$\Sigma\,(\partial R''/\partial x)\Delta(x)$	88.31
				$\Sigma[(\partial R''/\partial x)\Delta(x)]^2$	2275.43
				$\{\Sigma[(\partial R''/\partial x)\Delta(x)]^2\}^{1/2}$	47.70
final results of error analysis			Design	$\Delta_{worst\ case}(R'')$	$\Delta_{statistical}(R'')$
R"	global area-based resistance	10^{-6} h-ft^2-°F/Btu	688.7	88.3	47.7

Notes

1. The full scale for feedwater flow measurement is 4.8 x 10^6 lb_m/h
2. The full scale for SG pressure measurement is 1300 psi.

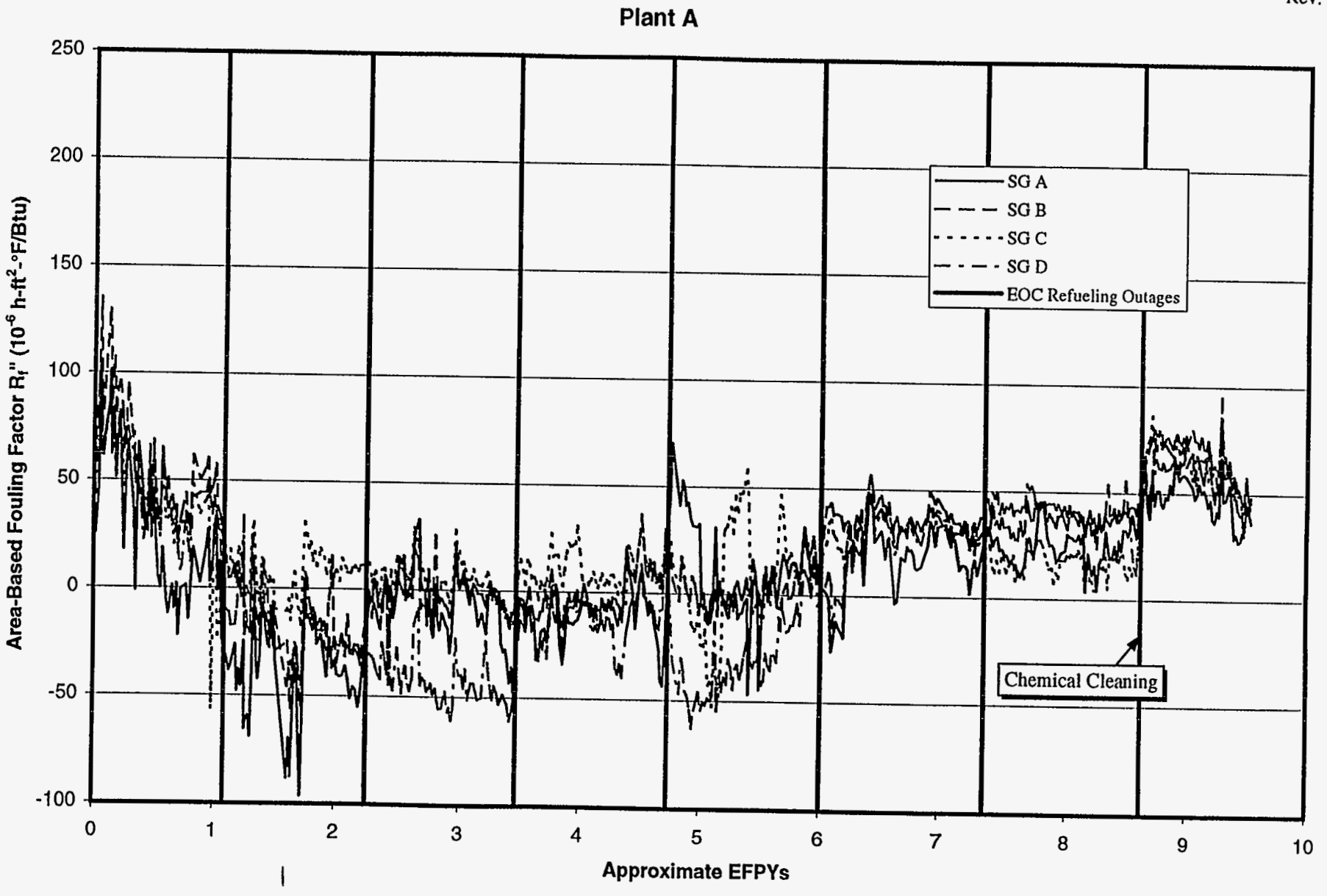

Figure C-A1. Historical Fouling Factor at Plant A (Using Feedwater Flow Measurements)

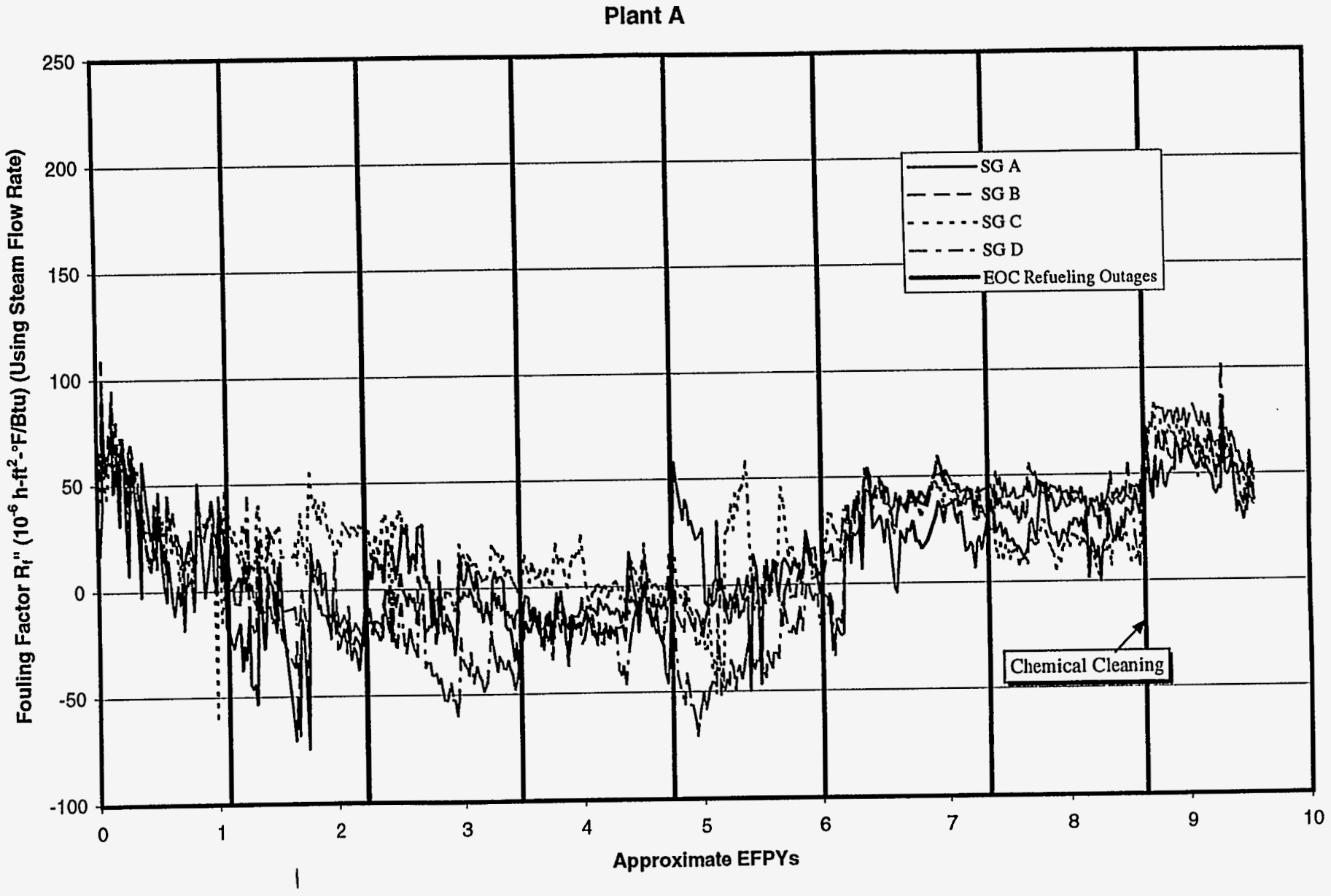

Figure C-A2. Historical Fouling Factor at Plant A (Using Steam Flow Measurements)

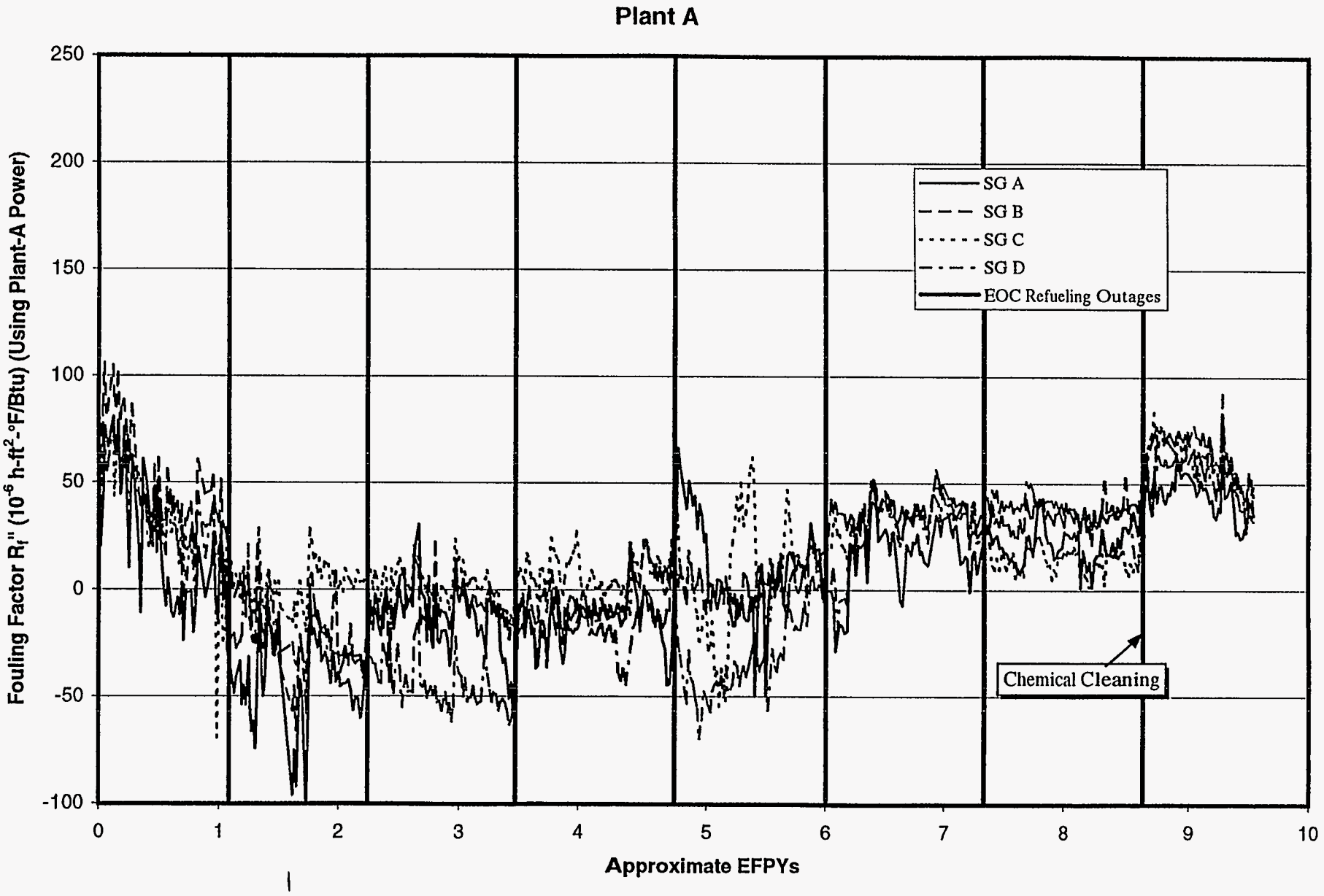

Figure C-A3. Historical Fouling Factor at Plant A (Using Plant A-Supplied Power)

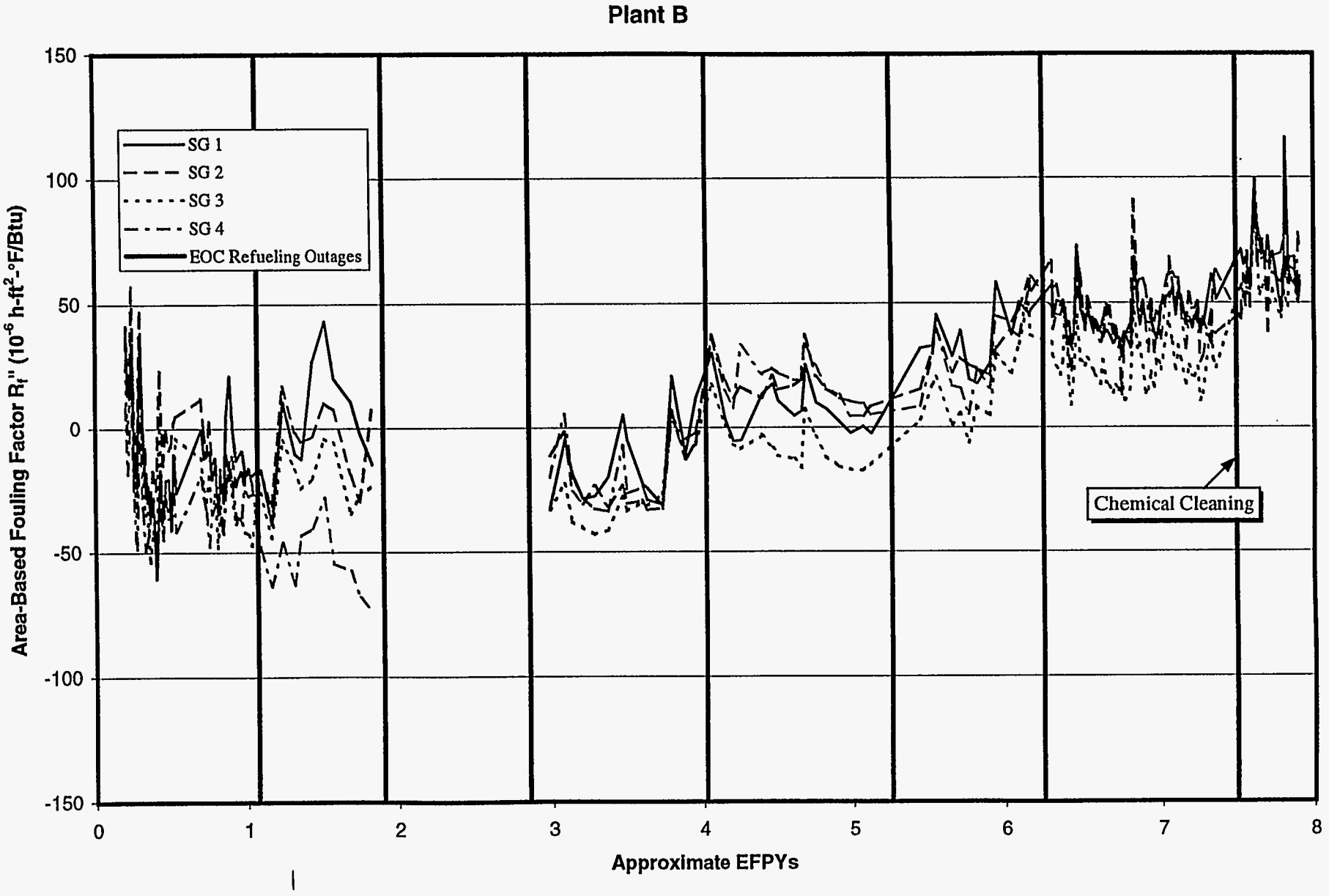

Figure C-B1. Historical Fouling Factor at Plant B (Using Feedwater Flow Measurements)

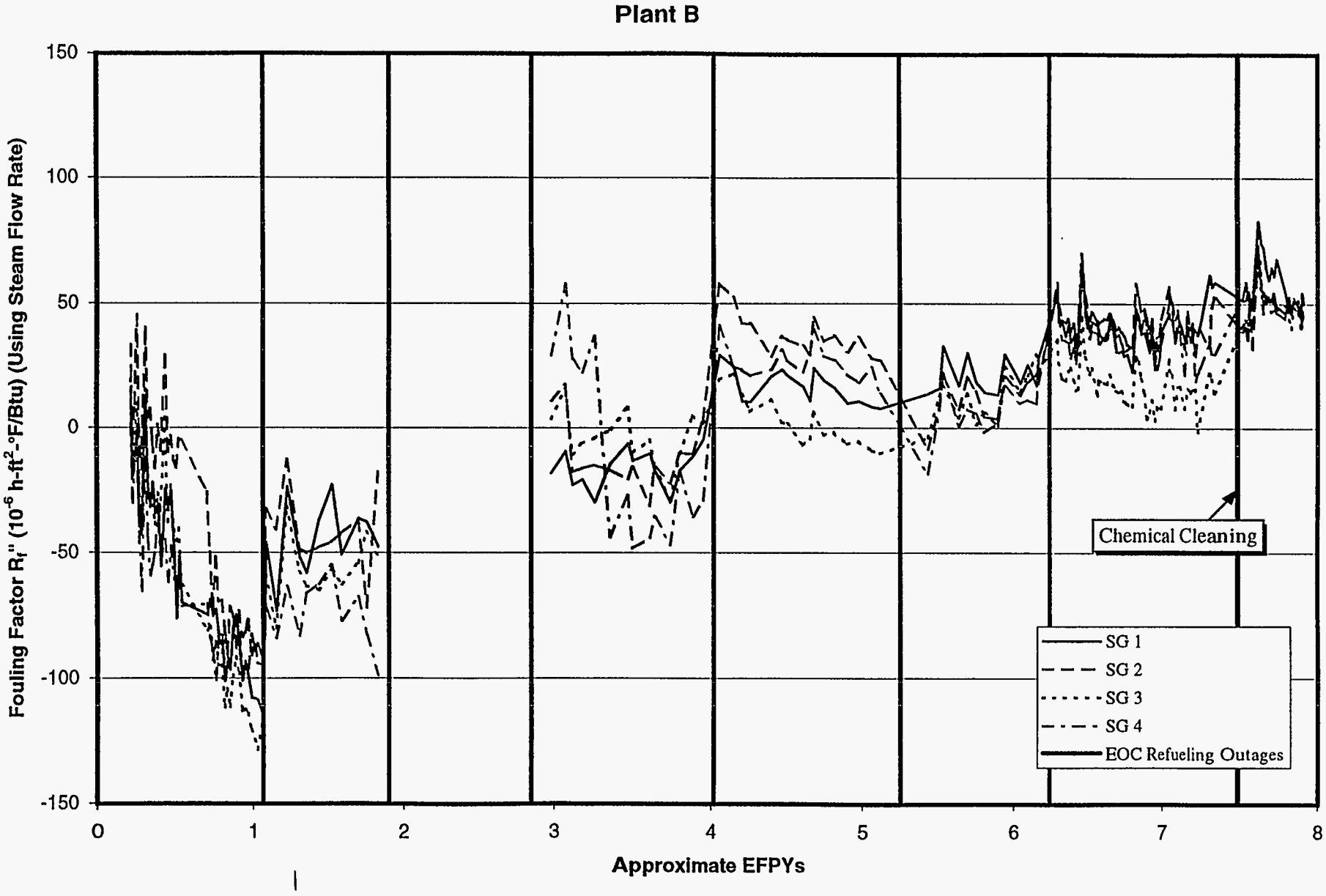

Figure C-B2. Historical Fouling Factor at Plant B (Using Steam Flow Measurements)

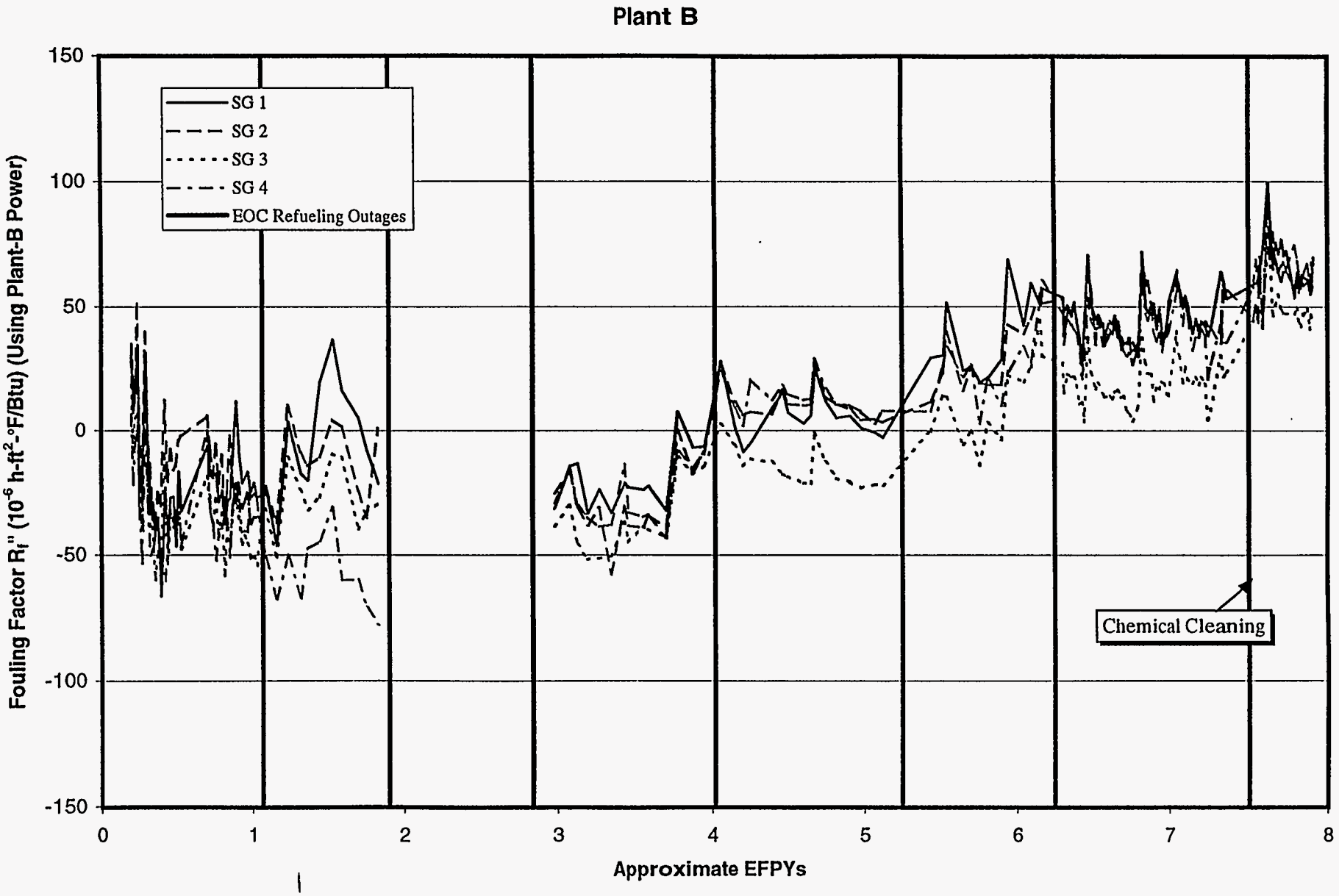

Figure C-B3. Historical Fouling Factor at Plant B (Using Plant B-Supplied Power)

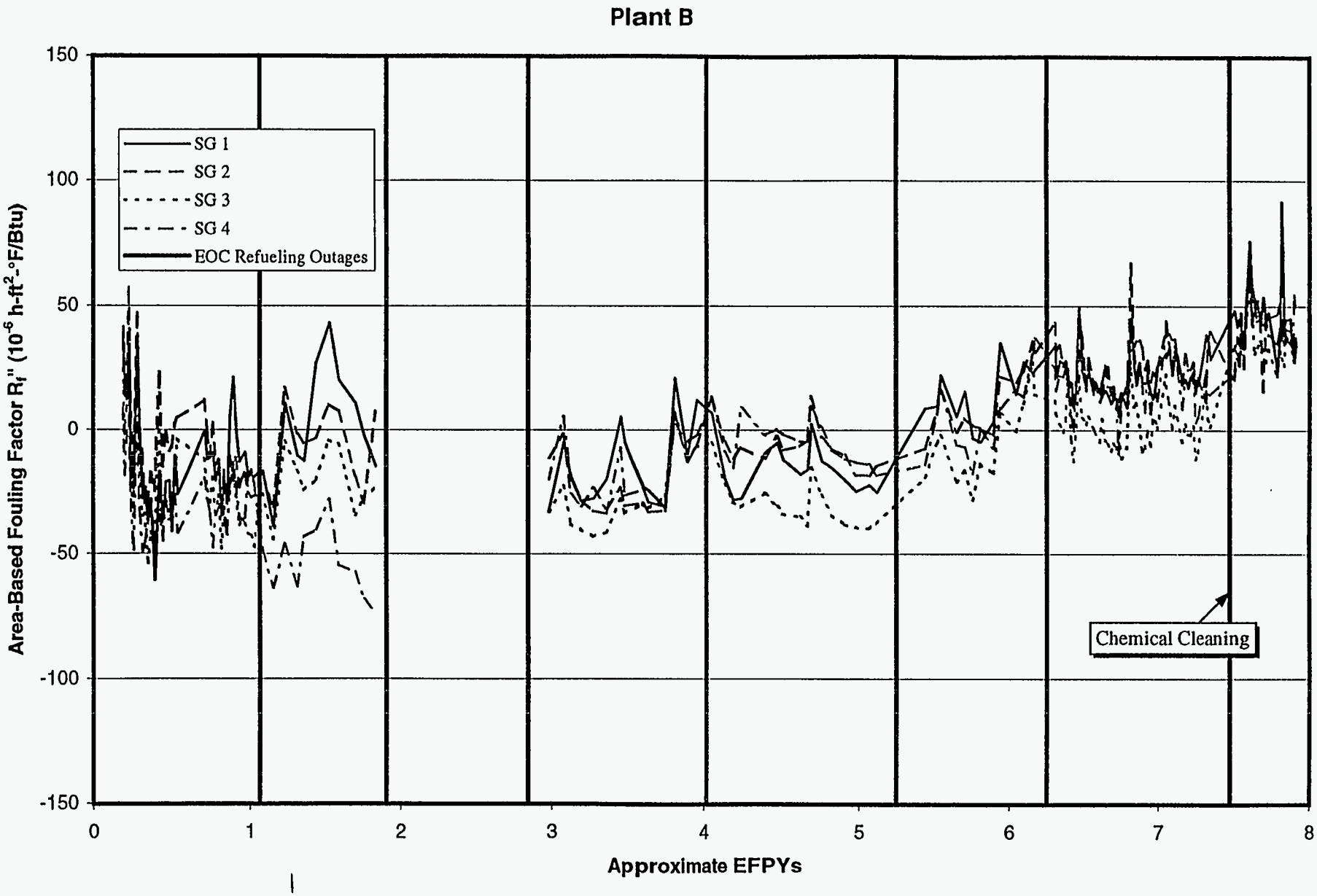

Figure C-B4. Historical Fouling Factor at Plant B (Using Feedwater Flow and Corrected T_{hot})

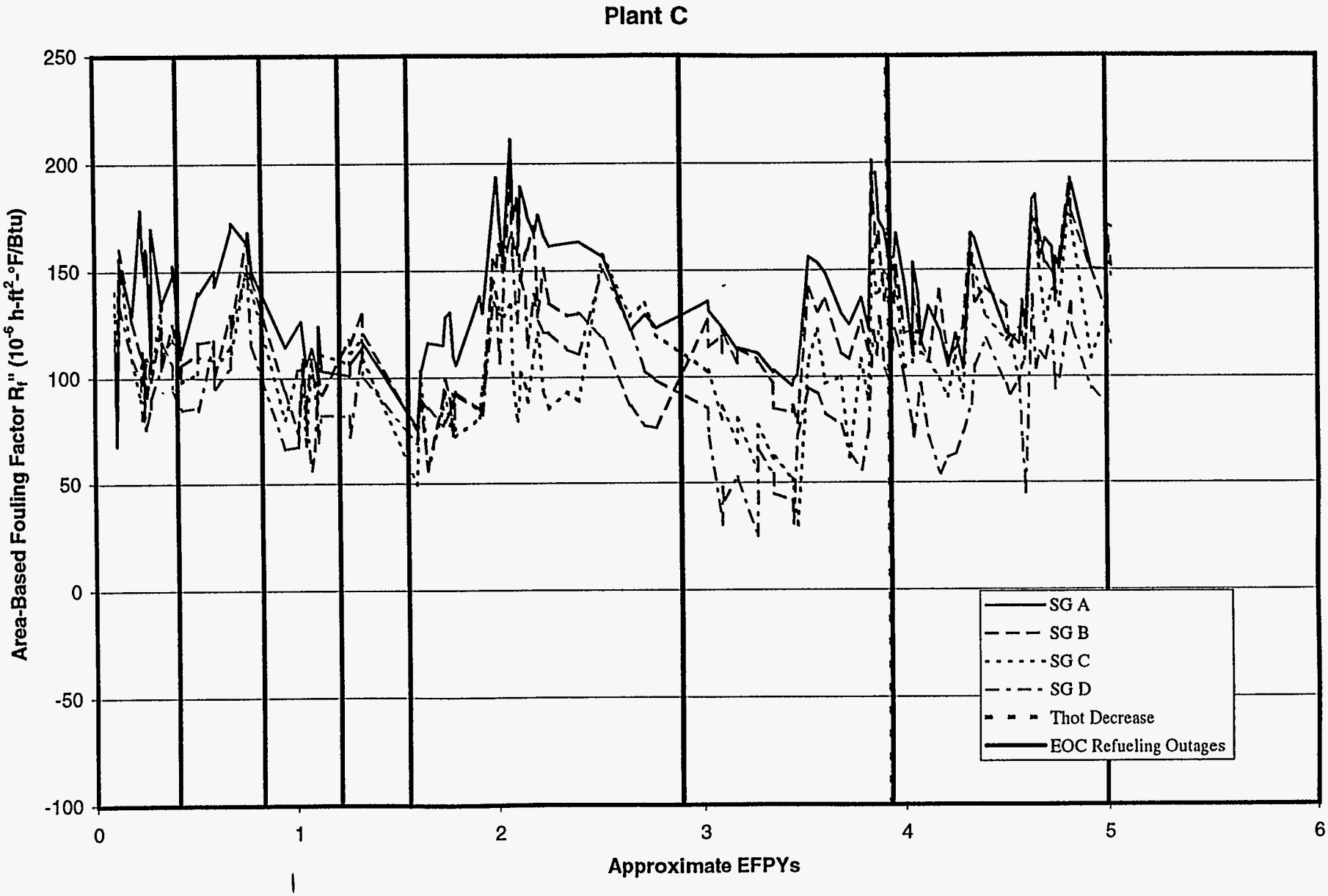

Figure C-C1. Historical Fouling Factor at Plant C (Using Feedwater Flow Measurements)

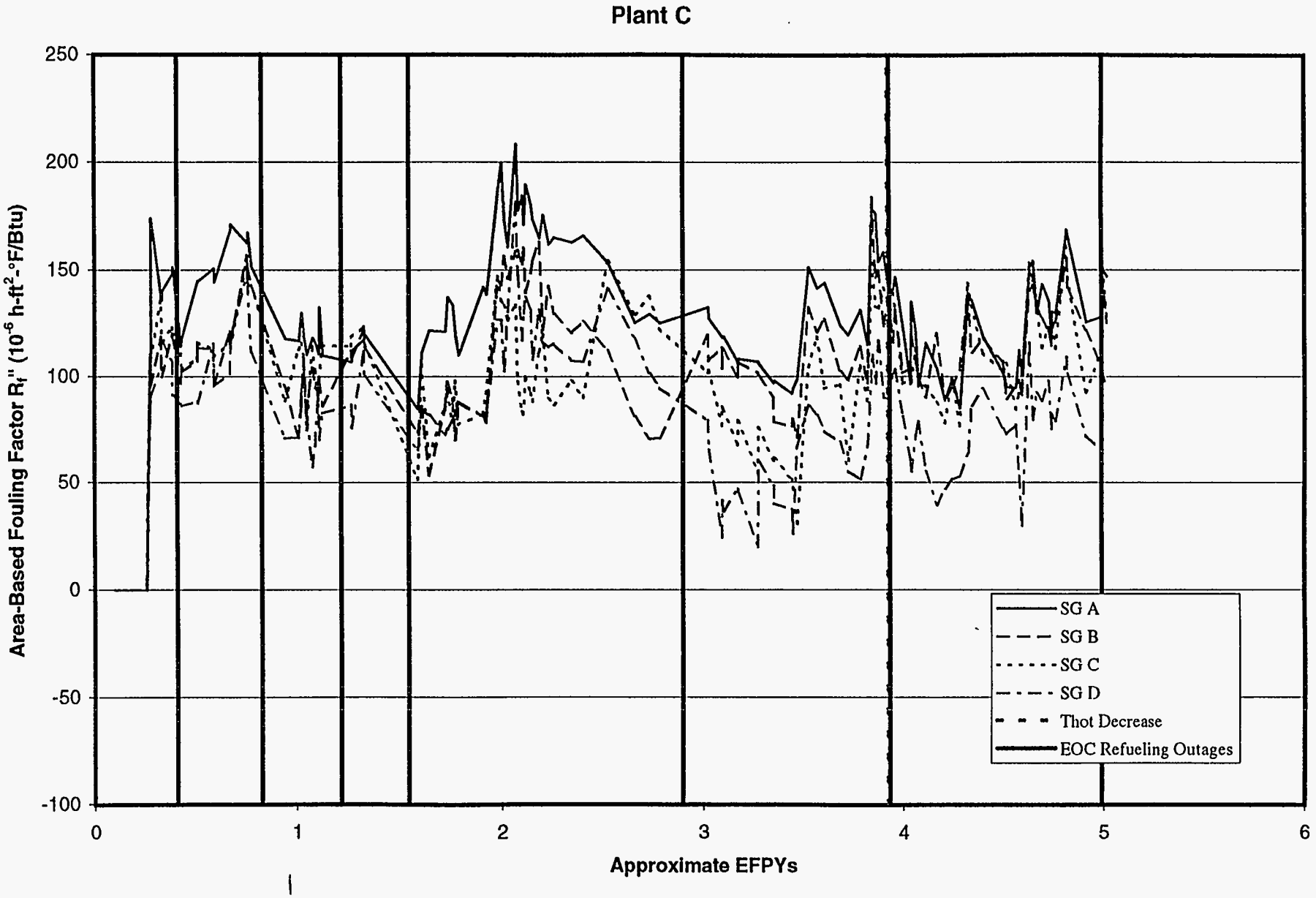

Figure C-C2. Historical Fouling Factor at Plant C (Using Steam Flow Measurements)

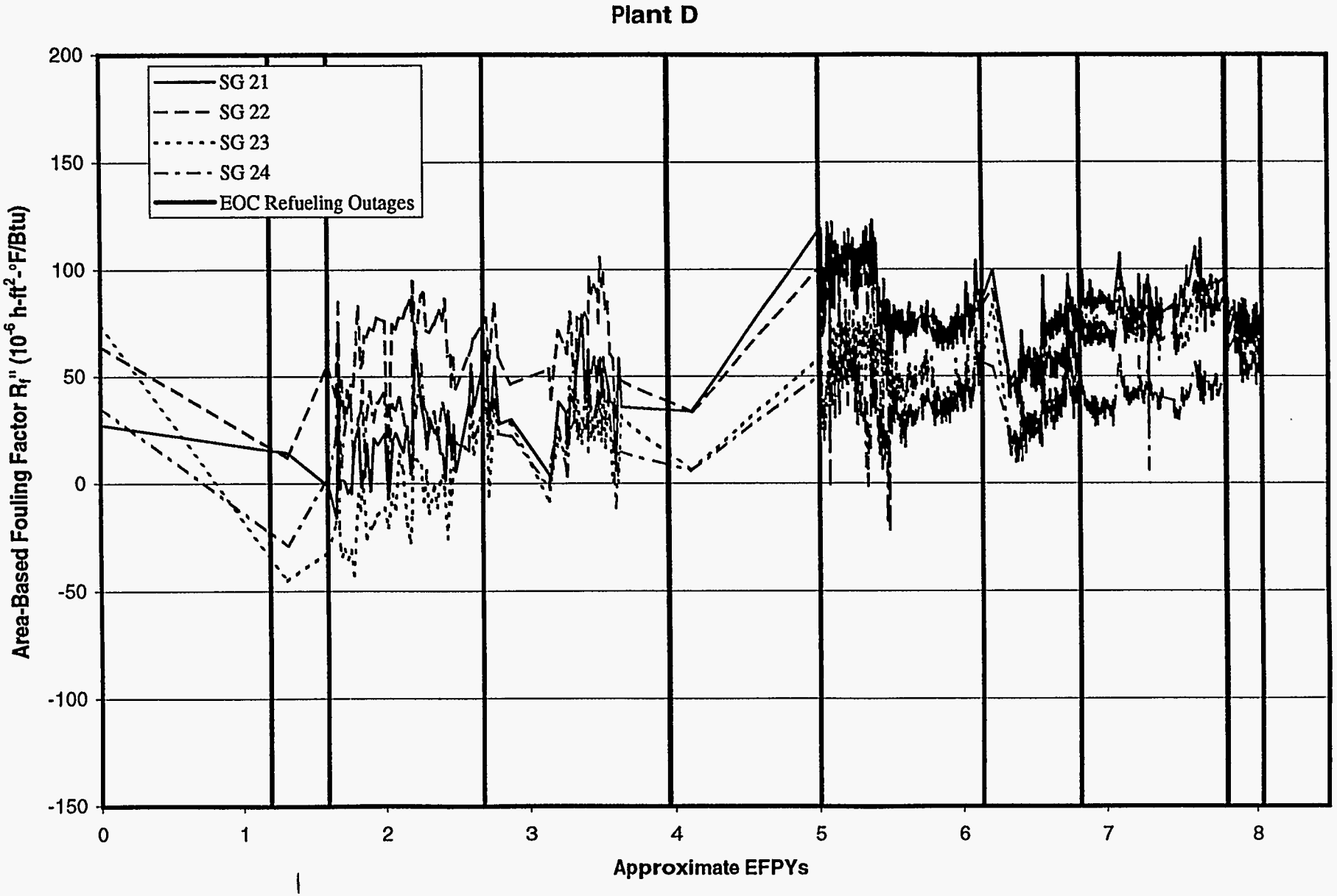

Figure C-D1. Historical Fouling Factor at Plant D
(Using Feedwater Flow Measurements)

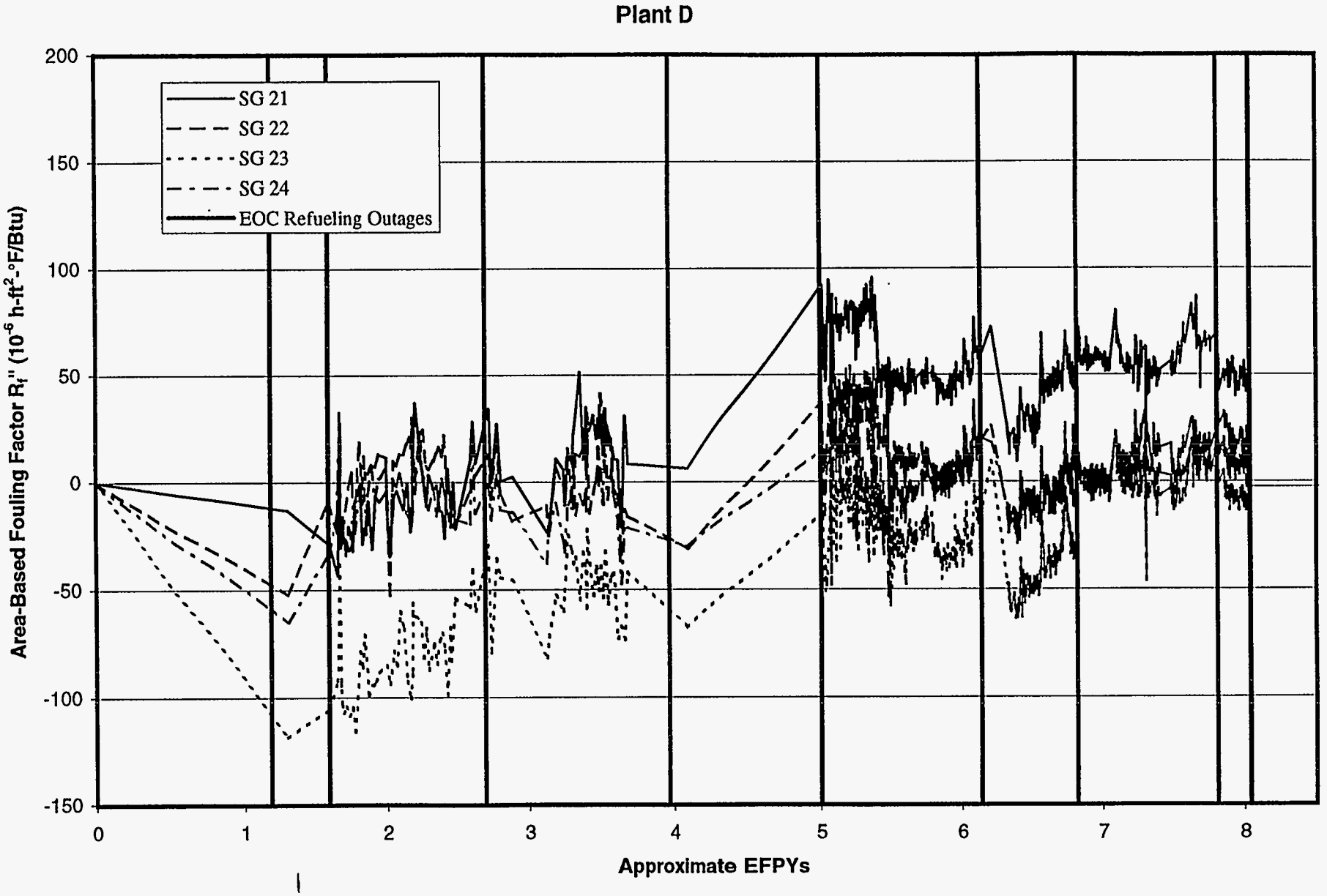

Figure C-D2. Historical Fouling Factor at Plant D (Relative to Initial Performance)

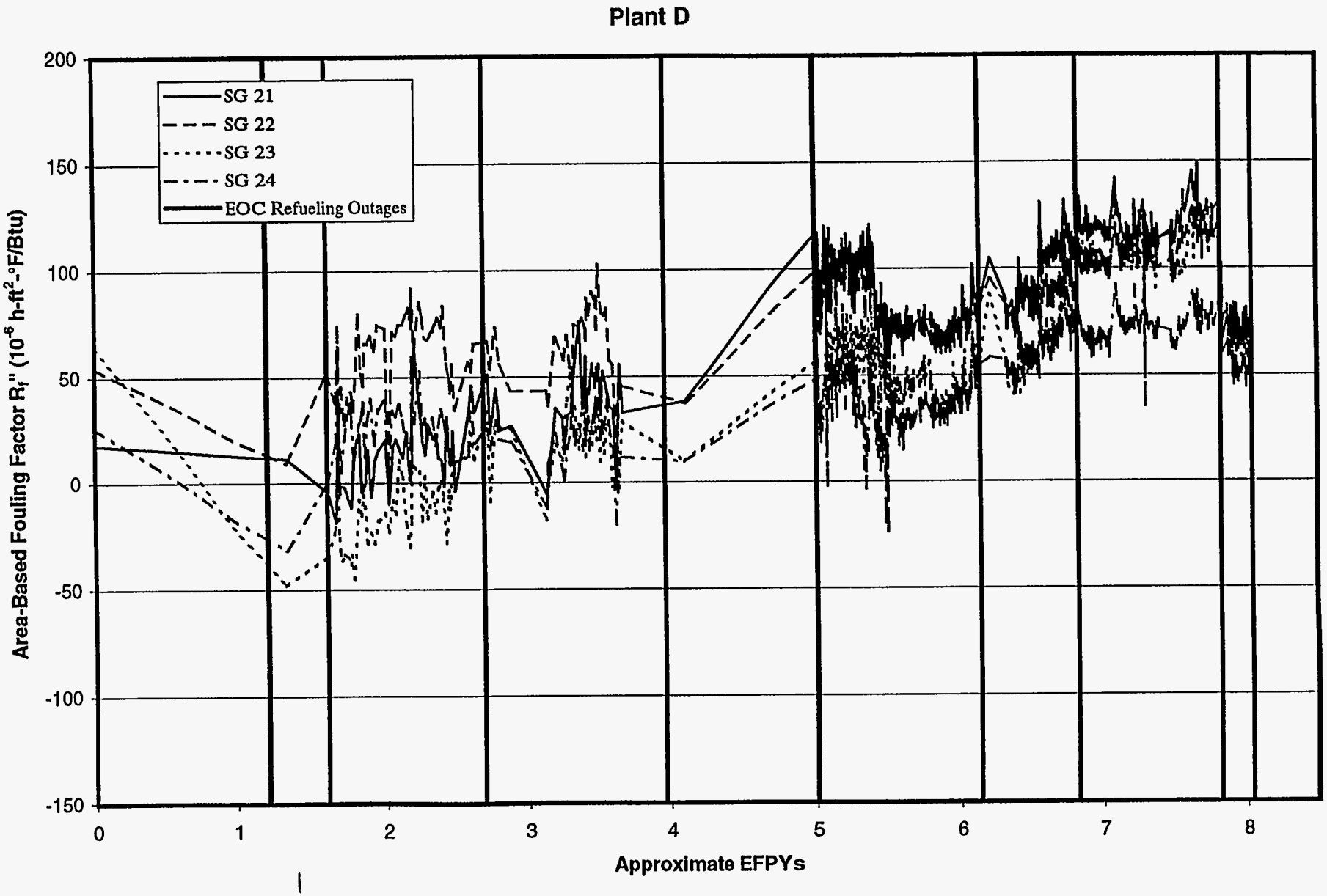

Figure C-D3. Historical Fouling Factor at Plant D (Using Plant-D Power)

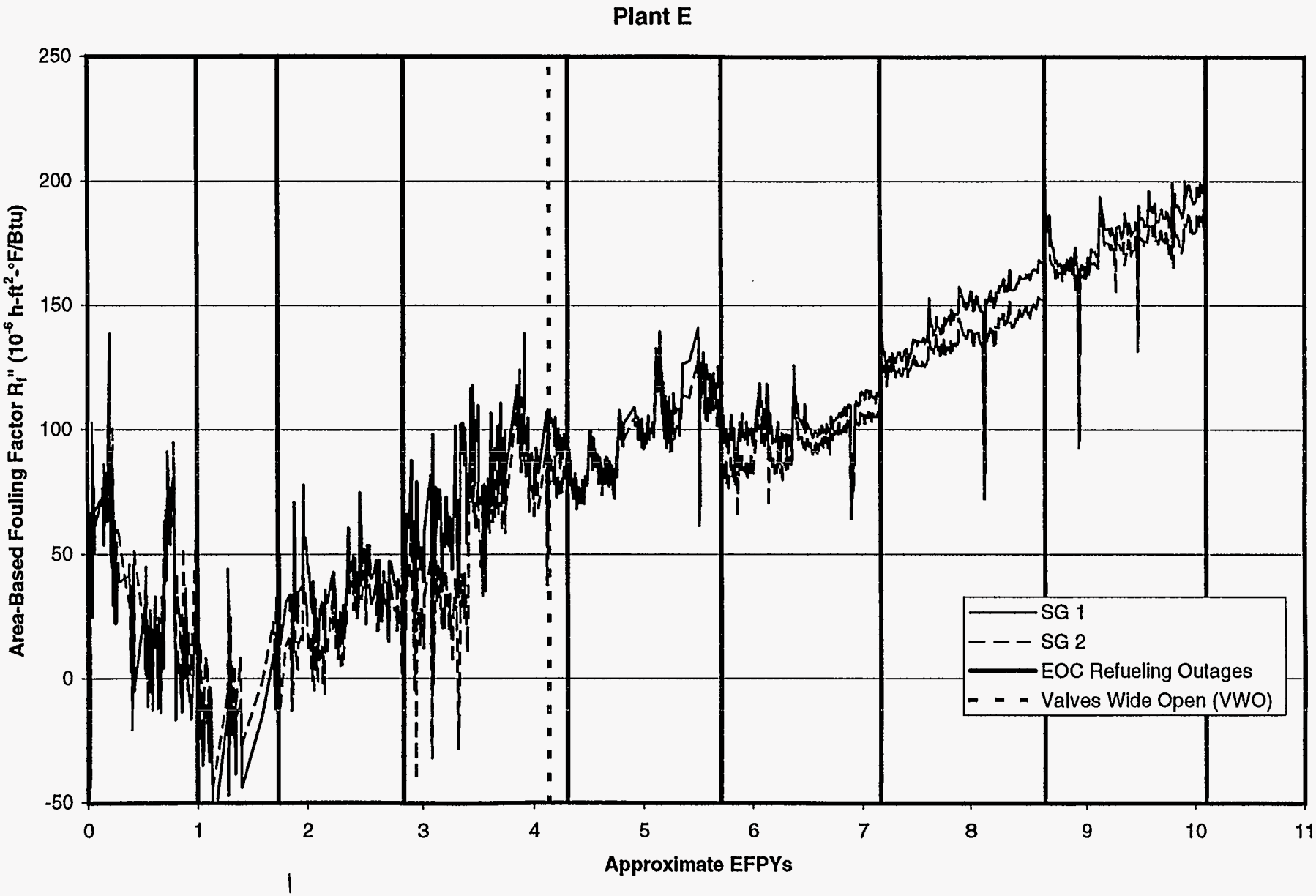

Figure C-E1. Historical Fouling Factor at Plant E (Using FW Flow Measurements)

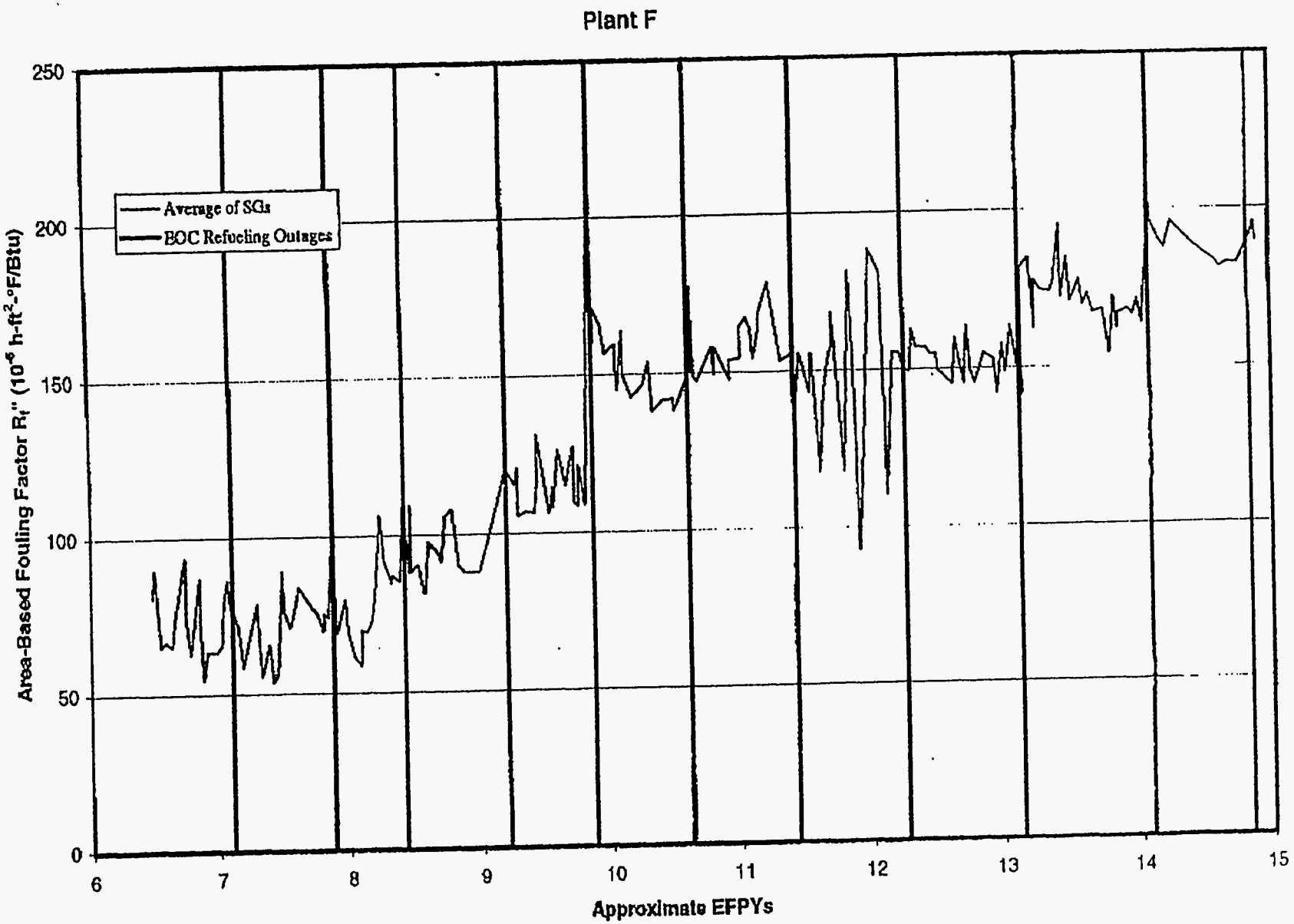

Figure C-F1. Historical Fouling Factor at Plant F

APPENDIX D

CAUSES OF PRESSURE LOSS FOR SGS AT FIVE US PLANTS – DETAILED EVALUATIONS

As discussed in Section V, the fouling factor methodology adjusts for changes in primary temperatures, thermal power, and heat-transfer area (e.g., plugged tubes). However, other possible causes of SG pressure loss must be evaluated before any calculated level of fouling can be attributed to secondary deposits at a particular plant. These evaluations are detailed below.

Effects of Fouling Factor Variables on SG Steam Pressure

While the fouling factor does adjust for changes in T_{hot}, T_{cold}, A, and Q, such changes can nevertheless affect the SG pressure. The sensitivity of SG pressure to each of these variables may be examined in the context of the overall heat transfer equation, introduced in Section IV and repeated here for convenience:

$$Q = UA \frac{T_{hot} - T_{cold}}{\ln\left(\frac{T_{hot} - T_{sat}(p_{sat})}{T_{cold} - T_{sat}(p_{sat})}\right)} \qquad [D\text{-}1]$$

The equation also allows predicted fouling factors calculated with the methods described in the Section IV to be translated into predicted pressure losses. Because thermal power (Q), primary temperatures (T_{hot} and T_{cold}), and heat-transfer area (A) appear explicitly in Eq. [D-1], their individual effects on SG steam pressure can be calculated with the proper partial derivatives. This separation allows the effects of variations or errors in heat-transfer area, reactor thermal power, and primary control temperature (T_{ave} for Plants A through D and T_{cold} for Plant E) to be individually quantified.

Results of this sensitivity analysis are presented in Tables D-1 through D-5 for each of the plants examined in this study. Note that there are three separate cases analyzed: (1) design values, (2) values that reflect early operation, and (3) values that reflect recent operation.* Using the values for most recent operation, the pressure loss that can be attributed to each cause may be calculated using the following equation:

$$\Delta p_{sat} = \frac{\partial p_{sat}}{\partial X} \Delta X \qquad [D\text{-}2]$$

where X represents A, T_{ave}, or Q. (Note that this calculation is an approximation since the partial derivative is not constant during the pressure decrease. However, as is clear from Tables D-1 through D-5, the values do not vary widely.) The results of this calculation for each variable are shown in Table D-6 under the heading "Sources That are Accounted for by the Fouling Factor Calculation." Best-estimate, lower-bound, and upper-bound results are included for Plant A

* Early operation values are based on the first 2-4 months of operating data available. Recent operating values are based on the most recent 2-4 months of data.

(both just prior to chemical cleaning and afterwards), Plant B (also before and after chemical cleaning), and Plants C, D, and E. Noteworthy results in the lower part of Table D-6 include

- Tube plugging has played a relatively minor role in reducing steam pressure at Plant A (1.6 psi) and Plant C (1.5 psi). The effect at Plant B is more significant (3.6 psi before chemical cleaning and 6.9 psi afterwards), and the effect at Plants D and E is even more pronounced (9.6 and 11.7 psi, respectively).
- The effect on steam pressure of primary temperature variations is shown compared to the initial primary temperatures characteristic of early operation. Plant A has seen a modest decrease of 3.3 psi, Plant B almost no change, Plant C a decrease of 52 psi, Plant D a decrease of 6 psi, and Plant E an increase of 5 psi. It is clear that this factor must be accounted for when discussing the size of steam pressure losses, as its effects are potentially large.

  Note that one possible reason for pressure decreases over plant life is the development of temperature asymmetries among the primary loops. For plants that control the high auctioneer T_{ave} (the highest-temperature loop), such asymmetries can lower the average primary temperature relative to the desired value. Flow anomalies within the reactor have been known to cause these asymmetries: Plant A, for example, has documented this phenomenon.
- Thermal power levels below 100% have slightly increased steam pressure at all 5 plants. However, the effect is relatively small (4 psi or less).
- Plant A's power uprate of 4.5% in 1988 caused a 15-psi drop in steam pressure. This step change in pressure matches the observed pressure drop in Figure B-A1. The other plants in the study did not change the rated thermal power.

Effects of Other Major Variables

Other potential sources of SG pressure loss include the following categories:

SOURCES THAT AFFECT INITIAL PERFORMANCE VS. IDEAL DESIGN PERFORMANCE. These factors can cause a steam generator to perform more poorly than expected, but they cannot account for an observed pressure loss over life. They can, however, decrease the performance margin available for accommodating fouling and plugging. Included are the following:

1. Pre-service tube plugging.
2. Initial primary temperatures different from the design values.
3. Initial primary tube velocity different from the design value.
4. Variation in tube wall thickness from the nominal value.
5. Variation in tube material thermal conductivity from the nominal value.

The effects of the first two on steam pressure are calculated using Eq. [D-2]. The effect of changes in primary-side velocity is calculated using the Dittus-Boelter correlation for internal flow through circular pipes (see, for example, p. 394 of Reference (16)):

$$R'' = \frac{1}{h} = \frac{1}{\frac{k}{d_i}\left(0.023 Re^{0.8} Pr^{0.3}\right)} \qquad [D\text{-}3]$$

where *Re* is the Reynolds number and *Pr* is the Prandtl number. Note that the calculations compare the resistance corresponding to the design value of primary flow rate with the resistances corresponding to a range of flow rates calculated from measured values of T_{hot}, T_{cold}, and thermal power.

The effects of wall thickness and material thermal conductivity variations are computed using the expression for thermal resistance through a cylindrical wall:

$$R'' = \frac{d_o}{2k} \ln\left(\frac{d_o}{d_i}\right) \qquad [D\text{-}4]$$

The change in this resistance is calculated for wall thicknesses of ±10% relative to the nominal thickness and for thermal conductivities of ±5% relative to the nominal value.

The effect of each of these causes is listed in the appropriately titled section of Table D-6 for each plant. In each case, pre-service plugging had a negligible effect on steam pressure. Initial primary temperatures, on the other hand, varied significantly from the originally specified design values. Plants A and B started up with T_{ave}'s that decreased the steam pressure about 9 psi and 7 psi, respectively, relative to what it would have been at the design temperatures. In contrast, Plant C experienced an initial steam pressure *increase* of about 14 psi due to an above-design T_{ave} during early operation.* Plant D exhibited an initial drop of 54 psi versus the design pressure; however, this is almost entirely because the utility chose to operate the plant at a nominal hot-leg temperature 8°F below the original design value. Plant E showed a modest initial increase of 2 psi versus the design pressure. Best-estimate predictions of steam pressure changes due to primary velocity differences from the design value range from -1 psi up to +4 psi (i.e., a relatively minor effect). No dimensional or material information was available to indicate that the tube wall thickness or conductivity deviated from nominal values; hence, the best-estimate changes in pressure due to these causes is zero for all plants. However, the bounding calculations shown in Table D-6 reveal that a wall thickness variation of 10% can cause steam pressure to be 9 psi to 16 psi lower (or higher) than design. Similarly, a 5% thermal conductivity variation can induce a 4 psi to 8 psi change in steam pressure.

SOURCES THAT ARE DUE TO DEPOSITS WITHIN THE TUBE BUNDLE. Such deposits may be primary or secondary in nature. Losses due to primary deposits are discussed in Appendix E. Best estimates of the fouling factors (and associated SG steam pressure losses) due to secondary deposits are discussed in Section III (see Table III-9). The results are summarized in Table D-6 under the above-titled heading. From these two tables, it is clear that only Plants E and F are believed to have highly resistant tube scale.

---

* It is important to note that the higher T_{ave} for Plant C reflected a higher-than-design thermal resistance of the Plant-C SGs. Although the initial T_{hot} was about equal to the design value, T_{cold} was about 3°F higher than design, suggesting that the SGs were less effective at removing heat than the design values would indicate.

SOURCES THAT ARE NOT DUE TO DEPOSITS WITHIN THE BUNDLE WHICH ARE CAPTURED BY THE FOULING FACTOR CALCULATION. These sources of pressure loss can also be expected to result in uncertainty in the fouling factor calculation. They include the following, all of which are summarized in Table D-6 under the above heading.

1. Uncertainty in SG pressure measurements. As indicated in Table C-1 this tolerance is estimated to be about ±5 to ±8 psi for each plant. This uncertainty is usually difficult to evaluate accurately because the maximum allowable tolerance on steam pressure measurement can be significantly larger than the actual tolerance achieved by the plant. However, these estimates are believed to be reasonably close to the actual uncertainties.
2. Additional pressure drop across the dryers and moisture separators (i.e., above the design value). Although this cause does not reflect fouling of the tube bundle, it nevertheless causes lower-than-expected pressure at the HP turbines. Tests at Plant A in February 1996 indicated that this pressure drop was about 4 psi larger than the design value. Plant B tracks the pressure drop between the top of the bundle and the main steam measurement location; this measurement has shown little net change since 1991, suggesting that the moisture separators are not actively fouling. Plant C did not report any information on this subject while Plant D indicated that no such measurements have been performed. Plant E has performed visual inspections of the moisture separators, observing a noticeable degree of fouling. Based on this observation and the Plant A measurements, Plant E is estimated to have 4 psi of added pressure drop due to this cause.*
3. Error in applied primary temperature. This can be caused by at least three separate problems:
   - T_{ave} Measurement Error. As with steam pressure measurement, determining the actual tolerances achieved by each plant (as opposed to the allowable limits) is difficult. The best estimates for each tolerance were reported in Table C-1, and the resulting calculated effect on steam pressure is shown in the upper- and lower-bound columns of Table D-6. These values range from 5 psi to 22 psi.
   - Hot-Leg Streaming. Reported calculations by one NSSS vendor indicate that a pressure loss of 10 psi is possible due to streaming. This phenomenon is caused by a nonuniform temperature through the pipe cross section where hot-leg temperature is measured. If the measured temperature is significantly higher than the bulk fluid temperature (e.g., even 0.5°F), then T_{ave} can be incorrectly decreased. Plants which control the average primary temperature (T_{ave}) rather than T_{cold} are potentially susceptible to this phenomenon. (Plants A through D control T_{ave}, while Plant E controls T_{cold}.) Another risk factor is the usage of low-neutron-leakage arrangements of fuel assemblies in the reactor core. Often the result is less thermal mixing, increasing the chance that the RTDs used to measure T_{hot} will be in error. Related is the distance of the RTDs from the reactor outlet; the smaller this distance, the poorer the mixing and the larger the potential effect of hot-leg streaming.

     In order to understand the effect of hot-leg streaming on primary temperature, consider Table D-7. When no streaming is taking place, the actual temperatures match the

* Note that another US utility has recently observed severe fouling of the moisture separators at one of its plants possessing Combustion Engineering Model 67 SGs. The estimated pressure recovery following a cleaning of these separators (13 psi) is considered to be a reasonable upper bound on the expected pressure loss due to separator fouling at a typical plant.

measurements (top line of each part of the table). Now suppose the hot-leg RTDs measure temperatures which average 4° greater than the actual temperature. This situation is reflected by the middle lines in Table D-7. Now the plant computer attempts to restore T_{ave} to the desired value by decreasing T_{hot} and T_{cold} by 2° (bottom lines in Table D-7). It is clear from the table that a hot-leg streaming effect of a certain magnitude (e.g., 4°) causes the reported T_{hot} and T_{cold} values to diverge by half that amount (i.e., T_{hot} increases by 2° and T_{cold} decreases by 2°). Meanwhile, the actual primary temperatures in this situation both decrease by 2°, or half the amount of the original streaming error. The potential effects of hot-leg streaming are explored for each plant below.

Plant A: Hot-leg streaming at Plant A during recent operation has been documented by the utility. Through the use of a reverse calorimetric procedure to back calculate hot-leg temperature, the error associated with hot-leg streaming was calculated to be 0.91°F at the beginning of Cycle 7 and 1.01°F at the beginning of Cycle 8. The average of these two values (0.96°F) is used in Table D-6 to calculate a corresponding best-estimate pressure loss of about 4 psi.

Plant B: According to the utility, the reactor core was modified to reduce neutron leakage at Plant B beginning in 1990. Examination of Figure B-B2 (parts a through d) indicates that the hot-leg and cold-leg temperatures begin to diverge at least as early as Cycle 6 (1992). Analysis of these values reveals that the measured T_{hot} increased about 2°F compared to initial operation while T_{cold} decreased by almost the same amount. The effect of this error on steam pressure is indicated in Table D-6; the best estimate is a 15 psi decrease.

Plant C: Like Plant B, Plant C has also attempted to minimize neutron leakage during the last few operating cycles by rearranging fuel in order to place lower-reactivity assemblies at the periphery of the reactor, a practice which increases the potential for significant hot-leg streaming effects. No definitive data or analyses have been provided by the utility regarding hot-leg streaming. However, the utility did report that RTD readings on a single pipe have varied as much as 7-8°F, indicating that streaming is taking place. In addition, calculated primary flow rates (which are based on primary temperature readings) have decreased substantially although no significant decrease was expected. These two signs suggest that hot-leg streaming is taking place. The current best estimate, reflected in Table D-6, is 3°F of streaming, which would lower steam pressure by about 13 psi.

Note that the primary temperatures at Plant C were intentionally lowered 4°F beginning in Cycle 6, and subsequently fell by another 1 to 1.5°F, most likely due to temperature asymmetry among the four loops. These temperature changes are unrelated to hot-leg streaming occurring within the pipe cross sections.

Plant D: Although Plant D did change fuel type as part of an effort to reduce neutron leakage during the EOC 5 outage, the evidence suggests that hot-leg streaming is not having a significant effect on Plant D. Specifically,

- Although the SG steam pressure decreased about 10-15 psi between the end of Cycle 4 and the beginning of Cycle 6, about 7 psi was lost due to plugging of Row 1 U-bend tubes during the EOC 4 refueling outage. The remaining loss (3 to 8 psi)

could be due to a number of other factors, including increased tube scale thermal resistance.

- Plant D's sister station also instituted the same low-leakage modifications as Plant D without observing any significant impact on steam pressure.
- Plant D primary temperatures do not show the divergence characteristic of hot-leg streaming (see Table D-7). In fact, the primary temperature history suggests a slight *increase* in steam pressure due to hot-leg streaming.

Plant E: Plant E controls T_{cold} rather than T_{ave} and is thus not susceptible to hot-leg streaming.

General Conclusions: Accurate quantitative estimates of hot-leg streaming require one or more of the following: a) detailed measurements of the temperature profile through the hot-leg pipe cross sections, b) a primary-side calorimetric enthalpy balance calculation to check for consistency in the temperature measurements (as was performed by Plant A), or c) more accurate temperature instrumentation not subject to streaming (e.g., ultrasonic techniques—see Reference (15) for further details on a specific application at one US plant). It may also be possible to analytically calculate the magnitude of hot-leg streaming by modeling the nuclear thermal hydraulics in the reactor and its outlet piping.

– Divider Plate Leakage. Leaks from the hot to the cold side of the primary channel head can cause three distinct effects that can lead to pressure loss: a) an inaccurate reading of the actual cold-leg temperature leaving the SG bundle, b) lower primary-side mass flow rate through the tube bundle and hence a lower primary-side velocity, which increases the primary boundary-layer thermal resistance, and c) an actual T_{cold} decrease due to the smaller primary mass flow rate through the tube bundle. All of these effects tend to cause the SG pressure to decrease. Note, however, that this problem has been primarily associated with the bolted connections typical of the CANDU SG design.

None of the plants involved in this study reported any knowledge of this phenomenon, and it is considered very unlikely that a significant leak could develop through the welded divider plates in US PWR SGs.* As a result, it is postulated that the induced primary temperature error is equal to an undetectable 10^{-4} times the primary temperature difference. As indicated in Table D-6, the effect on steam pressure is nearly zero. The upper-bound values (about 2 psi) are based on a 1% error in primary temperature difference caused by divider plate leakage.

Effects of Minor Contributors

Degradation of steam generator pressure could potentially be due in part to performance degradation of secondary cycle equipment, such as turbines, condensers, moisture separator reheaters, and feedwater heaters. The potential effect of changes in the secondary cycle can be empirically evaluated through the observed changes in feedwater temperature. Examining Figures B-A5, B-B6, B-C5, B-D5, and B-E5, we note that feedwater temperature at Plants A and

* Note that leakage is possible through threaded fastener holes, tongue-in-groove joints, or other breaches in the divider plate.

E has varied by up to 20°F, while Plants B, C, and D have seen smaller changes (10°F, 5°F, and 5°F, respectively). The steam pressure losses attributed to this cause for Plants A and E in Table D-6 were evaluated using a preliminary one-dimensional model of the SG based on the Dittus-Boelter correlation for single-phase cooling of the primary coolant and modified forms of the Chen correlation for subcooled and saturated forced convection boiling in the tube bundle. The values for Plants B, C, and D are estimates based on the results for Plants A and E and engineering judgment.

A second mechanism through which the secondary cycle performance may affect the steam generator pressure is the turbine back-pressure. This mechanism can only be active once steam generator pressure control is lost (i.e., the plant is operating in the VWO condition). When the turbine throttle valves are being actively controlled, variations in the turbine back-pressure are essentially canceled out. This is the case for Plants B, C, and D. However, at Plant A the throttle valves have been wide open since the beginning of Cycle 5, and Plant E operated in the VWO condition between late in Cycle 4 and the recent chemical cleaning.

Figure D-1 illustrates graphically how changes in the secondary cycle and SG fouling affect thermal power and SG pressure once the turbine throttle valves are wide open. The figure is based on data from a sister station of Plant E's and is to scale. The flatter line represents the overall heat-transfer equation [IV-4] at a given value of T_{cold} (since the plant is T_{cold}-controlled). The steeper line represents the approximate proportionality of thermal power and high-pressure turbine inlet pressure. For a constant turbine speed, which means a smaller mass flow rate approximately in proportion to any steam pressure decreases, this relationship is essentially a straight line as shown. As indicated on the figure, the plant will operate at the intersection of these two curves once the throttle valves are wide open. For decreases in primary temperature or SG fouling, the flatter curve moves down, lowering both pressure and thermal power. On the other hand, changes in the secondary cycle (e.g., changes in moisture carryover) can move the steeper curve in either direction as indicated on the figure. In one case, SG pressure is raised slightly but thermal power decreases. In the other case (e.g., remedial opening of the HP turbine inlet throat), SG pressure decreases slightly but thermal power and electrical output increase.

Summary of Pressure Losses

Using the results in Table D-6, Table D-8 summarizes the best-estimate pressure losses (relative to the initial performance) due to each postulated cause for the plants in this study, including Plant F. The most important conclusion apparent from this table is that the observed pressure

loss does not necessarily correlate well with secondary fouling. Plant A's pressure loss can largely be attributed to the 1988 power uprate. The loss at Plant B, meanwhile, is caused mainly by tube plugging and hot-leg streaming (22 of 36 psi). The remainder is due to other causes (perhaps including deposits that are more thermally resistive than would be consistent with total removal of secondary deposits during the 1995 chemical cleaning). Plant C has seen a pressure drop in excess of 60 psi, but this is mainly the result of reduced primary temperatures. The pressure loss at Plant D appears to be the result of a number of causes, potentially including a contribution from secondary tube scale. Plant E, on the other hand, is the only plant with for which secondary deposits are believed to be causing a major pressure loss. The 61-psi pressure recovery following the Plant-E chemical cleaning in 1996 supports this conclusion.

Thermal Power Degradation

Although steam pressure loss is one symptom of performance degradation, it should also be noted that thermal power can degrade, leading to the same loss in electrical power generation that can be caused by SG steam pressure loss. For the secondary system to properly do its job, it must receive sufficient steam pressure and the full level of thermal power input. Potential sources of thermal power loss include the following, each of which is evaluated in Table D-6 with regard to the pressure gain (or loss) that would accompany a thermal power decrease (or increase).

1. Feedwater Flow Measurement Error. This can be caused either by inaccuracies inherent in the measurement device, or a by a systematic error such as venturi fouling. Venturi meters are typically used to measure feedwater flow rate. They do so by measuring the pressure drop across a known geometry, which is subsequently converted to an average flow rate based on the geometry of the meter. If a layer of corrosion products accumulates on the surface of the venturi, then less flow will be passing through the meter for a given velocity, meaning that the meter measurement will be higher than the actual flow rate.* The result is an actual thermal-power level below the "measured" level based on a secondary calorimetric calculation.

   Plant A probably experienced significant venturi fouling during early cycles, as is evident from the mismatch between measured steam flow and calculated steam flow based on feedwater flow measurements (Figure B-A4b). However, during the last two cycles, feedwater and steam flow measurements agree closely, indicating that venturi fouling is minimal. As a consequence, the best-estimate for feedwater flow error in Table D-6 is zero. The upper-bound estimate incorporates a 0.5% venturi fouling error, plus the measurement uncertainty indicated in Table C-1.

   Plant B has also reported venturi fouling of up to 1%. However, recent operation (since 1992) is believed to reflect a total tolerance of ±0.5%, in large part because the venturis

* It is also possible for the meter to underreport the actual flow rate. This can happen if the venturi is calibrated while it is fouled, and then subsequently cleaned without being re-calibrated.

are cleaned during each refueling outage. As a result, the best-estimate for this error is zero, while the upper-bound estimate includes a 0.5% venturi fouling error (like Plant A).

Plant C has not reported any venturi fouling. Although Figure B-C4b shows a rather large systematic disagreement between feedwater and steam flow rates of 2-3% during the last cycle, the direction of the discrepancy is opposite of that expected for venturi fouling. Without further clarification, the same assumption is used as for Plants A and B (i.e., zero best-estimate error and 0.5% venturi fouling in the upper-bound case).

Plant D did not report significant venturi fouling. However, during Cycles 6 through 8, venturi bypass flow of approximately 4.5% caused the measured rate to be lower than the actual rate. See Appendix B for further details.

2. Feedwater temperature variations from the design value.
3. Outlet steam quality variations from the design value.
4. Blowdown flow rate variations from the design value.

The effects of the last three items are minor (less than 1 psi) as shown in Table D-6.

Table D-1. Sensitivity of Plant A Steam Generator Pressure to Other Parameters in Overall Heat Transfer Equation

Quantity	Description	Units	Design VWO	Early Operation	Recent Operation (Cycle 8)
nominal values of parameters in overall heat transfer coefficient equation (inputs)					
T_{hot}	hot leg temperature	°F	620.0	616.8	616.9
T_{cold}	cold leg temperature	°F	557.0	557.4	557.8
p_{sat}	steam generator dome pressure	psia	1000.0	974.7	986.1
A	total outside-tube surface area	ft^2	55,000	54,939	54,558
N_{tot}	total number tubes	--	5626	5620	5581
Q	steam generator thermal power	MWt	895	835	883
nominal values of parameters in overall heat transfer coefficient equation (calculated)					
p_{bundle}	mid-bundle pressure	psia	1011.5	986.2	997.6
T_{sat}	bundle saturation temperature	°F	545.97	542.90	544.30
Q	steam generator thermal power	Btu/h	3.053E+09	2.850E+09	3.013E+09
ΔT_{lm}	log-mean temperature difference	°F	33.09	36.54	35.16
R	global resistance to heat transfer	h-°F/Btu	1.084E-08	1.282E-08	1.167E-08
U	global heat transfer coefficient	Btu/h-ft^2-°F	1678	1420	1571
R"	global area-based resistance	10^{-6} h-ft^2-°F/Btu	596.0	704.4	636.6
calculation of dp_{sat}/dT_{sat} using Clapeyron relation: $dp_{sat}/dT_{sat} = h_{fg}/(Tv_{fg})$					
h_f	saturated liquid specific enthalpy	Btu/lb	544.3	540.4	542.2
h_g	saturated vapor specific enthalpy	Btu/lb	1192.5	1193.5	1193.0
h_{fg}	latent heat of vaporization at p_{sat}	Btu/lb	648.2	653.0	650.8
T	absolute bundle saturation temp.	°R	1005.6	1002.6	1004.0
v_f	saturated liquid specific volume	ft^3/lb	0.0216	0.0215	0.0216
v_g	saturated vapor specific volume	ft^3/lb	0.4404	0.4531	0.4473
v_{fg}	specific volume change upon vap.	ft^3/lb	0.4188	0.4315	0.4257
$\partial p_{sat}/\partial T_{sat}$	partial deriv. of sat. press. with T	psi/°F	8.32	8.16	8.23
partial derivatives of steam generator pressure					
effect of variations in reactor coolant loop temperature					
$\partial p_{sat}/\partial T_{cold/ave}$	partial deriv. wrt RCL temperature	psi/°F	8.32	8.16	8.23
effect of tube plugging					
$\partial p_{sat}/\partial A$	partial deriv. wrt heated area	psi/ft^2	0.00373	0.00437	0.00421
$\partial p_{sat}/\partial N_{plug}$	partial deriv. wrt no. tubes plugged	psi/tube plugged	-0.036	-0.043	-0.041
$\partial p_{sat}/\partial \%_{plug}$	partial deriv. wrt % tubes plugged	psi/1% plugged	-2.05	-2.40	-2.30
effect of variations in steam generator thermal power					
$\partial p_{sat}/\partial Q$	partial deriv. wrt thermal power	psi/(Btu/h)	-1.16E-07	-1.27E-07	-1.18E-07—
$\partial p_{sat}/\partial Q$	partial deriv. wrt thermal power	psi/MWt	-0.395	-0.432	-0.401
effect of variations in overall heat transfer coefficient (fouling factor)					
$\partial p_{sat}/\partial U$	partial deriv. wrt overall HT coeff.	psi/(Btu/h-ft^2-°F)	0.122	0.169	0.146
$\partial p_{sat}/\partial R_f$"	partial deriv. wrt fouling factor	psi/(10^{-6} h-ft^2-°F/Btu)	-0.344	-0.341	-0.361

Table D-2. Sensitivity of Plant B Steam Generator Pressure to Other Parameters in Overall Heat Transfer Equation

Quantity	Description	Units	Design VWO	Early Operation	Recent Operation (Cycle 8)
nominal values of parameters in overall heat transfer coefficient equation (inputs)					
T_{hot}	hot leg temperature	°F	609.7	608.8	608.9
T_{cold}	cold leg temperature	°F	546.7	545.6	545.7
p_{sat}	steam generator dome pressure	psia	857	841	852
A	total outside-tube surface area	ft^2	51,500	51,500	50,197
N_{tot}	total number tubes	--	3388	3388	3302
Q	steam generator thermal power	MWt	856	838	852
nominal values of parameters in overall heat transfer coefficient equation (calculated)					
p_{bundle}	mid-bundle pressure	psia	865	849	860
T_{sat}	bundle saturation temperature	°F	527.27	525.09	526.60
Q	steam generator thermal power	Btu/h	2.920E+09	2.859E+09	2.908E+09
ΔT_{lm}	log-mean temperature difference	°F	43.60	44.92	43.24
R	global resistance to heat transfer	h-°F/Btu	1.493E-08	1.571E-08	1.487E-08
U	global heat transfer coefficient	Btu/h-ft^2-°F	1300	1236 (1)	1340
R"	global area-based resistance	10^{-6} h-ft^2-°F/Btu	769.0	809.2	746.3
calculation of dp_{sat}/dT_{sat} using Clapeyron relation: $dp_{sat}/dT_{sat} = h_{fg}/(Tv_{fg})$					
h_f	saturated liquid specific enthalpy	Btu/lb	520.9	518.2	520.1
h_g	saturated vapor specific enthalpy	Btu/lb	1197.4	1197.9	1197.6
h_{fg}	latent heat of vaporization at p_{sat}	Btu/lb	676.5	679.7	677.5
T	absolute bundle saturation temp.	°R	986.9	984.8	986.3
v_f	saturated liquid specific volume	ft^3/lb	0.0211	0.0210	0.0211
v_g	saturated vapor specific volume	ft^3/lb	0.5233	0.5340	0.5266
v_{fg}	specific volume change upon vap.	ft^3/lb	0.5022	0.5130	0.5055
$\partial p_{sat}/\partial T_{sat}$	partial deriv. of sat. press. with T	psi/°F	7.38	7.27	7.34
partial derivatives of steam generator pressure					
effect of variations in reactor coolant loop temperature					
$\partial p_{sat}/\partial T_{cold/ave}$	partial deriv. wrt RCL temperature	psi/°F	7.38	7.27	7.34
effect of tube plugging					
$\partial p_{sat}/\partial A$	partial deriv. wrt heated area	psi/ft^2	0.00526	0.00539	0.00531
$\partial p_{sat}/\partial N_{plug}$	partial deriv. wrt no. tubes plugged	psi/tube plugged	-0.080	-0.082	-0.081
$\partial p_{sat}/\partial \%_{plug}$	partial deriv. wrt % tubes plugged	psi/1% plugged	-2.71	-2.78	-2.66
effect of variations in steam generator thermal power					
$\partial p_{sat}/\partial Q$	partial deriv. wrt thermal power	psi/(Btu/h)	-1.29E-07	-1.32E-07	-1.28E-07
$\partial p_{sat}/\partial Q$	partial deriv. wrt thermal power	psi/MWt	-0.439	-0.452	-0.437
effect of variations in overall heat transfer coefficient (fouling factor)					
$\partial p_{sat}/\partial U$	partial deriv. wrt overall HT coeff.	psi/(Btu/h-ft^2-°F)	0.208	0.225	0.199
$\partial p_{sat}/\partial R_f$"	partial deriv. wrt fouling factor	psi/(10^{-6} h-ft^2-°F/Btu)	-0.352	-0.343	-0.357

NOTES

1. The corresponding heat-transfer coefficient calculated for clean conditions using design T/H values and the design heat-transfer margin is 1420.

Table D-3. *Sensitivity of Plant C Steam Generator Pressure to Other Parameters in Overall Heat Transfer Equation*

Quantity	Description	Units	Design VWO	Early Operation	Recent Operation (Cycle 6)
nominal values of parameters in overall heat transfer coefficient equation (inputs)					
T_{hot}	hot leg temperature	°F	626.1	626.5	620.7
T_{cold}	cold leg temperature	°F	559.7	562.5	556.3
p_{sat}	steam generator dome pressure	psia	1100	1115	1052
A	total outside-tube surface area	ft^2	68,000	67,951	67,441
N_{tot}	total number tubes	--	4864	4861	4824
Q	steam generator thermal power	MWt	954	950	954
nominal values of parameters in overall heat transfer coefficient equation (calculated)					
p_{bundle}	mid-bundle pressure	psia	1107	1122	1059
T_{sat}	bundle saturation temperature	°F	557.06	558.71	551.62
Q	steam generator thermal power	Btu/h	3.256E+09	3.241E+09	3.257E+09
ΔT_{lm}	log-mean temperature difference	°F	20.34	22.17	23.94
R	global resistance to heat transfer	h-°F/Btu	6.246E-09	6.840E-09	7.352E-09
U	global heat transfer coefficient	Btu/h-ft^2-°F	2354	2151 (1)	2017
R"	global area-based resistance	10^{-6} h-ft^2-°F/Btu	424.7	464.8	495.8
calculation of dp_{sat}/dT_{sat} using Clapeyron relation: $dp_{sat}/dT_{sat} = h_{fg}/(Tv_{fg})$					
h_f	saturated liquid specific enthalpy	Btu/lb	558.6	560.7	551.6
h_g	saturated vapor specific enthalpy	Btu/lb	1188.8	1188.2	1190.7
h_{fg}	latent heat of vaporization at p_{sat}	Btu/lb	630.3	627.5	639.2
T	absolute bundle saturation temp.	°R	1016.7	1018.4	1011.3
v_f	saturated liquid specific volume	ft^3/lb	0.0220	0.0220	0.0218
v_g	saturated vapor specific volume	ft^3/lb	0.3978	0.3918	0.4181
v_{fg}	specific volume change upon vap.	ft^3/lb	0.3758	0.3698	0.3963
$\partial p_{sat}/\partial T_{sat}$	partial deriv. of sat. press. with T	psi/°F	8.91	9.01	8.62
partial derivatives of steam generator pressure					
effect of variations in reactor coolant loop temperature					
$\partial p_{sat}/\partial T_{cold/ave}$	partial deriv. wrt RCL temperature	psi/°F	8.91	9.01	8.62
effect of tube plugging					
$\partial p_{sat}/\partial A$	partial deriv. wrt heated area	psi/ft^2	0.00117	0.00153	0.00173
$\partial p_{sat}/\partial N_{plug}$	partial deriv. wrt no. tubes plugged	psi/tube plugged	-0.016	-0.021	-0.024
$\partial p_{sat}/\partial \%_{plug}$	partial deriv. wrt % tubes plugged	psi/1% plugged	-0.80	-1.04	-1.17
effect of variations in steam generator thermal power					
$\partial p_{sat}/\partial Q$	partial deriv. wrt thermal power	psi/(Btu/h)	-9.81E-08	-9.94E-08	-9.76E-08
$\partial p_{sat}/\partial Q$	partial deriv. wrt thermal power	psi/MWt	-0.335	-0.339	-0.333
effect of variations in overall heat transfer coefficient (fouling factor)					
$\partial p_{sat}/\partial U$	partial deriv. wrt overall HT coeff.	psi/(Btu/h-ft^2-°F)	0.034	0.048	0.058
$\partial p_{sat}/\partial R_f$"	partial deriv. wrt fouling factor	psi/(10^{-6} h-ft^2-°F/Btu)	-0.188	-0.224	-0.235

NOTES

1. The corresponding heat-transfer coefficient calculated for clean conditions using design T/H values and the design heat-transfer margin is 2715.

Table D-4. Sensitivity of Plant D Steam Generator Pressure to Other Parameters in Overall Heat Transfer Equation

Quantity	Description	Units	Design VWO	Early Operation	Recent Operation (Cycle 9)
nominal values of parameters in overall heat transfer coefficient equation (inputs)					
T_{hot}	hot leg temperature	°F	610.8	601.8	600.4
T_{cold}	cold leg temperature	°F	544.7	538.1	537.6
p_{sat}	steam generator dome pressure	psia	815	811	780
A	total outside-tube surface area	ft^2	46,350	51,500	49,653
N_{tot}	total number tubes	--	3388	3388	3388
Q	steam generator thermal power	MWt	856	852	851
nominal values of parameters in overall heat transfer coefficient equation (calculated)					
p_{bundle}	mid-bundle pressure	psia	823.3	818.5	788.2
T_{sat}	bundle saturation temperature	°F	521.6	520.9	516.6
Q	steam generator thermal power	Btu/h	2.920E+09	2.908E+09	2.904E+09
ΔT_{lm}	log-mean temperature difference	°F	48.92	41.07	45.45
R	global resistance to heat transfer	h-°F/Btu	1.675E-08	1.412E-08	1.565E-08
U	global heat transfer coefficient	Btu/h-ft^2-°F	1288	1375	1287
R"	global area-based resistance	10^{-6} h-ft^2-°F/Btu	776.5	727.3	776.9
calculation of dp_{sat}/dT_{sat} using Clapeyron relation: $dp_{sat}/dT_{sat} = h_{fg}/(Tv_{fg})$					
h_f	saturated liquid specific enthalpy	Btu/lb	513.9	513.1	507.8
h_g	saturated vapor specific enthalpy	Btu/lb	1198.7	1198.8	1199.7
h_{fg}	latent heat of vaporization at p_{sat}	Btu/lb	684.8	685.8	691.9
T	absolute bundle saturation temp.	°R	981.3	980.6	976.2
v_f	saturated liquid specific volume	ft^3/lb	0.0210	0.0209	0.0208
v_g	saturated vapor specific volume	ft^3/lb	0.5520	0.5555	0.5784
v_{fg}	specific volume change upon vap.	ft^3/lb	0.5310	0.5345	0.5576
$\partial p_{sat}/\partial T_{sat}$	partial deriv. of sat. press. with T	psi/°F	7.10	7.07	6.87
partial derivatives of steam generator pressure					
effect of variations in reactor coolant loop temperature					
$\partial p_{sat}/\partial T_{cold/ave}$	partial deriv. wrt RCL temperature	psi/°F	7.10	7.07	6.87
effect of tube plugging					
$\partial p_{sat}/\partial A$	partial deriv. wrt heated area	psi/ft^2	0.00645	0.00463	0.00537
$\partial p_{sat}/\partial N_{plug}$	partial deriv. wrt no. tubes plugged	psi/tube plugged	-0.088	-0.070	-0.079
$\partial p_{sat}/\partial \%_{plug}$	partial deriv. wrt % tubes plugged	psi/1% plugged	-2.99	-2.39	-2.67
effect of variations in steam generator thermal power					
$\partial p_{sat}/\partial Q$	partial deriv. wrt thermal power	psi/(Btu/h)	-1.37E-07	-1.19E-07	-1.24E-07
$\partial p_{sat}/\partial Q$	partial deriv. wrt thermal power	psi/MWt	-0.466	-0.406	-0.423
effect of variations in overall heat transfer coefficient (fouling factor)					
$\partial p_{sat}/\partial U$	partial deriv. wrt overall HT coeff.	psi/(Btu/h-ft^2-°F)	0.232	0.173	0.207
$\partial p_{sat}/\partial R_f$"	partial deriv. wrt fouling factor	psi/(10^{-6} h-ft^2-°F/Btu)	-0.385	-0.328	-0.343

Table D-5. Sensitivity of Plant E Steam Generator Pressure to Other Parameters in Overall Heat Transfer Equation

Quantity	Description	Units	Design VWO	Early Operation	Recent Operation (Cycle 8)
nominal values of parameters in overall heat transfer coefficient equation (inputs)					
T_{hot}	hot leg temperature	°F	611.0	606.5	606.4
T_{cold}	cold leg temperature	°F	553.0	553.2	554.0
p_{sat}	steam generator dome pressure	psia	900.0	927.6	862.6
A	total outside-tube surface area	ft^2	104,130	103,597	99,876
N_{tot}	total number tubes	--	9350	9340	9004
Q	steam generator thermal power	MWt	1705	1692	1696
nominal values of parameters in overall heat transfer coefficient equation (calculated)					
p_{bundle}	mid-bundle pressure	psia	910.0	937.6	872.6
T_{sat}	bundle saturation temperature	°F	533.4	536.9	528.4
Q	steam generator thermal power	Btu/h	5.818E+09	5.773E+09	5.788E+09
ΔT_{lm}	log-mean temperature difference	°F	42.21	36.71	46.99
R	global resistance to heat transfer	h-°F/Btu	7.255E-09	6.359E-09	8.118E-09
U	global heat transfer coefficient	Btu/h-ft^2-°F	1324	1518	1233
R"	global area-based resistance	10^{-6} h-ft^2-°F/Btu	755.5	658.7	810.8
calculation of dp_{sat}/dT_{sat} using Clapeyron relation: $dp_{sat}/dT_{sat} = h_{fg}/(Tv_{fg})$					
h_f	saturated liquid specific enthalpy	Btu/lb	528.2	532.6	522.0
h_g	saturated vapor specific enthalpy	Btu/lb	1195.6	1194.6	1196.8
h_{fg}	latent heat of vaporization at p_{sat}	Btu/lb	667.4	662.0	674.8
T	absolute bundle saturation temp.	°R	993.0	996.6	988.1
v_f	saturated liquid specific volume	ft^3/lb	0.0213	0.0214	0.0211
v_g	saturated vapor specific volume	ft^3/lb	0.4951	0.4791	0.5183
v_{fg}	specific volume change upon vap.	ft^3/lb	0.4738	0.4578	0.4972
$\partial p_{sat}/\partial T_{sat}$	partial deriv. of sat. press. with T	psi/°F	7.67	7.84	7.42
partial derivatives of steam generator pressure					
effect of variations in reactor coolant loop temperature					
$\partial p_{sat}/\partial T_{cold/ave}$	partial deriv. wrt RCL temperature	psi/°F	7.67	7.84	7.42
effect of tube plugging					
$\partial p_{sat}/\partial A$	partial deriv. wrt heated area	psi/ft^2	0.00266	0.00234	0.00315
$\partial p_{sat}/\partial N_{plug}$	partial deriv. wrt no. tubes plugged	psi/tube plugged	-0.030	-0.026	-0.035
$\partial p_{sat}/\partial \%_{plug}$	partial deriv. wrt % tubes plugged	psi/1% plugged	-2.77	-2.42	-3.15
effect of variations in steam generator thermal power					
$\partial p_{sat}/\partial Q$	partial deriv. wrt thermal power	psi/(Btu/h)	-2.59E-08	-2.21E-08	-3.28E-08
$\partial p_{sat}/\partial Q$	partial deriv. wrt thermal power	psi/MWt	-0.088	-0.076	-0.112
effect of variations in overall heat transfer coefficient (fouling factor)					
$\partial p_{sat}/\partial U$	partial deriv. wrt overall HT coeff.	psi/(Btu/h-ft^2-°F)	0.209	0.160	0.255
$\partial p_{sat}/\partial R_f$"	partial deriv. wrt fouling factor	psi/(10^{-6} h-ft^2-°F/Btu)	-0.367	-0.368	-0.388

Table D-6. Sources of Steam Generator Pressure Degradation at Five US Plants

		Plant A Before Chem Clean			Plant A Now (1/96-4/96)			Plant B Before Chem Clean			Plant B Now (3/96-5/96)			Plant C Now (2/96-6/96)			Plant D Now (4/95-6/95)			Plant E Before Chem Clean		
Steam generator type		Westinghouse Model F						Westinghouse Model 51						W Model E2			W Model 51			CE Model 3410		
Current EFPYs		8.63			9.54			7.49			7.91			5.02			8.05			10.02		
Design plugging margin for heat transfer		0%						0%						0%			10%			10%		
Current plugging level		0.63%			0.80%			1.32%			2.53%			1.32%			5.21%			3.70% (EOC 8)		
Design fouling factor (10^{-6} h-ft^2-°F/Btu)		28 before uprate / 1 after			1			60						56			55 (at 10% plugged)			44 (at 10% plugged)		
Current fouling factor (10^{-6} h-ft^2-°F/Btu)		-28 ± 19			-5 ± 19 (1)			21 ± 24			42 ± 24 (1)			30 ± 46			51 ± 89			172 ± 48.		
Nominal design dome pressure (psia)		1000						857						1100			815			900		
Design start-up dome pressure (psia)		1009						878						1106			837			941		
Actual start-up dome pressure (psia)		1003						877						1115			811			933		
Current dome pressure (psia)		986			975			852			841			1052			780			855		
Current total pressure loss vs. Initial Perf. (psi)		17			28			25			36			63			30			77		
Calculated remaining heat transfer margin		-5%			-9%			5%			0%			-31%			-12%			-12%		
Deposit Fouling Factors from Local Heat Transfer Analyses (10^{-6} h-ft^2-°F/Btu)		Lower Bound	Best Estimate	Upper Bound	Lower Bound	Best Estimate	Upper Bound	Lower Bound	Best Estimate	Upper Bound	Lower Bound	Best Estimate	Upper Bound	Lower Bound	Best Estimate	Upper Bound	Lower Bound	Best Estimate	Upper Bound	Lower Bound	Best Estimate	Upper Bound
Secondary freespan deposits		-30.0	-15.0	0.0	2.4	9.7	29.1	-15.0	28.8	107.0	2.4	9.7	29.1	-15.0	0.0	5.0	-3.5	65.4	148.6	51.1	185.2	363.8
Secondary flow blockage and extra friction	lower recirc ratio (2)	-5.8	5.3	17.8	flow paths open & little extra friction			-11.2	0.0	11.2	flow paths open & little extra friction			-4.3	0.0	4.3	-5.8	0.0	5.8	-4.5	6.0	19.5
	greater Δp in bundle	(3)						(3)						(3)			(3)			(3)		
Primary deposits		0.4	2.1	30.9	0.4	2.1	30.9	0.4	2.1	30.9	0.4	2.1	30.9	0.4	2.1	30.9	0.4	2.1	30.9	0.4	2.1	30.9
Total (10^{-6} h-ft^2-°F/Btu)		*-35.4*	*-7.6*	*48.8*	*2.8*	*11.8*	*60.1*	*-25.8*	*30.8*	*149.1*	*2.8*	*11.8*	*60.0*	*-18.8*	*2.1*	*40.1*	*-8.9*	*67.4*	*185.3*	*47.0*	*193.2*	*414.2*
SOURCES OF PRESSURE LOSS (psi)		Lower Bound	Best Estimate	Upper Bound	Lower Bound	Best Estimate	Upper Bound	Lower Bound	Best Estimate	Upper Bound	Lower Bound	Best Estimate	Upper Bound	Lower Bound	Best Estimate	Upper Bound	Lower Bound	Best Estimate	Upper Bound	Lower Bound	Best Estimate	Upper Bound
Sources That Affect Initial Performance vs. Ideal Design Performance (But Not Pressure Loss Since Start-Up)																						
Pre-service tube plugging		0.3	0.3	0.3	0.3	0.3	0.3	0.0	0.0	0.0	0.0	0.0	0.0	0.1	0.1	0.1	0.0	0.0	0.0	0.4	0.4	0.4
Initial RCL temps. different than design		-0.6	8.6	17.8	-0.6	8.6	17.8	-5.1	6.8	18.6	-5.1	6.8	18.6	-38.2	-13.8	10.6	14.8	53.6	92.5	-23.8	-1.5	20.8
Primary tube velocity different than design		-4.0	-3.1	-1.7	-5.2	-2.9	-0.5	-0.4	1.1	2.7	-0.4	1.1	6.9	-3.4	-2.2	-0.3	-2.5	-0.7	0.2	-5.8	-3.5	-2.9
Tube thickness variation from nominal		-12.3	0.0	12.5	-12.3	0.0	12.5	-15.2	0.0	15.4	-15.2	0.0	15.4	-8.6	0.0	8.7	-14.6	0.0	14.8	-16.1	0.0	16.3
Tube thermal conductivity variation from nominal		-5.5	0.0	6.1	-5.5	0.0	6.1	-6.8	0.0	7.6	-6.8	0.0	7.6	-3.9	0.0	4.3	-6.6	0.0	7.3	-7.2	0.0	8.0
Subtotal (psi) (not included in Total below)		*-22.2*	*5.8*	*35.0*	*-23.3*	*6.0*	*36.2*	*-27.5*	*7.9*	*44.3*	*-27.5*	*7.9*	*48.4*	*-54.0*	*-15.9*	*23.4*	*-8.9*	*53.0*	*114.8*	*-52.5*	*-4.6*	*42.5*
Sources That are Due to Deposits within the Tube Bundle																						
Secondary freespan deposits		-10.8	-5.4	0.0	0.9	3.5	10.5	-5.3	10.3	38.2	0.9	3.5	10.4	-3.5	0.0	1.2	-1.2	22.4	51.1	19.9	71.9	141.3
Secondary flow blockage and extra friction	lower recirc ratio (2)	-2.1	1.9	6.4	flow paths open & little extra friction			-4.0	0.0	4.0	flow paths open & little extra friction			-1.0	0.0	1.0	-2.0	0.0	2.0	-1.7	2.3	7.5
	greater Δp in bundle	(3)						(3)						(3)						(3)		
Primary deposits		0.1	0.7	11.2	0.1	0.7	11.2	0.1	0.7	11.0	0.1	0.7	11.0	0.1	0.5	7.3	0.1	0.7	10.6	0.2	0.8	12.0
Subtotal (psi)		*-12.8*	*-2.7*	*17.6*	*1.0*	*4.3*	*21.7*	*-9.2*	*11.0*	*53.2*	*1.0*	*4.2*	*21.4*	*-4.4*	*0.5*	*9.4*	*-3.0*	*23.2*	*63.7*	*18.3*	*75.0*	*160.7*
Sources That are NOT Due to Deposits within the Tube Bundle which are Captured in the Fouling Factor Calculation																						
Uncertainty in steam generator press. meas.		-6.5	0.0	6.5	-6.5	0.0	6.5	-4.8	0.0	4.8	-4.8	0.0	4.8	-7.5	0.0	7.5	-5.4	0.0	5.4	-6.0	0.0	6.0
Extra separator/dryer pressure drop		3.5	4.0	4.4	3.5	4.0	4.4	0.0	1.0	4.0	0.0	1.0	4.0	0.0	3.0	13.0	0.0	3.0	13.0	0.0	4.0	13.0
Error in applied primary temperature due to	$T_{cold/ave}$ meas. error	-4.6	0.0	4.6	-4.6	0.0	4.6	-5.9	0.0	5.9	-5.9	0.0	5.9	-12.2	0.0	12.2	-19.4	0.0	19.4	-22.3	0.0	22.3
	Hot leg streaming	0.0	4.0	5.9	0.0	4.0	5.9	0.0	14.7	22.0	0.0	14.7	22.0	0.0	12.9	34.5	-5.2	-3.1	6.9	T_{cold} control plant		
	Divider plate leakage	0.00	0.02	2.4	0.00	0.02	2.4	0.00	0.02	2.3	0.00	0.02	2.3	0.00	0.03	2.8	0.00	0.02	2.2	0.00	0.04	3.9
Error in reactor power calibration due to uncertainty in	FW flow including venturi fouling	-11.6	0.0	13.4	-11.6	0.0	13.4	-2.2	0.0	4.1	-2.2	0.0	4.1	-1.6	0.0	3.2	-1.8	0.0	3.6	-1.9	0.5	3.8
	FW temperature	-0.5	0.0	0.5	-0.5	0.0	0.5	-0.8	0.0	0.8	-0.8	0.0	0.8	-0.5	0.0	0.5	-0.5	0.0	0.5	-0.3	0.0	0.3
	Outlet steam quality	-0.5	0.0	0.5	-0.5	0.0	0.5	-0.5	0.0	0.5	-0.5	0.0	0.5	-0.4	0.0	0.4	-0.5	0.0	0.5	-0.3	0.0	0.3
	Blowdown flow	-0.02	0.0	0.02	-0.02	0.0	0.02	-0.2	0.0	0.2	-0.2	0.0	0.2	-0.2	0.0	0.2	-0.3	0.0	0.3	-0.17	0.0	0.17
Subcooling (feedwater temp. variations) (2)		-2.1	-0.7	0.0	-10.1	-3.4	0.0	-2.0	0.0	2.0	-1.0	0.0	1.0	-1.0	0.0	1.0	-1.0	0.0	1.0	-4.3	-1.4	0.0
Flow maldistribution in preheater														0.0	3.0	15.0						
Subtotal (psi)		*-22.4*	*7.2*	*38.3*	*-30.4*	*4.5*	*38.3*	*-16.4*	*15.7*	*46.6*	*-15.4*	*15.7*	*45.6*	*-23.4*	*19.0*	*90.2*	*-34.1*	*-0.1*	*52.8*	*-35.2*	*3.1*	*49.7*
Apparent fouling factor corresponding to this pressure loss (10^{-6} h-ft^2-°F/Btu)		*-62*	*20*	*106*	*-84*	*13*	*106*	*-46*	*44*	*131*	*-43*	*44*	*128*	*-99*	*81*	*384*	*-99*	*0*	*154*	*-91*	*8*	*128*
Net fouling factor after subtracting this component (10^{-6} h-ft^2-°F/Btu)		*34*	*-48*	*-134*	*79*	*-18*	*-111*	*66*	*-24*	*-110*	*85*	*-2*	*-86*	*129*	*-51*	*-354*	*150*	*51*	*-103*	*263*	*164*	*44*
Sources That are Accounted for by the Fouling Factor Calculation																						
Tube plugging since start-up		1.2	1.2	1.2	1.6	1.6	1.6	3.6	3.6	3.6	6.9	6.9	7.0	1.5	1.5	1.5	9.5	9.6	9.6	11.6	11.7	11.8
T_{cold}/T_{ave} variations vs. initial temperatures		-3.8	0.8	5.4	-1.3	3.3	7.9	-5.9	0.0	5.9	-5.2	0.7	6.7	39.5	51.7	63.9	-13.2	6.3	25.7	-26.7	-4.5	17.8
Variations in thermal power		-4.5	-3.6	-2.7	-3.6	-2.7	-1.8	-3.7	-2.8	-1.9	-2.8	-1.9	-0.9	-1.6	-0.8	0.0	-7.2	-3.6	0.0	-1.3	-0.7	0.0
Power uprate		13.9	15.4	17.0	13.9	15.4	17.0	No Uprate			No Uprate			No Uprate			No Uprate			No Uprate		
Subtotal vs. Initial Perf. (psi)		*6.8*	*13.9*	*20.9*	*10.6*	*17.7*	*24.7*	*-6.1*	*0.8*	*7.7*	*-1.1*	*5.8*	*12.7*	*39.4*	*52.4*	*65.4*	*-10.9*	*12.2*	*35.3*	*-16.4*	*6.6*	*29.7*
Summary																						
Best-Est. Total Loss vs. Initial Perf. (psi)		*18*			*26*			*28*			*26*			*72*			*35*			*85*		
Actual Total Loss vs. Initial Perf. (psi)		*17*			*28*			*25*			*36*			*63*			*30*			*77*		

(1) The fouling factor has been decreasing at Plants A and B since just after chemical cleaning. Plant A's has decreased about 11 10^{-6} and Plant B's has decreased about 4 10^{-6}.

(2) The values for Plants A and E are preliminary results of a one-dimensional heat transfer model of the steam generator using the Chen correlation for secondary resistance. The values for Plants B, C, and D are estimates based on engineering judgment.

(3) This effect may be evaluated using ATHOS modeling.

Table D-7. Example Hot-Leg Streaming Calculation

Instrument Readings	T_{hot}	T_{ave}	T_{cold}
No HL Streaming	600	570	540
HL Streaming (Transient)	604	572	540
HL Streaming (Steady-State)	602	570	538
Net Change	2	0	-2

Actual Temperatures			
No HL Streaming	600	570	540
HL Streaming (Transient)	600	570	540
HL Streaming (Steady-State)	598	568	538
Net Change	-2	-2	-2

Table D-8. Pressure-Loss Breakdowns – Non-Deposit Causes

Unit	Plant A		Plant B				Plant C	Plant D	Plant E		Plant F†
Year	1995	1996	1989	1990	1995	1996	1996	1995	1995	1996	1990
Operating Time (EFPY)	8.6	9.5	3.0	3.9	7.5	7.8	5.0	8.0	8.6	10.1	9.1
Tube Plugging	1.2	1.6	1.2	1.2	3.6	6.9	1.5	9.6	10.9	11.7	19.3
Power Uprate	15.4	15.4	–	–	–	–	–	–	–	–	–
Primary Temperature Variation	0.8	3.3	-2.9	0.7	0.0	0.7	51.7	6.3	-4.5	-4.5	*2.0*
Hot-Leg Streaming	4.0	4.0	0.0	0.0	14.7	14.7	12.9	-3.1	–	–	0.0
Thermal Power Variation	-3.6	-2.7	-3.7	-3.7	-2.8	-1.9	-0.8	-3.6	-0.7	-0.7	0.0
FW Temperature Variations	-0.7	-3.4	0.0	0.0	0.0	0.0	0.0	0.0	-1.0	-1.4	0.0
Flow Maldistribution in PH	–	–	–	–	–	–	3.0	–	–	–	–
FW Venturi Fouling**	0.0	0.0	0.0	0.0	0.0	0.0	0.0	0.0	0.5	0.5	*10.0*
Additional Separator/Dryer ΔP	4.0	4.0	0.5	0.5	1.0	1.0	3.0	3.0	3.5	4.0	*3.0*
Total Estimated Loss	**21.1**	**22.2**	**-4.9**	**-1.3**	**16.5**	**21.4**	**71.3**	**12.2**	**8.7**	**9.6**	**34.3**
Total Observed Loss	**17.0**	**28.4**	**-4.6**	**0.6**	**25.2**	**36.3**	**62.5**	**30.4**	**60.1**	**77.1**	**67.0***
Balance	**-4.1**	**6.2**	**0.3**	**1.9**	**8.7**	**14.9**	**-8.8**	**18.2**	**51.4**	**67.5**	**32.7**

* Does not reflect any pressure loss due to deposits observed between 1970 and 1980.

** Includes an adjustment for blowdown flow (17).

† Plant-F italicized values per Reference (17).

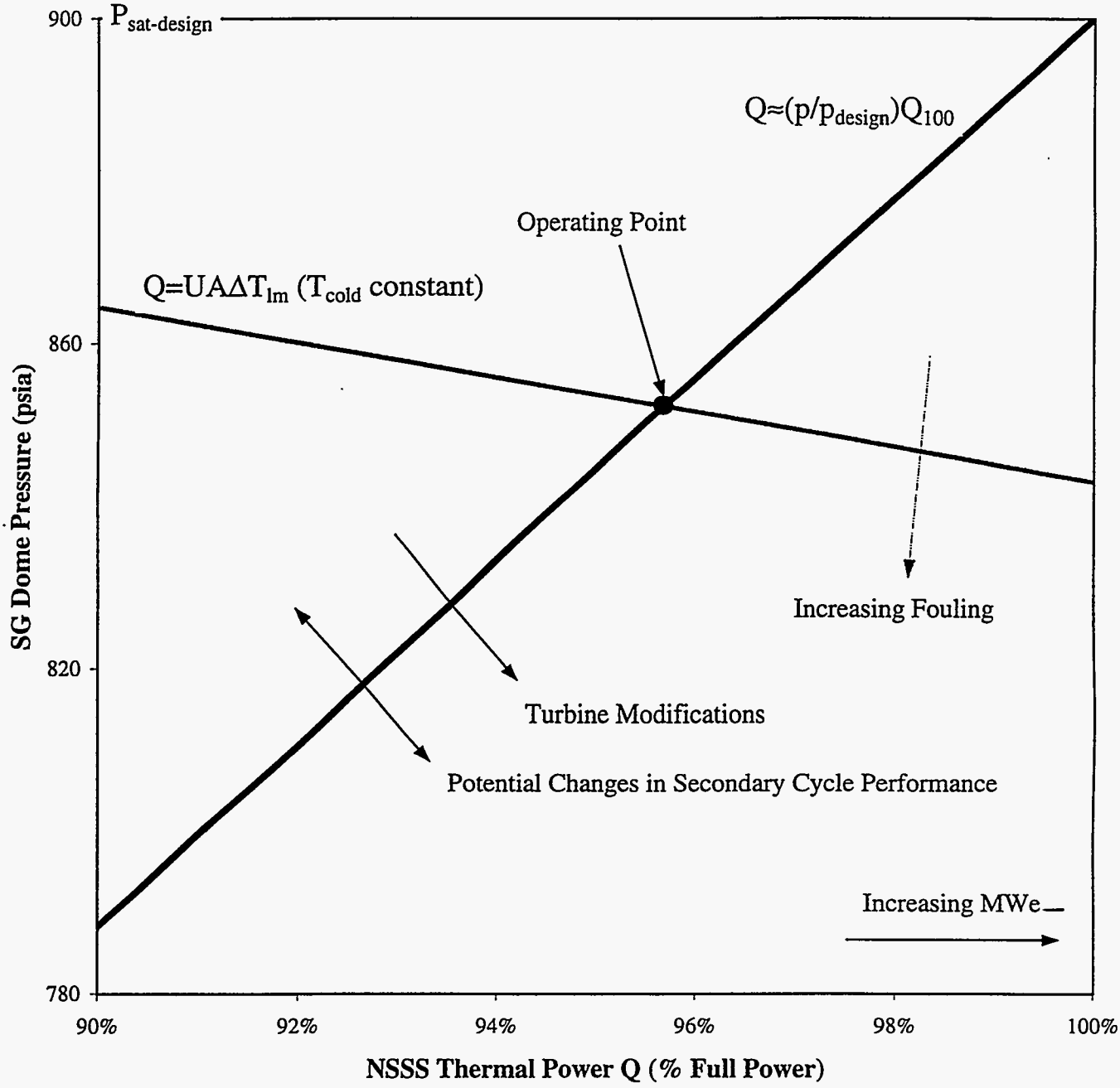

Figure D-1. Relationship Between SG Pressure and Thermal Power at Sister Unit to Plant E

APPENDIX E

IMPACT OF PRIMARY DEPOSITS ON THERMAL PERFORMANCE IN COMMERCIAL SGS

Because the secondary-side fluid in SGs boils, relatively concentrated solutions are possible, which can promote the formation of deposits. Hence, much effort has been spent examining secondary deposits and corrosion (e.g., numerous detailed tube-pull examinations have been documented in Electric Power Research Institute (EPRI) reports). On the other hand, the primary fluid remains subcooled, meaning that the concentrations of potentially corrosive species remain at the low levels of the original primary coolant, which is contained in a corrosion-resistant pressure boundary. As a consequence, much less work has been focused on potential primary-side (i.e., ID) corrosion films. Nevertheless, until the physical characteristics of the primary-side film are investigated, the potential contribution of an ID corrosion layer to the observed degradation in SG heat transfer capability cannot be ruled out.

In order to evaluate the heat-transfer role of primary films, the following characteristics must be considered:

- composition
- effective thermal conductivity (reflects both composition and morphology)
- deposit thickness

These properties have an impact on the potential for a particular corrosion layer to cause significant heat-transfer degradation. Based on a survey of EPRI tube pull reports, it seems that none of these variables has been measured consistently or frequently on actual pulled SG tubes in the US.* Pulled tubes have been examined most often on the secondary side where thicker deposit layers have been observed.

Composition. Like the secondary side, where corrosion layers are most often composed predominantly of iron oxides, primary-side layers are thought to contain primarily metal oxides. This conclusion is supported by tube examinations performed on SG tubes from several Electricité de France (EdF) plants (i.e., Dampierre, Gravelines, and Tricastin). These are plants which had been in operation for approximately 8-10 years at the time of the tube pulls. For over 40 tubes, the primary film constituents were the following, with average weight percents indicated (5):

Cr_2O_3	47%
Fe_3O_4	29%
NiO	23%

* As discussed later, some data have been taken on tubes pulled from overseas plants.

A literature survey of tube-pull reports for US plants did not reveal any similar detailed analyses of the ID surface film. A few tube exams have included reports of the ID layer components by element (References (6) through (10)). In addition to the main constituents of Alloy 600 and 690 (the typical tube materials), the following other elements were found in measurable quantities (not all were found in each test): Si, Ti, Al, Ca, P, S, O, Mn, Na, Cl, Zn, Zr.

Morphology. Based on discussions with three independent researchers (14), the following is noted regarding the structure of primary-side corrosion layers:

- The thickness is very uniform.
- Intergranular attack (IGA) penetrated the tube surface beneath the corrosion layer. The voids created by the IGA are believed to be oxide filled (as opposed to steam filled).
- No spalling of these films has been observed.

Effective Thermal Conductivity. In order to ascertain the effect of primary-side layers on heat transfer, the effective thermal conductivity of the layer must be determined, either by measurement or by calculation. No heat-transfer measurements for corrosion layers typical of PWR SG primary tubing are known to be available. It is believed that few if any experiments have been performed for this purpose due to the fact that secondary-side corrosion layers tend to be thicker than their primary-side counterparts and hence receive most of the attention. Consequently, calculation and/or estimation of the effective thermal conductivity must be performed.*

As a first step, thermal conductivity values for some solid metal oxides were compiled. This list is presented in Table E-1. As noted earlier, the bulk of primary films most likely comprise Cr_2O_3, Fe_3O_4, and NiO. However, a number of other oxides are included in the table to indicate the likely range of thermal conductivity values. All SI values are taken from Reference (11),† except for hematite (Fe_2O_3) and magnetite (Fe_3O_4), which are curve-fit values for 573 K taken from Reference (12). Conversion to English units is made based on standard conversion factors. The compounds are listed in order of increasing thermal conductivity. When possible, values were selected for temperatures close to typical primary-side SG temperatures (i.e., near 600°F). Comments regarding the characteristics of the samples used in the measurements are provided in the right-most column (e.g., some samples were single crystals while others consisted of pressed

* However, note that primary-side deposits are a major concern for SGs in PHWR plants (e.g., CANDU design) because of their use of carbon steel piping for primary components. Primary deposits in these SGs have been subjected to heat-transfer measurements.

† In some cases, averages of the values presented in (11) are reported in Table E-1.

powder). Note that the data in the table span the range from 0.2 to 53 BTU/hr-ft-°F.* In addition to magnetite and hematite (with thermal conductivities of 2.0 and 2.8 at 572°F), potentially relevant compounds include SiO_2 (1.0 at 578°F) and NiO (3.1-5.7 depending on temperature and porosity). Except for beryllium oxide, thermal conductivity values fall for the most part between 1.0 and 10, including the iron oxide, nickel oxide, and silica values. Based on this range and also the values for relevant compounds (i.e., Cr_2O_3, Fe_3O_4, NiO), the constituents of typical primary-side films are expected to have thermal conductivity values somewhere between 1.0 and 10.

The second step in computing effective thermal conductivity is accounting for possible porosity in the primary-side surface layer. If we assume a certain percentage of the film comprises pores that are filled with stagnant water, we can then compute the effective thermal conductivity from an equation developed by Bruggeman (13) for two-phase dispersions of one material within a matrix of another material:

$$\left(\frac{k_{eff} - k_d}{k_c - k_d}\right)\left(\frac{k_c}{k_{eff}}\right)^{1/3} = 1 - v_d \qquad \text{[E-1]}$$

In Eq. [E-1], k_c is the thermal conductivity of the matrix (in this case, the oxide components), k_d is the thermal conductivity of the dispersed material (in this case, water), and v_d is the volume fraction of the dispersed material.

Film Thickness. Because most of the attention on heat transfer loss has been focused on the secondary-side deposits, relatively few detailed examinations of primary-side oxide thickness have been recorded. However, several researchers have documented this thickness. Per References (5) and (14) (attached), three independent researchers who have examined numerous SG tubes all indicate that the primary-side oxide thickness after substantial operating times (i.e., approximately 5-10 EFPY) averages nearly 1 micron (0.04 mils), with possible maximum values near 5 microns (0.2 mils). The average thickness did not vary significantly among the plants involved (Doel 3 and 4 in Belgium; Dampierre, Gravelines, and Tricastin in France; and Ringhals 3 and 4 in Sweden). Nor was there substantial variation based on tube manufacturer: oxide thicknesses for Vallourec/Inphy tubing, Westinghouse/Huntington tubing, and Vallourec/Huntington tubing all averaged between 1 and 1.5 microns. In addition to these

* All subsequent references to thermal conductivity values are in BTU/hr-ft-°F unless otherwise indicated.

measurements, Reference (1) indicates that the primary film on the pulled tube at Plant F (reflecting over 15 EFPY) was less than 1 micron in thickness.

As a result of the above information, it is judged unlikely that a plant with less than 10 EFPY of operating time will have primary deposits thicker than the thickest samples described in Reference (5). Thus, 5 microns, or 0.2 mils, is believed to be a reasonable upper bound for primary oxide thickness, 1 micron is the best-estimate thickness, and 0.5 microns is taken as the lower-bound thickness.

Based on the best-estimate and bounding values for thickness and effective thermal conductivity developed above, the associated best-estimate and bounding fouling factors attributable to primary deposits are calculated and reported in Table E-2. For all plants, the best estimate value is 2 10^{-6} h-ft^2-°F/BTU and the conservative upper bound is about 30 10^{-6}.

Table E-1. Thermal Conductivities of Selected Solid Oxides[1]

Oxide	Temperature		Thermal Conductivity		Comments
	K	°F	W/m-K	BTU/h-ft-°F	
Co_2O_3	322	121	0.4	0.2	pressed powder
ZnO	323	122	0.6	0.3	pressed powder
CdO	320	117	0.7	0.4	pressed powder
Ni_2O_3	319	115	0.9	0.5	pressed powder
CuO	319	115	1.0	0.6	pressed powder
SiO_2	576	578	1.7	1.0	pure fused quartz
V_2O_5	673	752	1.8	1.0	
Zr_2O_3	673	752	2.1	1.2	
V_2O_5	473	392	2.6	1.5	
Ti_3O	575	576	2.9	1.7	
BaO	600	621	3.0	1.7	single crystal in argon
TiO	575	576	3.2	1.8	
Y_2O_3	673	752	3.3	1.9	single crystal; ±20%
Fe_3O_4	**573**	**572**	**3.4**	**2.0**	**crystalline wafers[2]**
Ti_5O	575	576	4.0	2.3	
Ti_6O	575	576	4.4	2.5	
Cr_2O_3	**333**	**140**	**4.5**	**2.6**	**pressed powder**
Fe_2O_3	573	572	4.9	2.8	crystalline wafers
TiO_2	473	392	5.0	2.9	polycrystalline
Sc_2O_3	573	572	5.0	2.9	sintered with zero open porosity
NiO	**673**	**752**	**5.3**	**3.1**	**25.7% porosity**
SrO	600	621	5.5	3.2	single crystal in argon
NiO	**673**	**752**	**7.2**	**4.2**	**polycrystalline, nonporous**
NiO	**473**	**392**	**7.4**	**4.3**	**25.7% porosity**
CeO_2	500	441	8.6	5.0	porous specimen
VO_2	373	212	9.8	5.7	
NiO	**473**	**392**	**9.9**	**5.7**	**polycrystalline, nonporous**
ZnO	673	752	11.0	6.4	polycrystalline
Ti_2O	575	576	11.5	6.6	
Al_2O_3	673	752	13.0	7.5	little or no porosity
CaO	600	621	14.0	8.1	single crystal in argon
ZnO	473	392	17.0	9.8	polycrystalline
MgO	575	576	17.5	10.1	
SnO_2	423	302	22.4	12.9	2% impurities
Al_2O_3	373	212	29.0	16.8	little or no porosity
BeO	673	752	91.0	52.6	nonporous

(1) All values taken from Reference (11) except as noted below.
(2) Values are based on a curve fit to actual data taken from Reference (12).
(3) Entries in bold describe oxides found in primary-side films.

Table E-2. Calculated Fouling Factors Associated with Primary Films*

Quantity	Lower Bound	Best Estimate	Upper Bound
Layer thickness (μm)	0.5	1	5
Layer thickness (mils)	0.020	0.039	0.197
Thermal conductivity (Btu/h-ft-°F)	4.6	1.8	0.6
Fouling factor (based on ID area) (10^{-6} h-ft^2-°F/BTU)	0.4	1.8	27.3
Fouling factor (based on OD area) (10^{-6} h-ft^2-°F/BTU)	0.4	2.1	30.9

*Based on Plant-A tube geometry. However, due to the very small thicknesses, these values also apply to the other plants.

MEMORANDUM

Number: M-3613-00-8, Rev. 0

To: RDV
36-13 File

From: Marc Kreider

Date: December 1, 1995

Subject: Telecons with Charles Laire (Laborelec), François Cattant (EPRI/NMAC) and Kjell Norring (Studsvik Energy)

Charles Laire (Laborelec-Belgium) – November 29, 1995

Based on his experimental work on numerous tubes, he indicated the following information regarding primary-side (ID) corrosion:

- Oxide layers were very thin - typically 1 micron or less.
- IGA on the ID surface penetrated only 15-20 microns at the most. The IGA surfaces, he believes, are oxide filled (not steam spaces). He doesn't believe that the IGA has a significant effect on heat transfer.
- In his experiments, no data on primary-side film composition was collected.
- Doel 4 had a similar experience to Callaway, i.e., chemical cleaning did not result in a significant steam pressure improvement, despite the success in removing corrosion products. Laire indicated that the theory why no pressure recovery was realized is that corrosion products may have been blocking preheater bypass flow prior to chemical cleaning. This blockage increased heat transfer. After chemical cleaning, this blockage may have been cleared, counteracting the beneficial effect of deposit removal.

François Cattant (EPRI/NMAC) – November 30, 1995

Based on his experimental work on numerous tubes from French SGs, he indicated the following information regarding primary-side (ID) corrosion:

- Primary-side oxide thickness depends somewhat on tube manufacturer:

Vallourec/Inphy:	1.5 microns average
Westinghouse/Huntington:	0.92 microns average
Vallourec/Huntington:	1.1 microns average

A maximum thickness from all samples was recorded to be 4 to 5 microns thick. These tubes were from Dampierre, Gravelines, and Tricastin, plants that had been in operation for about 10 years at the time of the tube pulls (ca. 1990).

Further details are available in EdF Document No. D5004/CTT/RA.90.128, dated Dec. 3, 1990, and titled "PWR Plants SGs: Composition and Thickness of Layers on ID Surfaces" [approximate translation from French].

- The main components of the film were oxides of Cr, Ni, and Fe.
- IGA on the primary side varied in thickness from 5-10 microns above the TS to 10-20 microns in the TS. No tests were performed to determined IGA composition. The grain-boundary thicknesses on the primary side were •0.5 microns.

Kjell Norring (Studsvik Energy - Sweden) – December 1, 1995

Based on his examination of tubes from Ringhals 3 and 4 (ca. 1990), he indicated the following information regarding primary-side (ID) corrosion:

- Oxide thickness averages approximately 1 micron; the thickness tends to be very uniform.
- No spalling of ID films has been observed.
- He does not believe that the structure of primary-side IGA is likely to be a source of reduced heat transfer.